Algebraic Field Theory on Causal Sets: Local Structures and Quantization Methods

Christoph Minz

PhD

University of York
Mathematics

September 2021

Abstract

I investigate aspects of classical and quantum real scalar field theory on *causal sets* — a discrete framework for space and time — using the algebraic perspective. After reviewing and generalizing necessary notation, I consider different discretizations of the Klein-Gordon field equations to describe the dynamics of a scalar field. I generalize a recently proposed discretization method that uses a *preferred past structure* (which assigns a specific past element to every element of a causal set) to lattices in Minkowski spacetime of any dimension. With numerical techniques, I analyse criteria to assign a preferred past structure to more general causal sets that are generated via *sprinkling* — a Poisson process on a given spacetime manifold. It turns out that there exists a method that is very successful in selecting a preferred past uniquely with high probability (for finite causal sets on Minkowski spacetime).

I review quantization methods and algebraic states. For the case of a finite causal set, I show how to construct a symplectic vector space with an inner product. The given structure lets me apply the method of *geometric quantization* to determine a quantum algebra and define a state, which is the *Sorkin-Johnston state* — commonly considered for quantum field theory on causal sets. Additionally, I discuss the relationship of the geometrically constructed quantum algebra to deformation quantization to motivate future applications like a non-perturbative construction of the quantum algebra for interacting field theories via geometric quantization.

Contents

List of Tables

List of Figures

Acknowledgements

First of all, I would like to thank my supervisors Kasia Rejzner and Eli Hawkins for their support, inspirations and help in the development of the ideas, methods and results of my PhD projects. My PhD research was funded by the Engineering and Physical Sciences Research Council (EPSRC) under the grant no. EP/N509802/1. Thanks goes also to Christopher Fewster for many discussions and improvements of the techniques used to obtain the results of our publication [38]. I would like to thank Atsushi Higuchi and Fay Dowker for their comments and suggested additions to this thesis.

I am grateful for many inspiring seminars, workshops, summer schools, and research conferences. In particular, I want to thank Sumati Surya, Stav Zalel, Ian Jubb, Alexei Daletskii for many helpful discussions and literature suggestions. Fleur Versteegen and Nomann X have shared their experiences with me when I was setting up the numerical simulations. Thanks goes also to the organisers and participants of the virtual conferences "Quantum Gravity 2020" and "The Virtual Causet" where interesting questions had been raised that improved the results of this thesis.

The simulations in this project were undertaken on the Viking Cluster, which is a high performance compute facility provided by the University of York. I am very grateful for computational support from the Research Computing team.

Last but not least, I want to thank my family for their support, and my PhD colleagues, the staff at the Department of Mathematics, and my housemates for a pleasant working and living atmosphere in York.

Author's Declaration

I declare that the work presented in this thesis, except where otherwise stated, is based on my own research carried out at the University of York and has not been submitted previously for any degree at this or any other university. Sources are acknowledged by explicit references.

Most results of Chapter 3 and Chapter 4 are published in Physical Review D 103.8 (2021): "Local Structure of Sprinkled Causal Sets" in collaboration with C. J. Fewster, E. Hawkins, and K. Rejzner [38]. My numerical investigations discussed in Chapter 3 were undertaken on the Viking Cluster, which is a high performance compute facility provided by the University of York, and the source code is publicly available via my online repositories listed in [76, 77]. In a side-project inspired by this publication, I developed a LaTeX-package for drawing Hasse diagrams for causal sets, which is available via CTAN [68].

A further publication "Quantization, Dequantization and Distinguished States" with my supervisors E. Hawkins, and K. Rejzner is in preparation.

Chapter 1

Introduction: Spacetime Manifolds and Causal Sets

1.1 Introduction, Prerequisites and Overview

Quantum field theory is often introduced as the area of theoretical physics that makes experimental predictions that have been verified to the highest precision, thus making quantum field theory a remarkable successful theory to describe the nature of elementary particles and their interactions. Elementary particles are understood via quantum fields, which are the quantized version of classical fields that obey certain equations of motions (e.o.m.) — relativistic field equations like the *Klein-Gordon equation* that we will also encounter in this thesis. Algebraic field theory takes an algebraic perspective on (classical and) quantum field theory and puts the formulation into a rigorous mathematical framework. The framework was developed not only to describe particle fields without gravitational interactions (in Minkowski spacetime) but also on more general, curved spacetime backgrounds.

Mathematical investigations of quantum fields on curved spacetime manifolds, in particular, where extremely strong gravitational fields can no longer be neglected lead to the prediction of effects that point beyond quantum field theory on curved spacetimes and the theory of general relativity to a theory of quantum gravity. Even though there are many candidates for such a theory, there has been no experimentally verified prediction beyond understood phenomena. Causal set theory is a framework for quantum gravity where the spacetime manifold is replaced by the discrete structure of causal sets. The general idea is that this discrete structure is important on a microscopic level, while on a much larger length scale a spacetime manifold "emerges" as a sufficiently precise approximation. A causal set does not only serve as a model to study quantum gravity, but due to its discrete nature, we may also construct models to investigate classical and quantum fields that are simpler than models on a spacetime manifold. In a longer perspective, such models may not only help to understand aspects of (algebraic) quantum field theory on causal sets, but may also serve to find solutions to problems in quantum fields on spacetimes once a suitable limiting process from the microscopic structure of causal sets to the macroscopic structure of spacetimes has been formulated.

In this thesis, I will discuss aspects of algebraic field theory of a real scalar

boson on causal sets and on spacetime manifolds in parallel highlighting common and distinct aspects. With this parallel approach, I want to guide our attention to important aspects and possible pitfalls that one needs to keep in mind to eventually formulate a mathematical rigorous limiting procedure to describe the "emergence" of spacetimes from causal sets, which is also referred to as the main conjecture ("Hauptvermutung") in causal set theory, see Surya [104]. The analogous formulation of causal sets and spacetimes may further inspire a view in terms of category theory, though I do not discuss category theory in this thesis. I will mainly focus on two aspects: first, the local structure of causal sets that is used to discretize the Klein-Gordon equations to describe the dynamics of the real scalar field, and second, the quantization of the symplectic space with a geometrical construction of the *Sorkin-Johnston state*.

As prerequisites, I assume a basic understanding of the concept of a manifold and the areas of differential geometry and quantum mechanics. Most necessary terms and notations are reviewed in introductory sections, listed in the glossary starting on p. 155, or given in the literature as referenced. The content of this thesis is structured as follows. In the following sections of this chapter, we review the causal structure that underlies causal sets and spacetimes. We will discuss classical field theory including the discretization of the field equations in Chapter 2 leading us to the local structure of causal sets that I analysed with numerical methods in Chapter 3. Most of the results of Chapter 3 and the analytic investigations into the *Poisson process* (called *sprinkling*) to generate causal sets from a spacetime discussed in Chapter 4 are published in Fewster, Hawkins, Minz, and Rejzner [38]. In Chapter 5, we take a look at *quantization methods* and aspects of quantum field theory, mostly those that are used for the geometrical construction of a quantum algebra and the Sorkin-Johnston state over a causal set in Chapter 6.

1.2 Causal Structures

At first, I review causal relations, something that spacetime manifolds and causal sets have in common. Afterwards, we look into the differences between spacetime manifolds and causal sets that will be important for the formulation of field equation and their solutions in Chapter 2. For a more detailed introduction to spacetime manifolds, in particular *globally hyperbolic spacetimes*, see the textbooks Penrose [89], Hawking and Ellis [47], and Wald [107].

1.2.1 Causal Relations

The causal structure of (causally ordered) spacetime manifolds and causal sets are partial orderings.

Definition 1.2.1. A **partially ordered set (poset)** $(S, \preceq)$ is a set S equipped with a binary relation $\preceq$ (the partial ordering) such that the following axioms are fulfilled for all $x, y, z \in S$

$$\text{reflexivity:} \qquad x \preceq x, \tag{1.1a}$$

$$\text{transitivity:} \qquad (x \preceq y \text{ and } y \preceq z) \Rightarrow x \preceq z, \tag{1.1b}$$

$$\text{anti-symmetry:} \qquad (x \preceq y \text{ and } y \preceq x) \Leftrightarrow x = y. \tag{1.1c}$$

If two elements x and y are ordered, but not equal ($x \preceq y$ and $x \neq y$), I write $x \prec y$. The set is **totally ordered** if all pairs of elements $x, y \in S$ are comparable,

$$\text{total order:} \qquad x \preceq y \text{ or } y \preceq x. \tag{1.2}$$

For many statements about posets, there are usually similar statements for the posets with reversed partial ordering. So it is useful to define it.

Definition 1.2.2. The **opposite poset** of a poset $\mathscr{S} = (S, \preceq)$ is the poset $\mathscr{S}^{\mathrm{op}} := (S, \preceq^{\mathrm{op}})$ such that

$$\forall x, y \in S: \qquad y \preceq^{\mathrm{op}} x \Leftrightarrow x \preceq y. \tag{1.3}$$

Note that $(\mathscr{S}^{\mathrm{op}})^{\mathrm{op}} = \mathscr{S}$ for any poset $\mathscr{S}$.

Definition 1.2.3. Let $(S, \preceq)$ be a poset. A **chain** is a totally ordered subset of S and an **antichain** is a subset $A \subseteq S$ such that

$$\forall x, y \in A: \qquad (x \preceq y \text{ or } y \preceq x) \Leftrightarrow x = y. \tag{1.4}$$

Definition 1.2.4. Let $(S, \preceq)$ be a poset and let $A \subseteq S$ be a subset. A subset $B \subset A$ is **convex in** A if

$$\forall x, y \in B : \forall z \in A: \qquad x \preceq z \preceq y \Rightarrow z \in B. \tag{1.5}$$

We simply say B is **convex** if B is convex in S.

Note that, in this thesis, I frequently use the common notation for open and closed intervals of integers or real numbers, (x, y) and $[x, y]$, respectively. I write $[x, y] \subset \mathbb{Z}$ or $[x, y] \subset \mathbb{R}$ etc. to make the number field explicit if it is not already clear from the context. More generally and slightly less common, let us also use the same notation to denote intervals of any partially ordered set.

Definition 1.2.5. Let $(S, \preceq)$ be a poset. For any pair of events $x, y \in S$, the **closed interval** from x to y is

$$[x, y] := \{z \in S \mid x \preceq z \preceq y\} \tag{1.6}$$

and the **open interval** from x to y is

$$(x, y) := \{z \in S \mid x \prec z \prec y\}\,. \tag{1.7}$$

It is obvious that closed intervals are convex. Given a poset $(S, \preceq)$ with $x, y \in S$, the closed interval $[x, y]$ can be understood as the intersection of the *future* of x with the *past* of y.

Definition 1.2.6. Let $(S, \preceq)$ be a poset. The **past** (J^-) and **future** (J^+) of an event $x \in S$ or a subset $A \subseteq S$ are

$$J^-(x) := \{y \in S \mid y \preceq x\}\,, \tag{1.8a}$$
$$J^+(x) := \{y \in S \mid x \preceq y\}\,, \tag{1.8b}$$
$$J^\mp(A) := \bigcup_{x \in A} J^\mp(x), \tag{1.8c}$$

and the **strict past/future** are, respectively,

$$J^\mp_*(x) := J^\mp(x) \setminus \{x\}, \tag{1.9a}$$
$$J^\mp_*(A) := \bigcup_{x \in A} J^\mp_*(x). \tag{1.9b}$$

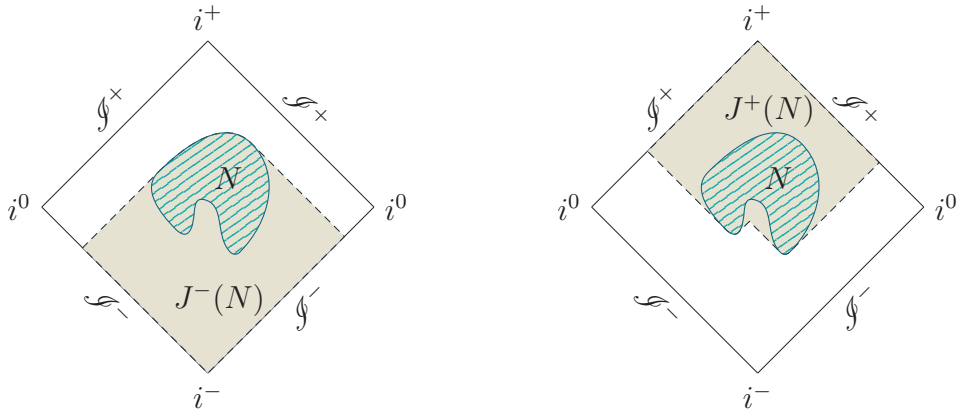

(a) Past of a compact region

(b) Future of a compact region

Figure 1.1: Penrose diagrams of Minkowski spacetime [88] showing (a) the past and (b) the future (dashed outline, grey) of a compact region $N \subset M$ (solid outline, line pattern, cyan). (*Notation of Penrose diagrams*: timelike past infinity i^-, timelike future infinity i^+, spacelike infinity i^0, past and future null infinity $\mathscr{I}^\mp$.)

Figure 1.1 shows an example of the past and future of a compact subset of Minkowski spacetime.

If it is necessary to emphasise a specific (sub)poset of events S over which an interval or past/future subset is determined, let us write $J^{\mp}[S](x)$.

The partial ordering on a *spacetime manifold* — an oriented, time-oriented Lorentzian manifold [107] — is determined by its time-orientation and its metric, where I use the signature $(+,-,-,\dots)$ throughout this thesis.

Definition 1.2.7 (after [107])**.** Let (M, g, u) be a spacetime manifold with metric g and a smooth vector field such that $\forall x \in M : g(u_x, u_x) > 0$ (time orientation). Let $I \subset \mathbb{R}$ be an open interval. Any tangent vector $X \in TM \setminus \{0\}$ is called

$$\textbf{timelike} \text{ or } \textbf{chronological} \text{ if} \qquad g(X,X) > 0, \tag{1.10a}$$

$$\textbf{null} \text{ or } \textbf{lightlike} \text{ if} \qquad g(X,X) = 0, \tag{1.10b}$$

$$\textbf{causal} \text{ if} \qquad g(X,X) \geq 0, \tag{1.10c}$$

$$\textbf{spacelike} \text{ if} \qquad g(X,X) < 0. \tag{1.10d}$$

A differentiable curve $\gamma : I \to M$ is called **timelike**, **null** or **lightlike**, **causal**, or **spacelike** if all tangent vectors $\dot{\gamma}(\tau)$ along the curve $\tau \in I$ have the respective property. A causal curve $\gamma : I \to M$ is called **past-directed** if $\forall \tau \in I : g\Big(u_{\gamma(\tau)}, \dot{\gamma}(\tau)\Big) < 0$ and **future-directed** if $\forall \tau \in I : g\Big(u_{\gamma(\tau)}, \dot{\gamma}(\tau)\Big) > 0$. A future-directed curve γ is **inextendible** if it does not approach a limit as the parameter $\tau \in I$ reaches the infimum and supremum of I.

A **timelike or spacelike geodesic** is a future-directed, timelike curve or a spacelike curve γ such that its length

$$L[\gamma] := \int_I \sqrt{\Big|g\Big(\dot{\gamma}(\tau), \dot{\gamma}(\tau)\Big)\Big|}\, \mathrm{d}\tau \tag{1.11}$$

is maximal or critical, respectively.

Definition 1.2.8. Let M be a spacetime manifold. I refer to an element $x \in M$ as **event**. Two events $x, y \in M$ are **causally ordered** $x \preceq y$ if there exists a future-directed, causal curve from x to y (or $x = y$), and they are **chronologically ordered** $x \ll y$ if there exists a future-directed, timelike curve from x to y. In this thesis, the spacetime is referred to as **causally ordered** if $(M, \preceq)$ is a poset. The partial ordering $\preceq$ is called the **causal relation**.

In context of the causal hierarchy (see Subsection 1.2.3), a causally ordered spacetime is usually just called a *causal* spacetime. In this thesis, however, I use the phrase *causally ordered* to make a distinction with causal sets.

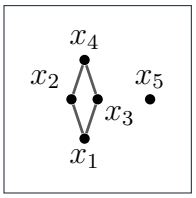

$$\left.\begin{array}{l} x_1 \prec * \, x_2 \\ x_2 \prec * \, x_4 \end{array}\right\} \Rightarrow x_1 \prec x_4$$

$$\left.\begin{array}{l} x_1 \prec * \, x_3 \\ x_3 \prec * \, x_4 \end{array}\right\} \Rightarrow x_1 \prec x_4$$

Figure 1.2: Hasse diagram of a causet with 5 events x_i ($i \in [1, 5]$) shown as vertices. One can read off the links from the edges of the graph (with the future directed towards the top of the page) and then determine the full causal structure using transitivity as shown on the right.

1.2.2 Causal Sets

One of the earliest references of causal set theory is by Bombelli, Lee, Meyer, and Sorkin [16] and a more recent review of the research area can be found in Surya [104]. Here, I review some of the common terms and notations.

Definition 1.2.9. A **causal set (causet)** is a partially ordered set $(C, \preceq)$ that is *locally finite*, i.e. the cardinality of every interval is finite,

$$\forall x, y \in C : \qquad \Big|[x, y]\Big| < \infty. \tag{1.12}$$

Similar to the spacetime manifolds, an **event** is an element of the causet and the **causal relation** is the partial ordering $\preceq$.

Definition 1.2.10. An event of a causet $(C, \preceq)$, $x \in C$, is **linked to** another event $y \in C$ when $[x, y] = \{x, y\}$ and $x \neq y$. In these circumstances, I write $x \prec * \, y$.

A causet is graphically represented by a *Hasse diagram* where the events are shown as vertices and the links as edges pointing up the page, see Figure 1.2 for an example. Let us use *linked chains* to define the causet analogue to (future-directed) causal curves.

Definition 1.2.11. Let $(C, \preceq)$ be a causet. A **path** is a chain $P \subseteq C$ such that for all $x \in P$ with $J^+_*(x) \cap P \neq \emptyset$ there exists a unique event $y \in P : x \prec * \, y$. The **set of paths from** x **to** y in C is denoted by $\text{paths}(x, y)$. A path from x to y is **minimal** (resp., **maximal**) if it has minimal (resp., maximal) cardinality among the elements of $\text{paths}(x, y)$.

Given a causet $(C, \preceq)$, the set of paths from an event $x \in C$ to itself, for example, is simply the set of the singleton, $\text{paths}(x, x) = \{\{x\}\}$, and for any pair of linked events $x \prec * \, y \in C$, we have $\text{paths}(x, y) = \{\{x, y\}\}$. In general, paths are the analogues to causal curves on spacetimes and maximal paths correspond to timelike geodesics, see Myrheim [82], Brightwell and Gregory [19], and Bachmat [7].

Especially in numerical applications with finite causets, it is useful to label the events and write the causal structure in terms of matrices.

Definition 1.2.12. Let C be a causet. A **labelling** of C is an injective function $l : C \to \mathbb{Z}$. It is **order-preserving** if $\forall x, y \in C : x \prec y \Rightarrow l(x) < l(y)$.

An order-preserving labelling is also called *natural* in Sorkin [100], however, the word "natural" has many other meanings so that I refrain from this term here. For a finite causet with cardinality n, it is convenient to use an (order-preserving) labelling that maps to the interval $[1, n] \subset \mathbb{Z}$.

Definition 1.2.13. Let C be a finite causet with cardinality $|C| = n$. The **(past) causal matrix (chain matrix)** $\boldsymbol{C}$ is the $n \times n$ matrix with components

$$\boldsymbol{C}^x{}_y := \begin{cases} 1 & y \prec x, \\ 0 & \text{otherwise.} \end{cases} \tag{1.13}$$

The **(past) link matrix** $\boldsymbol{L}$ is the $n \times n$ matrix with components

$$\boldsymbol{L}^x{}_y := \begin{cases} 1 & y \prec\!* \, x, \\ 0 & \text{otherwise.} \end{cases} \tag{1.14}$$

Given a finite causet C with cardinality n, we may use an order-preserving labelling $l : C \to [1, n] \subset \mathbb{Z}$ to index the matrices, then $\boldsymbol{C}$ and $\boldsymbol{L}$ are lower triangular with a vanishing diagonal.

1.2.3 Causal Hierarchy

In the following, we consider different properties of the causal structure of spacetimes and causets to see what they have in common and where they are distinct. More details of the causal hierarchy of spacetimes can be found in Minguzzi and Sánchez [67].

Recall from Definition 1.2.8 that on a spacetime manifold (M, g) we have the relation $\ll$ that is irreflexive in all the cases to be considered later on. A *totally vicious* spacetime manifold has a relation $\ll$ that is reflexive ($\forall x \in M : x \ll x$) and a spacetime is *not totally vicious* if

$$\exists x \in M : \qquad x \not\ll x. \tag{1.15}$$

All spacetimes with an irreflexive relation $\ll$,

$$\forall x, y \in M : \qquad x \ll y \Rightarrow x \neq y, \tag{1.16}$$

are called *chronologically ordered* (Minguzzi and Sánchez [67] only used the term "chronological"). Similarly, a spacetime is *causally ordered* if the (strict) causal

relation $\prec$ is irreflexive,

$$\forall x, y \in M : \qquad x \prec y \Rightarrow x \neq y. \tag{1.17}$$

The three conditions (1.15) (1.16) and (1.17) are not only fulfilled by the causal relation of the spacetime manifolds that are considered in this thesis, but also by the causal relation of all causets. For a causet, let the chronological relation $\ll$ be identical to the strict causal relation $\prec$ since only causal directions but not timelike or lightlike directions are defined. The fact that the spacetime manifolds considered in this thesis and causets in general are causally ordered has the physical interpretation of no closed causal curves (causal loops). Therefore, the anti-symmetry axiom (1.2) for the causal relation of spacetimes and causets is also known as the *axiom of acyclicity*. Since local finiteness is only a property of causets but not of spacetimes, I changed the common terms "chronological" and "causal" [67] to "chronologically ordered" and "causally ordered" to emphazise the differences between *causally ordered* spacetimes and *causal* sets.

For a spacetime M, the chronological relation induces sets of chronological past and future similarly to the strict causal pasts/futures given in Definition 1.2.6. For any event $x \in M$, let us denote these sets with $I^-(x)$ and $I^+(x)$. We say that a spacetime is *distinguishing* if $\forall x, y \in M : I^+(x) = I^+(y) \Rightarrow x = y$ and $\forall x, y \in M : I^-(x) = I^-(y) \Rightarrow x = y$. If we let the chronological ordering of a causet be given by its strict causal relation, we notice that it is not necessarily distinguishing. A simple example of a non-distinguishing causet is given in Figure 1.2, where events x_2 and x_3 both have the same strict past $\{x_1\}$ and future $\{x_4\}$.

The property of distinguishability is usually included in the causal hierarchy [67], see Figure 1.3. Here this property helps to emphasize some differences between spacetimes and causets. However, it is not necessary to define *global hyperbolicity*, see Bernal and Sánchez [14].

Definition 1.2.14. A causally ordered spacetime is **globally hyperbolic** if every closed causal interval in M is compact.

In the following, I consider only globally hyperbolic spacetimes and their discrete analogs. The compactness of closed causal intervals in a globally hyperbolic spacetime implies the local finiteness of causal intervals for its discrete counterparts.

There are other, equivalent definitions of global hyperbolicity for spacetime manifolds [14]. Most often, a globally hyperbolic spacetime manifold is defined as a spacetime that admits a *Cauchy surface*.

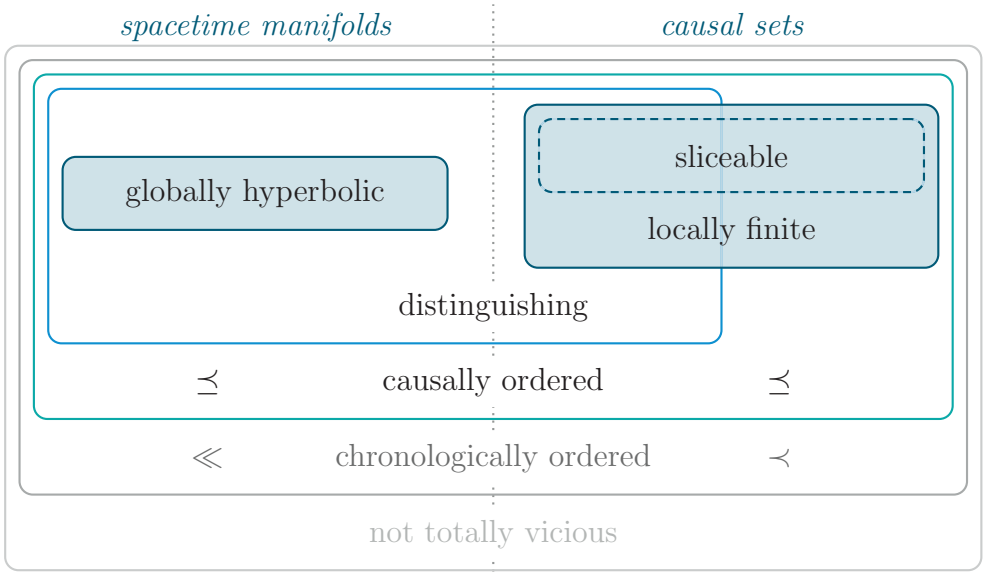

Figure 1.3: Illustration of the causal hierarchy with globally hyperbolic spacetimes and causal sets (shaded, dark blue) that are the main focus of this thesis. Sliceability (dashed) is an additional condition related to the causet equivalent of a Cauchy foliation that I introduce in Section 1.3. Note that causal sets are discrete models for globally hyperbolic spacetimes, but they may also model spacetime manifolds that are not globally hyperbolic.

Definition 1.2.15. Let M be a spacetime manifold. A **Cauchy (hyper)surface** is a submanifold $\Sigma \subset M$ such that every inextendible timelike curve in M intersects it exactly once.

Adapted from a general definition of manifold foliations in Lawson Jr [59], let us define the following.

Definition 1.2.16. Let M be a d-dimensional globally hyperbolic spacetime manifold. A **Cauchy foliation of** M is a partition into Cauchy surfaces, called **leaves**,

$$M = \bigcup_{\tau\in\mathbb{R}} \Sigma_\tau \qquad \big(\Sigma_\tau \cap \Sigma_{\tau'} = \emptyset \text{ if } \tau \neq \tau'\big), \tag{1.18}$$

where every event in M has a neighborhood $U \subset M$ and a system of local coordinates $x = (x^0, x^1, \ldots, x^{d-1}) : U \to \mathbb{R}^d$ such that for each leaf Σ_τ the time coordinate on $U \cap \Sigma_\tau$ is described by $x^0 = \tau$.

1.3 Characteristic Subsets of Causal Sets

Let us now focus on subsets of causets including the causet analogue of a Cauchy surface. First, we take a look at subsets that partition the past/future of a single causet event and the past/future of causet subsets. With this terminology, I discuss

some properties of antichains in causets in order to define the analogues of a Cauchy surface and a Cauchy foliation.

1.3.1 Layers, Steps and Ranks

The following conventions extend the notion of layers and ranks given in Dable-Heath, Fewster, Rejzner, and Woods [29] to subsets of events for some causet.

Definition 1.3.1. Let C be a causet and $k \in \mathbb{N}$. The **layer k past/future** of a point $x \in C$ is the set

$$L_k^-(x) := \left\{ y \in J^-(x) \;\middle|\; \left|[y,x]\right| - 1 = k \right\}, \tag{1.19a}$$

$$L_k^+(x) := \left\{ y \in J^+(x) \;\middle|\; \left|[x,y]\right| - 1 = k \right\}, \tag{1.19b}$$

respectively, as defined in Sorkin [101]. In extension, I define the layer k past/future of a subset $A \subseteq C$,

$$L_k^-(A) := \left\{ y \in J^-(A) \;\middle|\; \max_{x\in A}\left|[y,x]\right| - 1 = k \right\}, \tag{1.20a}$$

$$L_k^+(A) := \left\{ y \in J^+(A) \;\middle|\; \max_{x\in A}\left|[x,y]\right| - 1 = k \right\}, \tag{1.20b}$$

respectively. I denote the union of all layers from layer 0 to k by $L^\mp_{[0,k]}(x)$ and $L^\mp_{[0,k]}(A)$.
Following [29], the **k-layer past/future infinity** of C is the set

$$\mathcal{I}^\mp_{k\text{-layer}} := \left\{ x \in C \;\middle|\; \forall j \geq k : L_j^\mp(x) = \emptyset \right\}. \tag{1.21}$$

I call the 1-layer past/future infinity simply **past/future infinity** and write $\mathcal{I}^\mp := \mathcal{I}^\mp_{1\text{-layer}}$ for short.

Note that the past/future infinity of a causet C is equivalent to the set of events with empty strict past/future (the minimal/maximal events),

$$\mathcal{I}^\mp = \left\{ x \in C \;\middle|\; J_*^\mp(x) = \emptyset \right\}. \tag{1.22}$$

Definition 1.3.2. Let $(C, \preceq)$ be a causet and $k \in \mathbb{N}$. The **rank** of an event $y \in C$ relative to another event $x \in C$ is

$$\mathrm{rk}(y,x) := \begin{cases} \min\limits_{P\in\mathrm{paths}(x,y)} |P| - 1 & x \preceq y, \\ \infty & \text{otherwise.} \end{cases} \tag{1.23}$$

The **rank k past/future** of an event $x \in C$ is the set

$$R_k^-(x) := \left\{ y \in J^-(x) \;\middle|\; \mathrm{rk}(x,y) = k \right\}, \tag{1.24a}$$

$$R_k^+(x) := \left\{ y \in J^+(x) \;\middle|\; \mathrm{rk}(y,x) = k \right\}, \tag{1.24b}$$

respectively, as given in [29]. In extension, I define the rank k past and future of a subset $A \subseteq C$ is

$$R_k^-(A) := \left\{ y \in J^-(A) \;\middle|\; \max_{x \in A \cap J^+(y)} \mathrm{rk}(x,y) = k \right\}, \tag{1.25a}$$

$$R_k^+(A) := \left\{ y \in J^+(A) \;\middle|\; \max_{x \in A \cap J^-(y)} \mathrm{rk}(y,x) = k \right\}, \tag{1.25b}$$

respectively. I denote the union of all ranks from rank 0 to k by $R^{\mp}_{[0,k]}(x)$ and $R^{\mp}_{[0,k]}(A)$. The **k-rank past (or future) infinity** of C is the set

$$\mathcal{I}^{\mp}_{k\text{-rank}} := \left\{ x \in C \;\middle|\; \forall j \geq k : R_j^{\mp}(x) = \emptyset \right\}. \tag{1.26}$$

Since the layer numbers are determined by the cardinality of intervals, they heuristically encode information about the enclosed "volume". The rank numbers are determined by the cardinality of the minimal paths, thus they heuristically describe the length of paths that follow close to the lightcones in a spacetime embedding. There is a third, natural choice to partition the past/future of any causet event by using maximal paths, for which I define a *time step* function similar to the rank function.

Definition 1.3.3. Let $(C, \preceq)$ be a causet and $k \in \mathbb{N}$. The **(time) step** of an event $y \in C$ relative to another event $x \in C$ is

$$\mathrm{step}(y,x) := \begin{cases} \max\limits_{P \in \mathrm{paths}(x,y)} |P| - 1 & x \preceq y, \\ \infty & \text{otherwise.} \end{cases} \tag{1.27}$$

I define the **step k past/future** $S_k^{\mp}$ of an event $x \in C$ and a subset $A \subseteq C$ as well as the **k-step past/future infinity** $\mathcal{I}^{\mp}_{k\text{-step}}$ just as in Definition 1.3.2, replacing the function $\mathrm{rk}(y,x)$ by $\mathrm{step}(y,x)$.

For any causet C, the layer, rank, and step 0 past/future of an event $x \in C$ are the singleton $\{x\}$ and the layer, rank and step 1 past/future of x are equally given by all events that are linked to x in the past/future, but for $k \geq 2$ the layer, rank and step k pasts/futures are not necessarily identical. Examples of the past layers, ranks and steps are given in Figure 1.4, where I placed the example for the past steps between the layers (a) and ranks (c) in anticipation of the following

proposition. Note that the labels by the layer numbers in Figure 1.4a skip number 3, because there is no closed interval with cardinality 4 ending at the event labelled with 0. The ranks in Figure 1.4c are not arranged chronologically, because even very short minimal paths can reach far into the past of an event. The step partition in Figure 1.4b yields chronological increasing labels without skipping numbers. We also see that the largest layer number is greater than the largest step number that is in turn greater than the largest rank number. This brings me to the following statement.

Proposition 1.3.4. *Let C be a causet and $x \in C$ be any event. The unions of past/future partitions into layers, steps and ranks are related such that for any $k \in \mathbb{N}$:*

$$L^{\mp}_{[0,k]}(x) \subseteq S^{\mp}_{[0,k]}(x) \subseteq R^{\mp}_{[0,k]}(x). \tag{1.28}$$

Proof. Note that for any $y \preceq x \in C$, the cardinality (length) of the shortest path from y to x is less or equal to the length of the longest path from y to x, which is in turn less than or equal to $\big|[y,x]\big|$. So

$$\forall m \in [0,k] \subset \mathbb{N} : \forall y \in L^{-}_{m}(x) : \qquad y \in L^{-}_{[0,m]}(x) \Rightarrow y \in S^{-}_{[0,m]}(x), \tag{1.29a}$$

$$\forall n \in [0,k] \subset \mathbb{N} : \forall y \in S^{-}_{n}(x) : \qquad y \in S^{-}_{[0,n]}(x) \Rightarrow y \in R^{-}_{[0,n]}(x). \tag{1.29b}$$

In summary, $L^{-}_{[0,m]}(x) \subseteq S^{-}_{[0,m]}(x) \subseteq R^{-}_{[0,m]}(x)$, which is valid for any causet and thus also for the opposite causet. Since the relation of the opposite causet is reversed, the sequence holds for the future of any event $x \in C$ as well, $L^{+}_{[0,k]}(x) \subseteq S^{+}_{[0,k]}(x) \subseteq R^{+}_{[0,k]}(x)$. □

A similar statement also holds for the k-layer, -step, and -rank past/future infinities, for which one part is shown in [29, Lemma II.8].

The partitioning of past/future of any causet event into layers or ranks plays

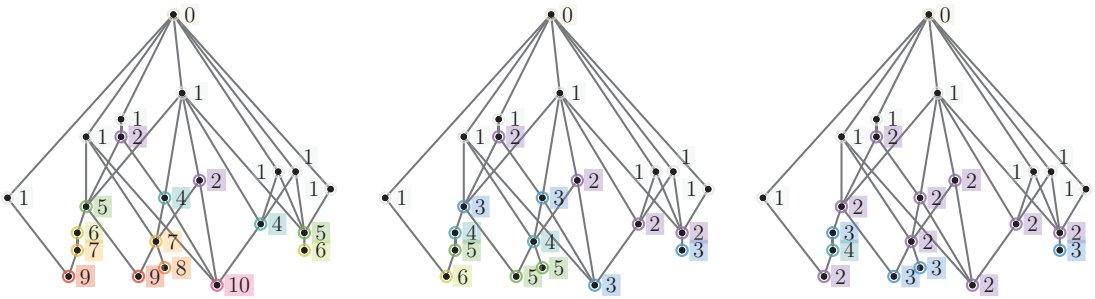

(a) Past layers (b) Past steps (c) Past ranks

Figure 1.4: Causet with an event labelled by 0 and past partitions labelled by 3 different methods.

an important role in the definition of discretized wave operators on causal sets. These discretizations typically involve a weighted sum taken over field values with weights determined by the layer or rank relative to the point where the operator is evaluated. For example, the discretizations studied in Sorkin [101], Benincasa and Dowker [11], Dowker and Glaser [35], Glaser [43], and Aslanbeigi, Saravani, and Sorkin [6] take a different number of layers into account depending on the spacetime dimension that is described by the causal set. The spacetime dimension is not a pre-defined property of a causet, but has to be estimated by the Myrheim-Meyer estimator [82, 65] or other approximations, see Reid [93], and Roy, Sinha, and Surya [97]. A more recent alternative approach given in Dable-Heath, Fewster, Rejzner, and Woods [29] proposes a discretization scheme for the wave operators that, while taking its inspiration from a discrete lattice in $1+1$ dimensions, has the potential to generalize to any dimension. Although this approach may not need the approximated spacetime dimension as an input, it does require the supplementation by a *preferred past structure* as discussed in Chapter 2. One part of my research projects was to investigate ways in which a preferred past may be associated intrinsically to a causal set and to evaluate their performance on sprinkled causets in Minkowski spacetime. We will come to this in Chapter 3.

1.3.2 Antichain Properties

As mentioned in Subsection 1.2.3, globally hyperbolic spacetimes admit Cauchy surfaces. Let us construct a similar notion for any causet from antichains.

Definition 1.3.5. Let $(C, \preceq)$ be a causet. An antichain $A \subseteq C$ is **maximal** (or *inextendible* [64]) if any event $x \in C$ is either an element of A or causally related to A, so that

$$J^-(A) \cup J^+(A) = C. \tag{1.30}$$

Let me give some rather obvious examples for finite causets.

Proposition 1.3.6. *The past and future infinities of a finite causet are maximal antichains.*

Proof. From Definition 1.3.1, recall that the events without any past layer in a *finite* causet C are in the past infinity $\mathcal{I}^-$. This is equal to the set of events with an empty strict past, see (1.22), which in turn means that every other causet event has a non-empty strict past. For any event x with a non-empty strict past there exists some event $y_1 \prec x$ that has an empty strict past or there exists another event $y_2 \prec y_1$ and so on. This process repeats until it terminates since the

causet is finite, so there exists some $k \in \mathbb{N}$ such that $y_k \in \mathcal{I}^-$ and $x \succ y_k$ due to transitivity. Therefore, the past infinity is a maximal antichain and $J^+(\mathcal{I}^-) = C$.

Because the argument applies to all *finite* causets, it also holds for any finite, opposite causet, and so also for the future infinity. □

It might seem that a maximal antichain is already a sufficient analogue for a Cauchy surface. However, there are further properties of Cauchy surfaces that are not necessarily fulfilled by maximal antichains in an analogous way.

Definition 1.3.7. A subset N of a globally hyperbolic spacetime manifold is **past/future-compact** if

$$\forall x \in N : J^{\mp}(x) \cap N \text{ is compact.} \tag{1.31}$$

A Cauchy surface Σ splits a globally hyperbolic spacetime into a past-compact subset $J^+(\Sigma)$ and a future-compact subset $J^-(\Sigma)$. The corresponding notion for causets is given by:

Definition 1.3.8. A subset S of a causet is **past/future-finite** if

$$\forall x \in S : J^{\mp}(x) \cap S \text{ is finite.} \tag{1.32}$$

Figure 1.5a shows a causet $(C, \preceq)$ that is not past but future-finite. Every element has a finite past and future, except for event z with an infinite past. The past infinity is

$$\mathcal{I}^- = C \setminus \{z\}, \tag{1.33}$$

which is an antichain and it is maximal, since $J^+(\mathcal{I}^-) = C$. However, it should

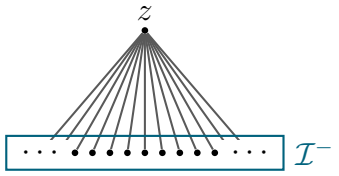

(a) Causet that is not past-finite ...

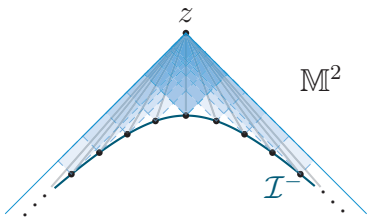

(b) ... and an embedding in 2-dimensional Minkowski spacetime

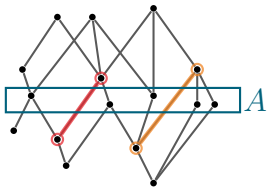

(c) Paths that do not intersect the antichain A

Figure 1.5: (a) An example of a causet that is not past-finite, because the event z has an infinite past (represented by dots to the left and right). The past of z coincides with the past infinity $\mathcal{I}^-$ in this example. (b) The same causet embedded in 2-dimensional Minkowski spacetime such that the spacetime interval between each event and z has the same volume (indicated by light shaded rectangles with a dashed outline, blue). Here the events of $\mathcal{I}^-$ fall on a hyperboloid (dark blue). (c) A causet with a maximal antichain A of 5 events crossed by 2 paths (thicker lines, red and orange) not intersecting A.

not be considered as an analogue of a Cauchy surface, since the future of the antichain $\mathcal{I}^-$ is not past-finite. To get a physical interpretation of this, notice that the antichain is also the layer 1 past of z and imagine the causet being embedded in $(1+1)$-dimensional Minkowski spacetime. When the events are embedded such that each spacetime interval from any event in $\mathcal{I}^-$ and the event z (i.e., each link) has equal spacetime volume and each event in $\mathcal{I}^-$ has distinct coordinates, then all events of $\mathcal{I}^-$ fall on a hyperboloid. We may distribute them uniformly along the hyperboloid as shown in Figure 1.5b. This hyperboloid (solid curve, dark blue) is not a Cauchy surface of Minkowski spacetime. So, let me make the following definition.

Definition 1.3.9. Let C be a causet. A **Cauchy antichain** is a maximal antichain $A \subseteq C$ such that its past $J^-(A)$ is future-finite and its future $J^+(A)$ is past-finite.

In the example of Figure 1.5a, only the maximal antichain $\{z\}$ is a Cauchy antichain.

As given in Definition 1.2.15, a Cauchy surface in a globally hyperbolic spacetime intersects any inextendible, future-directed timelike curve exactly once. However, this is not necessarily a property of a Cauchy antichain as demonstrated with an example in Figure 1.5c. The antichain A is Cauchy but there exist two paths (red and orange) that each connect an event in the past of A with an event in the future of A. These paths can be extended towards the past and future infinities to span some inextendible paths through the causet, but they do not intersect A. Because of the discreteness of causets, we cannot find an additional antichain property to ensure that the Cauchy antichain intersects any inextendible path. This phenomenon was also mentioned in Major, Rideout, and Surya [64].

There is one more property of Cauchy surfaces in globally hyperbolic spacetimes that will be important for the discussion of classical (and quantum) fields. A solution to normally hyperbolic field equations, e.g. the Klein-Gordon field equation, is fully determined over the entire spacetime by initial field data on a Cauchy surface. For the discrete setting, we will see in Section 2.3 that a Cauchy antichain is not sufficient to hold enough data for the discretized field equation to determine the solution over the entire causet. So it is necessary to specify a "thickening" method to add more layers to a Cauchy antichain and obtain Cauchy slices.

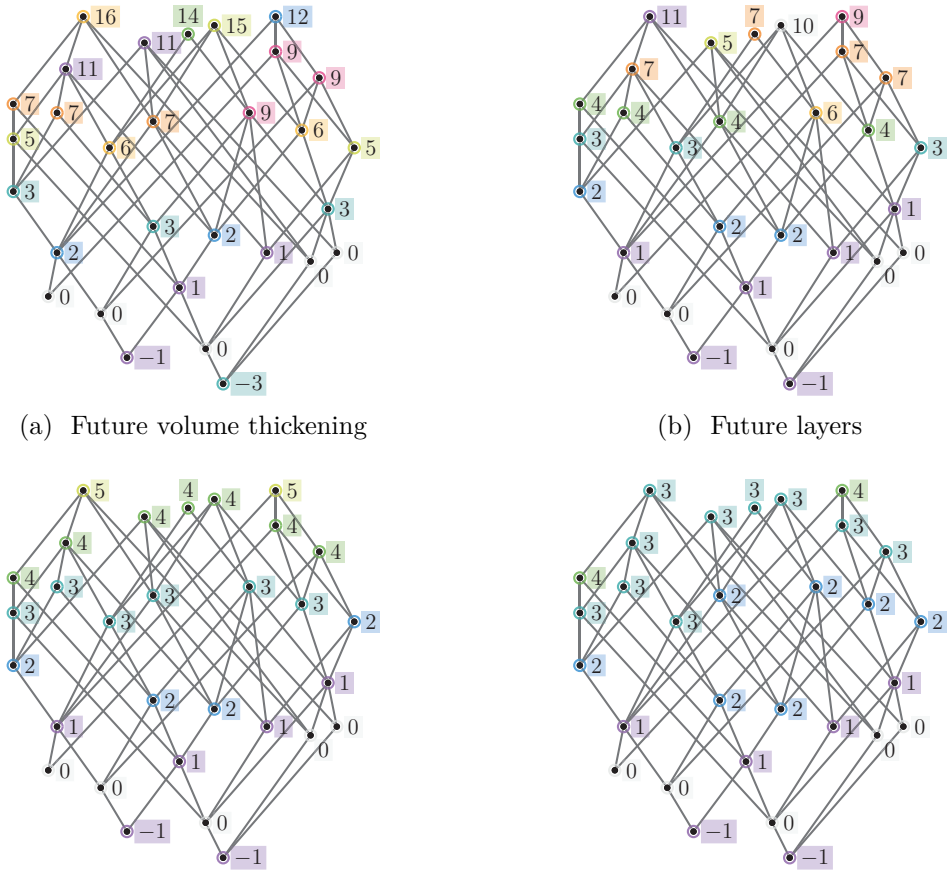

(a) Future volume thickening

(b) Future layers

(c) Future steps

(d) Future ranks

Figure 1.6: Future partitions of a Cauchy antichain (labelled by 0's) using four different methods on the same causet example.

1.3.3 Cauchy Slices

A definition for thickened antichains is given in Major, Rideout, and Surya [64].

Definition 1.3.10. Let A be an antichain in a causet and $k \in \mathbb{N}$. The **k-th past/future volume thickening** of an antichain A is the set

$$T_k^{\mp}(A) = \left\{ x \in J^{\mp}(A) \;\middle|\; \left| J_*^{\pm}(x) \setminus J_*^{\pm}(A) \right| \leq k \right\}. \tag{1.34}$$

An antichain A in a causet may also be "thickened" using any of the three methods defined in Subsection 1.3.1. For any $k \in \mathbb{N}$, the union of layers $L_{[0,k]}^{\mp}(A)$, steps $S_{[0,k]}^{\mp}(A)$ and ranks $R_{[0,k]}^{\mp}(A)$ are subsets of the past/future of the antichain A, respectively. Similarly to Proposition 1.3.4, for any $k \in \mathbb{N}$, we have

$$T_k^{\mp}(A) \subseteq L_{[0,k]}^{\mp}(A) \subseteq S_{[0,k]}^{\mp}(A) \subseteq R_{[0,k]}^{\mp}(A), \tag{1.35}$$

for example, see Figure 1.6. In [29], the *(future/past)* $(k+1)$*-layer Cauchy slice* is defined as the $(k+1)$-layer past/future infinity of the subcauset $J^{\pm}(A)$, which is $L_{[0,k]}^{\mp}(A)$ as I show in the following.

Proposition 1.3.11. *Let C be a causet. For any $k \in \mathbb{N}$, the union of past/future layers of a subset $A \subseteq C$ from the 0-th layer to the k-th layer is equivalently given by the $(k+1)$-layer future/past infinity of the subcauset $J^{\mp}(A)$,*

$$L^{\mp}_{[0,k]}(A) = \mathcal{I}^{\pm}_{(k+1)\text{-layer}}\Big[J^{\mp}(A)\Big]. \tag{1.36}$$

(Note that $\mathcal{I}^{\pm}_{(k+1)\text{-layer}}$ is taken over the subcauset in square brackets and not over the entire causet C.)

Proof. By definition, the set $L^{-}_{[0,k]}(A)$ is given as

$$\begin{aligned} L^{-}_{[0,k]}(A) &= \bigcup_{j=0}^{k} L^{-}_{j}(A) && \text{(1.37a)}\\ &= \Big\{ y \in J^{-}(A) \;\Big|\; \max_{x\in A}\Big|[y,x]\Big| - 1 \in [0,k] \subset \mathbb{N} \Big\} && \text{(1.37b)}\\ &= \Big\{ y \in J^{-}(A) \;\Big|\; \forall x \in A : 0 \leq \Big|[y,x]\Big| \leq k+1 \Big\}. && \text{(1.37c)} \end{aligned}$$

The cardinality of any such interval $[y,x]$ is between 0 and $k+1$ if the future j layer of y does not intersect the set $J^{-}(A)$ for any $j \geq k+1$. Recall that the future $(k+1)$ layer corresponds to an interval cardinality of $k+2$. Thus we have, equivalently

$$\begin{aligned} L^{-}_{[0,k]}(A) &= \Big\{ y \in J^{-}(A) \;\Big|\; \forall j \geq k+1 : L^{+}_{j}(y) \cap J^{-}(A) = \emptyset \Big\} && \text{(1.37d)}\\ &= \Big\{ y \in J^{-}(A) \;\Big|\; \forall j \geq k+1 : L^{+}_{j}\Big[J^{-}(A)\Big](y) = \emptyset \Big\} && \text{(1.37e)}\\ &= \mathcal{I}^{+}_{(k+1)\text{-layer}}\Big[J^{-}(A)\Big]. && \text{(1.37f)} \end{aligned}$$

To get the last lines, use the definition of $(k+1)$-layer future infinity (1.21) for the subcauset $J^{-}(A)$.

Since these arguments also hold for its opposite causet, the arguments also hold for the *future* (opposite signs and reversed intervals). □

Note that in particular $\mathcal{I}^{\pm}_{(k+1)\text{-layer}} \equiv \mathcal{I}^{\pm}_{(k+1)\text{-layer}}[C] = L^{\mp}_{[0,k]}(C)$ for any $k \in \mathbb{N}$, which could be empty sets for infinite causets. One might expect that $\mathcal{I}^{\pm}_{k\text{-layer}} = L^{\mp}_{[0,k-1]}(\mathcal{I}^{\pm})$ also for all $k > 0$, however, in an infinite causet C, the sets $\mathcal{I}^{\pm}$ might either be empty or do not necessarily correspond to the timelike and null future/ past infinities of a spacetime manifold, $i^{\pm}$ and $\mathscr{I}^{\pm}$, respectively.

Definition 1.3.12. Let A be a Cauchy antichain in a causet and $k \in \mathbb{N}_{*}$ (integers excluding zero). The **k-volume, k-layer, k-step past/future Cauchy slice S (of A)** are the sets $T^{\mp}_{k-1}(A)$, $L^{\mp}_{[0,k-1]}(A)$, $S^{\mp}_{[0,k-1]}(A)$, respectively.

I simply call it a k**-layer Cauchy slice** if

$$S = L^+_{[0,k-1]}\left(\mathcal{I}^-[S]\right) = L^-_{[0,k-1]}\left(\mathcal{I}^+[S]\right), \tag{1.38}$$

meaning it is a k-layer past and future Cauchy slice of its respective future and past infinity. Similarly, I define k-volume and k-step Cauchy slices.

I chose these definitions such that the 1-volume, 1-layer and 1-step Cauchy slices of a Cauchy antichain A are A itself. Notice that we cannot define a k-rank Cauchy slice in a similar way for any $k \in \mathbb{N}_*$, since the subset $R^{\mp}_{[0,k-1]}(A)$ for a given Cauchy antichain A is not necessarily convex. Looking at the example Figure 1.6d, the event labelled by 4 on the left has events with lower rank numbers not only in its past but also in its future. So the subset $R^+_{[0,3]}(A)$ is not convex.

The volume thickening of Cauchy antichains is convex, see Major, Rideout, and Surya [64]. Here we take a look at similar statements for the k-layer/step Cauchy slice of a Cauchy antichain.

Proposition 1.3.13. *Let A be a Cauchy antichain in a causet C. The k-layer past/future and k-step past/future Cauchy slice of A is convex for any $k \in \mathbb{N}_*$.*

Proof. Let S be the future k-layer Cauchy slice $L^+_{[0,k-1]}(A)$. If $k = 1$, then S is an (Cauchy) antichain — without a pair of related events — so that S is convex.

For $k > 1$, consider events $x \in A$, $z \in \mathcal{I}^+[S] \cap J^+(x)$, and $y \in [x, z]$ (as shown in Figure 1.7), where $\mathcal{I}^+[S]$ denotes the future infinity within the subcauset S (upper solid line, green). If $y = x$ or $y = z$, then $y \in S$; otherwise,

$$x \prec y \prec z \Rightarrow \left|[x, y]\right| < \left|[x, z]\right| \tag{1.39a}$$

$$\Rightarrow \exists j < k : y \in L^+_j(x), \tag{1.39b}$$

and more generally, $\forall x' \in J^-(y) \cap A$:

$$x' \prec y \prec z \Rightarrow \left|[x', y]\right| < \left|[x', z]\right| \leq k \tag{1.39c}$$

$$\Rightarrow \exists j' < k : y \in L^+_{j'}(x'). \tag{1.39d}$$

Because this is true for all y, $[x, z] \subseteq S$. It is also true for any x and z as in the assumptions, hence S is convex.

An analogous argument applies to the case of the k-step Cauchy slice, where the interval cardinalities have to be replaced by the length of the longest path (number of time steps) as formulated in Definition 1.3.3.

Both statements hold for any causet including its opposite causet so that they also hold for the k-layer/step *past* Cauchy slice of A. □

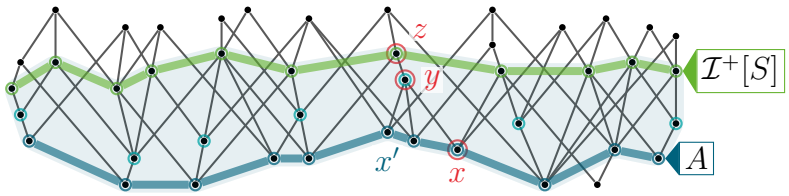

Figure 1.7: Example of a Cauchy antichain A (lower solid line across the causet, blue) and its 3-layer future Cauchy slice S (shaded, light blue). All paths connecting an event in the antichain A to an event in the slice's future infinity $\mathcal{I}^+[S]$ (upper solid line across the causet, green) are subsets of S.

The 3-layer future Cauchy slice S in Figure 1.7 is not a 3-layer past Cauchy slice, since $S' := L^-_{[0,2]}\big(\mathcal{I}^+[S]\big)$ is not identical to S. There is one event in the past of A that also lies in the layer 3 past of $\mathcal{I}^+[S]$. The subset S' that includes this event is a 3-layer (past and future) Cauchy slice.

With the definitions of Cauchy antichains and Cauchy slices, I now come to the definition of a *sliceable causet* (included in the causal hierarchy, see Figure 1.3).

Definition 1.3.14. Let C be a causet and let I be an interval of integers. A **slicing of** C is a sequence of Cauchy antichains $(A_k)_{k\in I}$ such that for all $k \in I$:

$$A_k \neq A_{k+1} \subset L^+_{[0,1]}(A_k) \tag{1.40}$$

and the sequence covers C, meaning that $\forall x \in C : \exists j \in I : x \in A_j$. The causet C is referred to as **slicable** if there exists a slicing of C.

Given a subset B of some causet, recall that $L^\pm_{[0,1]}(B) = S^\pm_{[0,1]}(B) = R^\pm_{[0,1]}(B)$, which give equivalent definitions of a slicing, and instead of using the future in (1.40), we could also use $A_{k-1} \subset L^-_{[0,1]}(A_k)$ as a slicing condition. If a causet is sliceable, its opposite is also sliceable.

Note that every finite causet is sliceable, since all of its maximal antichains are Cauchy. An example of a slicing for a finite causet is shown in Figure 1.8. However, sliceability is not guaranteed for infinite causets. A counter-example

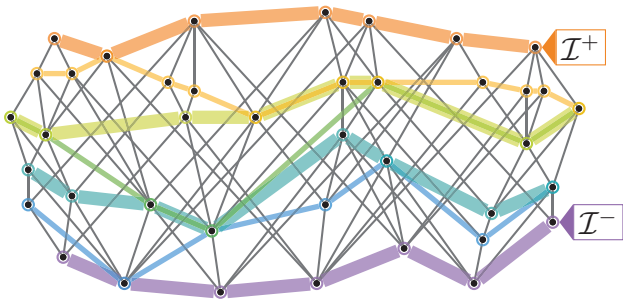

Figure 1.8: Example of a causet slicing. The sequence of seven Cauchy antichains (marked by semi-opaque lines with alternating thickness accross the causet) goes from the past infinity $\mathcal{I}^-$ to the future infinity $\mathcal{I}^+$.

to sliceable causets is shown in Figure 1.5a, which is a causet C that does have one Cauchy antichain $A = \{z\}$ but $L^-_{[0,1]}(A)$ does not contain a second Cauchy antichain that is different from A. The causet C cannot be covered by a sequence of Cauchy antichains and is hence not sliceable.

Before coming to discretization methods to find classical field equations on causal sets and the applications of Cauchy slices, let us review the kinematics of real scalar fields and observables, as well as discuss some aspects of scalar field dynamics on globally hyperbolic spacetimes.

Chapter 2

Classical Real Scalar Field Theory

In this chapter, I introduce the spaces of field configurations as well as off- and on-shell observables for the classical real scalar field theory. I assume from now on that any given spacetime manifold is globally hyperbolic and consider causets as their discrete analogues.

2.1 Field Kinematics

Physically measurable quantities are functions of fields, either on a (globally hyperbolic) spacetime manifold or a causal set. In this section, we review the kinematical structure of fields from the algebraic perspective. In the kinematic setting, there are no field equations constraining the space of fields, so the fields do not have a "dynamical behaviour" yet and they are referred to as *off-shell* field configurations. The main focus here lies on the classical real scalar field [12, 29].

2.1.1 Field Configurations and Off-Shell Observables

Definition 2.1.1. Let M be a spacetime manifold. The **space of real scalar field configurations** $\mathcal{E}(M)$ is the space of smooth functions,

$$\mathcal{E}(M) := \mathrm{C}^\infty(M, \mathbb{R}). \tag{2.1}$$

For a causet C, the configuration space is given by all functions

$$\mathcal{E}(C) := \{f : C \to \mathbb{R}\}, \tag{2.2}$$

since a causet does not have a smooth structure.

Given a finite causet C with cardinality $N = |C|$, notice that with a labelling (as defined in Definition 1.2.12) we can identify the configuration space with the N-dimensional Euclidean space $\mathcal{E}(C) \cong \mathbb{R}^N$. A field configuration can be represented by an N-dimensional real vector.

Let me set out some terms and notation that are commonly used for spacetimes [12] and here also adapted to causets.

Definition 2.1.2. Let $\mathcal{X}$ be a spacetime/causet. The **support of a function** $f \in \mathcal{E}(\mathcal{X})$ is the set

$$\operatorname{supp}(f) := \{x \in \mathcal{X} \mid f(x) \neq 0\}\,. \tag{2.3}$$

A function f has **spatial-compact/finite support** on $\mathcal{X}$ if there exists a compact/finite subset $K \subset \mathcal{X}$ such that

$$\operatorname{supp}(f) \subseteq J^+[\mathcal{X}](K) \cup J^-[\mathcal{X}](K), \tag{2.4}$$

and a function f has **past- or future-compact/finite support** if its support is past- or future-compact/finite, respectively, see Definition 1.3.7 and Definition 1.3.8.

I denote the corresponding configuration subspaces as:

$$\text{spatial-compact/finite :} \qquad \mathcal{E}_{\mathrm{s}}(\mathcal{X}) \subseteq \mathcal{E}(\mathcal{X}), \tag{2.5a}$$

$$\text{past-compact/finite :} \qquad \mathcal{E}_{\mathrm{p}}(\mathcal{X}) \subseteq \mathcal{E}(\mathcal{X}), \tag{2.5b}$$

$$\text{future-compact/finite :} \qquad \mathcal{E}_{\mathrm{f}}(\mathcal{X}) \subseteq \mathcal{E}(\mathcal{X}), \tag{2.5c}$$

$$\text{timelike-compact/finite :} \qquad \mathcal{E}_{\mathrm{t}}(\mathcal{X}) := \mathcal{E}_{\mathrm{p}}(\mathcal{X}) \cap \mathcal{E}_{\mathrm{f}}(\mathcal{X}). \tag{2.5d}$$

The space of configurations with compact support on a spacetime manifold M is written as $\mathcal{D}(M) := \mathrm{C}^\infty_{\mathrm{c}}(M, \mathbb{R})$ and the space of finitely supported functions on a causet C as $\mathcal{D}(C) := \Big\{ f \in \mathcal{E}(C) \;\Big|\; \big|\operatorname{supp}(f)\big| < \infty \Big\}$.

Figure 2.1 shows 2 examples of function supports that are (a) past compact and (b) future compact on Minkowski spacetime.

Note that on any finite causet C, $\mathcal{D}(C) = \mathcal{E}(C)$.

Definition 2.1.3. Let $\mathcal{X}$ be a spacetime manifold or a causet. The **algebra of observables** is the space of smooth, complex-valued functionals on the configuration space $\mathcal{E}(\mathcal{X})$,

$$\mathcal{F}(\mathcal{X}) := \mathrm{C}^\infty\Big(\mathcal{E}(\mathcal{X}), \mathbb{C}\Big) \tag{2.6}$$

equipped with point-wise addition and multiplication. Let us denote the space of **linear observables** as $\mathcal{F}_{\mathrm{lin}}(\mathcal{X}) \subset \mathcal{F}(\mathcal{X})$.

The notion of smoothness is straightforward in the case of a finite causet where the configuration space is isomorphic to $\mathbb{R}^N$. For arbitrary configuration spaces, in general, one has to use the Fréchet topology and Michal-Bastiani differentiability [66, 10, 83]. In the next two paragraphs, I review some of these notions only briefly as they are not necessary for the main focus on finite causets further below. For

more details, see Brouder, Dang, Laurent-Gengoux, and Rejzner [22].

Let $\mathcal{U} \subset \mathcal{E}(\mathcal{X})$ be an open subset in the Fréchet topology on $\mathcal{E}(\mathcal{X})$. A functional F has a *Gâteaux differential* at a point $\varphi \in U$ if the limit

$$\left\langle F^{(1)}(\varphi), \psi \right\rangle := \lim_{r \to 0} \frac{F(\varphi + r\psi) - F(\varphi)}{r} \tag{2.7}$$

exists for all directions $\psi \in \mathcal{E}(\mathcal{X})$. The observable is *Bastiani differentiable* on $\mathcal{U}$ if it has a Gâteaux differential for all $\varphi \in \mathcal{U}$ and $F^{(1)} : \mathcal{U} \times \mathcal{E}(\mathcal{X})$ with $\varphi \times \psi \mapsto F^{(1)}(\varphi)(\psi)$ is continuous on $\mathcal{U} \times \mathcal{E}(\mathcal{X})$. In [22], the k-th Bastiani derivative in directions $\psi_i \in \mathcal{E}(\mathcal{X})$ for $i \in [1, k] \subset \mathbb{N}$ is defined similarly, and I write

$$\left\langle F^{(k)}(\varphi), \bigotimes_{i=1}^{k} \psi_i \right\rangle := \left(\frac{\partial}{\partial r_1} \cdots \frac{\partial}{\partial r_k} F\left(\varphi + \sum_{i=1}^{k} r_i \psi_i \right) \right) \Bigg|_{r_1, \ldots, r_k = 0} . \tag{2.8}$$

The functional is *smooth* at $\varphi \in \mathcal{U}$ if the derivative $F^{(k)}(\varphi)$ exists for all $k \in \mathbb{N}$ and all $\psi_i \in \mathcal{E}(\mathcal{X})$. Observables are those functionals that are smooth at all points $\varphi \in \mathcal{E}(\mathcal{X})$, denoted by $F \in \mathcal{F}(\mathcal{X})$.

Given an observable $F \in \mathcal{F}(\mathcal{X})$, notice that (2.7) implies $F^{(1)}(\varphi) \in \mathcal{F}_{\text{lin}}(\mathcal{X})$. So the first derivative of a real-valued (or complex-valued) observable F at a point $\varphi \in \mathcal{E}(\mathcal{X})$ is an element of the (complexified) dual configuration space $F^{(1)}(\varphi) \in (\mathcal{E}^*)^{(\mathbb{C})}(\mathcal{X})$ — the space of compactly supported distributions. For the space of compactly supported functions $\mathcal{D}(M)$ on a spacetime manifold (M, g), the topology is locally convex, but not Fréchet, see Treves [105], and Rudin [98]. I denote the dual space to compactly/finitely supported functions by $\mathcal{D}^*(\mathcal{X})$.

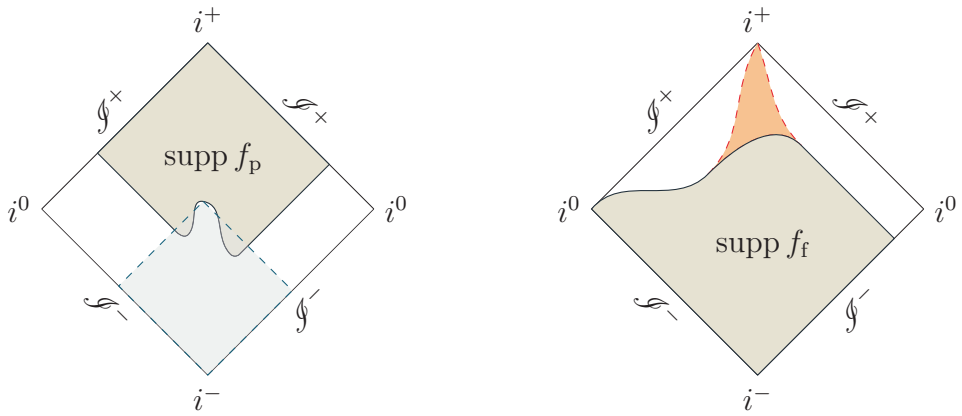

(a) Function f_p with past compact support.

(b) Function f_f with future compact support.

Figure 2.1: Penrose diagrams of Minkowski spacetime $\mathbb{M}$ showing (a) a function with past compact support $f_\text{p} \in \mathcal{E}_\text{p}(\mathbb{M})$ and (b) the future compact support of a function $f_\text{f} \in \mathcal{E}_\text{f}(\mathbb{M})$. In (a), past compactness of f_p is demonstrated for some point $x \in \operatorname{supp} f_\text{p}$ with a past $J^-(x)$ (dashed region) intersecting the support in two disjoint, compact subsets. A future compact support (b) may extend to spacelike infinity i^0 but not to the timelike future infinity i^+ (dashed region).

For example, let $\mathcal{X} = C$ be a finite causet with cardinality $|C| = N$ and let $\langle \cdot, \cdot \rangle$ be the complex extension of a pairing of elements of $\mathcal{E}(C)$. Any linear observable $\Phi_f \in \mathcal{F}_{\text{lin}}(C)$ is then represented by an element $f \in \mathcal{E}^{\mathbb{C}}(C)$ such that $\forall \varphi \in \mathcal{E}(C)$:

$$\Phi_f(\varphi) = \langle f, \varphi \rangle \, . \tag{2.9}$$

As mentioned in [29], there is a natural choice of a pairing so that $\Phi_f(\varphi) = f^{\mathsf{T}}\varphi$ with $\varphi \in \mathbb{R}^N$ and the transpose of $f \in \mathbb{C}^N$. The pairing in equation (2.9), however, is not fixed to a specific choice. For an infinite causet, the linear observable Φ_f may still be represented by some function f, but f must have finite support for the expression (2.9) to be finite, $f \in \mathcal{D}^{\mathbb{C}}(C)$.

Similarly, let us consider a globally hyperbolic spacetime $\mathcal{X} = M$ with a metric and a measure ϱ corresponding to some pairing $\langle \cdot, \cdot \rangle$ between elements of $\mathcal{E}(M)$ and $\mathcal{D}(M)$. Any linear observable $\Phi_f \in \mathcal{F}_{\text{lin}}(M)$ is analogously determined by a compactly supported function $f \in \mathcal{D}^{\mathbb{C}}(M)$ and the measure ϱ such that $\forall \varphi \in \mathcal{E}(M)$:

$$\Phi_f(\varphi) = \int_M f(x)\varphi(x)\varrho(x). \tag{2.10}$$

A natural choice for ϱ (and hence for the pairing) is the metric induced volume form dvol_M. When approximating a spacetime manifold by causets, the relations (2.9) and (2.10) (among other things) have to coincide in the limit of a causet sequence that gets increasingly denser in the approximated manifold [29].

In the following, let us turn the algebra of observables into an involutive algebra.

Definition 2.1.4 (see [33])**.** A ***-algebra** is an algebra $(\mathcal{A}, +, \cdot)$ over the field $\mathbb{C}$ that has an involution * i.e., a map $\mathcal{A} \to \mathcal{A}$ such that $\forall A, B \in \mathcal{A}, \forall c \in \mathbb{C}$:

$$\text{involutivity :} \qquad (A^*)^* = A, \tag{2.11}$$

$$\text{anti-linearity :} \qquad (cA)^* = \bar{c}A^*, \tag{2.12}$$

$$+ \text{ distributivity :} \qquad (A + B)^* = A^* + B^*, \tag{2.13}$$

$$\cdot \text{ anti-distributivity :} \qquad (A \cdot B)^* = B^* \cdot A^* \tag{2.14}$$

With the point-wise product of observables on a spacetime/causet $\mathcal{X}$ and the involution given by point-wise complex conjugation,

$$\forall \varphi \in \mathcal{E}(\mathcal{X}) : \qquad F^*(\varphi) := \overline{F(\varphi)}, \tag{2.15}$$

the algebra $\mathcal{F}(\mathcal{X})$ forms a *-algebra. Linear observables do not form a subalgebra. However, there are *-subalgebras constructed from *local* observables.

2.1.2 Local and Regular Observables

Before defining a notion of *locality* for observables on a spacetime manifold, first let us consider the case of a causet, where the notion is rather obvious.

Definition 2.1.5 (see [29])**.** Let C be a causet. An observable $F \in \mathcal{F}(C)$ is called **local** if its first derivative at $\varphi \in \mathcal{E}(C)$, $F^{(1)}(\varphi)$, evaluated at a point $x \in C$ only depends on x and the value of the field $\varphi(x)$. The space of local observables is denoted by $\mathcal{F}_{\mathrm{loc}}(C) \subset \mathcal{F}(C)$.

All linear observables on a causet C are local observables, $\mathcal{F}_{\mathrm{lin}}(C) \subset \mathcal{F}_{\mathrm{loc}}(C)$, since the first derivative of a linear observable corresponds to a constant element of $\mathcal{D}^{\mathbb{C}}(C)$. More generally, we have the algebra of *polynomial observables* $\mathcal{F}_{\mathrm{pol}}(C) \subset \mathcal{F}_{\mathrm{loc}}(C)$ that is generated by observables of the type

$$\Phi_f^{(k)}(\varphi) = \left\langle f, \varphi^k \right\rangle, \tag{2.16}$$

where the k-th power is an element-wise operation and $f \in \mathcal{D}^{\mathbb{C}}(C)$.

The analogous notion for a spacetime manifold is heuristically based on a "local coordinate free Taylor expansion" or in precise terms, the jet prolongation of a field configuration, as in the following.

Definition 2.1.6 (see [41])**.** Let M be a (globally hyperbolic) spacetime manifold and write $j_x^k(\varphi)$ for the k-th jet prolongation of $\varphi \in \mathcal{E}(M)$ at point $x \in M$. An observable $F \in \mathcal{F}(M)$ is **local** if there exists a density-valued function ρ on the jet bundle such that for all $\varphi_0 \in \mathcal{E}(M)$ there exists an open neighborhood $\mathcal{U}$ around φ_0 and an integer k such that

$$\forall \varphi \in \mathcal{U}: \qquad F(\varphi) = \int_M \rho\left(j_x^k(\varphi)\right). \tag{2.17}$$

The space of local observables is denoted by $\mathcal{F}_{\mathrm{loc}}(M) \subset \mathcal{F}(M)$.

On a spacetime manifold M, the space of local observables $\mathcal{F}_{\mathrm{loc}}(M)$ is not closed under the point-wise product. Its algebraic closure is called the space of *multilocal observables* $\mathcal{F}_{\mathrm{mloc}}(M)$, see Fredenhagen and Rejzner [41].

For a causet C, note that the algebra generated by linear observables $\mathcal{F}_{\mathrm{lin}}(C)$ under the point-wise product and involution (2.15) is a *-algebra. These are the *regular* observables denoted by $\mathcal{F}_{\mathrm{reg}}(C)$ [29], since they are analogous to non-singular observables on a spacetime manifold M.

Definition 2.1.7 (see also [94])**.** An observable $F \in \mathcal{F}(M)$ is **regular** if for all $\varphi \in \mathcal{E}(M)$ all derivatives $F^{(k)}(\varphi)$ are smooth ($\forall k \in \mathbb{N}$). Let us write $\mathcal{F}_{\mathrm{reg}}(M)$ for the space of regular observables.

2.2 Field Dynamics on Spacetimes

Let us now consider a scalar bosonic field described by the Klein-Gordon field equation. This section is only about (globally hyperbolic) spacetime manifolds so that I simply write $\mathcal{E}$ and $\mathcal{F}$ to denote the configuration space and space of observables, respectively. The content is a review of textbook chapters by Bär [8], and Benini and Dappiaggi [12], where I change the notation to be consistent with this thesis. I put emphasis on the short exact sequence of *Green hyperbolic operators* (as defined below) since it will be used in the derivation of the on-shell algebras of observables in Section 2.4. In Section 2.4, I will show that this sequence does not hold for causets in general and it will be necessary to find an alternative argument for causets that is still motivated by the discussion in this section.

Let (M, g) be a d-dimensional spacetime manifold with scalar curvature R and covariant d'Alembert operator $\Box = g^{\mu\nu}\nabla_\mu\nabla_\nu$ (using the summation convention over $\mu, \nu \in [0, d-1] \subset \mathbb{N}$). The Klein-Gordon operator $P_{\mathrm{KG}} : \mathcal{E} \to \mathcal{E}$ determines the dynamics of a *free* scalar field with mass parameter m and curvature coupling ξ (both are strictly positive),

$$P_{\mathrm{KG}} := -\Big(\Box + m^2 + \xi R\Big). \tag{2.18}$$

The Klein-Gordon equation is

$$P_{\mathrm{KG}}\varphi = 0 \tag{2.19}$$

with the solution space (*on-shell* configurations) denoted by

$$\mathcal{S} := \ker(P_{\mathrm{KG}}). \tag{2.20}$$

More generally, one could consider a normally hyperbolic operator,

$$P_{\mathrm{nh}} := -\Big(\Box + v \cdot \nabla + s\Big) \tag{2.21}$$

with a smooth vector field v and a smooth function s. For the case of the free scalar field, $v = 0$ and $s = \xi R + m^2$. For an interacting theory like the φ^4 theory, for example, one may consider the field equation linearised around a given field solution φ so that the smooth function depends on φ (coupled with strength λ), $s = \frac{\lambda}{2}\varphi^2 + \xi R + m^2$. In general, field equations are determined by an action functional using the Euler-Lagrange formalism. Note that for an easier transition to quantum fields later on, it is recommended to use the generalized Lagrangian formalism, see Brunetti, Dütsch, and Fredenhagen [23], and Fredenhagen and Rejzner [42, Sec. 2.3.2]. However, in the following, let us turn our attention to linear field equations.

For any linear partial differential operator P, there exists a *formal adjoint* P^* such that for any two functions $f_1, f_2 \in \mathcal{E}$, where $\operatorname{supp}(f_1) \cap \operatorname{supp}(f_2)$ is compact,

$$\langle P^* f_1,\, f_2\rangle = \langle f_1,\, P f_2\rangle \tag{2.22a}$$

$$\int_M (P^* f_1) f_2 \varrho = \int_M f_1 (P f_2) \varrho. \tag{2.22b}$$

The existence of a formal adjoint follows from Stokes' theorem and the uniqueness is a consequence of the non-degenerate pairing $\langle \cdot, \cdot \rangle$ (corresponding to the measure ϱ) of configurations $\mathcal{E}$ and test functions $\mathcal{D}$. If $P^* = P$, then P is called *formally self-adjoint*. Note that the pairing $\langle \cdot, \cdot \rangle$ in (2.22) is for elements of the configuration space and should not be confused with the Klein-Gordon inner product that is usually considered for solutions to the Klein-Gordon equation.

Proposition 2.2.1. *With the pairing determined by the metric-induced volume form, the Klein-Gordon operator* (2.18) *on a globally hyperbolic spacetime manifold of dimension d is formally self-adjoint.*

Proof. The coordinate expression (and summation convention for indices $\mu, \nu \in [0, d-1]$) for the Klein-Gordon operator (2.18) is

$$P_{\mathrm{KG}} = -\left(\frac{1}{\sqrt{|\det g|}} \partial_\mu \sqrt{|\det g|} g^{\mu\nu} \partial_\nu + m^2 + \xi R \right). \tag{2.23}$$

The metric induced volume measure is $\mathrm{dvol}_M = \sqrt{|\det g|}\mathrm{d}^d x$. When using partial integration with $P = P_{\mathrm{KG}}$ in (2.22) twice, the boundary terms vanish, since $\operatorname{supp}(f_1) \cap \operatorname{supp}(f_2)$ is compact, and the metric determinant factors cancel/complete with $\mathrm{d}^d x$ to the volume form so that $P^*_{\mathrm{KG}} = P_{\mathrm{KG}}$. □

Definition 2.2.2 (after [8])**.** Let P be a linear partial differential operator for a given spacetime manifold M. Recall Definition 2.1.2 with the subspaces of past/future-compactly supported configurations. The **retarded** and **advanced Green operators**, are the unique maps $E^+ : \mathcal{E}_{\mathrm{p}} \to \mathcal{E}$ and $E^- : \mathcal{E}_{\mathrm{f}} \to \mathcal{E}$, respectively, such that for any function f in the respective domain

$$P E^{\pm} f = f = E^{\pm} P f, \tag{2.24a}$$

$$\operatorname{supp}\Big(E^{\pm} f\Big) \subseteq J^{\pm}\Big(\operatorname{supp}(f)\Big). \tag{2.24b}$$

A **Green hyperbolic operator** is a linear partial differential operator that has both, retarded and advanced Green operators.

The retarded-minus-advanced operator combination

$$E := (E^+ - E^-) : \mathcal{E}_{\mathrm{t}} \to \mathcal{E} \tag{2.25}$$

is called the **Pauli-Jordan operator**.

In the perspective reviewed here, the Klein-Gordon operator P and the Pauli-Jordan operator E are morphisms on $\mathcal{E}$ (or its complex extension). More generally, the Klein-Gordon operator may be understood as a morphism $\tilde{P} : \mathcal{E}^{\mathbb{C}} \to (\mathcal{E}^*)^{\mathbb{C}}$ so that the Pauli-Jordan morphism $\pi^\sharp_{\mathrm{off}} : (\mathcal{E}^*)^{\mathbb{C}} \to \mathcal{E}^{\mathbb{C}}$ is the map constructed from the retarded and advanced morphisms to $\tilde{P}$, see Bär, Ginoux, and Pfäffle [9]. The operator E is determined by $\pi^\sharp_{\mathrm{off}}$ and it also depends on the choice of a pairing $\langle \cdot, \cdot \rangle$ between the elements of $\mathcal{E}^{\mathbb{C}}$ and its dual. This implicit dependence of the Pauli-Jordan operator E on the pairing will become important in the construction of the Sorkin-Johnston state in Chapter 6. I continue using the operator E as of Definition 2.2.2 in order to review the analogue formulation for causal sets in Section 2.3, following the arguments of Sorkin [102], and [103].

All normally hyperbolic operators are Green hyperbolic operators and the formal adjoints of the Green operators are $E^{\pm *} = E^{\mp}$ [12]. Notice that I use a sign convention where the field operator P has a leading minus sign (due to the Lagrangian formalism) so that the retarded/advanced Green operator $E^\pm$ is equivalent to the negative of the retarded/advanced Green operator of $-P = \Box + m^2 + \xi R$.

Lemma 2.2.3 (see [12])**.** *Let P be a Green hyperbolic operator on a spacetime manifold. The operator P and its Pauli-Jordan operator form an exact sequence*

$$0 \xrightarrow{E} \mathcal{E}_{\mathrm{t}} \xrightarrow{P_{\mathrm{t}}} \mathcal{E}_{\mathrm{t}} \xrightarrow{E} \mathcal{E} \xrightarrow{P} \mathcal{E} \tag{2.26a}$$

with

$$\{0\} = \ker(P_{\mathrm{t}}), \tag{2.26b}$$

$$\mathrm{img}(P_{\mathrm{t}}) = \ker(E), \tag{2.26c}$$

$$\mathrm{img}(E) = \ker(P). \tag{2.26d}$$

The subscript on P_{t} only highlights the different domain (additionally to the colouring) of P.

Proof. Recall from Definition 2.1.2 that $\mathcal{E}_{\mathrm{t}} = \mathcal{E}_{\mathrm{p}} \cap \mathcal{E}_{\mathrm{f}}$.
(2.26b) $\Rightarrow$**:** If $f = 0$, then automatically $P_{\mathrm{t}} f = 0$, because P is linear.
(2.26b) $\Leftarrow$**:** If $f \in \ker(P_{\mathrm{t}})$, then

$$0 = E^\pm P_{\mathrm{t}} f \overset{(2.24a)}{=} f. \tag{2.27}$$

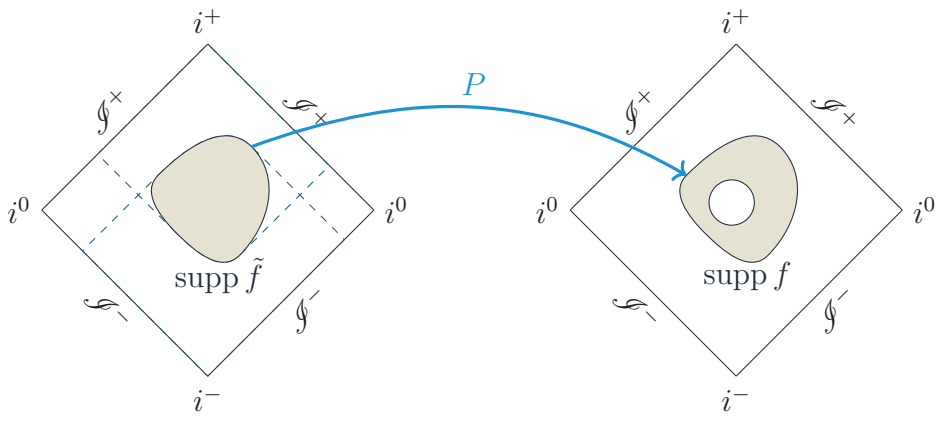

(a) The support of $\tilde{f} \in \mathcal{D}(\mathbb{M})$ remains compact under P.

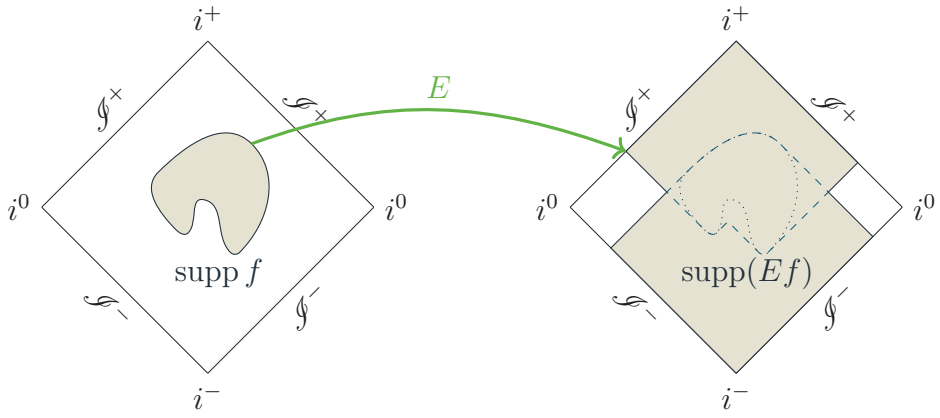

(b) The support of $f \in \mathcal{D}(\mathbb{M})$ becomes spatially compact under E.

Figure 2.2: Penrose diagrams of Minkowski spacetime $\mathbb{M}$ showing the change of function supports (grey) under the action of (a) a Green hyperbolic operator P (blue) and (b) its Pauli-Jordan operator E (green).

(2.26c) $\Rightarrow$: If $f \in \mathrm{img}(P_\mathrm{t}) \subseteq \mathcal{E}_\mathrm{t}$, then $\exists \tilde{f} \in \mathcal{E}_\mathrm{t} : f = P_\mathrm{t}\tilde{f}$ and

$$Ef \overset{(2.25)}{=} E^+P_\mathrm{t}\tilde{f} - E^-P_\mathrm{t}\tilde{f} \overset{(2.24a)}{=} \tilde{f} - \tilde{f} = 0. \tag{2.28}$$

(2.26c) $\Leftarrow$: If $f \in \ker(E) \subset \mathcal{E}_\mathrm{t}$, then $E^+f = E^-f =: \tilde{f}$ by (2.25) and

$$\left(\mathrm{supp}\,\tilde{f} \overset{(2.24b)}{\subset} J^+(\mathrm{supp}\,f) \cap J^-(\mathrm{supp}\,f)\right) \Rightarrow \tilde{f} \in \mathcal{E}_\mathrm{t}. \tag{2.29}$$

So (2.24a) yields $f = P_\mathrm{t}\tilde{f}$ and hence $f \in \mathrm{img}(P_\mathrm{t})$.

(2.26d) $\Rightarrow$: If $f \in \mathrm{img}(E)$, then $\exists \tilde{f} \in \mathcal{E}_\mathrm{t} : f = E\tilde{f}$ and

$$Pf \overset{(2.25)}{=} PE^+\tilde{f} - PE^-\tilde{f} \overset{(2.24a)}{=} \tilde{f} - \tilde{f} = 0. \tag{2.30}$$

(2.26d) $\Leftarrow$**:** Let $\chi \in \mathcal{E}_{\mathrm{p}}$ be a smooth cutoff function and $f \in \ker(P)$, so that $f^- := \chi f \in \mathcal{E}_{\mathrm{p}}$ and $f^+ := f - f^- \in \mathcal{E}_{\mathrm{f}}$. Because

$$Pf^+ = Pf - Pf^- = 0 - Pf^-, \tag{2.31}$$

note that $Pf^\pm \in \mathcal{E}_{\mathrm{t}}$. By property (2.24a), $f^\pm = E^\mp P f^\pm = \mp E^\mp P f^-$, so

$$f = f^- + f^+ = (E^+ - E^-)Pf^- \overset{(2.25)}{=} EPf^-. \tag{2.32}$$

Hence f is also in the image of E. □

An example of a Green hyperbolic operator P and its Pauli-Jordan operator E acting on some functions on Minkowski spacetime are shown in Figure 2.2.

In Section 2.4, we will discuss the algebra of classical observables with a Poisson bracket that can be expressed in terms of the Pauli-Jordan operator. Using Lemma 2.2.3, I will derive a symplectic space for the Klein-Gordon theory on spacetimes. A similar argument (yet not quite the same) will lead us to the symplectic space for a causet.

2.3 Field Dynamics on Causal Sets

In this section, let us review the field dynamics for the scalar field on causets analogously to the case of globally hyperbolic spacetimes in the previous section, mostly following Sorkin [102], and [103]. In order to generalize the Klein-Gordon equation to a causet, we must find a suitable discretization of the d'Alembertian. For a shorter notation, I simply denote the configuration space of a given causet by $\mathcal{E}$.

2.3.1 Discretization of the d'Alembertian and the Preferred Past

The partition of the past of a causet event into layers or ranks (see Section 1.3) plays an important role in the definition of discretized wave operators on causal sets, see Sorkin [101], Benincasa and Dowker [11], Dowker and Glaser [35], Glaser [43], and Aslanbeigi, Saravani, and Sorkin [6]. For a causet C discretizting a d-dimensional (Minkowski) spacetime manifold at some microscopic length scale ℓ, the d'Alembertian in the *generalized causet box* discretization $\Box^{\mathrm{GCB}}$ acting on a field configuration $\varphi \in \mathcal{E}$ at event $x \in C$ is given by

$$\left(\Box^{\mathrm{GCB}}\varphi\right)(x) = c_0\varphi(x) + \sum_{i=1}^{k_d} c_i \sum_{z \in L_i^-(x)} \varphi(z). \tag{2.33}$$

For 2-dimensional Minkowski spacetime, the necessary number of layers is $k_2 = 3$ with coefficients $(c_0, c_1, c_2, c_3) = (2, -4, 8, -4)/\ell^2$ [101], for 4-dimensional Minkow-

ski spacetime, the parameters are set to $k_4 = 4$ and

$$\Big(c_0, c_1, c_2, c_3, c_4\Big) = \frac{4}{\sqrt{6}\ell^2}\Big(1, -1, 8, -16, 8\Big), \tag{2.34}$$

and the generalization to other dimensions is given in [6].

The properties of this discretization are that $\Box^{\mathrm{GCB}}$ is retarded (only depends on the past of event x), independent of a possible labelling of events ("label invariance"), and the weights c_i are global constants ("neighbourly democracy") [6]. However, using this technique, there is a different discretization for every spacetime dimension, which is usually unknown for an arbitrary causet. One might estimate the dimension at least "locally" — for some causal interval — by the Myrheim-Meyer estimator [82, 65] or other approximations [93, 97] and then use the respective discretization on said interval. Furthermore, the summations in (2.33) run over the entire past layers $L_i^-(x)$ yielding possibly infinite sums when the past of the event x is infinite.

A more recent, alternative approach [29] proposes a discretization scheme for the wave operators that has the potential to be used without knowing the spacetime dimension beforehand. However, this method requires the specification of a supplementary structure.

Definition 2.3.1 (after [29])**.** Let C be a causet. A **preferred past (or future) structure** is a map from causet events that are not in the 2-layer past (or future) infinity, $\Lambda^{\mp} : C \setminus \mathcal{I}^{\mp}_{\text{2-layer}} \to C$, such that

$$\Lambda^{\mp}(x) \in R_2^{\mp}(x). \tag{2.35}$$

Let Λ^- be some preferred past structure for a causet C and let $\varphi \in \mathcal{E}$. A discretized d'Alembertian adapted from a 2-dimensional lattice $\Box^{\mathrm{2D}}$, as proposed in Dable-Heath, Fewster, Rejzner, and Woods [29], is a map $\Box^{\mathrm{2D}}\varphi : C\setminus\mathcal{I}^-_{\text{2-layer}} \to \mathbb{R}$. For any $x \in C$, it is the weighted sum over the values of φ on $[\Lambda^-(x), x]$. With the open interval $I_x = (\Lambda^-(x), x)$, the cardinality $k = |I_x|$, and a fundamental length scale ℓ, it is given by

$$\left(\Box^{\mathrm{2D}}\varphi\right)(x) = c_0\varphi(x) + c_1 \sum_{z\in I_x} \varphi(z) + c_2\varphi\left(\Lambda^-(x)\right), \tag{2.36a}$$

$$\Big(c_0, c_1, c_2\Big) = \frac{2}{\ell^2}\left(1, -\frac{2}{k}, 1\right). \tag{2.36b}$$

This expression yields the correct continuum limit (taken over a sequence of increasingly finer lattices) for 2-dimensional Minkowski spacetime [29]. It is hoped that at least a similar expression might also hold in higher dimensions.

In the following, I construct a generalization of the d'Alembertian that holds for regular lattices in any spacetime dimension d. Let δ_r be a lattice parame-

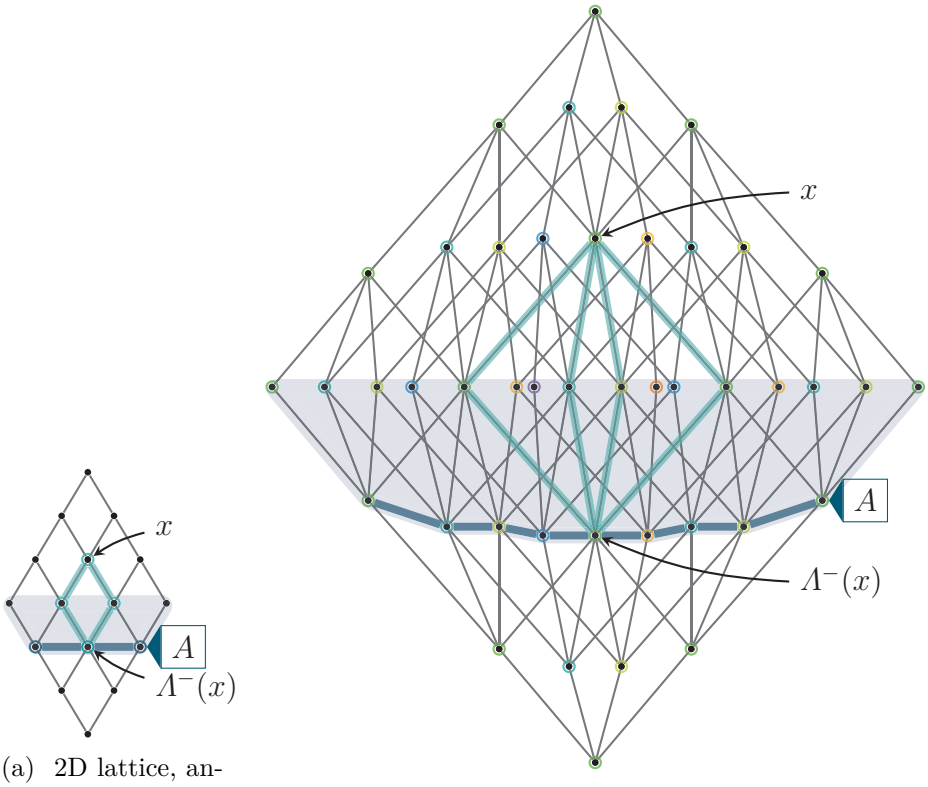

(a) 2D lattice, animated in [78]

(b) 3D lattice, animated in [79]

Figure 2.3: Subcausets of infinite regular lattices, (a) 4×4 lattice that embeds in $(1+1)$-dimensional Minkowski spacetime, and (b) lattice that is composed of layers, from front to back: 1×1 (purple), 2×2 (blue), 3×3 (cyan), 4×4 (green), 3×3 (lime), 2×2 (yellow), 1×1 (orange), and it embeds in $(1+2)$-dimensional Minkowski spacetime (lattice of squares in spatial dimensions). Both lattices show (part of) a Cauchy antichain A and a *pure diamond* (marked in cyan; see Subsection 2.3.2) with its tip event x sticking out of the respective 2-layer future Cauchy slices, while its *preferred past* $\Lambda^-(x)$ lies in A. For animated versions of the lattice subsets in 2-, 3- and 4-dimensional Minkowski spacetime, follow the links [78, 79, 80].

ter that I will derive from the fundamental length scale ℓ below. Consider d-dimensional Minkowski spacetime $\mathbb{M}^d$ with standard coordinates and basis vectors $\boldsymbol{e}_0 = (1,0,\dots,0)$, $\dots$, $\boldsymbol{e}_{d-1} = (0,\dots,0,1)$. For all $i,j \in [0,d-1] \subset \mathbb{N}$ and all $n_0, n_1, \dots, n_{d-1} \in \mathbb{Z}$, I place a single event at each *distinct* coordinate tuple given by (note that this defines all lattice sites multiple times)

$$\delta_r \boldsymbol{e}_i + \delta_r \boldsymbol{e}_j + \sum_{l=0}^{d-1} 2n_l \delta_r \boldsymbol{e}_l. \tag{2.37}$$

This yields a regular lattice that reduces to the lattice considered in [29] in the 2-dimensional case. Subsets of the $(1+1)$- and $(1+2)$-dimensional lattices are shown in Figure 2.3.

I define a preferred past structure Λ^- for the lattice by

$$\Lambda^-(x) = x - 2\delta_r \boldsymbol{e}_0. \tag{2.38}$$

This yields the causet interval $\left[\Lambda^-(x), x\right]$ as shown by highlighted links (cyan) in Figure 2.3. The d'Alembertian of a field φ at x is determined by the field values at the preferred past event $\Lambda^-(x)$ and the intermediate events $x_j^\pm \in I_x := \left(\Lambda^-(x), x\right)$ (for all $j \in [1, d-1] \subset \mathbb{N}$) at

$$x_j^\pm = x - \delta_r \boldsymbol{e}_0 \pm \delta_r \boldsymbol{e}_j. \tag{2.39}$$

The lattice constant δ_r is determined by the fundamental length scale ℓ such that

$$\ell^d \Big|[x, y]\Big| \asymp \mathrm{vol}_{\mathbb{M}^d}\left(J^+[\mathbb{M}^d](x) \cap J^-[\mathbb{M}^d](y)\right) \tag{2.40}$$

holds asymptotically, for very large causet intervals $[x, y]$. With the given coordinates (2.37), the volume element is a square (hyper)octahedron, so

$$\ell^d = \frac{1}{d!}(2\delta_r)^d. \tag{2.41}$$

In dimension 2, it is the "volume" of a 2-dimensional pyramid with base $2\delta_r$ and height $2\delta_r$, so $\frac{1}{2}2\delta_r \times 2\delta_r = 2\delta_r^2$. In dimension 3, the 2D octahedron is the base and the pyramid height is $2\delta_r$ yielding $\frac{1}{3}2\delta_r \times 2\delta_r^2$. This pattern continues to higher dimensions, leaving us with the general expression (2.41).

The dimension d is related to the cardinality $k := |I_x|$ by $2(d-1) = k$, so the physical dimension factor for the d'Alembertian is

$$\delta_r^2 = \frac{1}{4}\Gamma\left(\tfrac{k+4}{2}\right)^{\frac{4}{k+2}} \ell^2, \tag{2.42}$$

where I replaced the factorial by the Gamma function with later generalizations including odd values of k in mind.

Now I Taylor expand the fields $\varphi\left(x_j^\pm\right)$ and $\varphi\left(\Lambda^-(x)\right)$ around x,

$$\begin{aligned}\varphi\left(x_j^\pm\right) = \Bigg(1 - \delta_r\frac{\partial}{\partial t} \pm \delta_r\frac{\partial}{\partial x^j} + \frac{\delta_r^2}{2}\frac{\partial^2}{\partial t^2} \mp \delta_r^2\frac{\partial}{\partial t}\frac{\partial}{\partial x^j} \\ + \frac{\delta_r^2}{2}\frac{\partial^2}{\partial (x^j)^2} + \mathcal{O}(\delta_r^3)\Bigg)\varphi(x),\end{aligned} \tag{2.43a}$$

$$\sum_{x_j^\pm \in I_x} \varphi\left(x_j^\pm\right) = \left(k - k\delta_r\frac{\partial}{\partial t} + \frac{k\delta_r^2}{2}\frac{\partial^2}{\partial t^2} + \delta_r^2\nabla^2 + \mathcal{O}(\delta_r^3)\right)\varphi(x), \tag{2.43b}$$

$$\varphi\left(\Lambda^-(x)\right) = \left(1 - 2\delta_r\frac{\partial}{\partial t} + 2\delta_r^2\frac{\partial^2}{\partial t^2} + \mathcal{O}(\delta_r^3)\right)\varphi(x). \tag{2.43c}$$

Notice that the linear combination

$$\begin{aligned}&\frac{3k-2}{4}\varphi(x) - \sum_{z \in I_x}\varphi(z) + \frac{k+2}{4}\varphi\left(\Lambda^-(x)\right) \\ &= \frac{k-2}{2}\delta_r\frac{\partial\varphi}{\partial t}(x) + \delta_r^2(\Box\varphi)(x) + \mathcal{O}(\delta_r^3)\end{aligned} \tag{2.44}$$

contains the d'Alembertian, but also a time derivative of the field at x. In the 2-dimensional case where $k = 2$, the time derivative does not contribute and the expression divided by ℓ^2 yields the d'Alembertian in the limit $\ell \to 0$ (using a sequence of refined lattices as in [29]). In all other cases, it is necessary to add further correction terms compensating the time derivative.

Note that the time derivative describes the normal vector of the horizontal Cauchy slice as marked in Figure 2.3 (shaded, light blue). So I express it using the next preferred past following the preferred past structure, with the Taylor expansion

$$\varphi\left((\Lambda^- \circ \Lambda^-)(x)\right) = \left(1 - 4\delta_r \frac{\partial}{\partial t} + 8\delta_r^2 \frac{\partial^2}{\partial t^2} + \mathcal{O}(\delta_r^3)\right) \varphi(x). \tag{2.45}$$

With this extra term, we obtain the d'Alembertian generalized to the regular lattice in any dimension

$$\left(\Box^{\text{lat}}\varphi\right)(x) = c_0\varphi(x) + c_1 \sum_{z \in I_x} \varphi(z) + c_2\varphi\left(\Lambda^-(x)\right) + c_3\varphi\left(\Lambda^{-2}(x)\right), \tag{2.46a}$$

$$(c_0, c_1, c_2, c_3) = \frac{4}{\Gamma\left(\frac{k+4}{2}\right)^{\frac{4}{k+2}} \ell^2} \left(\frac{3k+2}{8}, -1, \frac{3k-2}{4}, \frac{2-k}{8}\right), \tag{2.46b}$$

abbreviating $\Lambda^- \circ \Lambda^-$ to Λ^{-2}. Note that this generalization of the d'Alembertian is a map that is only defined at events in $C \setminus \mathcal{I}^-_{\text{4-rank}}$ (or for events $C \setminus \mathcal{I}^-_{\text{2-layer}}$ that have a preferred past with $k = |I_x| = 2$).

The d'Alembertian operator (2.46) is valid on the lattices for any dimension, since the dimensional dependence is captured by the cardinality k of the interval $(\Lambda^-(x), x)$. It remains to show if and how the 4 coefficients c_i have to be modified for generic causets using statistics generated from given spacetime manifolds by a *sprinkling process*. In Chapter 4, I will have a closer look at the Poisson process of sprinkling, however, I will leave a more detailed analysis of the discretization method and an estimation of the coefficients for sprinkled causets to future research projects.

Alternatively to the generalization (2.46), I suggest to consider a slicing such that for each preferred past interval $[\Lambda^-(x), x]$, there exists a Cauchy antichain A through $\Lambda^-(x)$ and its 2-layer future Cauchy slice includes the semi-closed interval $[\Lambda^-(x), x)$ — as shown by the examples in Figure 2.3. Then the d'Alembertian can also be computed from the field values of the preferred past interval and the field values of the events in the set

$$I'_x = \left(J^-(x) \cap A\right) \setminus \{\Lambda^-(x)\}. \tag{2.47}$$

Following this idea, one defines yet another generalization of the d'Alembertian operator that does not include the $\Lambda^{-2}(x)$ term, but instead a term depending on the event set I'_x.

A quantitative comparison of the different discretization approaches is not included here. However, in Chapter 3, we will discuss how a preferred past structure could be assigned intrinsically in sprinkled causets (on Minkowski spacetime).

2.3.2 Diamonds

For an event $x \in C$ in an arbitrary causet, the rank 2 past $R_2^-(x)$ generally contains more than one event, so a preferred past structure (as in Definition 2.3.1) is a choice of rank 2 past events. In Chapter 3, I will analyse six methods for selecting subsets of $R_2^-(x)$ with the aim to find one method that (among other things) selects singleton sets with high probability. To this end, I introduce further properties of the open causal intervals spanned between an event and any of the events in its rank 2 past, and also of the events within such intervals.

Definition 2.3.2. Let C be a causet and let $x, y \in C$ such that $\mathrm{rk}(y, x) = 2$. A **diamond** is the closed interval $[x, y]$ with **diamond size** k given by

$$k = \Big|(x, y)\Big| = \Big|[x, y]\Big| - 2. \tag{2.48}$$

The diamond $[x, y] \subseteq C$ is a **past diamond of** y and a **future diamond of** x. Given some preferred past (future) structure $\Lambda^{\mp}$ on C, the **preferred past (future) diamond** of x is the diamond $[\Lambda^-(x), x]$ (the diamond $[x, \Lambda^+(x)]$).

An event in the open interval (x, y) can either be only linked to x and y, or it is related to other events in this set, which leads me to the following diamond properties.

Definition 2.3.3. Let $[x, y]$ be a k-diamond in the causet $(C, \preceq)$. Let us call an event $z \in (x, y)$ **perimetral** if $x \prec\!* \, z \prec\!* \, y$. The number of perimetral events is

$$\mathrm{prm}(y, x) := \Big|\{z \in (x, y) \mid x \prec\!* \, z \prec\!* \, y\}\Big|. \tag{2.49}$$

An event $z \in (x, y)$ is **internal** if it is not perimetral. There are

$$\begin{aligned} \mathrm{itn}(y, x) &:= \Big|(x, y)\Big| - \mathrm{prm}(y, x) \\ &= k - \mathrm{prm}(y, x) \end{aligned} \tag{2.50}$$

internal events in (x, y). A **pure** diamond is a diamond with $\mathrm{itn}(y, x) = 0$.

Notice that the number of perimetral events of a diamond (2.49) is the same as the number of minimal paths from y to x. As an example, consider some causet $(C, \preceq)$ and two events $x, y \in C$ such that their interval $[x, y]$ is a 4-diamond. For it to be a 4-diamond, there has to be at least one event z such that $x \prec\!* \, z \prec\!* \, y$,

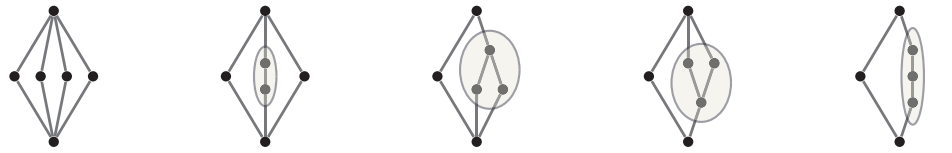

prm: 4, pure | prm: 2, itn: 2 | prm: 1, itn: 3 | prm: 1, itn: 3 | prm: 1, itn: 3

Figure 2.4: Types of 4-diamonds. From left to right, the pure 4-diamond, followed by the 4-diamond with two internal events (ellipse), and three 4-diamonds with three internal events.

but the remaining three events can have an arbitrary causal structure, so there are the 5 distinct 4-diamonds drawn in Figure 2.4.

The preferred past diamonds in the d-dimensional lattices Figure 2.3 are examples of pure 2^{d-1}-diamonds. In generic or sprinkled causets, a preferred past structure with similar diamond sizes is more likely to include non-pure diamonds. For a detailed, numerical analysis of the possibility to assign a preferred past structure to sprinkled causets intrinsically, see Chapter 3.

2.3.3 Green Operators

In this section, I follow closely the discussion in [29]. Let C be some fixed causet (with configuration space $\mathcal{E}$) and let P be any retarded discretization of a normally hyperbolic operator, as described in Subsection 2.3.1. Consider the inhomogeneous field equation for a field $\varphi \in \mathcal{E}$,

$$P\varphi = Kf \tag{2.51}$$

with some source field $f \in \mathcal{E}$ and a retarded operator $K : \mathcal{E} \to \mathcal{E}$ that determines a weight for the source field values on the events of the past diamond for each causet event as discussed in [29]. For simplicity, we may choose the identity operator for K here, so the source field only influences the field equations locally.

Definition 2.3.4 (after [29])**.** The **retarded** and **advanced Green operators**, are the maps $E^+ : \mathcal{E}_\mathrm{p} \to \mathcal{E}$ and $E^- : \mathcal{E}_\mathrm{f} \to \mathcal{E}$ (see Definition 2.1.2), respectively, given by

$$E^+ := P^{-1}K, \tag{2.52a}$$

$$E^- := (E^+)^*, \tag{2.52b}$$

where the star denotes the adjoint with respect to some (real-valued) pairing $\langle \cdot, \cdot \rangle$. The **Pauli-Jordan operator** is

$$E = E^+ - E^-. \tag{2.53}$$

If P^{-1} and hence E^+ exists, P is referred to as **Green hyperbolic**.

Similar to my remark in the review of normally hyperbolic operators on spacetime manifolds, the Klein-Gordon operator P may be understood rather as a morphism $\widetilde{P} : \mathcal{E}^{\mathbb{C}} \to (\mathcal{E}^*)^{\mathbb{C}}$ so that the Green functions are $\widetilde{E}^+ : (\mathcal{E}^*_{\mathrm{p}})^{\mathbb{C}} \to \mathcal{E}^{\mathbb{C}}$ and $\widetilde{E}^- : (\mathcal{E}^*_{\mathrm{f}})^{\mathbb{C}} \to \mathcal{E}^{\mathbb{C}}$, and they determine the Pauli-Jordan morphism $\pi^\sharp_{\mathrm{off}} = \widetilde{E}^+ - \widetilde{E}^-$. I will use the bilinear form π_{off} corresponding to this morphism to define a Poisson bracket for off-shell observables in Section 2.4. For now, I continue with the Green operators as given in Definition 2.3.4.

For a finite causet C, recall the Klein-Gordon operator P_{KG} for a *massless* boson in the discretization $\Box^{\mathrm{lat}}$ that I introduced in Subsection 2.3.1. With the described preferred past structure Λ^- and the subsets $I_1(x) := (\Lambda^-(x), x)$, $I_2(x) := \{\Lambda^-(x)\}$ and $I_3(x) := \{\Lambda^{-2}(x)\}$, it has a matrix representation with components

$$(\boldsymbol{P}_{\mathrm{KG}})^x{}_y := \begin{cases} -\ell^{-2} & y = x \in \mathcal{I}^-_{\text{4-rank}}, \\ -c_0 & y = x \notin \mathcal{I}^-_{\text{4-rank}}, \\ -c_i & y \in I_i(x), i \in \{1,2,3\}, \\ 0 & \text{otherwise}, \end{cases} \tag{2.54}$$

where $\mathcal{I}^-_{\text{4-rank}}$ stands for the 4-rank past infinity, see Definition 1.3.2. Using an order-preserving labelling, the matrix $\boldsymbol{P}_{\mathrm{KG}}$ is lower triangular, or *retarded*, with a nowhere vanishing diagonal. So the retarded Green operator $\boldsymbol{E}^-$ exists. The advanced Green operator $\boldsymbol{E}^-$ is given by $(\boldsymbol{E}^+)^{\mathsf{T}}$ when we use the natural pairing. For a massive boson, one may add the mass term as a perturbation term later on, see Dable-Heath, Fewster, Rejzner, and Woods [29, Sec. III.E].

Note that the exact sequence given in Lemma 2.2.3 for spacetime manifolds does not hold for the Green operators on a causet, since it is not guaranteed that $EP = 0$ and $PE = 0$. Hence, I will use an alternative for the solution space with a symplectic form as discussed in Section 2.4. However, first let us briefly consider an application of Green operators to study field solutions under *local* changes of a given causet.

2.3.4 Relative Cauchy Evolution

In the following, I take a brief look at the application of *relative Cauchy evolution* to causets. Relative Cauchy evolution was introduced in Brunetti, Fredenhagen, and Verch [26] for perturbations of a background metric in locally covariant quantum field theory on curved spacetime manifolds. In Rejzner [94, Ch. 8], it is discussed in the context of effective quantum gravity. The idea of the application to causal set theory was first considered in Dable-Heath, Fewster, Rejzner, and Woods [29]. I review this application and give an illustration in the following.

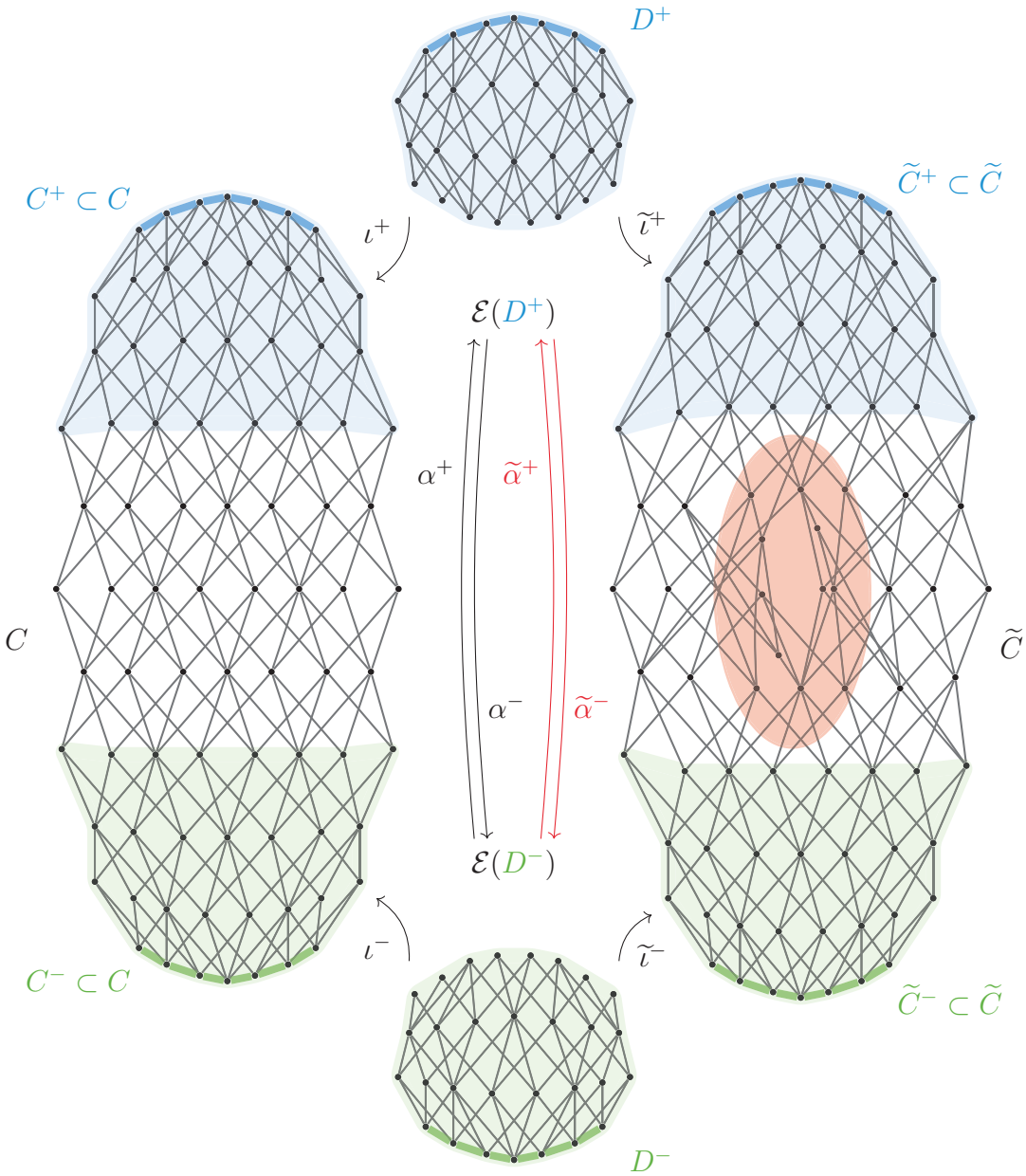

Figure 2.5: Relative Cauchy evolution between 2 causets, a causet C (left) and a modified/perturbed causet $\widetilde{C}$ (right), while the 4-step Cauchy slices $D^{\mp}$ embed as subsets in both causets via $\iota^{\mp}$ and $\widetilde{\iota}^{\mp}$, respectively. The configuration spaces over the Cauchy slices are isomorphic if the Cauchy evolutions α^+ and $\widetilde{\alpha}^+$ exist. The causets are equal up to a finite region (red ellipse). For animated versions of the causets C, $D^{\mp}$, and an alternative perturbation embedded in 3-dimensional Minkowski spacetime, follow the links [72, 73, 74, 75].

Let C be a causet with a j-step Cauchy slice C^- (for some $j > 2$ depending on the discretization method) that is the embedding of another causet D^- via the order-preserving map $\iota^- : D^- \to C$ such that $C^- = \iota^- D^-$. For example, in a finite causet, we may take the j-step past infinity $C^- = \mathcal{I}^-_{j\text{-step}}$, or in an infinite causet with a Cauchy antichain A, consider the j-step future Cauchy slice $C^- = S^+_{[0,j-1]}(A)$. Let the initial field values be given by a source function $f = \varphi^-$ that is only supported on $C^- \subset C$. All such initial field values form a subset of timelike-finitely supported configurations denoted as $\mathcal{E}_{C^-}(C) \subset \mathcal{E}_{\mathrm{t}}(C)$ (see Definition 2.1.2). The pullback of the embedding map is the isomorphism $(\iota^-)^{\leftarrow} : \mathcal{E}_{C^-}(C) \to \mathcal{E}(D^-)$. Notice the unusual notation with a left pointing arrow $^{\leftarrow}$ for the pullback to avoid confusion with the numerous other meanings of the commonly used * symbol in the superscript.

For all events in the future of C^-, the j-step Cauchy problem (initial value problem) over C has the inhomogeneous field equation $P_{\mathrm{KG}}\varphi = \varphi^-$ with the solution $\varphi = E^+\varphi^-$. Any solution is fully described by the Cauchy data φ^- and the solution space is given by

$$\mathcal{S}^+(C) := E^+\mathcal{E}_{C^-}(C) \tag{2.55}$$

as introduced in [29]. Additionally, let there be another Cauchy slice $C^+ \subset C$ in the future of C^-, analogously given by a causet D^+ such that $|D^+| = |D^-|$, an embedding ι^+ such that $C^+ = \iota^+ D^+$, and the configuration subspace $\mathcal{E}_{C^+}(C) \subset \mathcal{E}_{\mathrm{t}}(C)$. Let $\mathit{\Pi}_{C^+} : \mathcal{E}(C) \to \mathcal{E}_{C^+}(C)$ be the projector that restricts any field configuration to the part compactly supported on C^+. With this notation, let us define the map

$$\alpha^+ = (\iota^+)^{\leftarrow} \mathit{\Pi}_{C^+} E^+ \left((\iota^-)^{\leftarrow}\right)^{-1}. \tag{2.56}$$

This map yields a solution on the future causet D^+ from a field configuration on the past causet D^- via the field equations on the causet C. A *Cauchy evolution* is such a map $\alpha^+ : \mathcal{E}(D^-) \to \mathcal{E}(D^+)$ that is a bijection. A graphical example is given in the left of Figure 2.5.

If the Cauchy evolution exists, we can compare solutions to another causet $\widetilde{C}$ that also has a past and a future Cauchy slice $\widetilde{C}^{\mp} \subset \widetilde{C}$ that are identified with the "Cauchy slice" causets $S^{\mp}$ via the embeddings $\tilde{\iota}^{\mp}$. While the past and the future Cauchy slices of C and $\widetilde{C}$ are isomorphic, the causets can differ between these Cauchy slices as illustrate by a red ellipse in Figure 2.5. I assume that the map $\tilde{\alpha}^+ : \mathcal{E}(D^-) \to \mathcal{E}(D^+)$ is also a Cauchy evolution i.e., an isomorphism.

Definition 2.3.5 (after [29])**.** Given a setting as described above, the **relative Cauchy evolution** is the isomorphism $\mathrm{rce} : \mathcal{S}^+(C) \to \mathcal{S}^+(C)$ such that

$$\mathrm{rce}(\varphi) := E^+\Big((\iota^-)^{\leftarrow}\Big)^{-1}(\widetilde{\alpha}^+)^{-1}(\iota^+)^{\leftarrow}\Pi_{D^+}\varphi. \tag{2.57}$$

Let $\mathcal{F}^+(C)$ be the algebra of observables over $\mathcal{S}^+(C)$. Every observable $F \in \mathcal{F}^+(C)$ has the relative Cauchy evolution given by the pullback $\mathrm{rce}^{\leftarrow}F$.

In Brunetti, Fredenhagen, and Verch [26, Thm. 4.3.], it was shown that the functional derivative of the relative Cauchy evolution (for spacetime manifolds) with respect to the metric tensor is a divergence-free quantity determined by the energy-momentum tensor. So similarly for causets, the relative Cauchy evolution may contain information about the analogue of the energy-momentum tensor for causets. However, a more detailed study of relative Cauchy evolution for causets is beyond the scope of this thesis.

2.4 Classical Poisson Algebras and Symplectic Spaces

With the Pauli-Jordan operator E as given in Definition 2.2.2 for spacetime manifolds and in Definition 2.3.4 for causets, let us turn our attention to the off-shell and on-shell algebras of observables, equipped with a *Poisson structure* additionally to the commutative algebra structure.

Definition 2.4.1. A **Poisson algebra** is a commutative algebra $\mathcal{F}$ with a bilinear map, called the **Poisson bracket**,

$$\{\cdot, \cdot\} : \mathcal{F} \times \mathcal{F} \to \mathcal{F} \tag{2.58}$$

such that the following properties hold for all $F_1, F_2, F_3 \in \mathcal{F}$

$$\text{anti-symmetry:} \qquad \{F_1, F_2\} = -\{F_2, F_1\}, \tag{2.59a}$$

$$\text{Leibniz's rule:} \qquad \{F_1F_2, F_3\} = \{F_1, F_3\}F_2 + F_1\{F_2, F_3\}, \tag{2.59b}$$

$$\text{Jacobi identity:} \qquad 0 = \{F_1, \{F_2, F_3\}\} + \{F_2, \{F_3, F_1\}\} + \{F_3, \{F_1, F_2\}\}. \tag{2.59c}$$

2.4.1 Peierls Brackets and Off-Shell Algebras

To turn the algebra of (off-shell) observables $\mathcal{F}(\mathcal{X})$ over a (globally hyperbolic) spacetime or causet $\mathcal{X}$ into a Poisson algebra, I apply the method of Peierls [87] to define a Poisson bracket. The *Peierls bracket* is equivalent to the canonical bracket used in classical mechanics, but it is more generally defined, directly from

the Lagrangian formalism and without requiring a Cauchy foliation or the existence of a Hamiltonian formalism [94, Ch. 4]. For the review in the following, it shall be enough to look into the properties of the bracket to construct a Poisson algebra.

Recall that any linear observable $\Phi_f \in \mathcal{F}_{\text{lin}}(\mathcal{X})$ is determined by a function $f \in \mathcal{D}^{\mathbb{C}}(\mathcal{X})$ via (2.9) on a causet and (2.10) on a spacetime. The Peierls bracket of two linear observables $\Phi_{f_1}, \Phi_{f_2} \in \mathcal{F}_{\text{lin}}(\mathcal{X})$ is a constant observable (not depending on the point of evaluation $\varphi \in \mathcal{E}(\mathcal{X})$),

$$\{\Phi_{f_1}, \Phi_{f_2}\}(\varphi) := \pi_{\text{off}}(f_1, f_2), \tag{2.60}$$

where π_{off} is the bilinear map corresponding to the Pauli-Jordan map $\pi_{\text{off}}^\sharp$ as mentioned in Section 2.2 for spacetime manifolds and in Subsection 2.3.3 for causets. The Peierls bracket generalizes to any pair of observables $F_1, F_2 \in \mathcal{F}(\mathcal{X})$ at any point $\varphi \in \mathcal{E}(\mathcal{X})$, for which I write

$$\{F_1, F_2\}(\varphi) = \pi_{\text{off}}\left(F_1^{(1)}(\varphi), F_2^{(1)}(\varphi)\right). \tag{2.61}$$

For a (finite) causet with order-preserving labelling, I have a metric g determined by the inner product $\langle \cdot, \cdot \rangle$, so the Peierls bracket has the following expression in summation convention,

$$\{F_1, F_2\}(\varphi) = F_{1,m} E^m{}_k g^{kn} F_{2,n} =: F_{1,m} E^{mn} F_{2,n}, \tag{2.62}$$

where the derivatives are shortened as $F_{,m} := (F^{(1)}(\varphi))_m$.

Proposition 2.4.2 (see [29])**.** *For a given causet C, the Peierls bracket is a Poisson bracket on the algebra $\mathcal{F}(C)$.*

Proof. Since $F_1^{(1)}(\varphi), F_2^{(1)}(\varphi) \in \mathcal{F}(C)$ and the Pauli-Jordan operator E are linear, the Peierls bracket is bilinear. It is also anti-symmetric because E is anti-symmetric.

The functional derivative in the definition implies that the first argument and thus also the bracket fulfills Leibniz's rule.

In the non-interacting case, E does not depend on the fields, so that its functional derivative does not contribute. Using the short-hand notation of (2.62) (also for infinite causets), we have a summation over the 3 permutations $\sigma = (i, j, k) \in \{(1, 2, 3), (2, 3, 1), (3, 1, 2)\}$,

$$\left\{F_i, \{F_j, F_k\}\right\}(\varphi) = F_{i,m} E^{mn} (F_{j,o} E^{op} F_{k,p})_{,n} \tag{2.63a}$$

$$= E^{mn} E^{op} \left(F_{i,m} F_{j,o,n} F_{k,p} + F_{i,m} F_{j,o} F_{k,p,n}\right), \tag{2.63b}$$

$$\sum_\sigma \Big\{F_i,\, \{F_j,\, F_k\}\Big\}\,(\varphi) = E^{mn}E^{op}\Big(F_{1,m}F_{2,o,n}F_{3,p} + F_{1,m}F_{2,o}F_{3,p,n} + F_{2,m}F_{3,o,n}F_{1,p} + F_{2,m}F_{3,o}F_{1,p,n} + F_{3,m}F_{1,o,n}F_{2,p} + F_{3,m}F_{1,o}F_{2,p,n}\Big) \tag{2.63c}$$

$$= 2E^{mn}E^{[op]}\Big(F_{1,m}F_{2,n,(o}F_{3,p)} + F_{2,m}F_{3,n,(o}F_{1,p)} + F_{3,m}F_{1,n,(o}F_{2,p)}\Big). \tag{2.63d}$$

To get to the last line, we relabel $m \leftrightarrow o$ and $n \leftrightarrow p$ in every other term in the brackets, which is compatible with the double contraction with $E^{mn}E^{op}$. Then note that each pair of two summands combines to twice the symmetric term in indices o and p. The last line vanishes as the symmetrised terms are contracted with the anti-symmetric Pauli-Jordan operator. □

On a spacetime manifold M, the extension of the Peierls bracket $\{\cdot,\cdot\}$ is not closed on the space of observables $\mathcal{F}(M)$. However, it has been shown in Brunetti, Fredenhagen, and Rejzner, Brunetti, Fredenhagen, and Ribeiro [24, 25] that there exists a subspace of (strongly) micro-causal observables, denoted as $\mathcal{F}_{(\mathrm{s})\mu\mathrm{c}}(M)$, under which the bracket is closed and $\Big(\mathcal{F}_{(\mathrm{s})\mu\mathrm{c}}(M), \{\cdot,\cdot\}\Big)$ is a Poisson algebra.

2.4.2 On-Shell Algebras and Symplectic Spaces

Due to Lemma 2.2.3, the solution space (2.20) to the Klein-Gordon field equation on a spacetime manifold (M, g) is equivalently given by

$$\mathcal{S}(M) = \mathrm{img}(E). \tag{2.64}$$

The equivalent statement does not hold for every causet C because in the non-trivial case $\mathrm{img}(E) \neq \ker(P)$, but $\mathrm{img}(E) \supset \ker(P) = \{0\}$ since P is invertible by construction. The retarded Green operator E^+ is determined by P^{-1} and the advanced Green operator E^- is its adjoint, see Definition 2.3.4.

For any spacetime/causet $\mathcal{X}$, let us use the space

$$\mathcal{S}(\mathcal{X}) = \mathrm{img}(E) = \mathrm{img}(\pi^\sharp_{\mathrm{off}}) \tag{2.65}$$

and equip it with a symplectic form determined by the non-degenerate Poisson bivector of the on-shell algebra (corresponding to the Poisson bracket) as in the following. Recall from the subsection before that the free field, off-shell Poisson algebra is $(\mathcal{F}_{\mu\mathrm{c}}(M), \{\cdot,\cdot\})$ for any spacetime manifold M, and $(\mathcal{F}(C), \{\cdot,\cdot\})$ for any causet C.

The on-shell algebra on a spacetime manifold M is obtained as the quotient of the off-shell algebra by the ideal generated by the equations of motion. For

regular observables (see Definition 2.1.7), the algebra is quotiented by the ideal generated by linear observables Φ_{Pf} of the form (2.10). Because $\mathrm{img}(P) = \ker(E)$ for a Green hyperbolic operator P (as shown in Lemma 2.2.3), this is equivalent to quotienting by the ideal generated by linear observables $\Phi_{f'}$ with some spatially supported function f' in the kernel of E. By continuity, this extends to all (also singular) observables in $\mathcal{F}_{\mu c}(M)$ and it yields a quotient algebra for the free field dynamics.

As Lemma 2.2.3 does not hold for every causet C, we quotient the algebra by the ideal generated by linear functionals that vanish on $\mathcal{S}(C)$. Using this quotient to obtain the on-shell algebra shall be considered as the more general condition [29] in contrast to the one proposed in [103].

I denote the on-shell algebra of (micro-causal) observables on the spacetime/ causet $\mathcal{X}$ by $\big(\mathcal{P}(\mathcal{X}), \{\cdot,\cdot\}\big)$. The Poisson bracket is non-degenerate and the inverse of the corresponding Poisson bivector π is a symplectic form ω on the solution space $\mathcal{S}(\mathcal{X})$.

For a spacetime manifold $\mathcal{X} = M$ with metric g, for example, let me formulate an explicit expression for the symplectic form. I take any two compactly supported functions $f_1, f_2 \in \mathcal{D}$ that determine two solutions $\psi_1 = Ef_1, \psi_2 = Ef_2$. With the metric induced volume measure, the symplectic form for the two solutions is given by the expression

$$\omega\left(\psi_1, \psi_2\right) = \int_M \psi_1 f_2 \, \mathrm{dvol}_M. \tag{2.66}$$

Let Σ be a Cauchy surface of M and n a future pointing normal vector field. At first, I split the integral into the future and past of the Cauchy slice and replace f_2 in each integral by the respective identity expression of the Green operators $E^{\mp}$. Then a double partial integration (p. int.) leaves boundary integrals over the Cauchy hypersurface only, because $P\psi_1 = 0$ (for any formally self-adjoint Green hyperbolic operator $P = P^*$),

$$\begin{aligned}
\omega\left(\psi_1, \psi_2\right) &\overset{(2.24)}{=} \int_{J^+(\Sigma)} \psi_1 \left(PE^- f_2\right) \, \mathrm{dvol}_M + \int_{J^-(\Sigma)} \psi_1 \left(PE^+ f_2\right) \, \mathrm{dvol}_M && \text{(2.67a)} \\
&\overset{\text{p. int.}}{=} \int_\Sigma \psi_1 \nabla_n \left(E^- f_2\right) \, \mathrm{d}\Sigma - \int_\Sigma \left(\nabla_n \psi_1\right) \left(E^- f_2\right) \, \mathrm{d}\Sigma \\
&\quad - \int_\Sigma \psi_1 \nabla_n \left(E^+ f_2\right) \, \mathrm{d}\Sigma + \int_\Sigma \left(\nabla_n \psi_1\right) \left(E^+ f_2\right) \, \mathrm{d}\Sigma && \text{(2.67b)} \\
&\overset{(2.25)}{=} \int_\Sigma \Big(\psi_2 \nabla_n \psi_1 - \psi_1 \nabla_n \psi_2\Big) \, \mathrm{d}\Sigma. && \text{(2.67c)}
\end{aligned}$$

The solutions ψ_1, ψ_2 are uniquely determined by the Cauchy data on Σ, and they are spatial compactly supported on M, thus compactly supported on Σ (see Figure 2.6).

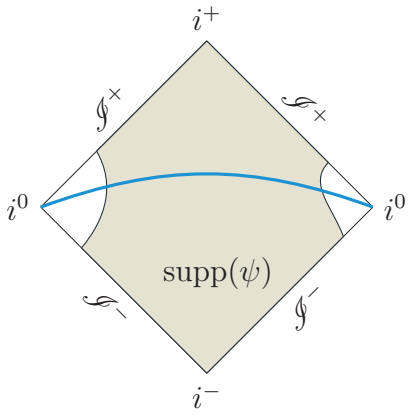

Figure 2.6: A Cauchy surface (solid line, blue) in Minkowski spacetime has a compact intersection with the support (shaded, grey) of a solution ψ.

I write the symplectic form of $\big(\mathcal{S}(\mathcal{X}), \omega\big)$ on a spacetime/causet $\mathcal{X}$ in terms of an inner product $\langle \cdot, \cdot \rangle$ and the inverse of the Pauli-Jordan operator restricted to $\mathcal{S}(\mathcal{X})$, E^{-1}_{on}, so for any $\psi_1, \psi_2 \in \mathcal{S}(\mathcal{X})$

$$\omega(\psi_1, \psi_2) = \left\langle \psi_1, E^{-1}_{\text{on}} \psi_2 \right\rangle . \tag{2.68}$$

In Chapter 6, I will discuss how an algebra of quantum observables on a causet $\mathcal{X} = C$ is geometrically constructed starting from the symplectic space with inner product, $(\mathcal{S}(C), \omega, \langle \cdot, \cdot \rangle)$.

2.4.3 Resolvent Set and Spectrum

In order to make a final note on the Pauli-Jordan operator for a causet in the next subsection as well as to establish some notation that I will use in the construction of a physical Hilbert space later on, let us take a brief digression to review some functional analysis, see Reed and Simon [91, Sec. VI.3].

Definition 2.4.3. Let $\mathcal{H}$ be a Hilbert space (or more generally a Banach space) with identity operator $\mathbb{1} \in \text{End}(\mathcal{H})$ and $D \in \text{End}(\mathcal{H})$ some (unbounded) operator. Let $\mathcal{B}(\mathcal{H})$ be the space of bounded (linear) operators. The **resolvent set** of the operator resol(D) is the set of all complex numbers for which $\lambda\mathbb{1} - D$ has a bounded (left and right) inverse $R \in \mathcal{B}(\mathcal{H})$, called the **resolvent** at λ,

$$\text{resol}(D) := \{\lambda \in \mathbb{C} \mid \exists R \in \mathcal{B}(\mathcal{H}) : (\lambda\mathbb{1} - D)R = R(\lambda\mathbb{1} - D) = \mathbb{1}\} . \tag{2.69}$$

The **spectrum** of the operator spec(D) is

$$\text{spec}(D) := \text{resol}(D)^{\complement} = \mathbb{C} \setminus \text{resol}(D). \tag{2.70}$$

To recall the change of a spectrum under a linear transformation, suppose that the spectrum of some operator D on a Hilbert space $\mathcal{H}$ is given. When we scale

the operator by some constant $c_1 \in \mathbb{C} \setminus \{0\}$ and translate it by $c_0 \in \mathbb{C}$ to obtain a new operator

$$\tilde{D} = c_1 D + c_0 \mathbb{1}, \tag{2.71}$$

the resolvent set of the transformed operator is

$$\begin{aligned} \operatorname{resol}(\tilde{D}) &= \left\{ \tilde{\lambda} \in \mathbb{C} \;\middle|\; \exists \tilde{R} \in \mathcal{B}(\mathcal{H}) : \left(\tilde{\lambda}\mathbb{1} - \tilde{D}\right) \tilde{R} = \mathbb{1} \right\} && \text{(2.72a)} \\ &= \left\{ \tilde{\lambda} = c_1\lambda + c_0 \in \mathbb{C} \;\middle|\; \exists \tilde{R} \in \mathcal{B}(\mathcal{H}) : (\lambda\mathbb{1} - D)\, c_1 \tilde{R} = \mathbb{1} \right\} && \text{(2.72b)} \\ &= c_1 \operatorname{resol}(D) + c_0, && \text{(2.72c)} \end{aligned}$$

where only the right inverses are printed here (but the linear transformation is also valid for the left inverses). Notice that in the last line the resolvent set is transformed analogously to (2.71). Consequently, also the spectrum is scaled and translated by the values $c_1 \in \mathbb{C} \setminus \{0\}$ and $c_0 \in \mathbb{C}$, respectively.

2.4.4 The Spectrum of the Pauli-Jordan Operator for a Causal Set

As a final note on the Pauli-Jordan operator E for a causet, I want to take a look at the spectrum of E. For a finite causet C, the Pauli-Jordan operator is given by a matrix $\boldsymbol{E}$ and the spectrum is the set of its eigenvalues. The multiplicity of the eigenvalue 0 is the dimension of the kernel of E and the number of non-zero eigenvalues (including their multiplicity) determine the dimension N of the solution space $\mathcal{S}(C)$.

Recall from Section 2.3 that E has different discretizations, so here I look into the methods from X, Dowker, and Surya [113] and Dable-Heath, Fewster, Rejzner, and Woods [29] for a 8×8 lattice, see Figure 2.7a. The respective matrices are expressed in terms of the causal matrix $\boldsymbol{C}$ and the link matrix $\boldsymbol{L}$ (see Definition 1.2.13),

$$\boldsymbol{E}_{\mathrm{DSX}} = \frac{1}{2}\left(\boldsymbol{C} - \boldsymbol{C}^{\mathsf{T}}\right), \tag{2.73a}$$

$$\boldsymbol{E}_{\mathrm{2D}} = \frac{1}{4}\left(\boldsymbol{L} + \boldsymbol{C}\boldsymbol{L} - \boldsymbol{L}^{\mathsf{T}} - \boldsymbol{L}^{\mathsf{T}}\boldsymbol{C}^{\mathsf{T}}\right), \tag{2.73b}$$

where $\boldsymbol{E}_{\mathrm{2D}}$ is written as in [29]. The spectra of $\boldsymbol{E}_{\mathrm{DSX}}$ and $\boldsymbol{E}_{\mathrm{2D}}$ are shown in Figure 2.7. Note that the spectra are purely imaginary, hence I only drew the imaginary part in Figure 2.7. When finding the spectrum of a large matrix $\boldsymbol{E}$ with a numerical algorithm, one needs to remember that there might be a numerical inaccuracy or slow convergence that may yield some eigenvalue with a small but non-zero real or imaginary part, which is in fact exactly 0.

All eigenvalues in Figure 2.7 (except for 0) occur once, but are paired with their complex conjugates, so that the spectrum is symmetric around 0 (and the solution

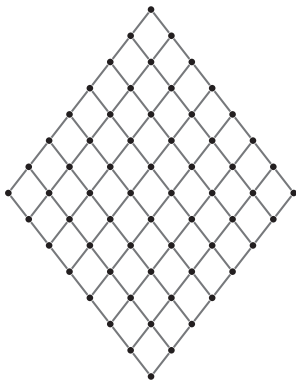

(a) 8×8 lattice

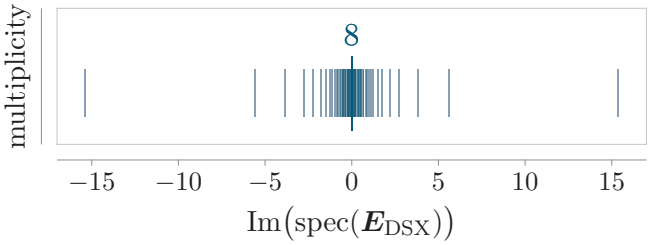

(b) The purely imaginary spectrum of (2.73a).

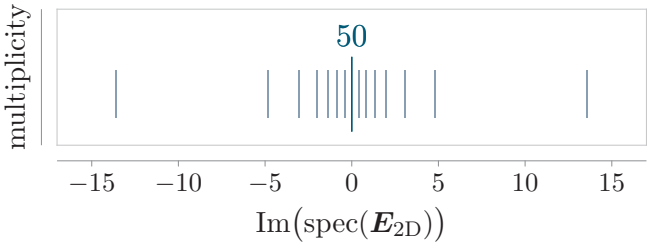

(c) The purely imaginary spectrum of (2.73b).

Figure 2.7: Spectra of two different discretizations of the Pauli-Jordan operator for an 8×8 lattice (a). All spectral values have a vanishing real part and the imaginary parts as shown in the plots, where only the eigenvalue 0 occurs multiple times, 8 times in (b) and 50 times in (c).

space is even-dimensional). For the DSX discretization shown in Figure 2.7b, the eigenvalue 0 has a multiplicity of 8, and in the 2D lattice discretization shown in Figure 2.7c, 0 occurs 50 times. The multiplicity of the eigenvalue 0 is the dimension of the kernel of $\boldsymbol{E}$ under the respective discretization. Because the 2D lattice discretization gives a much larger kernel (at least applied to the regular lattice), this discretization method might overcome the small kernel problem of the DSX method, which led Sorkin [103] to the conclusion that the equations of motion might only hold in an approximate sense by including eigenvectors with eigenvalues close to 0 when constructing the on-shell algebra and the solution space. Note, however, that at this point I cannot make a conclusive statement. It will be necessary to make a more in depth analysis of the newly proposed discretization method and its performance on sprinkled causets.

Chapter 3

Local Structure of Causal Sets

For the discretization of the d'Alembertian in the scalar field equation on causal sets, I reviewed in Section 2.3 a supplementary, local structure called a *preferred past*. Given some causet C, a preferred past structure $\Lambda^- : C \backslash \mathcal{I}^-_{\text{2-layer}} \to C$ is a map that assigns to each event $x \in C \backslash \mathcal{I}^-_{\text{2-layer}}$ an event in its rank 2 past $R^-_2(x)$. Since the rank 2 past is very rarely a singleton for arbitrary causets, we have to make choices when defining a specific preferred past structure. I defined the intervals between events and their rank 2 past events as *diamonds* and specified some diamond properties in Subsection 2.3.2. In the following, let us discuss some methods that may be used to determine a preferred structure intrinsically by selecting diamonds that are unique, at least with high probability on finite causets. To obtain quantitative results and compare causets representing different dimensions, I conducted numerical simulations on Minkowski spacetime of dimension $1+1$ to $1+3$.

3.1 Setup of the Numerical Investigations

For the numerical investigations, the source code was developed with MATLAB and the simulations were conducted on the Viking high performance computing cluster of the University of York. One may find the source code that was used to generate simulation data at my GitHub account [76]. The simulation outputs are raw data files that are further evaluated and charted with the source code provided at a second repository [77].

3.1.1 Sprinkling on Minkowski Spacetime Subsets

For each dimension $d = 1+1$, $1+2$ and $1+3$ of a Minkowski spacetime $\mathbb{M}^d$, consider some pair of events p, q in $\mathbb{M}^d$ that form a non-empty causal interval $U = J^+(p) \cap J^-(q)$. On the subset U, I repeat a *sprinkling process* ten thousand times with a fixed sprinkling density parameter ρ such that each sprinkle has an expected cardinality of six thousand events. The sprinkling process is a Poisson process with uniform probability density over the subset U. More details on sprinkling processes for arbitrary spacetime manifolds will be discussed in Chapter 4.

The described process yields an ensemble of *sprinkles* (individual outcomes of a sprinkling process) that corresponds to a grand-canonical ensemble on U.

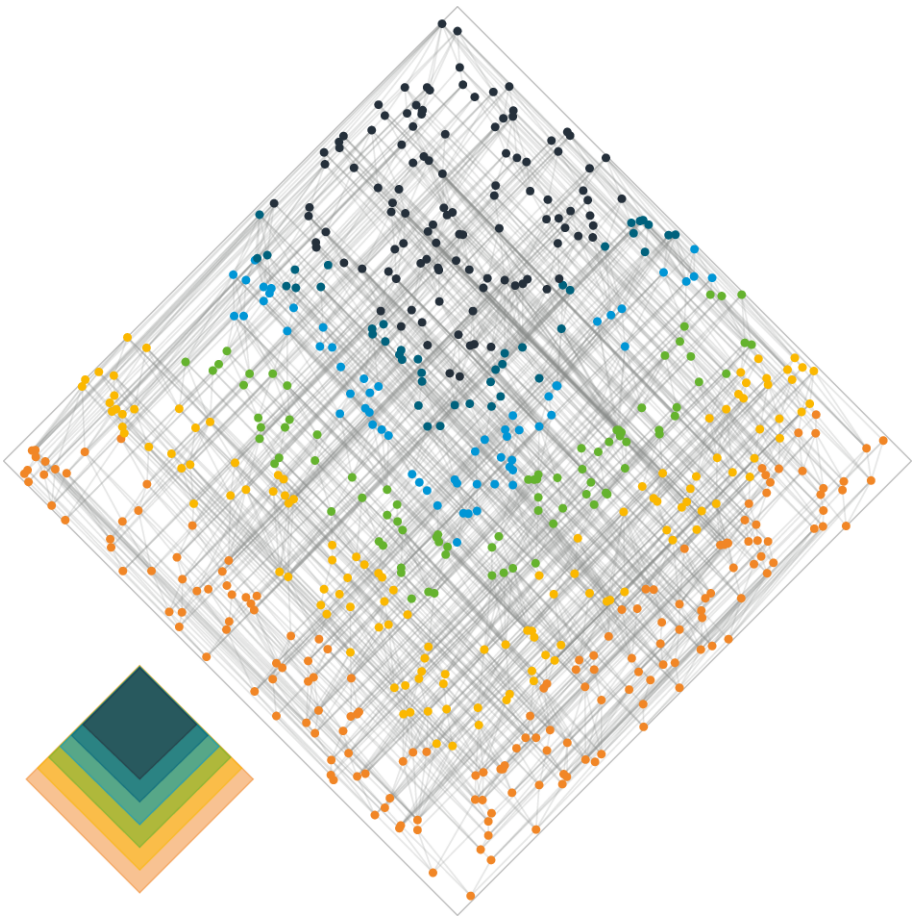

Figure 3.1: Example causal set of 600 events sprinkled in a causal interval of $(1+1)$-dimensional Minkowski spacetime. To analyse the effects of the past infinity, we observe the events that are sprinkled in reduced region U_i, from the entire sprinkling region $i = 0$ (no reduction) up to $i = 5$ (smallest observation region, black shade), $U_5 \subset U_4 \subset U_3 \subset U_2 \subset U_1 \subset U_0 = U$.

For each event x in each sprinkled causet, we consider every event $y \in R_2^-(x)$ in the rank 2 past of x and count the number of perimetral and internal events in the corresponding diamond $[y, x]$. The counts are accumulated over all the ten thousand sprinkles so that we obtain results averaging over tens of millions of rank 2 past events. The implementation of the sprinkling process is given below in Subsection 3.1.2.

Because the sprinkling region U is compact, all sprinkles are finite and we expect effects from the past boundary of U only, because the preferred past structure is a retarded structure. To mitigate these effects, we set up various *observation regions* as subsets of U. For $i \in \{0, 1, \ldots, 5\}$, fix points $p_i \in \mathbb{M}^d$ along the straight line from p to q in $\mathbb{M}^d$ such that the observation regions $U_i = J^+(p_i) \cap J^-(q)$ have a volume

$$V_i = 2^{-di/4} V_0. \tag{3.1}$$

So we obtain 6 regions per causal interval U of Minkowski space to compare. For

each index $i \in \{0, 1, \ldots, 5\}$, we consider all rank 2 past diamonds in U whose future tip is contained in $U_i \subset U$. The sequence of subsets is illustrated in Figure 3.1 with an example sprinkle of six hundred events (one order of magnitude smaller than the actual sprinkles used in the numerical investigations).

3.1.2 Implementation of the Sprinkling Process and Diamond Counting

The sprinkling region is a causal interval U in d-dimensional Minkowski spacetime (where $d \in \{2, 3, 4\}$). Using Lorentz invariance of the sprinkling measure, we may, without loss, take U to be the Cauchy development of a ball of radius R centred a the origin of the $t = 0$ hyper-surface in standard inertial coordinates. A single sprinkle is then obtained in the following steps.

1. Randomly choose the sprinkle cardinality $n \in \mathbb{N}$ according to the Poisson distribution with mean $\langle n \rangle = 6000$.
2. The sprinkle comprises n events, each of which has a spacetime position x chosen independently from a uniform distribution on U w.r.t. the volume measure. This is achieved by setting

$$x = \left(t_{\text{sign}}(1-h)R, rR\frac{\vec{v}}{|\vec{v}|} \right), \tag{3.2}$$

   where:

   a) $t_{\text{sign}} \in \{-1, 1\}$ is the uniformly chosen sign of the time coordinate.

   b) $h = u_h^{1/d}$ is determined by a uniformly distributed random number $u_h \in [0, 1]$.

   c) $r = h u_r^{1/(d-1)}$ is the radial scaling determined by a uniformly distributed random value $u_r \in [0, 1]$.

   d) $\vec{v} \in \mathbb{R}^{d-1}$ is a vector with components that are independently chosen from a normal distribution with zero mean and unit variance, such that the resulting normalised vectors $\vec{v}/|\vec{v}|$ are uniformly distributed on the unit $(d-2)$-sphere.

This procedure is repeated ten thousand times to results from millions of data points.

The source code (given in [76]) is divided in individual MATLAB functions, which are called in sequence from wrapper functions. A list of the individual functions with a short description is shown in Table 3.1. After a set of data files is created with these routines, the MATLAB functions listed in the second repository [77] are used to evaluate the raw data and generate plots with the LaTeX TikZ data visualization tools.

File name	Short description
causet_new_sprinkle.m	Generates a matrix of coordinates for n events for a d-dimensional sprinkling region of a specified shape (here: 'bicone') using a specified pseudo-random number stream. It also returns information about the events in the regions U_i as described above.
metric_flat.m	$d \times d$ matrix as metric of d-dimensional Minkowski spacetime with signature $(+, -, -, \ldots)$.
causet_edit_relate.m	Causal matrix for a sprinkled causet determined by the event coordinates and the metric.
causet_get_links.m	Computes the link matrix from the causal matrix.
causet_find_Aset.m	Events in the causal interval of an event pair.
causet_find_infsteps.m	Events in the k-step past/future infinity.
causet_find_layer.m	Events in the k-th past/future layer of an event.
causet_find_linkgeodesics.m	Searches for all maximal paths between a pair of events.
causet_find_preftimes.m	Rank 2 past selection for an event that has past/future diamonds with specified numbers of perimetral and internal events — all w.r.t. a criterion (see Subsection 3.2.2).
causet_get_statistics.m	Main function that goes through the list of criteria and analyses all rank 2 past events for every causet event of a single sprinkle. It computes probability distributions for the multiplicity of past diamonds and their proper time separation, their distribution along the past hyperboloid and more, for all diamonds in a region U_i as well as for every criterion individually.
ensemble_get_statistics.m	Repeats causet_get_statistics.m for a specified number of iterations, each with a new random sprinkling. Additionally to the diamond statistics in each region U_i for $i \in \{0, 1, \ldots, 5\}$, it analyses the diamonds along one timelike geodesic (maximal path) through each entire sprinkle.
runjobs_generate_statistics.m	Wrapper function that is called by a script from the computing cluster and executes ensemble_get_statistics.m for a small number of sprinkling runs, while other instances of the same function call may run in parallel. Each of these calls saves the data to an individual job file.
runjobs_combine_statistics.m	Combines the data of the ten thousand sprinkles distributed to several hundred or thousand job files to a single dataset for each dimension $d \in \{2, 3, 4\}$ after all jobs are completed.

Table 3.1: List of MATLAB functions and their short description that are published in the GitHub repository [76]. Some helper and older test functions are omitted here, but are described in the repository.

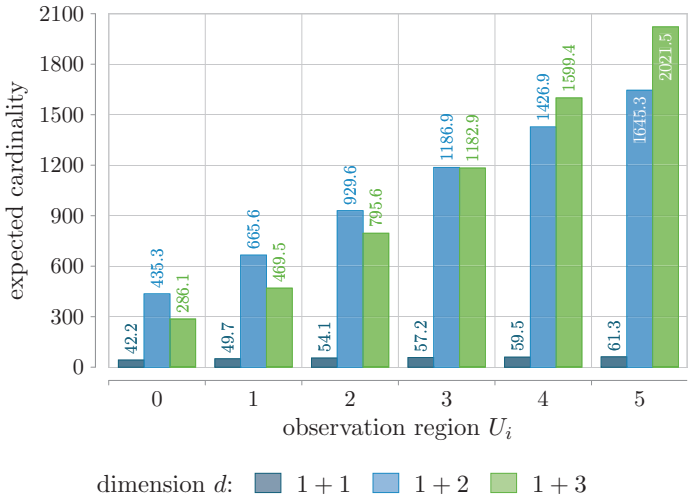

Figure 3.2: Expected cardinality of the rank 2 past for a random event x that is not in the 2-layer past infinity of a sprinkle on the closed interval U of $(1+1)$- (darkest blue shade), $(1+2)$- (lighter blue shade), and $(1+3)$-dimensional Minkowski spacetime (lightest/green shade). For all dimensions, the expected cardinality of $R_2^-(\mathsf{x})$ increases with the observation region U_i from $i = 0$ to $i = 5$.

3.2 Subsets of the Rank 2 Pasts

We want to determine some methods to select subsets of the rank 2 past that are singleton for each event of a causet, at least with high probability. First, we take a look at the expected size of the rank 2 past for an arbitrary event in a sprinkled causet within the numerical setting discussed above. Second, we motivate and formulate criteria to select subsets of the rank 2 pasts in Subsection 3.2.2, and show that the subsets selected by the criteria are non-empty in Subsection 3.2.3.

3.2.1 Cardinality of the Rank 2 Pasts and Desired Selection Qualities

Let C be a causet with expected cardinality of six thousand events, sprinkled in the causal interval of Minkowski spacetimes in dimension $d \in \{2, 3, 4\}$ as described above. A random event $\mathsf{x} \in C \setminus \mathcal{I}^-_{\text{2-layer}}$ (not in the 2-layer past infinity) has a rank 2 past with an expected cardinality as shown in Figure 3.2. We can see that the expected cardinality of the rank 2 past $R_2^-(x)$ grows with the cardinality of the past $J^-(x)$ for all three dimensions d, since the past of x becomes larger with decreasing volume (increasing index i) of the observation region U_i. In arbitrary large sprinkles, this growth is unbounded and events in infinite causal sets typically have infinitely many links to their past, thus also infinitely many elements in the rank 2 past.

Even though the rank 2 past of an event in a sprinkled causet can be very large even for finite causets, we may distinguish the rank 2 past events by the number

of perimetral and internal events in the corresponding past diamonds. In this way, we will be able to select a singleton subset with high probability (at least for finite causets).

Below we set out six methods for selecting a subset $S(x) \subset R_2^-(x)$ for each event $x \in C \setminus \mathcal{I}^-_{\text{2-layer}}$. The first criterion was proposed in Dable-Heath, Fewster, Rejzner, and Woods [29], while the others are newly introduced. We compare the subsets $S(x)$ selected by each method so that we can identify the one that performs best in relation to three qualitative measures:

- the selected sets $S(x)$ should be singletons with high probability, across all points x in each sprinkle in the ensembles studied
- the distribution of proper time separations between x and the event(s) in $S(x)$ should have low variance and small expectation value, across the ensembles as before
- the distribution of the unit-normalized separation vectors between x and the event(s) in $S(x)$, should be approximately uniformly distributed on the unit hyperboloid, across each ensemble.

The third of these is intended to ensure Lorentz invariance of the preferred past structure, in a statistical sense, in the limit of large sprinkles.

3.2.2 Criteria for Selecting Rank 2 Past Subsets

Again, let C be one of the sprinkled causets in one of the ensembles. Consider any event $x \in C \setminus \mathcal{I}^-_{\text{2-layer}}$ and any of its rank 2 past events $y \in R_2^-(x)$. All the past diamonds $[y, x]$ can be grouped by their number of minimal paths $\text{prm}(x, y)$ and their number of internal events $\text{itn}(x, y)$ as given in Definition 2.3.3. We introduce 6 criteria that select events in the rank 2 past whose corresponding diamonds have a specific size (and a specific number of internal events). We evaluate these selection criteria against the desirable features described before.

To begin, define some notation. For any causet event $x \in C \setminus \mathcal{I}^-_{\text{2-layer}}$, let

$$D^-_{\max \text{prm}}(x) := \underset{y \in R_2^-(x)}{\arg\max} \Big(\text{prm}(x, y) \Big) \tag{3.3}$$

denote the set of events y in the past of x with past diamond of maximal number of perimetral events. Here, arg max (and similarly arg min) of a function yields the set of points of the function domain, where the function becomes maximal (or minimal, respectively). Let

$$D^-_{\text{pure}}(x) := \Big\{ y \in R_2^-(x) \;\Big|\; \text{itn}(x, y) = 0 \Big\} \tag{3.4}$$

be the set of events corresponding to pure past diamonds only. We now set out the six criteria that are compared in our simulations. For $i \in \{1, 2, \ldots, 6\}$, rule i selects a subset $D^-_{\text{crit}\,i}(x) \subset R_2^-(x)$ of the rank 2 past of each event $x \in C \setminus \mathcal{I}^-_{\text{2-layer}}$.

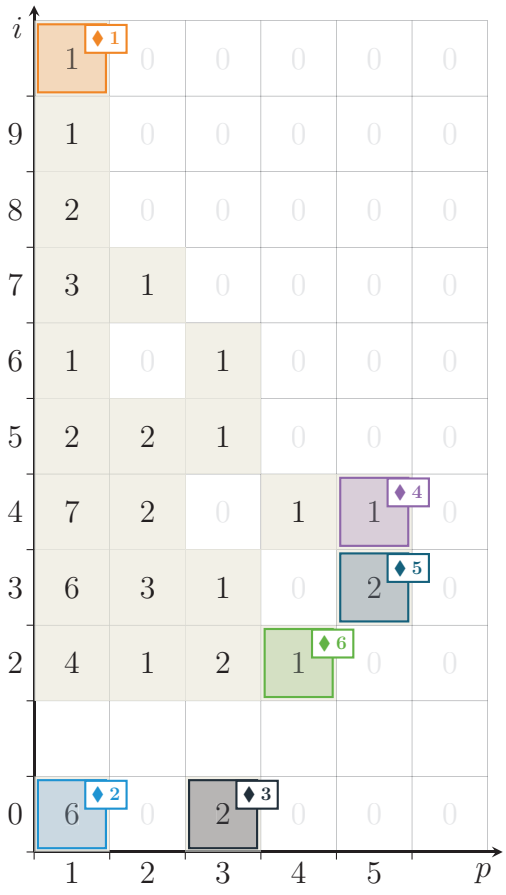

Figure 3.3: Example matrix of the number of past diamonds for an event in a sprinkled causet to demonstrate the six criteria. The p-axis labels the number of perimetral points and the i-axis represents the number of internal events (note that diamonds with one internal event do not exist). Thus, in this example there are seven diamonds with one perimetral and four internal events. The selection for each of the six criteria is labeled. Criterion 6, in particular, picks one of the singletons (which are the ones in this matrix).

To motivate our first criterion, consider a regular lattice as depicted in Figure 2.3 for dimensions $d = 2$ and $d = 3$, which has an obvious choice of a preferred past for every element x characterized as the largest past diamond (as labelled by $\Lambda^-(x)$ in the graphics). As discussed in Section 2.3, this preferred past structure yields a good approximation to the d'Alembertian in the continuum limit. So the first criterion comprising those $y \in R_2^-(x)$ such that the diamond $[y, x]$ is one of

◆ **1** the largest diamonds ("maximal layer rule" proposed in [29]),

$$D^-_{\text{crit }1}(x) := \underset{y \in R_2^-(x)}{\arg\max} \Big|[y, x]\Big|. \tag{3.5}$$

For the sprinkled causets, it will turn out that choosing the largest diamond is not the best criterion, since it tends to yield a very large proper time separation between x and y that is only limited by the finite past cardinality of x in our simulation (as expected from the discussion of the size of the rank 2 past in arbitrarily large sprinkles in Subsection 3.2.1). In order to get the smallest proper time, we consider

◆ **2** the smallest diamonds,

$$D^-_{\text{crit }2}(x) := \underset{y \in R_2^-(x)}{\arg\min} \Big|[y, x]\Big|. \tag{3.6}$$

We will see that these diamonds correspond to the smallest proper time separation, but they are not unique for regular lattices (see Figure 2.3) nor for typical events in a sprinkled causet. In further criteria, we consider maximizing and minimizing the diamond properties of the number of internal and perimetral events. Physically, perimetral events of a diamond $[y, x]$ in the sprinkle are points that fall very close to the boundary of the causal interval from y to x within $\mathbb{M}^d$, while internal events form time-like paths between these two events. As the d'Alembertian describes the propagation of light, we want to maximize the number of perimetral events, so I consider

♦ **3** the largest (or maximal perimetral) pure diamonds,

$$\begin{aligned} D^-_{\text{crit }3}(x) &:= \underset{y\in D^-_{\text{pure}}(x)}{\arg\max} \Big|[y,x]\Big| \\ &= \underset{y\in D^-_{\text{pure}}(x)}{\arg\max} \Big(\text{prm}(x,y)\Big); \end{aligned} \tag{3.7}$$

♦ **4** the diamonds with the most internal events among the diamonds with the most perimetral events,

$$D^-_{\text{crit }4}(x) := \underset{y\in D^-_{\max \text{prm}}(x)}{\arg\max} \Big(\text{itn}(x,y)\Big); \tag{3.8}$$

♦ **5** the diamonds with the least internal events among the diamonds with the most perimetral events,

$$D^-_{\text{crit }5}(x) := \underset{y\in D^-_{\max \text{prm}}(x)}{\arg\min} \Big(\text{itn}(x,y)\Big). \tag{3.9}$$

It might be expected that criterion 4 does not perform the best as it yields diamonds that may also contain a larger number of internal events. This presumption will be supported by the comparison of the results for criteria 3–5. Criteria 3 and 5 can still be refined and we suggest one possible improvement, which will give even better results. The sixth criterion is designed to combine the best features of criteria 3 and 5. Our results will show that criterion 5 selects a single rank 2 past event with high probability, but its proper time distribution has a large variance. On the other hand, criterion 3 yields a prominent peak for the proper time separation, but with a lower probability of selecting a singleton. This suggests the following rule:

♦ **6** Consider the sets of rank 2 past events y so that $[y, x]$ contains $i \in \mathbb{N}$ internal events and $p \in \mathbb{N}_*$ perimetral events,

$$D^-_{i,p}(x) := \Big\{ y \in R^-_2(x) \;\Big|\; \text{itn}(x,y) = i, \text{prm}(x,y) = p \Big\}. \tag{3.10}$$

If there is at least one singleton among (3.10), then choose the singleton with the indices

$$j(x) := \min\Big\{ i \in \mathbb{N} \;\Big|\; \big|D^-_{i,p}(x)\big| = 1 \Big\}, \tag{3.11a}$$

$$q(x) := \max\Big\{ p \in \mathbb{N}_* \;\Big|\; \big|D^-_{j(x),p}(x)\big| = 1 \Big\} \tag{3.11b}$$

to minimize the number of internal events first and then maximize the number of perimetral events. Only if there is no singleton, $j(x) = \infty$, take the same subset as criterion 5,

$$D^-_{\text{crit}\,6}(x) := \begin{cases} D^-_{j(x),q(x)}(x), & \text{if } j(x) < \infty, \\ D^-_{\text{crit}\,5}(x), & \text{otherwise.} \end{cases} \tag{3.12}$$

The sixth criterion yields events that correspond to diamonds with a size between the size of the diamonds selected by criteria 3 and 5. If criterion 3 selects a singleton, criterion 6 selects the same singleton. The subset selected by criterion 6 is only non-singleton if there is no singleton among all the subsets (3.10), so that it selects the same subset as criterion 5. Note that this list of criteria is not exhaustive and one might consider further criteria determined by other diamond properties.

Notice that similar criteria could be considered for subsets of the rank 2 future $R^+_2(x)$ for any causet event $x \in C \setminus \mathcal{I}^+_{\text{2-layer}}$. The statistics for rank 2 future subsets are equivalent to the statistics for rank 2 past subsets, because of the time symmetry for the causal intervals of Minkowski spacetimes and the invariance of sprinkling probability.

3.2.3 Non-Emptiness of the Selected Subsets

All criteria presented above yield non-empty subsets of the rank 2 past for all events outside the 2-layer past infinity, see Figure 3.3 for an example, and below for the proofs.

Note that a causet event that is not part of the 2-layer past infinity has a non-empty rank 2 past, so I can make the following arguments.

Lemma 3.2.1. *If $x \in C \setminus \mathcal{I}^-_{\text{2-layer}}$ for some causet C, then $R^-_2(x)$ contains at least one event that spans a pure diamond with x.*

Proof. Take any event $y_0 \in R^-_2(x)$. Either $[y_0, x]$ is pure or it contains internal events including at least one event y_1 that is also two links in the past of x, $y_1 \in R^-_2(x)$. The diamond $[y_1, x] \subset [y_0, x]$ is either pure or contains yet another internal event that is also in the rank 2 past, $y_2 \in R^-_2(x)$. This process may be repeated until it terminates (because $[y, x]$ is finite) leading to a past diamond

$[y_i, x]$ with $y_i \in R_2^-(x)$ for some $i \in \mathbb{N}$ such that the diamond has no internal events (it is pure). □

For example, the two smallest diamonds (the 1- and the 2-diamond) are pure. Out of the two possible 3-diamonds, one is pure and the other contains a 1-diamond, and so on.

Proposition 3.2.2. *Let $x \in C \setminus \mathcal{I}^-_{\text{2-layer}}$ for some causet C. All subsets of its rank 2 past that are determined by the six criteria (defined in Sec. 3.2.2) are non-empty.*

Proof. Non-emptiness of the subsets for criteria 1 (largest diamonds) and 2 (smallest diamonds) is a direct consequence of the fact that the functions

$$\arg\max_{y \in R_2^-(x)} \Big|[y, x]\Big| \qquad \text{and} \qquad \arg\min_{y \in R_2^-(x)} \Big|[y, x]\Big|$$

are taken over the non-empty set $R_2^-(x)$. For criterion 3 (largest pure diamonds), we consider the subset of pure diamonds only, which is non-empty as shown in Lemma 3.2.1, so that the arg max function yields again a non-empty subset. Criteria 4 and criteria 5 take the extrema of two properties in succession, so that their selections are non-empty. Finally, criterion 6 yields either a singleton or the same result as criterion 5 if there are no singletons among all subsets $D^-_{i,p}(x)$ as defined in (3.10). Any singleton is by definition non-empty and we have just shown that the rank 2 past subset given by criterion 5 is non-empty as well. So in summary, all criteria yield a non-empty subset of rank 2 events for any causet event that has a non-empty rank 2 past. □

3.3 Comparison of the Diamond Criteria

In this section, we compare the six criteria according to the 3 qualities listed in the previous section. For each of the Minkowski spacetimes of dimensions $1+1$, $1+2$ and $1+3$, the sprinkling ensemble is a set of ten thousand sprinkled causets, each with a cardinality of six thousand events.

3.3.1 Cardinality of the Rank 2 Past Subsets

Figure 3.4 displays the size distribution of the sets selected by each criterion, in dimensions $1+1$ (top), $1+2$ (middle) and $1+3$ (bottom), using observation region U_2 with volume (3.1) to mitigate edge effects. To indicate how the results depend on the observation region, each bar is accompanied by horizontal red and black lines corresponding to the values that would be obtained if observing the entire sprinkling region U_0, or the smallest region U_5, respectively. Note that the

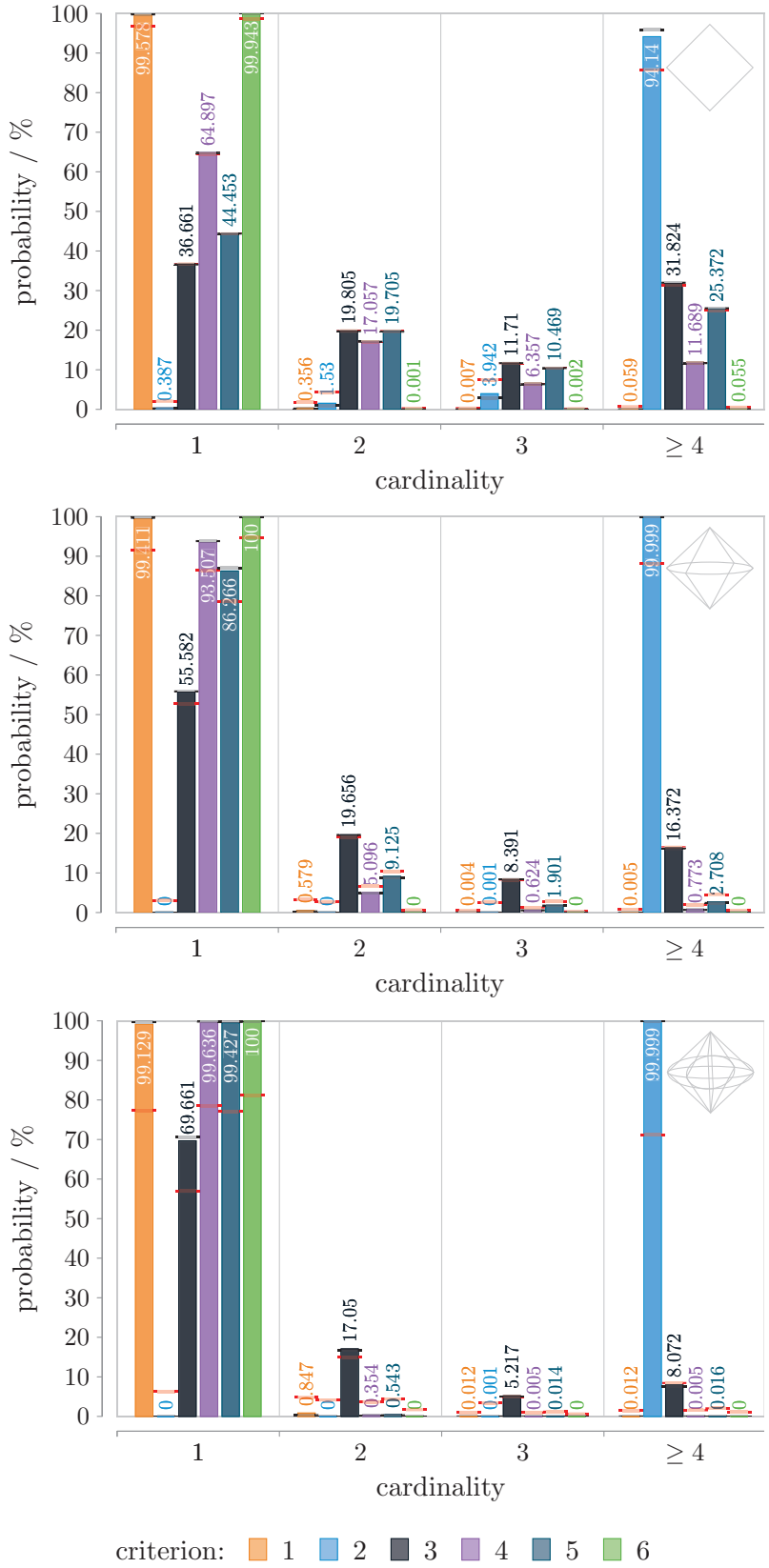

Figure 3.4: Probability distributions for the cardinality of the subset of the rank 2 pasts that are selected by the six criteria, observed for the region U_2. The spacetime dimension increases from top to bottom. The horizontal lines across each column indicate the value obtained using the entire sprinkling region U_0 in red and the smallest observation region U_5 in black.

latter deviates less from the bar than the former, indicating that edge effects are substantially ameliorated when using U_2, even though the influence of the past infinity increases with dimension.

The probability of selecting a singleton (unique rank 2 past event) increases with the spacetime dimension to almost certainty at dimension $1+3$ for all criteria but the second and third criterion. The third criterion, selecting the rank 2 past events associated to the largest pure diamonds, also shows an increase in the probability for a unique preferred past with increasing spacetime dimension, but for about 30% of the events there is still more than one rank 2 past event selected at dimension $1+3$. The second criterion selects mostly the 1-diamonds that are formed by a single 3-path (smallest possible diamond), so that the number of rank 2 past events is very large and, furthermore, increases with the spacetime dimension. The first criterion performs very well across our results for all three dimensions. Criterion 6 selects a singleton if and only if there is at least one singleton among the subsets (3.10) for any $i \in \mathbb{N}, p \in \mathbb{N}_*$. The chance to find an event in region V_2 for which criterion 6 selects more than one rank 2 past event is almost as low as 1 in 925,000 for dimension $1+2$. For the observation region U_2 in dimension $1+3$, criterion 6 selects a singleton with certainty within our numerical accuracy, so that the probability to find a non-singleton is less than 10^{-7}.

Criterion 6 has the highest probability to select a unique rank 2 past event, followed in order by criteria 1, 4, 5, 3, 2, where criteria 1, 4, and 5 are equally good at dimension $1+3$.

3.3.2 Proper Time Separation for the Rank 2 Past Subsets

In the numerical setup, we fixed the sprinkling density ρ such that the expected cardinality of sprinkled causets in the sprinkling region U of d-dimensional Minkowski spacetime is six thousand events. Since each sprinkled causet is embedded in U, we can compare the statistics of proper time separation measured in length units $\sqrt[d]{1/\rho}$ between sprinkled events and their rank 2 past events selected by each criterion. The results are shown in Figure 3.5. Once again, we display the proper time distributions in dimensions $d = 1+1$ (top), $d = 1+2$ (middle) and $d = 1+3$ (bottom) for all selected past diamonds of the events in observation region U_2.

Criteria 4 and 5 yield proper time distributions that broaden with increasing spacetime dimension, while the peaks of criteria 2, 3, and 6 are more pronounced and get sharper with increasing spacetime dimension. The maxima of the probability distributions for 2, 3, and 6 roughly stay at the same position, meaning that the time increment by the corresponding diamonds is very similar across the dimensions. Heuristically, this means that a "diamond" clock ticking with the rate given by any of the preferred pasts constructed from the criteria 2, 3, or 6 is

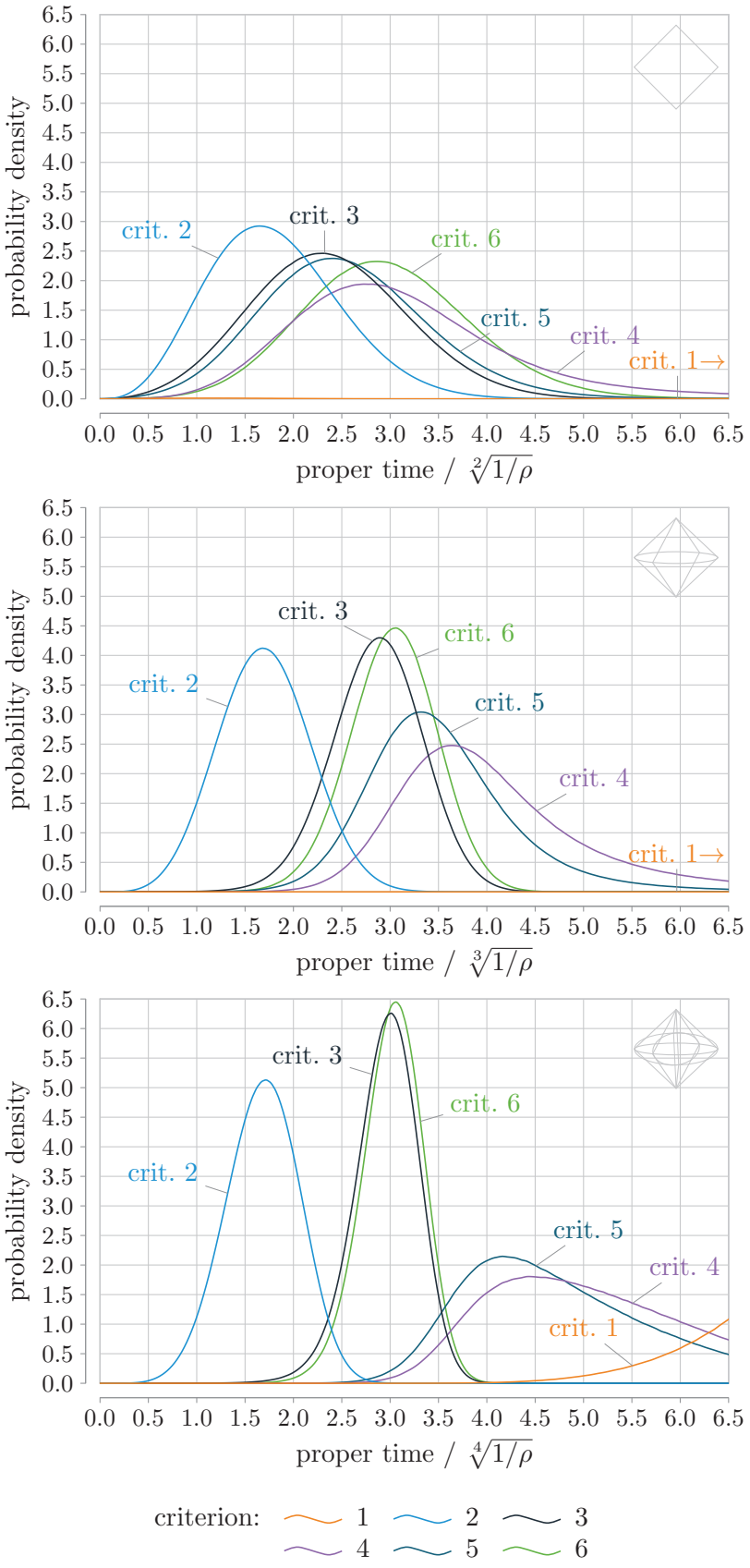

Figure 3.5: Probability distributions for the proper time separations between each causet event and its preferred past, according to the six criteria. The histograms have a bin size of a twentieth of the time scale $\sqrt[d]{1/\rho}$.

independent of the emergent dimension at macroscopic scale (at least for the three spacetime cases investigated here).

In $(1+3)$-dimensional Minkowski space, about 70% of the subsets selected by criterion 3 (largest pure diamonds) are singleton (see Figure 3.4) so that the same subsets are selected by criterion 6 as well. Other singletons selected by criterion 6 span diamonds with almost the same size. This is reflected in very similar proper time distributions for criteria 3 and 6 in dimension $1+3$.

Criterion 1 yields the worst result here, since the diamonds corresponding to the rank 2 past events in $D^-_{\text{crit}\,1}(x)$ (for a causet event $x \in C \setminus \mathcal{I}^-_{\text{2-layer}}$) can have any size almost up to the entire past of x in C. In Figure 3.5, the probability densities for criterion 1 reach their maxima at approximately 37 for dimension $d = 1+1$, at 14.5 for dimension $d = 1+2$ and around 7.2 for dimension $d = 1+3$ in units $\sqrt[d]{1/\rho}$, thus falling far beyond the plotting range of the proper time axes.

When looking at the proper time separation, we find that criterion 6, followed by criterion 3 and 2 perform best giving a probability distribution with relatively low expectation value and variance.

3.3.3 Distribution of the Rank 2 Past Subsets along the Unit Hyperboloid

Even though discrete subset of Minkowski spacetime, like any sprinkle, break Lorentz symmetry, the entire configuration space for the spacetime (see details in Chapter 4) is Lorentz invariant since it includes all transformed versions of the sprinkle. If the distributions of rank 2 past events selected by most criteria are uniform in the limit of large sprinkles, the selected subsets tend to be Lorentz invariant. We check this by viewing the relative coordinates $(x_0, x_1, \dots)$ of all rank 2 past events $D^-_{\text{crit}\,n}(x)$ corresponding to the criterion n with respect to each event x (positioned at the origin in these relative coordinates) and project it onto the unit past hyperboloid, i.e. dividing by the proper time separation

$$\tau = \sqrt{x_0^2 - r^2}, \qquad \text{where} \qquad r^2 = \sum_{i=1}^{d-1} x_i^2. \tag{3.13}$$

For example, see the scatter plots for criteria 1 and 6 at dimension $1+2$ in Figure 3.6. The data points in the scatter plots are shaded corresponding to the observation region U_i ($i \in [2,5]$) to which the event x belongs. These plots suggest, by eye, that the events selected by criterion 1 tend to cluster around the central point on the unit hyperboloid while those selected by criterion 6 are more uniformly distributed. This is investigated more systematically in the following and shown in Figure 3.7 for a single sprinkled causet of each ensemble.

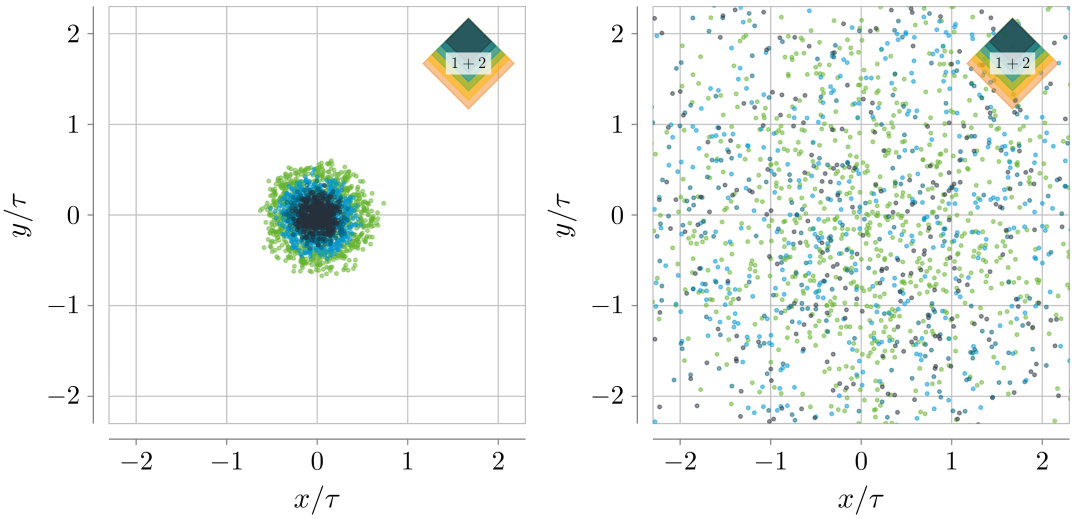

(a) Criterion 1 in dimension 3

(b) Criterion 6 in dimension 3

Figure 3.6: Scatter plots of the rank 2 past events distributed along the unit hyperboloid for dimensions $1+2$ and all observation regions U_i ($i \in [2,5]$ from lighter to darker shades, green, blue, dark blue, black) for criteria 1 (a) and 6 (b). Both plots are for single sprinkles with about six thousand events.

In order to obtain the graphs of Figure 3.7, we define the rescaled coordinate ρ_d such that its differential $\mathrm{d}\rho_d$ describes equal volume slices along the radial direction of the unit hyperboloid. It is the product of the volume of the unit $d-2$ sphere S_{d-2} and the integral over the hyperbolic radius up to the value $u' = \operatorname{arsinh}(r/\tau)$,

$$\rho_d = S_{d-2} \int_0^{u'} \sinh^{d-2}(u)\, \mathrm{d}u. \tag{3.14}$$

Evaluate these integrals to find ρ_d as function of the normalized radial coordinate r/τ,

$$\rho_{1+1} = 2 \operatorname{arsinh} \frac{r}{\tau}, \tag{3.15a}$$

$$\rho_{1+2} = 2\pi \left(\sqrt{1 + \left(\frac{r}{\tau}\right)^2} - 1 \right), \tag{3.15b}$$

$$\rho_{1+3} = 4\pi \left(\frac{1}{4} \sinh\left(2 \operatorname{arsinh} \frac{r}{\tau}\right) - \frac{1}{2} \operatorname{arsinh} \frac{r}{\tau} \right). \tag{3.15c}$$

Note that the hyperbolic radius $u' = \operatorname{arsinh}(r/\tau)$ is the rapidity (with respect to the inertial coordinates) of the inertial motion connecting the point on the hyperboloid to the origin.

All criteria but the first yield a constant distribution falling off at values close to the outer boundary of the sprinkling region at dimensions $1+1$ and $1+2$. Boundary effects at dimension $1+3$ are more pronounced, so that we only have criteria 2, 3, and 6 with a close to uniform distribution. Criterion 1 has a strong

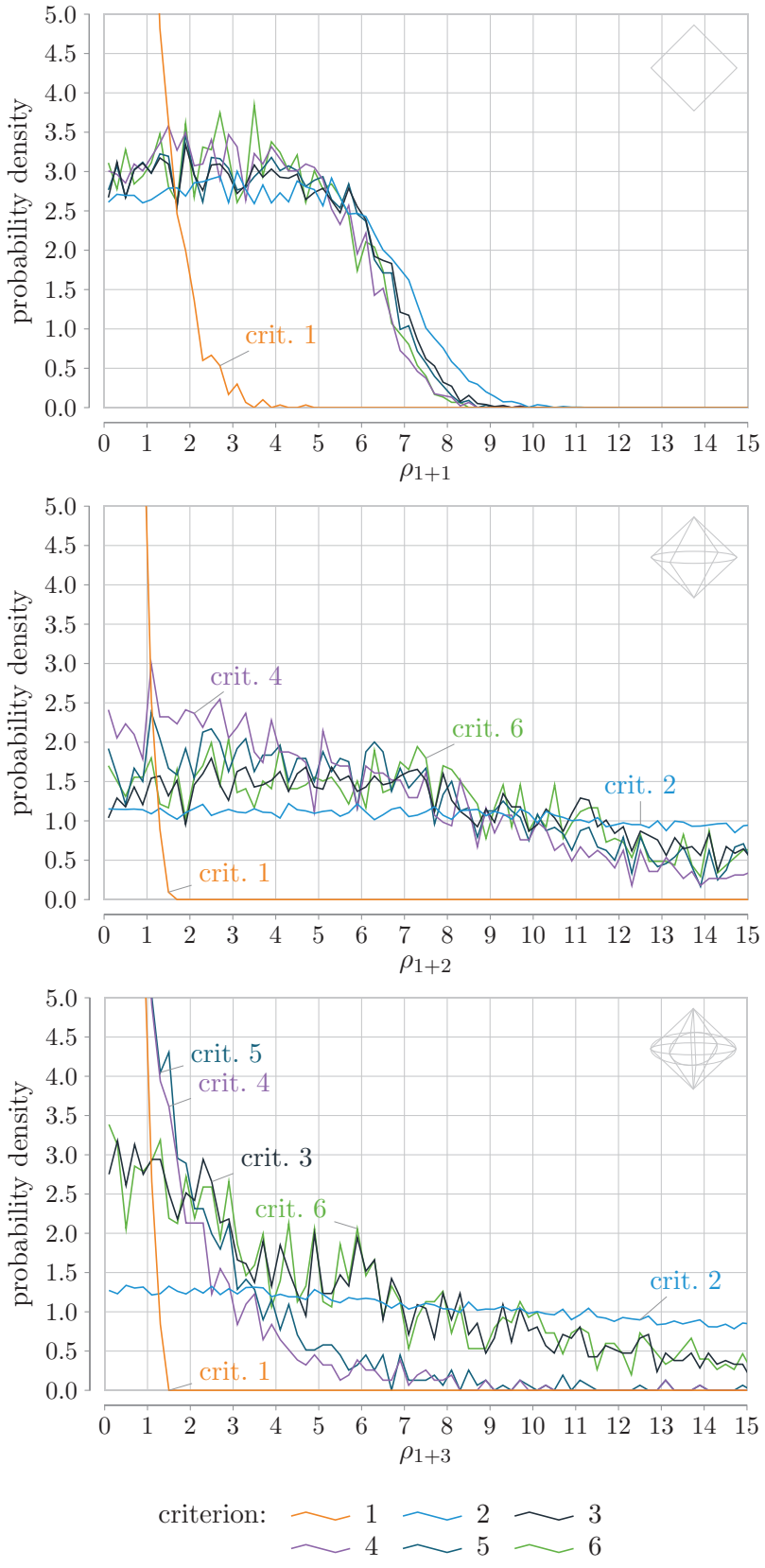

Figure 3.7: Probability distributions of the rank 2 past subsets projected onto the unit hyperboloid, for all six criteria at observation volume U_2 for a single sprinkle (of about six thousand events) in Minkowski spacetime of dimension $1+1$ (top), $1+2$ (middle) and $1+3$ (bottom).

bias to select rank 2 events close to the central point on the unit hyperboloid for all investigated Minkowski spacetimes, because the selected events correspond to the largest diamond so that they tend to be as close as possible to the bottom tip of the entire sprinkling region U. Comparing similar plots for all observation regions U_i (not shown), we find that the distributions are getting more and more homogeneous from $i = 0$ to $i = 5$, except for criterion 1, which concentrates more and more around the origin when decreasing the observation region.

In combination of the characteristics, we find that criterion 6 has the highest probability for a unique rank 2 past event, while also yielding a sharply peaked proper time distribution with a maximum at low proper time separation, and tend to give a uniform distribution along the unit hyperboloid. The next part of this section is focused on this criterion only.

3.3.4 Diamond Sizes for Criterion 6

The analysis presented in the previous part of the section indicates that criterion 6 has the best performance among those studied. We proceed to investigate criterion 6 in more depth by computing the resulting distribution of diamond sizes spanned between the causet event x and the elements of $D^-_{\mathrm{crit}\,6}(x)$. The plots in Figure 3.8 show the probability distribution of the diamond size. The plot legends list the actual size of the respective observed volumes as fraction of the entire sprinkling region. In brackets, we denote the fractions of the causets that are within the observation regions and have a non-empty rank 2 past.

Note the change of the histograms when reducing the observation region U_i from $i = 0$ (light/orange shade) to $i = 5$ (black shade), because the diamonds that are getting smaller towards the past infinity are excluded. Especially for $d = 1+3$, the reduction from observation region U_0 to the first smaller region U_1 causes a strong increase in the diamond sizes.

Figure 3.8 indicates that the expectation value of the distributions shifts to larger values with increasing dimension. This is shown quantitatively in Figure 3.9, where I extended the numerical analysis to Minkowski spacetimes of dimensions $1+4$ and $1+5$. For each dimension, I compute the roots of the standardized momenta of the diamond sizes from the probability function $p_{\mathrm{crit}\,6}(k)$ (see Figure 3.8): the expectation value k_{ex}, square root of the variance (standard deviation) k_{std}, and cube root of the skewness k_{skew},

$$k_{\mathrm{ex}} := \sum_{k=0}^{\infty} p_{\mathrm{crit}\,6}(k)k, \tag{3.16a}$$

$$k_{\mathrm{std}} := \left(\sum_{k=0}^{\infty} p_{\mathrm{crit}\,6}(k)\Big(k - k_{\mathrm{ex}}\Big)^2\right)^{\frac{1}{2}}, \tag{3.16b}$$

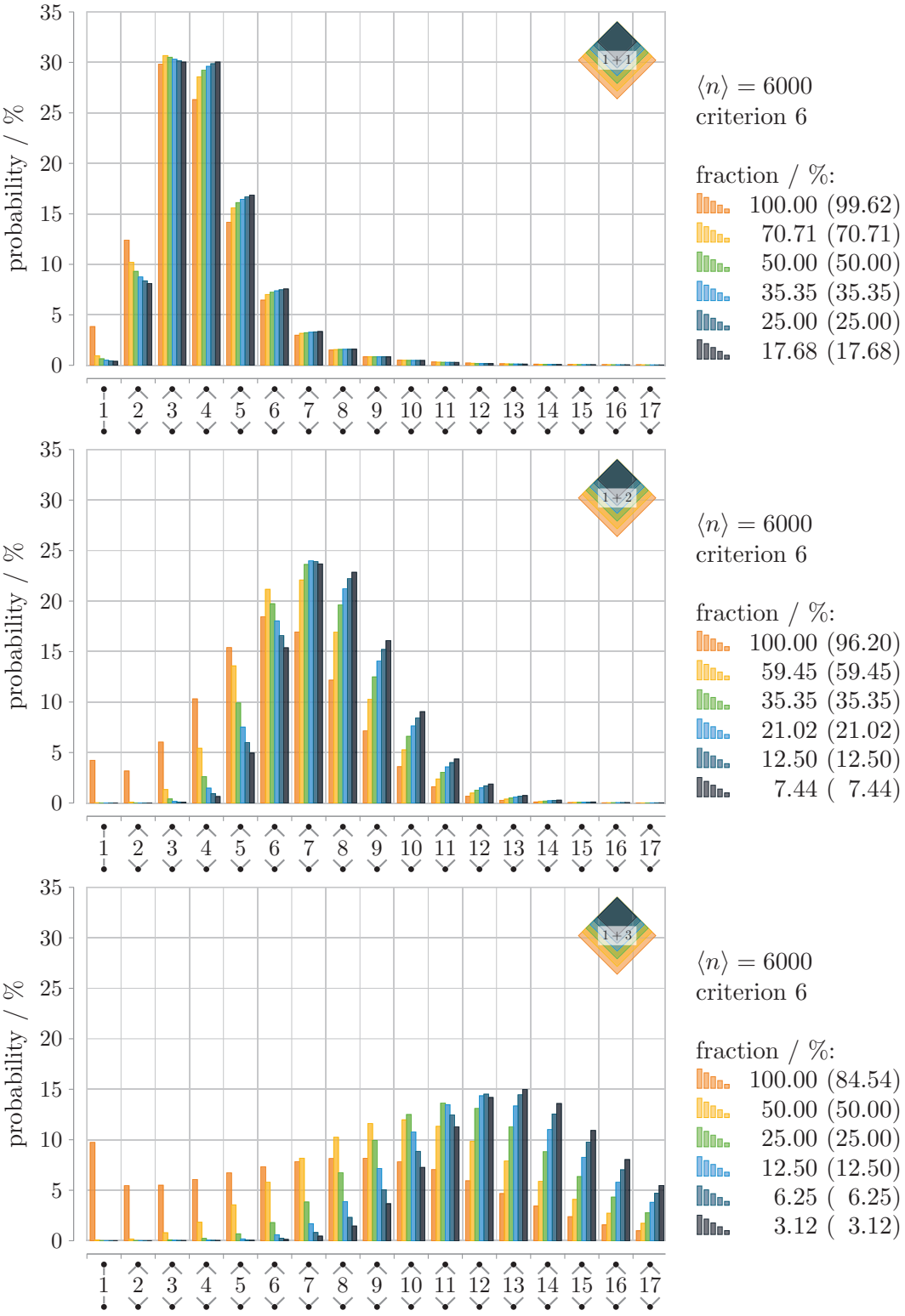

Figure 3.8: Probability distribution of diamond cardinalities and how they change by shrinking the observed region U_i from $i = 0$ (light/orange shade) to $i = 5$ (black shade). The plot legends show the observation volume (and causet fraction that has at least one preferred past). The spacetime dimension increases from $1 + 1$ (top plot) to $1 + 3$ (bottom plot). Along the horizontal axis, the histogram bins are labelled by the diamond size.

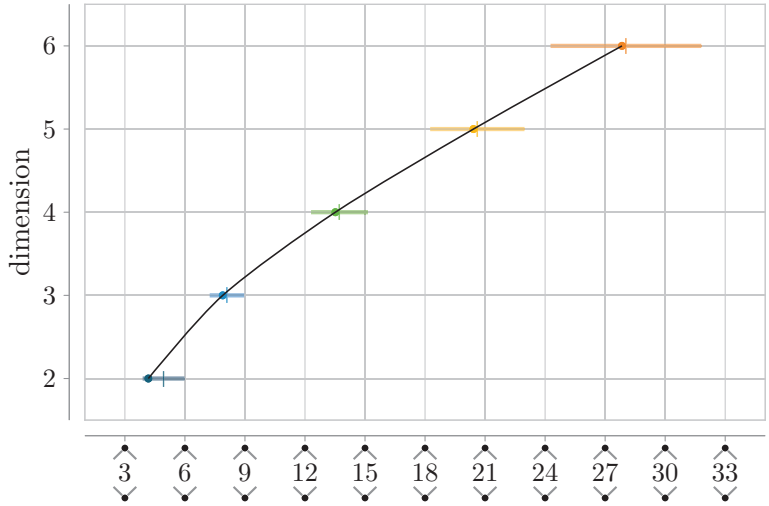

Figure 3.9: Sizes of diamonds with their tip in observation region U_5 (black bars in Figure 3.8) for criterion 6 and Minkowski spacetime dimensions from $1+1$ (dark blue) to $1+5$ (orange). The expectation value is marked by a circle and the square root of the variance (standard deviation) is depicted as a horizontal line. The line extends by one standard deviation to the right and by one to the left from the center that is marked by a small vertical line. The horizontal offset from the circle mark to the vertical line mark is a quarter of the cube root of the skewness.

$$k_{\text{skew}} := \frac{1}{k_{\text{std}}} \left(\sum_{k=0}^{\infty} p_{\text{crit}\,6}(k) \Big(k - k_{\text{ex}} \Big)^3 \right)^{\frac{1}{3}} . \tag{3.16c}$$

Recall from the lattice discretization of the d'Alembertian discussed in Subsection 2.3.1 that the lattice diamond size k_{lat} is related to the spacetime dimension by $k_{\text{lat}} = 2(d-1)$. While the plot in Figure 3.9 shows an increase of the expected diamond size with increasing dimension d, the expected diamond size in the sprinkles is larger than the value corresponding to the lattice discretization. The increase in Figure 3.9 is also not quite linear, so that a generalization of the lattice discretization to sprinkled causal sets with a preferred past structure selected by criterion 6 might only work approximately. However, the generalization of the lattice method to sprinkled causets requires a more detailed investigation that goes beyond the scope of my simulations. To get a more in-depth analysis, it will be necessary to compare solutions of the field equations on a spacetime manifold with the solutions of the discretized field equations for sprinkled causets on the same manifold.

3.4 Diamonds along Timelike Geodesics

I also investigated the diamond size and its expected proper time separation in more generality. In Fewster, Hawkins, Minz, and Rejzner [38], we considered the

maximal paths between the events with the minimal and maximal time coordinates of a given sprinkle in U. Such paths are analogous to timelike geodesics and may be regarded as potential observer trajectories. We computed the expected diamond size and proper time separation between next-to-nearest neighbours along such paths.

In the following, I improve upon our results published in [38]. The ensemble size of ten thousand sprinkles per dimension gave sufficient data to obtain the results presented before. However, for the additional results of the geodesic paths, the ensemble size of ten thousand sprinkles was rather small yielding stronger random noise in the results. I chose an equal expected sprinkling cardinality across all dimensions so that the geodesics in dimension $1+1$ had a length about one order of magnitude larger than the geodesics in dimension $1+3$. This resulted in fewer data points in dimension $1+2$ and yet even fewer in dimension $1+3$ and might have elongated or compressed the distributions for the proper time separation by diamonds. Another potential imprecision might have been caused by the fact that we chose the start and end events of the geodesics via the minimal and maximal coordinate time, respectively. Thus the time distributions might have a slightly elongated tail compared with randomly chosen start and end points.

To avoid these (potential) problems, I modified the setup such that the geodesic paths have roughly the same length across all dimensions and with more data points in higher dimensions. It will turn out, however, that our original results were quite similar and the improved results shown below yield primarily smoother plots (due to the larger amount of data points).

3.4.1 Modified Numerical Setup

Similarly to the previous setup described in Section 3.1, I consider sprinkles on causal intervals of Minkowski spacetime. I do not only investigate the dimensions $d = 1+1$, $1+2$ and $1+3$ as before, but I also include the dimension $1+4$. The sprinkling density will be set such that the length of maximal paths is roughly 11 for any dimension, meaning that each geodesic gives about nine data points for the diamonds of next-to-nearest neighbouring events along the path. For each sprinkle in the four ensembles, two events, a start and end event, are uniformly chosen at random from events that are present in sub-regions at the top and bottom of the sprinkling region, as highlighted (orange) in Figure 3.10 for a sprinkle in 2-dimensional Minkowski spacetime.

As in the previous setup, I chose standard coordinates with the origin in the center of the region and the tips at coordinates $\left(\pm\tau/2, 0, 0, \dots\right)$ where τ is the proper time separation by the causal interval. The start and end region of the geodesics are determined by causal intervals between the region's tips and the

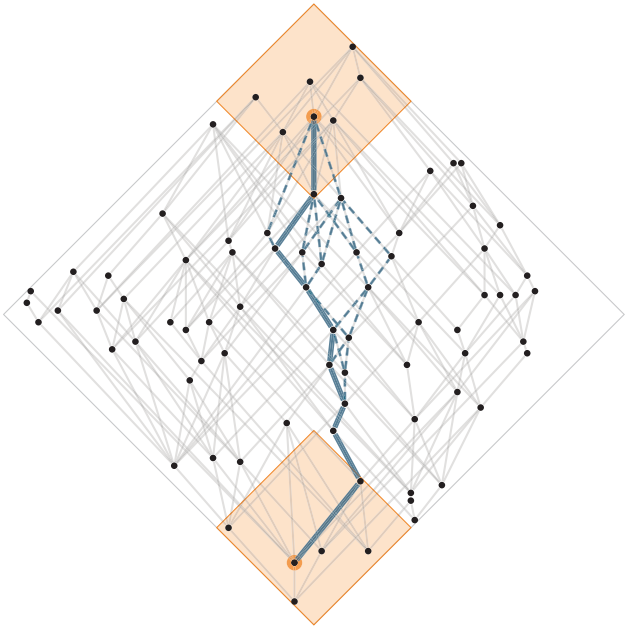

Figure 3.10: Sprinkle of 80 events in a causal interval of $(1+1)$-dimensional Minkowski spacetime. A start event and an end event (orange) are uniformly chosen at random from a subregion (shaded, orange) in the past and future of the sprinkling region. The geodesics connecting both events are drawn with dashed line and one (uniformly chosen at random) is shown with a solid line (blue).

dimension d	2	3	4	5
expected cardinality $\langle N \rangle$	80	440	2420	13310
number of sprinkles	1×10^7	5×10^6	6.25×10^5	1.4×10^5
total computation time / h	54	638	2279	24497
fail rate / %	0.081	0.048	0.029	0.017
start fail rate / %	0.040	0.024	0.015	0.006
end fail rate / %	0.041	0.024	0.014	0.011
expected start count	7.84	8.30	8.79	9.30
expected end count	7.84	8.30	8.80	9.30
expected geodesic length	11.32	11.40	11.15	10.89

Table 3.2: The first three rows list the input parameters for the modified simulations. The seven rows below the middle line show the results: the total computation time in hours adding the computation times of CPU cores that ran in parallel on the Viking cluster (at the University of York), the fail rates as the percentage of sprinkles without an event in the start or end region, the expected number of events in the start and end region, and the expected length of the maximal paths between the uniformly chosen start and end event for the sprinkles (among those sprinkles that did not fail to have a geodesic in the described setup).

points $\left(\pm(\tau/2 - \tau_{\text{sub}}), 0, 0, \dots\right)$ with

$$\tau_{\text{sub}} = 0.035 \sqrt[d]{N} \tau. \tag{3.17}$$

The start and end event are chosen uniformly at random from the events that fall within the respective sub-region, (orange) circled events in Figure 3.10.

The parameters are chosen as listed in Table 3.2. Even though the sub-regions for the start and end of the geodesics contain an expected number of 7 to 9 events (see next-to-last rows in Table 3.2), one or even both of these might be empty for

a given sprinkle. In such a case, the sprinkle is counted as "failed" — Table 3.2 shows the fail rates in per cent.

Note that it is very likely that there are more than one geodesic between the start and end events for a given sprinkle. Consider the pure diamonds between next-to-nearest neighbours along the geodesic drawn with a solid line in Figure 3.10. From past to future, these diamonds have sizes: 1, 1, 1, 2, 2, 1, 3, 1. At every diamond with size larger than 1, there is another choice of maximal path. Additionally there can be even more geodesics following a different set of events. Figure 3.10 shows all possible paths with dashed lines. Thus in the following results, I distinguish between two cases. In one case, I consider all geodesics for the chosen start and end point, and in a second case, I uniformly choose only one of all the possible geodesics at random.

3.4.2 Results for the Diamonds and Their Proper Time Separation

In the following, I discuss the diamond results for the described setup in dimensions 2–5. Note that all diamonds are pure, since the timelike geodesics are the maximal paths.

Figure 3.11 shows the probability distributions of the diamond sizes and their proper time separations between the next-to-nearest neighbour events along all geodesics. The histograms of the diamond sizes in Figure 3.11a are sorted from dimension 2–5, with different shades (and colors) for each dimension. Pictograms of the sprinkling regions and the geodesics are included in the top right-hand corners. All histograms peak at 1-diamonds and are roughly the same for the sprinkles in the causal intervals of Minkowski spacetimes in dimensions 2–5. An observer travelling along a geodesic path in a causet might be unable to identify the spacetime dimension from the local structure of diamonds, when they analyse the diamonds along a short timelike geodesic.

Because each sprinkle is embedded, I have coordinates to assign a proper time separation to the diamonds and thus determine a ticking rate of a 'diamond clock' for an observer following a geodesic path, see Figure 3.11b. The expectation values are marked with dashed lines and listed in Table 3.2. In units where $\rho = 1$, the expected proper times are quite close and a clock that is ticking in accordance with the diamonds shows a similar time passing along an equal path length (number of diamonds) in all dimensions. The distributions of the proper time separation are also very similar to the results for criterion 2 in dimension 2, see Figure 3.5, since that criterion selects the smallest diamonds. However, here I observe almost the same statistics for the timelike geodesics in all dimension (from 2–5). This evidence supports the discussion from Carlip [27] suggesting a dimensional reduction to dimension 2 for an observer in causal set theory at very small scales.

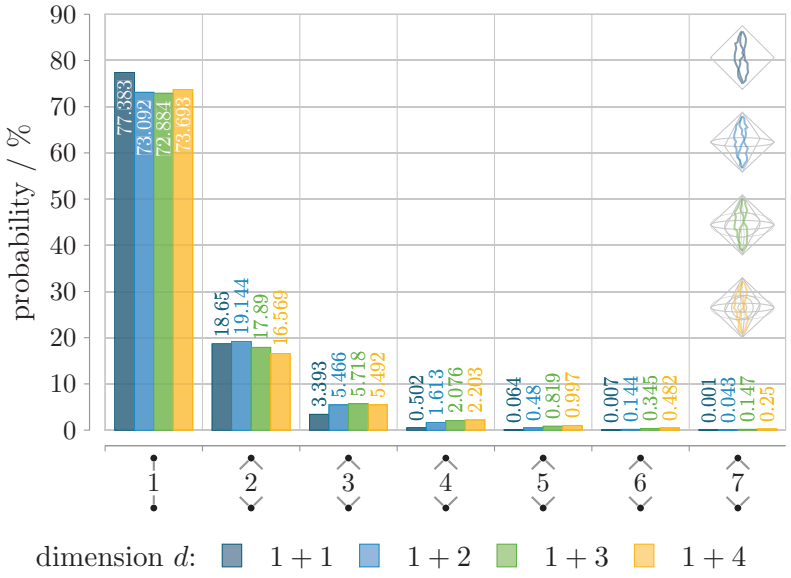

(a) Probability distribution of the diamond sizes

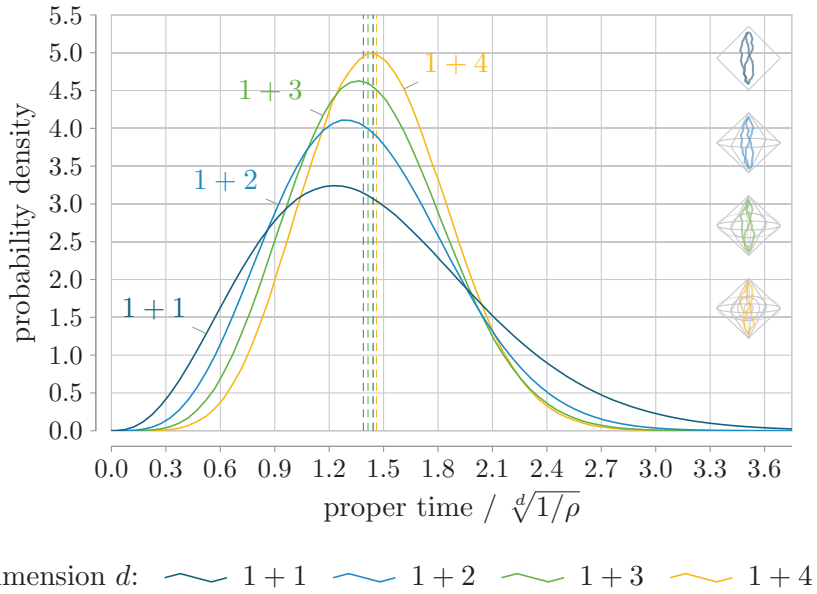

(b) Probability distribution of the proper time separations in sprinkling units $\sqrt[d]{1/\rho}$

Figure 3.11: Probability distributions for the diamonds along *any* of the geodesics connecting one start with one end event in the sprinkles.

dimension d	2	3	4	5
all geodesics in [38]	1.236	1.193	1.278	
all geodesics	1.442	1.388	1.414	1.461
single geodesic	1.407	1.324	1.335	1.374

Table 3.3: Expected values for the proper time separation between next-to-nearest neighbour diamonds along geodesics in sprinkling units $\sqrt[d]{1/\rho}$. The first row shows the previous results obtained for geodesics between the events with minimal and maximal time coordinate in six thousand event sprinkles published in [38].

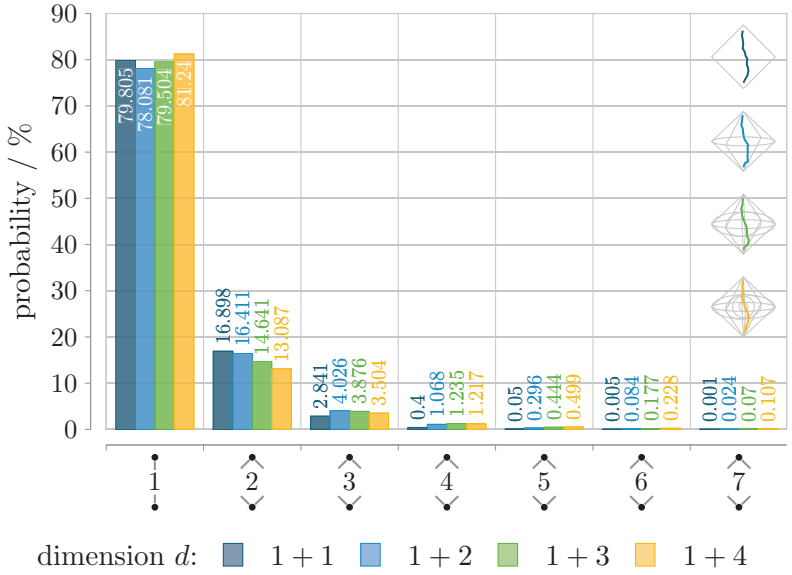

(a) Probability distribution of the diamond sizes

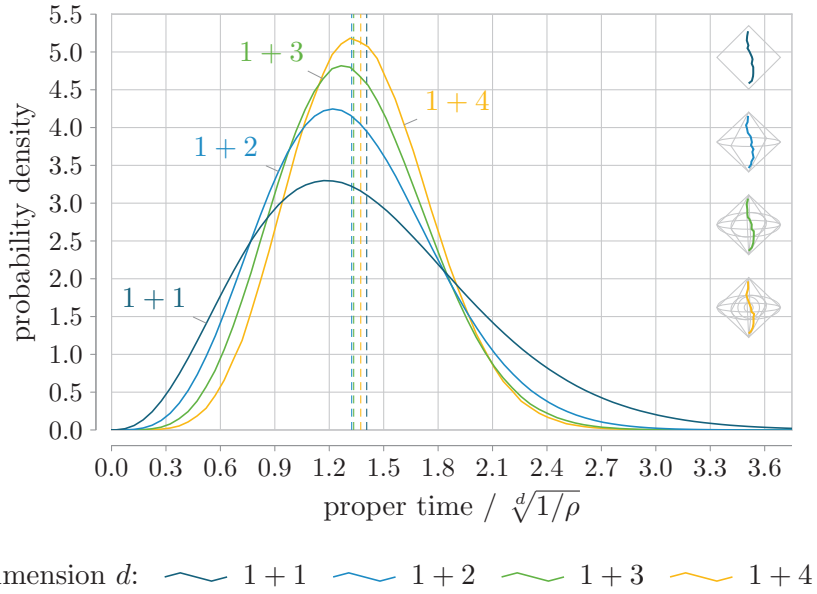

(b) Probability distribution of the proper time separations in sprinkling units $\sqrt[d]{1/\rho}$

Figure 3.12: Probability distributions for the diamonds along a *single* geodesic per sprinkle (uniformly chosen at random) connecting one start with one end event.

Most diamonds are likely to be counted many times in the results in Figure 3.11, since the data includes *all* geodesics between the fixed start and end event (per sprinkle). In contrast, Figure 3.12 shows the results of a similar analysis, but now only for one geodesic per sprinkle, uniformly chosen at random. The single geodesic results are very similar to the previous results that considered all geodesics. However, there are minor differences. Most remarkably, the probability for the (pure) k-diamonds is largest when $k = d$ (for the investigated dimensions from

2–5). One may extend the results to the trivial case of dimension 1, where all diamonds are 1-diamonds (with probability 1).

The expected proper times for all geodesics and a single geodesic per sprinkle are very similar, shown in the last two rows of Table 3.2. One row above, the table also shows the results from our publication [38] where we took the average over ten thousand sprinkles, each with the same expected cardinality of six thousand for the dimensions 2 to 4 (see description of the numerical setup in Section 3.1). In the paper, we found expected path lengths of 137.4 events in $(1 + 1)$-, 26.2 events in $(1 + 2)$-, and 8.1 events in $(1 + 3)$-dimensional Minkowski spacetime. The expected path length in dimension 4 given there is shorter than 11 despite an almost 3 times larger sprinkle cardinality — compared to the cardinality 2420 for dimension 4 in the setup discussed here. However, the expected lengths in the paper were calculated indirectly via the diamond count, while the new expected lengths (see last two rows of Table 3.2) are now directly measured which gives more accurate results.

In summary, the similar expected proper times across all (investigated) dimensions is consistent with the idea of a dimensional reduction to dimension 2 at very small length scales discussed in Carlip [27], and Abajian and Carlip [1]. However, at this point, I cannot make a conclusive argument, since I only conducted sprinkles on Minkowski spacetimes in dimensions 2–5 and I did not include a more detailed comparison with other method that are used to estimate the dimension (like the Myrheim-Meyer estimator [82, 65]).

Chapter 4

Causal Set Sprinkling on Spacetimes

Let us start this chapter by constructing the probability space for sprinkling on any globally hyperbolic spacetime. Afterwards, we consider applications of the Poisson probability measure to compute the expectation values of past infinity cardinalities in sprinkled causets, and to compute the expectation value for the proper time separation of diamonds as functions of the diamond size in Minkowski spacetimes of arbitrary dimension. However, the precise construction of the probability space may also find other applications. For example, it may facilitate a more general discussion of the continuum limit of causal sets, like previously considered for compact spacetime manifolds in Bombelli [15].

4.1 The Sprinkling Process

Throughout this section, let M be a fixed d-dimensional spacetime manifold with metric g. The Poisson process called sprinkling randomly selects a finite subset as a causal set from the spacetime M, see Sorkin [101]. For the construction of a probability space for the sprinkling process, we need to find a space of "possible outcomes", an appropriate class of measurable subsets (a σ-algebra), and a probability measure.

We review the sample space of sprinkling on M and compact subsets of the manifold $U \subset M$ based on the considerations by Albeverio, Kondratiev, and Röckner [4]. This framework was constructed for applications in quantum theory (see Albeverio, Kondratiev, and Röckner [3]) but, as we will see, may be applied to causal set theory. The construction provides a Borel σ-algebra over the configuration space and leads to the discussion of the Poisson probability measure for the subsets U and the entire manifold M. For an introduction to Poisson processes, see also Kingman [53].

4.1.1 Sprinkling Probability Spaces

In the literature, the term 'sprinkling' is used to refer to the random Poisson process as well as to an element of the configuration space [101]. Here we want to make the notions more distinct and put the sprinkling process in a more formal language.

Definition 4.1.1. The **sprinkling configuration space** is the set of all locally finite subsets of M,

$$Q := \{S \subset M \mid \forall \text{ compact } U \subset M : |S \cap U| < \infty\}. \tag{4.1}$$

A **sprinkle** is an element of Q and the Poisson process is called **sprinkling** on M.

To find the σ-algebra $\mathrm{B}\sigma(Q)$ over this configuration space — the space of subsets of Q to which we can assign a probability — first, consider a compact subset $U \subset M$ and notice that the σ-algebra is constructed from open subsets so that it is similar to a topological space. The sprinkling configuration space Q_U for U is the (disjoint) union of configuration spaces $Q_{U,n}$ with fixed cardinalities n,

$$Q_{U,n} := \{S \subset U \mid |S| = n\}, \tag{4.2}$$

$$Q_U = \bigcup_{n=0}^{\infty} Q_{U,n}. \tag{4.3}$$

The n-fold Cartesian product U^n has the n-fold product topology. Let F_n denote the fat diagonal of the Cartesian product, which is the subset of all n-tuples that have at least one pair of identical elements. Deleting F_n, we obtain the configuration space of n *indistinguishable* points in U,

$$\widetilde{Q}_{U,n} := U^n \setminus F_n, \tag{4.4}$$

with the subspace topology. As there is no physical significance to the order in which a set of spacetime events is listed, the configuration space $Q_{U,n}$ is the image of

$$\begin{aligned} \Sigma_{U,n} : \widetilde{Q}_{U,n} &\to Q_{U,n}, \\ (x_1, x_2, \ldots, x_n) &\mapsto \{x_1, x_2, \ldots, x_n\}, \end{aligned} \tag{4.5}$$

which maps all $n!$ permutations of some n-tuple to the same set of n events. So the configuration space $Q_{U,n}$ is the quotient by the n-th symmetric group acting on the n-tuples and endowed with the quotient topology induced by $\Sigma_{U,n}$. Taking the disjoint union over n, see (4.3), we find the disjoint union topology on Q_U and the Borel σ-algebra $\mathrm{B}\sigma(Q_U)$. Finally, the inverse limit over all configuration spaces Q_U leads to the Borel σ-algebra $\mathrm{B}\sigma(Q)$.

So far, we have the configuration space Q with the Borel σ-algebra. For the probability space $(Q, \mathrm{B}\sigma(Q), \mu)$, it remains to specify the Poisson probability measure

$$\mu : \mathrm{B}\sigma(Q) \to [0, 1] \tag{4.6}$$

that corresponds to the sprinkling process on M with a given positive constant that we call the *sprinkling density* ρ. The measure restricted to any compact subset $U \subset M$ is determined by the metric induced volume measure on the spacetime (M, g). For every measurable spacetime subset $O \in \mathrm{B}\sigma(M)$ the volume measure ν assigns a positive real value

$$\nu(O) := \int_O \sqrt{|\det g|}\, \mathrm{d}^d x \tag{4.7}$$

(including the metric factor in some coordinate chart). The sprinkling measure is defined using the product measure ν^n for subsets of the Cartesian product U^n and its push-forward by the map $\Sigma_{U,n}$.

Definition 4.1.2. The **Poisson (probability) measure** μ_U with **sprinkling density** ρ **on any compact subset** U of the manifold M with volume measure ν assigns a probability to each subset in $\mathrm{B}\sigma(Q_U)$ such that for every $n \in \mathbb{N}$ and $B_n \in \mathrm{B}\sigma(Q_{U,n})$

$$\mu_U(B_n) = \mathrm{e}^{-\rho\nu(U)} \frac{\rho^n}{n!} \nu^n \left(\Sigma_{U,n}^{-1}(B_n)\right). \tag{4.8}$$

where $\Sigma_{U,n}^{-1}$ denotes the pre-image by (4.5).

Note that the exponential factor normalizes μ_U to a probability measure so that $\mu_U(Q_U) = 1$. The sprinkling process on M is obtained by an inverse limit over the measures μ_U for all compact subsets $U \subset M$ as an application of the Hahn-Kolmogorov theorem so that the Poisson measure μ is uniquely determined by the measure family of μ_U for all U, see Parthasarathy [86, Thm. 4.2]. It is a measure μ on Q with the following property: for all compact subsets $U \subset M$ and all $B \in \mathrm{B}\sigma(Q_U)$,

$$\mu(B_U) = \mu_U(B), \tag{4.9a}$$

$$\text{where} \qquad B_U := \{S \in Q \mid S \cap U \in B\}. \tag{4.9b}$$

It is shown in Albeverio, Kondratiev, and Röckner [4, Sec. 2.2] that the following integral formula holds

$$\int_Q \exp\left(\sum_{x \in S} f(x)\right) \mathrm{d}\mu(S) = \exp\left(\rho \int_M \left(\mathrm{e}^{f(x)} - 1\right) \mathrm{d}\nu(x)\right) \tag{4.10}$$

for every compactly supported, continuous function f on M, where the integral on the left-hand side runs over all sprinkles $S \in Q$. This provides an alternative definition of μ; see Albeverio, Kondratiev, and Röckner [4, Sec. 2] for more details.

In summary, this construction yields the probability spaces $\left(Q_U, \mathrm{B}\sigma(Q_U), \mu_U\right)$ for all compact subsets $U \subset M$ and $\left(Q, \mathrm{B}\sigma(Q), \mu\right)$ for any spacetime manifold (M, g).

n	$a(n)$
0	1
1	1
2	2
3	5
4	**16**
5	63
6	318
7	2045
8	16999
9	183231
10	2567284
11	46749427
12	1104891746
⋮	⋮

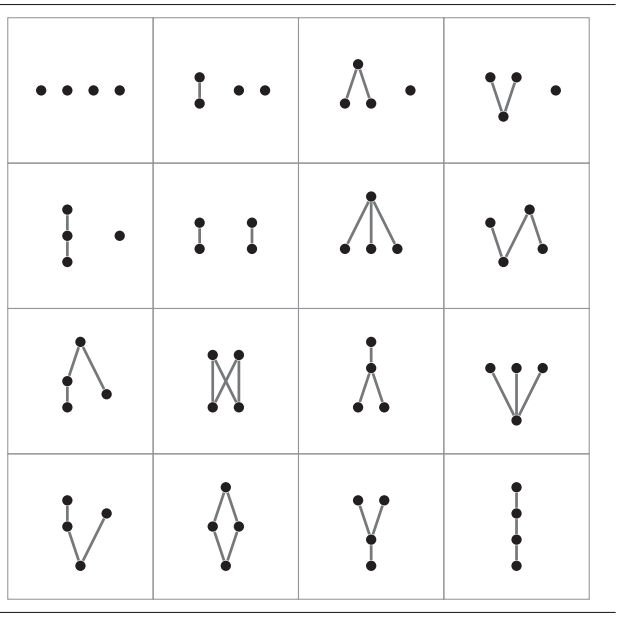

Table 4.1: First elements of the integer sequence A000112: number of partial ordered sets (posets) with n indistinguishable elements. The Hasse diagrams for all possible 4-event causets are shown on the right.

4.1.2 Causet Isomorphism Classes

For all sprinkles $S \in Q$ and all events $x, y \in S$, the partial order $x \preceq_S y$ is the causal relation of the spacetime manifold $(M, \preceq_M)$ restricted to the subset S,

$$x \preceq_S y \Leftrightarrow x \preceq_M y. \tag{4.11}$$

Two sprinkles are isomorphic, denoted by the symbol $\sim$, if there exists a bijection between them that preserves the causal relation. The sprinkles $S \in Q$ that are isomorphic to a given causet $(C, \preceq)$ form an isomorphism class $[C] \subset Q$, which is the set of all possible sprinkles in M that are isomorphic to C.

For every compact subset $U \subset M$, any sprinkle $S \in Q_U$ has a finite cardinality $|S|$ and, for any fixed cardinality n, there is a finite number $a(n)$ of distinct causet isomorphism classes, forming an integer sequence labelled as A000112 in the On-Line Encyclopedia of Integer Sequences [85]. A closed expression for the term $a(n)$ of this sequence is unknown, but the first sixteen terms have been computed, see Brinkmann and McKay [21] — and the first twelve terms are given in Table 4.1. To the right of the table, we show all $a(n) = 16$ causets for $n = 4$ as Hasse diagrams. For cardinalities up to 5, one can embed every causet in a causal interval of $(1 + 1)$-dimensional Minkowski spacetime. Among the 318 causets with cardinality six, there are three causets that cannot be embedded in $(1 + 1)$-dimensional Minkowski spacetime, shown in Figure 4.1. The crown causet (shown in the middle of Figure 4.1) may be seen as light propagating along the exterior of

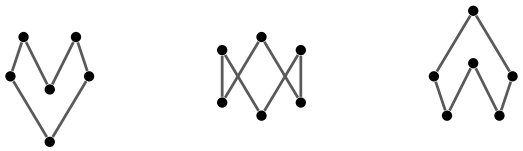

Figure 4.1: The three causets with six events that do not embed in $(1+1)$-dimensional Minkowski spacetime.

a regular 2-simplex, from the three vertices (represented by the three past events) to the centres of the edges that connect the vertices (represented by the three future events). I made animations for the crown causet (including an event for the 2-face of the 2-simplex) as well as for the other two causets shown in Figure 4.1, which are available under the links [69, 70, 71]. The causets of Figure 4.1 can be spotted repeatedly as the fundamental constituent of the causets in Figure 2.3b and Figure 2.5.

I denote a random sprinkle that arises from sprinkling into U with density ρ by $\mathsf{S} \in Q_U$ using a sans-serif font. If the sprinkle with the causal relation $\preceq_M$ is isomorphic to a given $(C, \preceq)$, I write $(\mathsf{S}, \preceq_M) \sim C$, or simply $\mathsf{S} \sim C$ for short. The probability for a random sprinkle to be isomorphic to C is

$$\Pr(\mathsf{S} \sim C) = \mu_U\Big([C]_U\Big). \tag{4.12}$$

Here we use the fact that any causet isomorphism class $[C]_U$ is a measurable set in $\mathrm{B}\sigma(Q_U)$ (ultimately due to the causal relation describing a closed subset of Q_U). For example, the causet $\mathfrak{:}$ (two causally related events) has equivalence class

$$[\mathfrak{:}]_U = \Big\{\{x_1, x_2\} \in Q_U \;\Big|\; x_1 \prec x_2\Big\}, \tag{4.13}$$

with pre-image

$$\Sigma_{U,2}^{-1}\Big([\mathfrak{:}]_U\Big) = \Big\{(x_1, x_2) \in \widetilde{Q}_{U,2} \;\Big|\; (x_1 \prec x_2) \vee (x_2 \prec x_1)\Big\} \tag{4.14}$$

in $\widetilde{Q}_{U,2}$. Using (4.6) and the label permutations $\sigma_{12} = \{(1,2),(2,1)\}$, the probability of sprinkling a causal set of this type into U is

$$\begin{aligned} \Pr\left(\mathsf{S} \sim \mathfrak{:}\right) &= \mu_U\Big([\mathfrak{:}]_U\Big) && \text{(4.15a)} \\ &= \mathrm{e}^{-\rho\nu(U)}\frac{\rho^2}{2!}\sum_{(i,j)\in\sigma_{12}}\int_U \mathrm{d}\nu(x_i)\int_{J^+(x_i)\cap U}\mathrm{d}\nu(x_j). && \text{(4.15b)} \end{aligned}$$

Both terms of the sum have equal volume, so that the expression simplifies to twice the double integral of one labelling. For a causal interval U of 2-dimensional Minkowski spacetime, the sum becomes $\frac{1}{2!}\nu(U)^2$ as shown in Section 4.2.

For any compact subset U of a spacetime manifold, the probability for a random sprinkle S to have exactly n events is

$$\Pr\Big(|\mathsf{S}| = n\Big) = \mu(Q_{U,n}) \tag{4.16a}$$

$$= \mathrm{e}^{-\rho\nu(U)}\frac{\rho^n}{n!}\nu(U)^n. \tag{4.16b}$$

Note that according to Bayes' theorem, the probability $\Pr(\mathsf{S} \sim C)$ (and similarly for sprinkles on subsets U) splits as

$$\Pr\Big(\mathsf{S} \sim C\Big) = \Pr\Big(\mathsf{S} \sim C \;\Big|\; |\mathsf{S}| = |C|\Big)\Pr\Big(|\mathsf{S}| = |C|\Big) \tag{4.17}$$

since $\Pr\Big(|\mathsf{S}| = |C| \;\Big|\; \mathsf{S} \sim C\Big) = 1$. This relation is useful whenever a computation of the conditional probability $\Pr\Big(\mathsf{S} \sim C \;\Big|\; |\mathsf{S}| = |C|\Big)$ is necessary or there are different methods to compute it, for example, the one we will encounter below.

4.1.3 Past Infinity in Finite Sprinkles

Consider a random sprinkle S on any compact spacetime subset $U \in M$ and the canonical ensemble given by sprinkles distributed according to the sprinkling measure described before but with fixed cardinality n. For any $j \in \mathbb{N}$, the expected cardinality of the j-layer past infinity is given by a sum over the set $A(n)$ of all causets $(C, \preceq)$ with cardinality n (as shown in Table 4.1 for $n = 4$),

$$\mathbb{E}\Big(|\mathcal{I}^-_{j\text{-layer}}| \;\Big|\; |\mathsf{S}| = n\Big) = \sum_{C \in A(n)} \Pr\Big(\mathsf{S} \sim C \;\Big|\; |\mathsf{S}| = n\Big)\Big|\mathcal{I}^-_{j\text{-layer}}[C]\Big|. \tag{4.18}$$

Here $\mathcal{I}^-_{j\text{-layer}}[C]$ denotes the j-layer past infinity of the causet C, see Definition 1.3.1. Because a general expression for the sets $A(n)$ is unknown, let us use a different method to compute the expectation values.

Note that the expectation value is equally given by the sum over all events $x_i \in \mathsf{S}$ (all independently given by an identical volume denoted with a random event $\mathsf{x} \in \mathsf{S}$)

$$\mathbb{E}\Big(|\mathcal{I}^-_{j\text{-layer}}| \;\Big|\; |\mathsf{S}| = n\Big) = \sum_{i=1}^{n} \Pr\Big(x_i \in \mathcal{I}^-_{j\text{-layer}}[\mathsf{S}] \;\Big|\; |\mathsf{S}| = n\Big) \tag{4.19a}$$

$$= n\Pr\Big(\mathsf{x} \in \mathcal{I}^-_{j\text{-layer}}[\mathsf{S}] \;\Big|\; |\mathsf{S}| = n\Big) \tag{4.19b}$$

$$= \frac{n\Pr\Big(\mathsf{x} \in \mathcal{I}^-_{j\text{-layer}}[\mathsf{S}]\Big)}{\Pr\Big(|\mathsf{S}| = n\Big)}. \tag{4.19c}$$

An event sprinkled at position $x_i \in U$ is part of the 1-layer past infinity of a sprinkle with cardinality n if all other $(n-1)$ events do not fall in its past region $U_{x_i} = J^-(x_i) \cap U$ but appear in the remaining region $U \setminus J^-(x_i)$. So

$$\frac{\mathbb{E}\Big(|\mathcal{I}^-_{1\text{-layer}}| \;\Big|\; |\mathsf{S}| = n\Big)}{n} = \frac{1}{\nu(U)^n}\int_U \Big(\nu(U) - \nu(U_x)\Big)^{n-1}\,\mathrm{d}\nu(x). \tag{4.20}$$

Similarly, for the 2-layer past infinity, a sprinkled event at x is in the 2-layer past infinity if it has any number $k \in \mathbb{N}$ of pairwise spacelike separated events to its past and the remaining $n-k-1$ events are found again in the rest of the sprinkling region $U \setminus J^-(x)$. So the integral reads

$$\frac{\mathbb{E}\Big(|\mathcal{I}^-_{\text{2-layer}}| \;\Big|\; |\mathsf{S}| = n\Big)}{n} = \frac{1}{\nu(U)^n} \sum_{k=0}^{n-1} \int_U \binom{n-1}{k} \Big(\nu(U) - \nu(U_x)\Big)^{n-1-k} \times P_k(U_x) \nu(U_x)^k \, \mathrm{d}\nu(x), \tag{4.21}$$

where the weight $P_k(U_x)$ is the probability that the k events form a subcauset $C_{k,\dots,1}$ of pairwise spacelike separated events within the region U_x. This probability is given by

$$P_k(U_x) = \Pr\Big(\mathsf{S}_x \sim_{U_x} C_{k,\dots,1} \;\Big|\; |\mathsf{S}_x| = k\Big) \tag{4.22a}$$

$$= \frac{\mu_{U_x}\Big([C_{k,\dots,1}]_{U_x}\Big)}{\mu_{U_x}\Big(Q_{U_x}\Big)} \tag{4.22b}$$

where S_x is a random sprinkle on U_x.

The normalized expected sizes of higher j-layer past infinities (with $j \in \mathbb{N}$) are computed with the same integral (4.21) as for the 2-layer past infinity. However, in general we have to account for all possible arrangements of the k events to the past of position $x \in U$ such that an event at x is part of the j-layer past infinity. Thus the probability weight (4.22) has to be replaced by the sum

$$P^{(j)}_k(U_x) = \sum_{C^{(j)}} \Pr\Big(\mathsf{S}_x \sim_{U_x} C^{(j)} \;\Big|\; |\mathsf{S}_x| = k\Big) \tag{4.23}$$

running over all causets $C^{(j)}$ with cardinality k such that the event x with a subsprinkle isomorphic to $C^{(j)}$ in its past is in the j-layer past infinity. All causets $C^{(j)}$ can have at most $j-1$ layers. For $j = 1$, the sum is trivially 1 since $k = 0$, and for $j = 2$, there is only one term, the k-event yielding (4.22).

In the full grand canonical ensemble of all sprinkles, the cardinality n is determined by the Poisson process with a fixed sprinkling density ρ, which leads to the normalized expectation values for the j-layer past infinity

$$\frac{\mathbb{E}\Big(|\mathcal{I}^-_{j\text{-layer}}|\Big)}{\rho\nu(U)} = \mathrm{e}^{-\rho\nu(U)} \sum_{n=1}^{\infty} \frac{\Big(\rho\nu(U)\Big)^{n-1}}{n!} \mathbb{E}\Big(|\mathcal{I}^-_{j\text{-layer}}| \;\Big|\; |\mathsf{S}| = n\Big). \tag{4.24}$$

In the following, we compute these expectation values for causal intervals of $(1+1)$-dimensional Minkowski spacetime as examples.

4.2 Sprinkling on Intervals of Minkowski Spacetime

For causal intervals of 2-dimensional Minkowski space, we formulate the probability for a causet in terms of a combinatorial method. This leads us to the computation of the probability for a causet event to be in the 1- and 2-layer past infinities and their asymptotic behaviour for infinite sprinkles on 2-dimensional Minkowski spacetime.

4.2.1 Sprinkle Probabilities from 2D-Orders

We use the correspondence between sprinkles on causal intervals U of $(1+1)$-dimensional Minkowski spacetime and their *2D-orders*, see Winkler [110] and [111], to compute probabilities of obtaining an element of any given causet isomorphism class when sprinkling into U. A 2D-order is the product of two total orders.

Starting with an example, consider the sprinkles $S \in Q_U$ that are isomorphic to the 3-chain causet $\vdots$. Using standard null coordinates (u, v) and excluding a set of measure zero, we restrict to those sprinkles comprising events at $(u_i, v_i), i \in \{1, 2, 3\}$ such that $u_1 < u_2 < u_3$ and $v_1 < v_2 < v_3$. One such sprinkle is pictured in Figure 4.2. Similarly to (4.15), the probability for a random sprinkle S into U to be isomorphic to $\vdots$ is

$$\begin{aligned}\Pr\Big(\mathsf{S} \sim \vdots\Big) &= \left(3! \int_0^1 \mathrm{d}u_1 \int_{u_1}^1 \mathrm{d}u_2 \int_{u_2}^1 \mathrm{d}u_3 \int_0^1 \mathrm{d}v_1 \int_{v_1}^1 \mathrm{d}v_2 \int_{v_2}^1 \mathrm{d}v_3\right) \\ &\quad \times \left(\mathrm{e}^{-\rho\nu(U)} \frac{\rho^3}{3!} \nu(U)^3\right) \qquad (4.25a) \\ &= \frac{1}{3!} \left(\mathrm{e}^{-\rho\nu(U)} \frac{\rho^3}{3!} \nu(U)^3\right), \qquad (4.25b)\end{aligned}$$

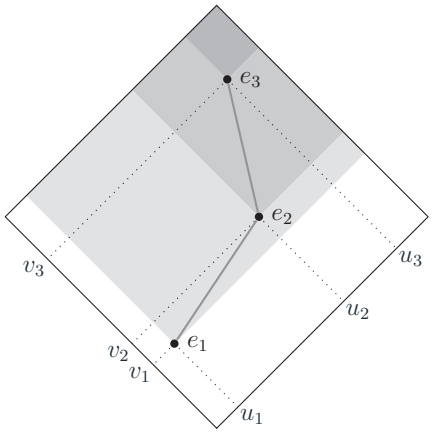

Figure 4.2: Sprinkle with three events in a causal interval of $(1+1)$-dimensional Minkowski spacetime that is isomorphic to the 3-chain causet $\vdots$. The futures of the events are shaded.

where we have pulled out a volume factor and correspondingly scaled the null coordinates such that they range over the unit interval. The six-fold integral in (4.25) has a factor of 3!, since there are that many distinct labellings (total orders) of the events by their u-coordinate. Compare (4.25) with (4.17) to find the conditional probability for "the sprinkled causet is the 3-chain given that the sprinkle has three events",

$$\Pr\Big(\mathsf{S} \sim \vdots \;\Big|\; |\mathsf{S}| = 3\Big) = \frac{1}{3!}. \tag{4.26}$$

Now, we consider another method to determine this conditional probability by combinatorial means.

Let S be any finite sprinkle on a causal interval of (1+1)-dimensional Minkowski spacetime, comprising events with null coordinates (u_i, v_i) $(1 \leq i \leq n = |S|)$. We say that the sprinkle is *non-degenerate* if all the u-coordinates are distinct and all the v-coordinates are distinct. In this case we may, without loss, assume that the events are labelled so that the u_i form a strictly increasing sequence. Then the causal relation of S induces a total order on the v-coordinates, $v_i \leq v_j$. The product of the two total orders in (u, v) is a 2D-order, see Brightwell, Henson, and Surya [20]. Non-degenerate sprinkles with equal cardinality that induce the same total order are necessarily isomorphic, but two non-degenerate sprinkles in the same isomorphism class can induce different orders. This can be seen in Figure 4.3, which displays an example of non-degenerate sprinkles inducing each of the six distinct total orders. Of these, there are two that are in the same isomorphism class, while the others correspond to distinct causets. So, let me define the following.

Definition 4.2.1. Let C be a finite causet and consider all of its embeddings in a causal interval U of 2-dimensional Minkowski spacetime given by the isomorphism class $[C]$. Labelling the events of any non-degenerate sprinkle $S \in [C]$ by integers

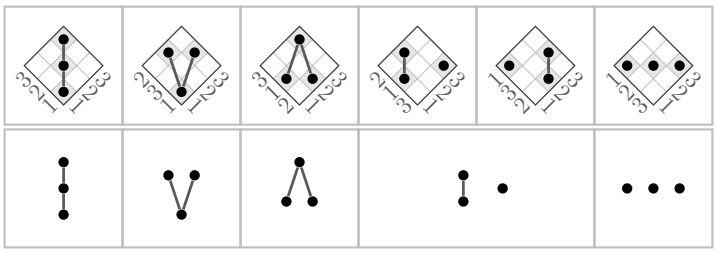

Figure 4.3: Choosing an event labelling by an increasing u-coordinate (upwards on the right of the diamonds), there exist six distinct total orders along the v-coordinate (upwards on the left of the diamonds). The corresponding five causets are shown at the bottom. These diagrams (as well as all Hasse diagrams in this thesis) are drawn with my LaTeX-package [68], which is based on this combinatorial technique.

increasing with the u-coordinate, the **2D-order multiplicity** $m\big([C]\big) \in \mathbb{N}$ is the number of distinct total orders of the event labels along the v-coordinate induced by all non-degenerate sprinkles in $[C]$.

In the case where $[C]$ has no representative embedded in $(1+1)$-dimensional Minkowski spacetime, the 2D-order multiplicity is 0; on the other hand, every causet that can be embedded in $(1+1)$-dimensional Minkowski spacetime can be embedded non-degenerately. A random sprinkle S in $(1+1)$-dimensional Minkowski spacetime is almost surely non-degenerate. While the combinatorics of random 2D-orders (including the 2D-order multiplicity) has been studied in the large cardinality limit, see Winkler [111], I use this idea to compute sprinkling probabilities for *finite* causets in the following.

Proposition 4.2.2. *Let U be a causal interval of $(1+1)$-dimensional Minkowski spacetime. If C is a finite causet with cardinality n, the probability that a random sprinkle into U with cardinality n has the same causal structure as C is determined by the 2D-order multiplicity and the causet cardinality,*

$$\Pr\big(\mathsf{S} \sim C \;\big|\; |\mathsf{S}| = n\big) = \frac{m\big([C]_U\big)}{n!}, \tag{4.27}$$

consequently,

$$\Pr\big(\mathsf{S} \sim C\big) = \frac{m\big([C]_U\big)}{(n!)^2}\big(\rho\nu(U)\big)^n e^{-\rho\nu(U)}. \tag{4.28}$$

Proof. There are $n!$ distinct total orders of the v-coordinate for a given labelling of the n event sprinkle. Each of these total orders has the same probability. Therefore, the probability for the random sprinkle S to be isomorphic to C given a cardinality n is the 2D-order multiplicity $m([C]_U)$. □

4.2.2 Past Infinity of Sprinkles in 2D-Minkowski Spacetime

In the following, we use this combinatorial method from above to determine the expected size of the 1- and 2-layer past infinity of random sprinkles in causal intervals of $(1+1)$-dimensional Minkowski spacetime. We analytically evaluate these probabilities, compare the analytic computations with results of simulations, and discuss the past infinity in the infinite causet limit.

Recall the general results Subsection 4.1.3. The conditional expectation values (canonical ensemble) are easier to compute analytically and approximates the grand-canonical ensemble for larger sprinkling cardinalities, as we will see in the following.

For 2-dimensional Minkowski spacetime, express the position x of an event in

null coordinates $x = (u', v')$ ranging over $u', v' \in [0, a]$ or rescaled over $u, v \in [0, 1]$ for a total volume of $\nu(U) = a^2$, so that $\nu(U_x) = a^2 uv$. Evaluating (4.20), we find the normalized expected size of the 1-layer past infinity for cardinality n,

$$\frac{\mathbb{E}\Big(|\mathcal{I}^-_{\text{1-layer}}| \;\Big|\; |\mathsf{S}| = n\Big)}{n} = \frac{\mathrm{h}_n}{n} \tag{4.29a}$$

$$\asymp \frac{1}{n}\left(\ln(n) + \gamma + \frac{1}{2n} + \mathcal{O}(n^{-2})\right), \tag{4.29b}$$

where h_n is the n-th harmonic number,

$$\mathrm{h}_n := \sum_{k=1}^{n} \frac{1}{k}. \tag{4.30}$$

The asymptotic behavior for large n is shown on the right-hand side of (4.29) where γ is the Euler-Mascheroni constant. For large n, these asymptotics agree with the known results for random 2D-orders, for which the 1-layer past infinity is referred to as the set of minimal points of the partially ordered sets [110, 111]. Furthermore, I have the following results.

The normalized expectation value in the grand-canonical ensemble may be given in terms of the entire exponential integral Ein, which is the generating function of harmonic numbers,

$$\frac{\mathbb{E}\Big(|\mathcal{I}^-_{\text{1-layer}}|\Big)}{\rho a^2} = \frac{\mathrm{Ein}(\rho a^2)}{\rho a^2} \tag{4.31a}$$

$$= \frac{1}{\rho a^2}\Big(\ln(\rho a^2) + \gamma + \Gamma(0, \rho a^2)\Big). \tag{4.31b}$$

The symbol $\Gamma(0, z)$ is the incomplete Gamma function, which falls off rapidly in the limit $z \to \infty$, so that the asymptotic behavior (for $\rho \to \infty$) is the same as for the conditional expectation value (4.29). The cardinality of the 1-layer past infinity of causal sets has also been studied in order to find entropy bounds on Cauchy horizons, see [95].

I complement the previous result by calculating the expected size of the 2-layer past infinity. The subset $U_x = J^-(x) \cap U$ in (4.22) is now given by a causal interval of (1+1)-dimensional Minkowski spacetime for all positions $x \in U$, the probability $P_k(U_x)$ is given by Proposition 4.2.2 as the x-independent expression

$$P_k(U_x) = \frac{1}{k!}. \tag{4.32}$$

There is only the total order $v_k < v_{k-1} < \cdots < v_1$ along the v-coordinate that corresponds to k events being spacelike separated, assuming the u-coordinates are arranged in ascending order, $u_1 < u_2 < \cdots < u_k$. Hence the integration (4.21)

	$n =$	1	2	5	10	15	50	100	200
$\mathcal{I}^-_{\text{1-layer}}$	analytic	100.0	75.00	45.67	29.29	22.12	8.998	5.187	2.939
	simulated	100.0	74.96	45.61	29.28	22.09	8.986	5.191	2.941
$\mathcal{I}^-_{\text{2-layer}}$	analytic	100.0	100.0	80.83	57.96	45.70	20.13	11.94	6.906
	simulated	100.0	100.0	80.79	57.97	45.61	20.14	11.93	6.910

(a) Normalized expectation values $\mathbb{E}\big(|\mathcal{I}^-_{\text{1,2-layer}}| \;\big|\; |\mathsf{S}| = n\big)/\%$ for the size of the past infinity for fixed causet cardinalities n.

	$\rho a^2 =$	1	2	5	10	15	50	100	200
$\mathcal{I}^-_{\text{1-layer}}$	analytic	79.66	65.96	43.76	28.80	21.90	8.978	5.182	2.938
	simulated	79.96	66.03	43.77	28.79	21.91	8.966	5.181	2.941
$\mathcal{I}^-_{\text{2-layer}}$	analytic	97.82	93.08	76.43	56.63	45.10	20.08	11.92	6.902
	simulated	97.96	93.27	76.49	56.59	45.10	20.05	11.92	6.910

(b) Normalized expectation values $\mathbb{E}\big(|\mathcal{I}^-_{\text{1,2-layer}}|\big)/\%$ for the size of the past infinity for fixed sprinkling densities ρ.

Table 4.2: Normalized expectation values for the 1-layer ($\mathcal{I}^-_{\text{1-layer}}$) or 2-layer ($\mathcal{I}^-_{\text{2-layer}}$) past infinity for ensembles with increasing causet cardinalities n (top half), and increasing sprinkling density ρ (bottom half) in units of the inverse volume a^{-2}, respectively. Simulated values are computed as averages over 100000 sprinkles.

yields the expression

$$\frac{\mathbb{E}\Big(|\mathcal{I}^-_{\text{2-layer}}| \;\Big|\; |\mathsf{S}| = n\Big)}{n} = \frac{1}{n}\sum_{k=0}^{n-1}\frac{\mathrm{h}_n - \mathrm{h}_k}{k!} \tag{4.33a}$$

$$\asymp \frac{\mathrm{e}}{n}\left(\ln(n) + \tilde{\gamma} + \frac{1}{2n} + \mathcal{O}(n^{-2})\right) \tag{4.33b}$$

with the constant

$$\tilde{\gamma} = \gamma - \frac{1}{\mathrm{e}}\sum_{k=0}^{\infty}\frac{\mathrm{h}_k}{k!} = \gamma - \mathrm{Ein}(1) \approx -0.21938. \tag{4.34}$$

We do not have an expression for the expectation value in the grand-canonical case, however, the summation in (4.24) is quickly converging so that it can be computed numerically with sufficient accuracy.

Table 4.2 shows some examples for the normalized expectation values at fixed cardinalities n (canonical, 4.2a) and fixed sprinkling densities ρ (grand-canonical, 4.2b). The numbers are presented as a percentage, since they may also be interpreted as the probabilities that an event randomly chosen from a sprinkle is in the 1- or 2-layer past infinity, respectively. The simulations results below the analytic results are computed from the cardinalities of the past infinities averaged over one hundred thousand sprinkles. Note that the values for the two ensembles

dimension d	2	3	4	5	6	7	8
sphere volume S_{d-2}	2	2π	4π	$2\pi^2$	$\frac{8}{3}\pi^2$	π^3	$\frac{16}{15}\pi^3$
causal volume factor α_d	2	$\frac{12}{\pi}$	$\frac{24}{\pi}$	$\frac{160}{\pi^2}$	$\frac{360}{\pi^2}$	$\frac{2688}{\pi^3}$	$\frac{6720}{\pi^3}$

Table 4.3: Unit sphere volume S_{d-2} and proportionality factor α_d between the d-th power of the proper time of a causal interval and its Minkowski spacetime volume.

become asymptotically equal as the cardinality increases. Furthermore, the values decrease with increasing sprinkle cardinality so that sufficiently many events in sprinkles of more than two hundred events lie outside the 2-layer past infinity and thus have non-empty rank 2 pasts. As the sprinkle size increases, the proportion of the sprinkle lying in past infinity tends to zero and the influence of the past infinity on the preferred pasts becomes negligible.

4.2.3 Proper Time Separation of Diamonds

The numerical results discussed in Section 3.3 suggested a relation between the size of diamonds and their tip to tip proper time separation. Here we will use the probability measure to compute the relation and compare it to numerical results for d-dimensional Minkowski spacetime.

Consider d-dimensional Minkowski spacetime $\mathbb{M}^d$ and two points $y \prec x \in \mathbb{M}^d$. The d-th power of the proper time separation τ_{yx} of the causal interval U_{yx} is related by [93]

$$\tau_{yx}^d = \frac{2^{d-1}d(d-1)}{S_{d-2}}\nu(U_{yx}) =: \alpha_d \nu(U_{yx}), \tag{4.35}$$

where

$$S_{d-2} = 2\frac{\pi^{\frac{d-1}{2}}}{\Gamma\left(\frac{d-1}{2}\right)} \tag{4.36}$$

is the unit sphere volume in dimension $d-2$. The proportionality factor α_d and the sphere volume S_{d-2} for dimensions 2 to 8 are given in Table 4.3.

Let $C^{(k)}$ be the abstract causet of the "interior" of a k-diamond such that one event is spacelike separated to all other $k-1$ events. A random pair of events y, x in a random sprinkle S in Minkowski spacetime $\mathbb{M}^d$ is a k-diamond if $(\mathsf{y},\mathsf{x})_{\mathsf{S}} \sim C^{(k)}$.

As a first simple approach, we may take a causal interval U_{yx} between two points $y \prec x \in \mathbb{M}^d$ and use the probability measure $\mu_{U_{yx}}$ to find the probability for a random sprinkle S_{yx} on U_{yx} to be isomorphic to $C^{(k)}$,

$$\Pr\left(\mathsf{S}_{yx} \sim C^{(k)}\right) = \mu_{U_{yx}}\left([C^{(k)}]_{U_{yx}}\right) \tag{4.37}$$

The expectation value for the proper time separation between the tips of U_{yx} given that the sprinkle S_{yx} is a k-diamond is then computed as an average over all diamond volumes, normalized by the sprinkling density. Thus I use the measure $\lambda = \rho\nu(U_{yx})$ to compute

$$\mathbb{E}\Big(\tau_{yx} \,\Big|\, \mathsf{S}_{yx} \sim C^{(k)}\Big) \asymp \left(\frac{\alpha_d}{\rho}\right)^{\frac{1}{d}} \int_0^\infty \frac{1}{k!}\lambda^{k+\frac{1}{d}}\mathrm{e}^{-\lambda}\,\mathrm{d}\lambda \tag{4.38a}$$

$$\asymp \left(\frac{\alpha_d}{\rho}\right)^{\frac{1}{d}} \frac{\Gamma\left(k+\frac{1}{d}+1\right)}{k!}. \tag{4.38b}$$

This expression is a good approximation but is only asymptotically accurate (for arbitrary large sprinkling regions) since it does not consider finite sprinkles.

For finite sprinkles, first fix a causal interval U in d-dimensional Minkowski spacetime, and let $\delta(\cdot)$ be the indicator function which is 1 whenever its argument is true and 0 otherwise (as generalization of the Kronecker delta). The expectation value of the proper time separation between two random events y and x whose interval is a k-diamond in a random sprinkle S in U is given by

$$\mathbb{E}\Big(\tau_{\mathsf{yx}} \,\Big|\, (\mathsf{y},\mathsf{x})_{\mathsf{S}} \sim C^{(k)}\Big) = \int_{Q_U} \frac{\sum\limits_{x,y\in S} \tau_{xy}\delta\Big((y,x)_S \sim C^{(k)}\Big)}{\max\left(1, \sum\limits_{x,y\in S} \delta\Big((y,x)_S \sim C^{(k)}\Big)\right)}\,\mathrm{d}\mu_U(S). \tag{4.39}$$

Since the summation in the integrand's denominator counts k-diamonds, I use the maximum function to avoid an ill-defined expression when there are no k-diamonds in a sprinkle S (for which the numerator becomes 0 as well). The random variables in the numerator and denominator are not independent. However, in very large sprinkles like the numerical setting of $n = 6000$ from Section 3.1, it is almost certain to find diamonds for any size $k \ll n$ with a large number of occurrences. Hence, we may get a good approximation for the expectation value by adding all proper time separations of k-diamonds and divide by their number. For a large, fixed sprinkle cardinality n, it reads

$$\mathbb{E}\Big(\tau_{\mathsf{yx}} \,\Big|\, (\mathsf{y},\mathsf{x})_{\mathsf{S}} \sim C^{(k)}, |\mathsf{S}| = n\Big) = \frac{\int_{Q_{U,n}} \sum\limits_{x,y\in S} \tau_{yx}\delta\Big((y,x)_S \sim C^{(k)}\Big)\,\mathrm{d}\mu_U(S)}{\int_{Q_{U,n}} \sum\limits_{x,y\in S} \delta\Big((y,x)_S \sim C^{(k)}\Big)\,\mathrm{d}\mu_U(S)}. \tag{4.40}$$

The denominator of (4.40) is the normalization of the probability measure here and corresponds to the expected number of k-diamonds N_k. For this expression, fix 3 out of n events $x, y, z \in S$ of a sprinkle S in U such that $k-1$ out of the remaining $n-3$ events are placed in the subregion $U_{yx} \setminus U_{yzx}$ and $U \setminus U_{yx}$ contains

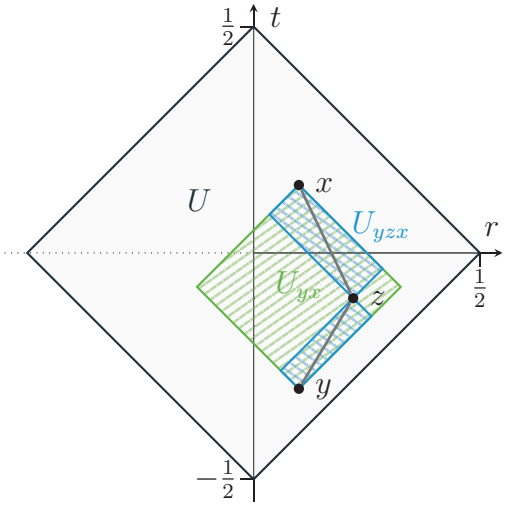

Figure 4.4: Diamond subregion U_{xy} (increasing line pattern, green) and the link subregion U_{xzy} (decreasing line pattern, blue) in the sprinkling region (causal interval) U of d-dimensional Minkowski spacetime. The computations are done in relative coordinates t and r as shown by the coordinate system in the background.

$n-(k+2)$ events. Figure 4.4 shows an example for the three events in U. So

$$\mathbb{E}\Big(N_k \,\Big|\, |\mathsf{S}| = n\Big) = \frac{1}{\nu(U)^n}\binom{n}{3}\binom{n-3}{k-1}\int_U \int_{U\cap J^-(x)} \Big(\nu(U)-\nu(U_{yx})\Big)^{n-k-2} \\ \times \nu(U_{yx})^k \Pr\Big(\mathsf{S}_{yx} \sim C^{(k)} \,\Big|\, |\mathsf{S}_{yx}| = k\Big)\, \mathrm{d}\nu(y)\, \mathrm{d}\nu(x). \tag{4.41}$$

The conditional probability for the sub-sprinkle $\mathsf{S}_{yx} \subset \mathsf{S}$ to form a k-diamond (including x and y as its tips) is independent of the integration variables. It is given by the normalized integral

$$\Pr\Big(\mathsf{S}_{yx} \sim C^{(k)} \,\Big|\, |\mathsf{S}_{yx}| = k\Big) = \frac{1}{\nu(U_{yx})}\int_{U_{yx}} \Big(\nu(U_{yx})-\nu(U_{yzx})\Big)^{k-1}\, \mathrm{d}\nu(z) \tag{4.42}$$

that describes the relative probability for $k-1$ events to be in the region $U_{yx}\setminus U_{yzx}$ for any event z with $y \prec\!* z \prec\!* x$, see Figure 4.4.

The numerator of (4.39) is a similar integration yielding the expected total proper time separation of all k-diamonds T_k,

$$\mathbb{E}\Big(T_k \,\Big|\, |\mathsf{S}| = n\Big) = \frac{1}{\nu(U)^n}\binom{n}{3}\binom{n-3}{k-1}\int_U \int_{U\cap J^-(x)} \Big(\nu(U)-\nu(U_{yx})\Big)^{n-k-2} \\ \times \alpha_d^{\frac{1}{d}} \nu(U_{yx})^{k+\frac{1}{d}} \Pr\Big(\mathsf{S}_{yx} \sim C^{(k)} \,\Big|\, |\mathsf{S}_{yx}| = k\Big)\, \mathrm{d}\nu(y)\, \mathrm{d}\nu(x). \tag{4.43}$$

The conditional probability (4.42) and the binomials appear in both expressions (4.41) and (4.43) and cancel out. Let $\tau = \sqrt{\alpha_d \nu(U)}$ be the proper time separation

between the tips of the sprinkling region U, so that we have the normalized integral

$$\varepsilon_d^p(n,k) = \frac{1}{\nu(U)^2} \int_U \int_{U\cap J^-(x)} \left(1 - \left(\frac{\tau_{yx}}{\tau}\right)^d\right)^{n-k-2} \left(\frac{\tau_{yx}}{\tau}\right)^{kd+p} \mathrm{d}\nu(y)\, \mathrm{d}\nu(x). \quad (4.44)$$

The expected proper time separation of a k-diamond given a sprinkle with $n \gg k$ events is then given by

$$\mathbb{E}\Big(\tau_{\mathsf{yx}} \;\Big|\; (\mathsf{y},\mathsf{x})_{\mathsf{S}} \sim C^{(k)}, |\mathsf{S}| = n\Big) = \frac{\varepsilon_d^1(n,k)}{\varepsilon_d^0(n,k)}\tau. \quad (4.45)$$

Note that the dimension τ is determined by the sprinkling cardinality n such that $\tau = (\alpha_d n)^{\frac{1}{d}} \sqrt[d]{1/\rho}$.

For the integrals (4.44), make use of the Poincare invariance of Minkowski spacetime. Choose a coordinate system with origin at the center of the region U and with time axis aligned along the tips as shown in Figure 4.4. The angular part, i.e. the volume of the $(d-2)$-sphere (4.36) separates from the time and radial coordinates in the x- and y-integration (see Table 4.3 for its values). So we are left with four integrals in normalized coordinates. The x-integrals range over

$$t_x \in \left[-\frac{1}{2}, \frac{1}{2}\right], \qquad r_x \in \left[0, \frac{1}{2} - |t_x|\right]. \quad (4.46)$$

The y event has to be in the past of x, somewhere in the region $U \cap J^-(x)$ with normalized tip-to-tip proper time

$$\hat{\tau}_x := \frac{\tau_x}{\tau} = \sqrt{\left(t_x + \frac{1}{2}\right)^2 - r_x^2}. \quad (4.47)$$

Therefore, the normalized y-coordinates range over

$$t_y \in \left[-\frac{1}{2}\hat{\tau}_x, \frac{1}{2}\hat{\tau}_x\right], \qquad r_y \in \left[0, \frac{1}{2}\hat{\tau}_x - |t_y|\right]. \quad (4.48)$$

The proper time separation of the k-diamond region U_{yx} is

$$\hat{\tau}_{yx} := \frac{\tau_{yx}}{\tau} = \sqrt{\left(\frac{1}{2}\sqrt{\left(t_x + \frac{1}{2}\right)^2 - r_x^2} - t_y\right)^2 - r_y^2}. \quad (4.49)$$

In these coordinates, the normalized integral (4.44) becomes

$$\varepsilon_d^p(n,k) = (\alpha_d S_{d-2})^2 \int_{t_x}\int_{r_x}\int_{t_y}\int_{r_y} \left(1 - \hat{\tau}_{yx}^d\right)^{n-k-2} \hat{\tau}_{yx}^{kd+p} (r_y r_x)^{d-2}\, \mathrm{d}r_y \mathrm{d}t_y \mathrm{d}r_x \mathrm{d}t_x. \quad (4.50)$$

Note that the expectation value (4.45) is for a fixed sprinkle cardinality n and the respective value for a fixed sprinkling density ρ (grand canonical) is

$$\mathbb{E}\Big(\tau_{\mathsf{yx}} \;\Big|\; (\mathsf{y},\mathsf{x})_{\mathsf{S}} \sim C^{(k)}\Big) = \mathrm{e}^{-\lambda} \sum_{n=k+2}^{\infty} \frac{\lambda^n}{n!} \mathbb{E}\Big(\tau_{\mathsf{yx}} \;\Big|\; (\mathsf{y},\mathsf{x})_{\mathsf{S}} \sim C^{(k)}, |\mathsf{S}| = n\Big). \quad (4.51)$$

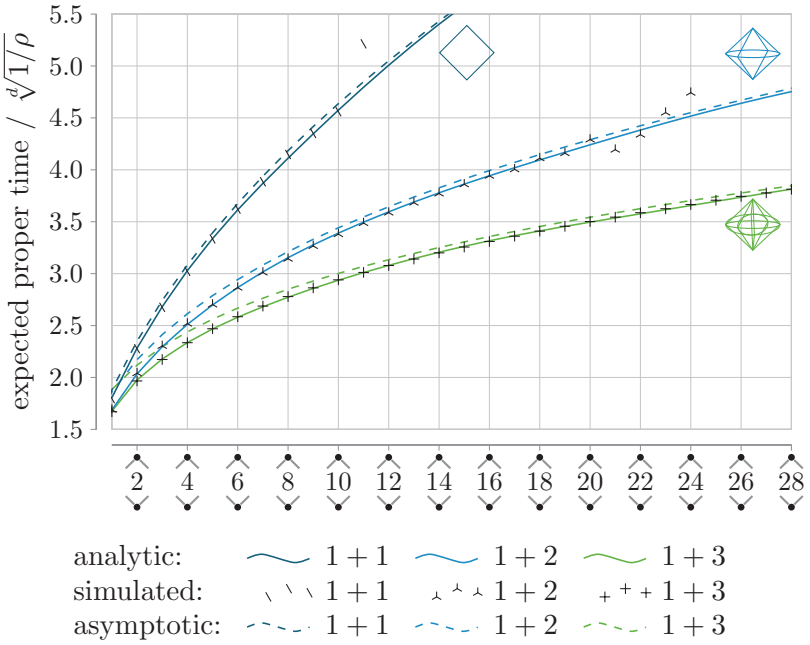

Figure 4.5: Comparison of the diamond proper time separation determined by three different methods for Minkowski spacetime of dimension $1+1$ to $1+3$. The solid lines show the results of (4.45) where the integrals (4.50) have been numerically evaluated with a quasi Monte-Carlo method in Mathematica; the cross marks show the results of the sprinkling simulations for an expected sprinkling cardinality of $\langle n \rangle = 6000$ where random errors increase with the diamond size; and the dashed lines are the asymptotic expression (4.38).

However, as we have seen for the past infinity calculations in Subsection 4.2.2, the ensembles give almost equal values for very large n (as in our case). Thus, it will suffice to evaluate the integrals (4.50) numerically, compute (4.45), and compare the results with a numerical sprinkling process.

The results are shown in Figure 4.5. There is a nearly perfect agreement between the analytic expression (4.45) (solid lines) and the simulation results with an expected sprinkling cardinality of $\langle n \rangle = 6000$ (cross marks). Only for large diamond size (in dimensions $1+1$ and $1+2$), the simulation results show random errors because the respective large diamonds are rare throughout sprinkles with about six thousand events. The match between the analytic values (computed with a "quasi Monte-Carlo", numerical integration method in Mathematica) and the sprinkling simulations confirms the assumptions for the transition from (4.40) to (4.39). Additionally, notice the close approximation of the analytic curves by the much simpler expression of the asymptotic behaviour (4.38), plotted with dashed lines in Figure 4.5.

Chapter 5

Quantization and States

In Chapter 2, I constructed a Poisson algebra for the free classical scalar field. In this chapter, I want to construct the corresponding quantum field theory. First, I review different *methods of quantization*: deformation quantization (see Weinstein [108], Rieffel [96], and Kontsevich [57]), geometric quantization (see Woodhouse [112], and Borthwick and Uribe [18]), and Toeplitz quantization (see De Monvel and Guillemin [30]). A general overview over quantization methods is also given in Ali and Engliš [5] and more mathematical details can be found in the textbooks by Landsman [58], and Dereziński and Gérard [31]. Second, I consider the algebraic description of physical observations as *states* on a constructed quantum algebra, in particular, to review the Sorkin-Johnston state.

Note that the methods discussed in this chapter are important for the algebraic formulation of quantum field theory as well, however, the central aspects of algebraic quantum field theory are the Haag-Kastler axioms [46] and their modification in the perturbative approach, see Fredenhagen and Rejzner [42], Rejzner [94], and Hawkins and Rejzner [49], which are not discussed in this thesis. I will only focus on the mathematical aspects that are relevant for the construction of a quantum algebra for the classical Poisson algebras $(\mathcal{P}, \{\cdot, \cdot\})$ and the symplectic spaces $(\mathcal{S}, \omega)$ for spacetime manifolds and causets as reviewed and discussed in Chapter 2. This will lead us to the construction of the Sorkin-Johnston state, in particular, for a finite causet in Chapter 6.

5.1 Quantization Methods

Quantum observables form a non-commutative algebra $\mathfrak{A}_\hbar$. For the commutator of two elements $A_1, A_2 \in \mathfrak{A}_\hbar$, we write

$$[A_1, A_2]_- := A_1 A_2 - A_2 A_1. \tag{5.1}$$

Quantization is a procedure that turns the given classical Poisson algebra $(\mathcal{P}, \{\cdot, \cdot\})$ into a non-commutative algebra $\mathfrak{A}_\hbar$. Dirac's original idea was to identify the commutator of the quantum algebra with the quantization of the Poisson bracket, which reads in terms of a quantization map $Q_\hbar : \mathcal{P} \to \mathfrak{A}_\hbar$, for any $F_1, F_2 \in \mathcal{P}$,

$$\Big[Q_\hbar(F_1), Q_\hbar(F_2)\Big]_- = \mathrm{i}\hbar Q_\hbar\Big(\{F_1, F_2\}\Big). \tag{5.2}$$

However, the Groenewold-van Hove, no-go theorem [44, 106] states that such a quantization map does not exist. Using the little-o notation, for some functions f and g of a real parameter $\hbar$,

$$f(\hbar) = \mathrm{o}\Big(g(\hbar)\Big) :\Leftrightarrow \lim_{\hbar\to 0} \frac{f(\hbar)}{g(\hbar)} = 0, \tag{5.3}$$

this problem is solved by weakening Dirac's condition to

$$\Big[Q_\hbar(F_1),\, Q_\hbar(F_2)\Big]_- = \mathrm{i}\hbar Q_\hbar\Big(\{F_1,\, F_2\}\Big) + \mathrm{o}(\hbar). \tag{5.4}$$

The extension of the pointwise product of classical observables to higher powers of the quantization parameter $\hbar$ such that Dirac's condition (5.4) holds, in particular, is also the main idea of deformation quantization.

5.1.1 Formal Deformation Quantization

Given a spacetime or a causet $\mathcal{X}$, recall the construction of a classical, on/off-shell Poisson algebra from Chapter 2. Formal deformation quantization is a generalization of the classical pointwise product of the Poisson algebra to a star product.

Definition 5.1.1. Let $(\mathcal{P}, \{\cdot,\cdot\})$ be a Poisson algebra. A **star product** $\star$ is a product on the space of formal power series $\mathcal{P}[[\hbar]]$ such that for all $F_1, F_2 \in \mathcal{P}$:

$$F_1 \star F_2 = \sum_{k=0}^{\infty} B_k(F_1, F_2)\hbar^k, \tag{5.5}$$

where B_k are bilinear maps fulfilling the conditions, $\forall F_1, F_2, F_3 \in \mathcal{P}$:

$$\text{associativity:} \qquad (F_1 \star F_2) \star F_3 = F_1 \star (F_2 \star F_3), \tag{5.6a}$$

$$\text{pointwise product:} \qquad B_0(F_1, F_2) = F_1 F_2. \tag{5.6b}$$

The star product $\star$ is

$$\textbf{Poisson compatible} \text{ if} \qquad B_1(F_1, F_2) - B_1(F_2, F_1) = \mathrm{i}\,\{F_1,\, F_2\}\,, \tag{5.6c}$$

$$\textbf{unital} \text{ if} \qquad F_1 \star 1 = 1 \star F_1 = F_1, \tag{5.6d}$$

$$\textbf{self-adjoint} \text{ if} \qquad \overline{F_1 \star F_2} = \overline{F_2} \star \overline{F_1}, \tag{5.6e}$$

and it is **differential** if all B_k are bi-differential maps.

Heuristically, the second condition (5.6b) ensures that the star product is the pointwise product in the classical limit (formally $\hbar \to 0$), which is also known as von Neumann's condition. Poisson compatibility is usually also included as a main condition for a star product, since it describes Dirac's idea of obtaining the Poisson bracket from the commutator in the classical limit [58, Ch. II]. The

additional properties (Poisson compatibility, unitality, self-adjointness) are similar to the ones given in Schlichenmaier [99]. Note that the parameter $\hbar$ is treated as a formal parameter here and, in general, such power series do not converge, hence they are called *formal*.

5.1.2 Strict Deformation Quantization and (De)Quantization Maps

While we can treat the formal parameter $\hbar$ as a number for polynomial observables (2.16) and the power series converge due to a finite number of terms, this is no longer true for arbitrary (non-polynomial) observables. However, in reality, the quantization parameter is not formal, so let us now consider the strict version of deformation quantization. First, we need to review some general terminology [33].

Definition 5.1.2. A **normed vector space** is a vector space $\mathcal{V}$ with a norm i.e., a function $\|\cdot\|$ that fulfills the following axioms for all elements $v, w \in \mathcal{V}$ and all $c \in \mathbb{C}$:

$$\text{positivity:} \qquad \|v\| \geq 0, \tag{5.7a}$$

$$\text{zero element:} \qquad \|v\| = 0 \Leftrightarrow v = 0, \tag{5.7b}$$

$$\text{scalar multiplication:} \qquad \|cv\| = |c|\|v\|, \tag{5.7c}$$

$$\text{triangle inequality:} \qquad \|v + w\| \leq \|v\| + \|w\|. \tag{5.7d}$$

Definition 5.1.3. A **Banach *-algebra** is a *-algebra $\mathfrak{A}$ (see Definition 2.1.4) that is also a normed vector space, complete in the metric induced by the norm, and the norm fulfills the conditions, for all elements $A_1, A_2 \in \mathfrak{A}$:

$$\text{unital (if } \mathfrak{A} \text{ is unital):} \qquad \|\mathbb{1}\| = 1, \tag{5.8a}$$

$$\text{involution compatibility:} \qquad \|A_1^*\| = \|A_1\|, \tag{5.8b}$$

$$\text{Banach inequality:} \qquad \|A_1 A_2\| \leq \|A_1\|\|A_2\|. \tag{5.8c}$$

Definition 5.1.4. A **C*-algebra** is a Banach *-algebra $\mathfrak{A}$ with a norm that, for all $A \in \mathcal{A}$, also satisfies the

$$\text{C*-property:} \qquad \|A^* A\| = \|A\|^2. \tag{5.9}$$

Strict deformation quantization involves a family of C*-algebras $(\mathfrak{A}_\hbar)_{\hbar \in I}$ parametrized by $\hbar$ for some parameter range $I \subseteq \mathbb{R}$ including the classical limit $\hbar = 0$. In the following, I have $I = [0, \infty)$ and denote $I_* := I \setminus \{0\}$. However, for some constructions of geometric quantization later on, I will see that the quantization parameter has to take values in $I_* = \left\{ \frac{1}{p} \;\middle|\; p \in \mathbb{N}_* \right\}$, where the classical limit $\hbar \to 0$ is equivalent to $p \to \infty$.

To construct the on-shell algebras, let $\big(\mathcal{S}(\mathcal{X}), \omega\big)$ be the symplectic space on a spacetime/causet $\mathcal{X}$ as discussed in Subsection 2.4.2. Since the construction is fully analogous for a causet C and a spacetime M, I shorten $\mathcal{S}(\mathcal{X})$ to $\mathcal{S}$ in further expressions.

At the value $\hbar = 0$, let us use some C*-algebra $\mathfrak{A}_0$ of bounded functions that includes at least all functions vanishing at infinity,

$$\mathrm{C}_0(\mathcal{S}, \mathbb{C}) \subseteq \mathfrak{A}_0 \subseteq \mathrm{C}_\mathrm{b}(\mathcal{S}, \mathbb{C}), \tag{5.10}$$

with the supremum norm,

$$\|F\| := \sup_{\varphi \in \mathcal{S}} |F(\varphi)| \tag{5.11}$$

for all $f \in \mathrm{C}_\mathrm{b}(\mathcal{S}, \mathbb{C})$. The Poisson bracket (determined by the inverse of the symplectic form ω) is defined on a dense *-subalgebra $\mathcal{A}_0 \subseteq \mathfrak{A}_0$.

Definition 5.1.5. A **quantization** Q is a family of linear maps from the classical *-algebra $\mathcal{A}_0 \subseteq \mathfrak{A}_0$ to the C*-algebra of quantum observables $\mathfrak{A}_\hbar$ parametrized by $\hbar \in I$,

$$Q_\hbar : \mathcal{A}_0 \to \mathfrak{A}_\hbar \tag{5.12}$$

that respects the involution, $\forall F \in \mathcal{A}_0 : Q_\hbar(F)^* = Q_\hbar(\overline{F})$, and if there exists a unit $1 \in \mathcal{A}_0$, it is also unital, $Q_\hbar(1) = \mathbb{1}$.

Definition 5.1.6. A **dequantization** Υ is a family of linear maps

$$\Upsilon_\hbar : \mathfrak{A}_\hbar \to \mathfrak{A}_0, \tag{5.13}$$

that respects involution, $\forall A \in \mathfrak{A}_\hbar : \Upsilon_\hbar(A^*) = \overline{\Upsilon_\hbar(A)}$, and if there exists a unit $\mathbb{1} \in \mathfrak{A}_\hbar$, it is also unital, $\Upsilon_\hbar(\mathbb{1}) = 1$.

Note that in general for a quantization Q, a dequantization Υ and any observable $F \in \mathcal{A}_0$: $(\Upsilon_\hbar \circ Q_\hbar)(F) \neq F$.

I now consider a continuous field for the family of C*-algebras $(\mathfrak{A}_\hbar)_{\hbar \in I}$ over the quantization range I as defined in Dixmier [32], and [33].

Definition 5.1.7. Let I be a topological space and let $(\mathfrak{A}_\hbar)_{\hbar \in I}$ be a family of C*-algebras. A **continuous field of C*-algebras** is a triple $\Big(I, (\mathfrak{A}_\hbar)_{\hbar \in I}, \Gamma\Big)$ with vector fields $\Gamma \subseteq \prod_{\hbar \in I} \mathfrak{A}_\hbar$ such that

1. Γ is a linear subspace of $\prod_{\hbar \in I} \mathfrak{A}_\hbar$, closed under multiplication and involution,
2. for every $\hbar \in I$ the set $\{A(\hbar) \in \mathfrak{A}_\hbar | A \in \Gamma\}$ is dense in $\mathfrak{A}_\hbar$, and

3. for every element $A \in \Gamma$ the norm function $n_A : I \to \mathbb{R}$ defined by

$$n_A(\hbar) := \|A(\hbar)\| \tag{5.14}$$

is continuous, $n_A \in \mathrm{C}(I, \mathbb{R})$, as well as

4. if a vector field $A' \in \prod_{\hbar \in I} \mathfrak{A}_\hbar$ fulfills the condition that for all $\hbar \in I$ and for all real constants $\delta > 0$ there exists a neighborhood $N_\hbar \subset I$ of $\hbar$ such that

$$\exists A \in \Gamma : \forall \hbar' \in N_\hbar : \qquad \|A'(\hbar') - A(\hbar')\| \leq \delta, \tag{5.15}$$

then $A' \in \Gamma$.

The elements of Γ are called (continuous) **sections** of the field.

Products and the involution of any vector fields $A_1, A_2 \in \prod_{\hbar \in I} \mathfrak{A}_\hbar$ are computed pointwise, $A_1 A_2 : \hbar \mapsto A_1(\hbar) A_2(\hbar)$ and $A_1^* : \hbar \mapsto A_1(\hbar)^*$, respectively.

If I is locally compact, then the subset of sections $\mathfrak{A} \subseteq \Gamma$ that have a continuous norm function vanishing at infinity, $n_A \in \mathrm{C}_0(I, \mathbb{R})$, is a C*-algebra with the supremum norm

$$\|A\| := \sup_{\hbar \in I} \|A(\hbar)\|. \tag{5.16}$$

The triple $(I, (\mathfrak{A}_\hbar)_{\hbar \in I}, \mathfrak{A})$ is also referred to as a *C*-bundle* in Kirchberg and Wassermann [54].

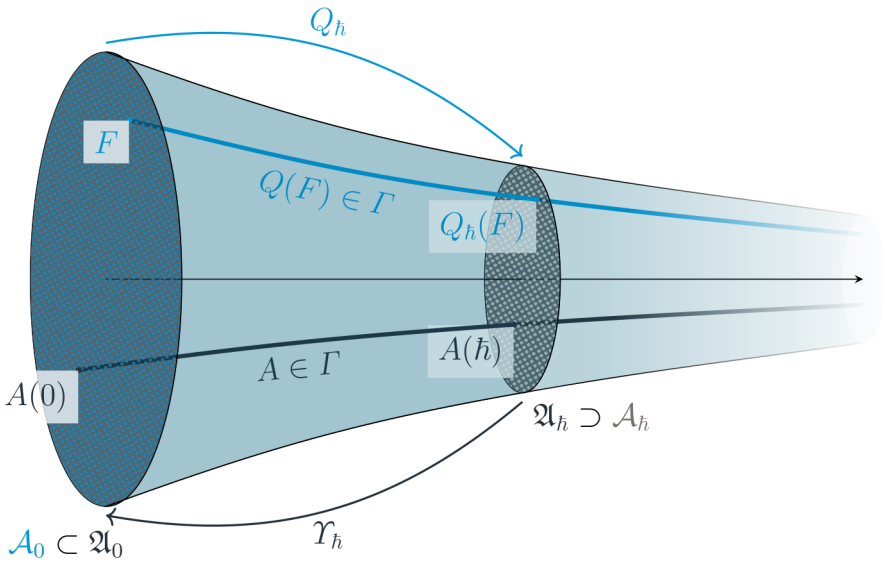

Figure 5.1: Continuous field of C*-algebras $(I, (\mathfrak{A}_\hbar)_{\hbar \in I}, \Gamma)$ with (continuous) sections $Q(F)$ (upper solid line, blue) and A (lower solid line, black), a family of quantization maps $(Q_\hbar)_{\hbar \in I}$ and dequantization maps $(\Upsilon_\hbar)_{\hbar \in I}$. At each value $\hbar \in I$ (horizontal axis), there is a quantum algebra $\mathfrak{A}_\hbar$ (ellipse, black) with a dense Poisson subalgebra $\mathcal{A}_\hbar$ (dotted patterns, blue/gray).

As an example, for any $F \in \mathcal{A}_0$, let us define the vector field

$$Q(F) : \hbar \mapsto \begin{cases} F & \hbar = 0, \\ Q_\hbar(F) & \hbar \in I_*. \end{cases} \tag{5.17}$$

My aim is to determine a quantization such that there exists a continuous field of C*-algebras where these vector fields are continuous sections as illustrated in Figure 5.1. I want the quantization to admit a star product in the following sense [58].

Definition 5.1.8. The **quantization star product** $\star_Q$ of a quantization — if it exists — is the star product (5.5) with operators $B_{Q,k} : \mathcal{A}_0 \times \mathcal{A}_0 \to \mathcal{A}_0$, such that for all $k \in \mathbb{N}$ and for all $F_1, F_2 \in \mathcal{A}_0$, the k-th order remainder

$$R_Q^k(F_1, F_2, \hbar) := \frac{1}{\hbar^k} \left\| Q_\hbar(F_1)Q_\hbar(F_2) - \sum_{j=0}^{k} Q_\hbar\Big(B_{Q,j}(F_1, F_2)\Big)\hbar^j \right\| \tag{5.18}$$

vanishes in the classical limit,

$$\lim_{\hbar \to 0} R_Q^k(F_1, F_2, \hbar) = 0. \tag{5.19}$$

Definition 5.1.9 (after [48])**.** An **infinite order strict deformation quantization** is a quantization Q such that

1. there exists a continuous field of C*-algebras $\Big(I, (\mathfrak{A}_\hbar)_{\hbar \in I}, \Gamma\Big)$ with

$$\forall F \in \mathcal{A}_0 \subseteq \mathfrak{A}_0 : \qquad Q(F) \in \Gamma, \tag{5.20}$$

2. the quantization star product $\star_Q$ exists, and
3. the star product is Poisson compatible.

Heuristically, the star product of two functions $F_1 \star_Q F_2$ of an infinite order strict quantization Q is an asymptotic expansion of $Q_\hbar^{-1}\Big(Q_\hbar(F_1)Q_\hbar(F_2)\Big)$, even though the inverse $Q_\hbar^{-1}$ usually does not exist even if the star product exists.

Sections of a continuous field of C*-algebras (constructed from an infinite order strict deformation quantization) may be considered as well-behaved in the following sense.

Definition 5.1.10. Let $\Big(I, (\mathfrak{A}_\hbar)_{\hbar \in I}, \Gamma\Big)$ be a continuous field of C*-algebras for an infinite order strict deformation quantization Q. A section $A \in \Gamma$ of the continuous field of C*-algebras is **Q-quantization expandable** (*quantization*

expandable or Q-expandable for short) if for any $k \in \mathbb{N}$

$$\exists F_0, \dots, F_k \in \mathcal{A}_0 : \qquad \lim_{\hbar \to 0} \frac{1}{\hbar^k} \left\| A(\hbar) - \sum_{j=0}^{k} Q_\hbar(F_j)\hbar^j \right\| = 0 \tag{5.21}$$

and it is **Υ-dequantization expandable** (*dequantization expandable or Υ-expandable* for short) if for any $k \in \mathbb{N}$

$$\exists F_0, \dots, F_k \in \mathcal{A}_0 : \qquad \lim_{\hbar \to 0} \frac{1}{\hbar^k} \left\| \Upsilon_\hbar\Big(A(\hbar)\Big) - \sum_{j=0}^{k} F_j\hbar^j \right\| = 0. \tag{5.22}$$

Denote the space of Υ-expandable sections by $\Gamma_\Upsilon \subseteq \Gamma$ and let $\Sigma^k_\Upsilon(\cdot, \hbar) : \Gamma_\Upsilon \to \mathcal{A}_0[[\hbar]]$ map to the expansion of any section $A \in \Gamma_\Upsilon$ by the functions from (5.22) truncated at order k,

$$\Sigma^k_\Upsilon(A, \hbar) := \sum_{j=0}^{k} F_j\hbar^j. \tag{5.23}$$

It is immediately seen that the quantization section $Q(F) \subset \Gamma$ for any $F \in \mathcal{A}_0$ is Q-expandable with $F_0 = F$ and $F_k = 0$ for all $k > 0$. Furthermore, if the space of Υ-expandable sections forms a *-subalgebra of Γ, then dequantization also admits a star product (which is not necessarily Poisson compatible).

Definition 5.1.11. The **dequantization star product** $\star_\Upsilon$ is the star product (5.5) with operators $B_{\Upsilon,k} : \mathcal{A}_0 \times \mathcal{A}_0 \to \mathcal{A}_0$ such that for all $k \in \mathbb{N}$ and any dequantization expandable sections $A_1, A_2 \in \Gamma_\Upsilon \subseteq \Gamma$, the expansion map intertwines $\star_\Upsilon$ with the product on Γ, meaning

$$\Sigma^k_\Upsilon(A_1A_2, \hbar) = \sum_{j=0}^{k} B_{\Upsilon,j}\Big(\Sigma^k_\Upsilon(A_1, \hbar), \Sigma^k_\Upsilon(A_2, \hbar)\Big)\hbar^j \mod \hbar^{k+1}. \tag{5.24}$$

Definition 5.1.12. Let $\Big(I, (\mathfrak{A}_\hbar)_{\hbar \in I}, \Gamma\Big)$ be a continuous field of C*-algebras. An **infinite order strict deformation dequantization** is a dequantization Υ such that

1. the dequantization of any section $A \in \Gamma$,

$$\Upsilon(A) : \mathcal{S} \times I \to \mathbb{C}, \qquad \Upsilon(A)(x, \hbar) \mapsto \Upsilon_\hbar\Big(A(\hbar)\Big)(x), \tag{5.25}$$

   is a continuous function $\Upsilon(A) \in \mathrm{C}(\mathcal{S} \times I, \mathbb{C})$,
2. the dequantization star product $\star_\Upsilon$ exists, and
3. the star product is Poisson compatible.

Note that the algebras constructed with deformation quantization are abstract and independent of a specific formulation of operators on a Hilbert space.

Constructing of a strict deformation quantization, a corresponding continuous field of C*-algebras $\left(I, (\mathfrak{A}_\hbar)_{\hbar\in I}, \Gamma\right)$ and a corresponding strict deformation dequantization can be quite complicated for an arbitrary quantum field theory. However, I will show the construction and relation between different quantization methods (including deformation quantization) in the case of a (finite-dimensional) symplectic vector space in Chapter 6. This construction will start with the geometric method reviewed in the following.

5.1.3 Geometric Quantization

For more details on geometric quantization, reviewed in the following, consider the textbook of Woodhouse [112].

Definition 5.1.13. Let $(\mathcal{S}, \omega)$ be a real symplectic manifold. A **quantization bundle** is a Hermitian line bundle $\mathcal{L}_\hbar \to \mathcal{S}$ with connection $\nabla_\hbar$ such that its curvature $R^{\mathcal{L}_\hbar}$ is proportional to the symplectic form,

$$R^{\mathcal{L}_\hbar} := (\nabla_\hbar)^2 = -\frac{\mathrm{i}}{\hbar}\omega, \tag{5.26}$$

parametrized by the quantization parameter as before, $\hbar \in I_*$. The connection preserves the Hermitian inner product on $\mathcal{L}_\hbar$.

The existence of such a quantization bundle is guaranteed when the symplectic form ω is closed and for any closed 2-surface Σ in $\mathcal{S}$:

$$\frac{1}{2\pi\hbar}\int_\Sigma \omega \in \mathbb{Z}, \tag{5.27}$$

but it is not necessarily unique. This is known as the *prequantization (or integrality) condition*, see Ali and Engliš [5, Sec. 2].

For geometric quantization, it is also necessary to choose a *physical* Hilbert space $\mathcal{H}_\hbar \subset \mathrm{L}^2(\mathcal{S}, \mathcal{L}_\hbar)$, a subspace of square-integrable, $\mathcal{L}_\hbar$-valued sections. In some cases, the space $\mathcal{H}_\hbar$ is determined by a polarization.

Definition 5.1.14 (after [5])**.** Let $(\mathcal{S}, \omega)$ be an $2N$-dimensional, real, symplectic manifold and $\mathcal{L}_\hbar \to \mathcal{S}$ a quantization bundle. A (complex) **polarization** is a subbundle $P \subset (\mathrm{T}\mathcal{S})^{\mathbb{C}}$ that is involutive, $X, Y \in \Gamma(P) \implies [X, Y] \in \Gamma(P)$, and maximally isotropic (Lagrangian), $\forall X, Y \in \Gamma(P) : \omega(X, Y) = 0$ and $\forall x \in \mathcal{S} : \dim_{\mathbb{C}} P_x = N$. We say that a section $\psi \in \Gamma(\mathcal{S}, \mathcal{L}_\hbar)$ is **polarized** if $\forall X \in \Gamma(P) : \nabla_{\hbar,X}\psi = 0$. The **physical Hilbert space** $\mathcal{H}_\hbar \subset \mathrm{L}^2(\mathcal{S}, \mathcal{L}_\hbar)$ is a subspace constructed from polarized, square-integrable sections of $\mathcal{L}_\hbar$.

Compact Kähler manifolds are well-studied examples with a polarization determined by a compatible *complex structure*, see Bordemann, Meinrenken, and

Schlichenmaier [17], Karabegov and Schlichenmaier [51], and Schlichenmaier [99].

Definition 5.1.15 (see Da Silva [28])**.** For any $x \in \mathcal{S}$, a **complex structure** on the tangent space $\mathrm{T}_x\mathcal{S}$ is a linear map $J_x : \mathrm{T}_x\mathcal{S} \to \mathrm{T}_x\mathcal{S}$ such that $J_x^2 = -\mathbb{1}$. An **almost complex structure** is a smooth field of complex structures, $J : \mathrm{T}\mathcal{S} \to \mathrm{T}\mathcal{S}$ (with $J^2 = -\mathbb{1}$). The **Nijenhuis tensor** for an almost complex structure J is a tensor N_J such that for any two vector fields $X, Y \in \Gamma(\mathrm{T}\mathcal{S})$ (with Lie bracket $[X, Y]$):

$$N_J(X,Y) := [JX, JY] - J[JX, Y] - J[X, JY] - [X, Y]. \tag{5.28}$$

The theorem by Newlander and Nirenberg [84] states that an almost complex structure J is a complex structure on $\mathrm{T}\mathcal{S}$ if $N_J = 0$.

Definition 5.1.16 (see [31])**.** A **Kähler manifold** is a symplectic manifold $(\mathcal{S}, \omega)$ with a complex structure $J : \mathrm{T}\mathcal{S} \to \mathrm{T}\mathcal{S}$ that is compatible with the symplectic form, meaning there exists a bilinear form η on $\mathrm{T}\mathcal{S}$ such that

$$\forall v_1, v_2 \in \mathrm{T}\mathcal{S} : \qquad \eta(v_1, v_2) = \omega(v_1, Jv_2). \tag{5.29}$$

A pair of a symplectic form and a bilinear form (ω, η) is called **Kähler** if it fulfills this relation.

For a Kähler manifold, consider the split of the complexified tangent bundle by the complex structure $J : \mathrm{T}\mathcal{S} \to \mathrm{T}\mathcal{S}$ and its linear extension to the complexified tangent bundle $\mathrm{T}^{\mathbb{C}}\mathcal{S}$ (where it has eigenvalues $\pm\mathrm{i}$) into the holomorphic and anti-holomorphic tangent bundles,

$$\mathrm{T}^{\mathbb{C}}\mathcal{S} = \mathrm{T}^{1,0}\mathcal{S} \oplus \mathrm{T}^{0,1}\mathcal{S}. \tag{5.30}$$

The anti-holomorphic tangent bundle is a polarization $\overline{P}_J = \mathrm{T}^{0,1}\mathcal{S}$ — called the Kähler polarization — such that the polarized sections are holomorphic.

For the more general case of a symplectic manifold without pre-defined complex structure, I will consider an alternative construction of the physical Hilbert space. Given a symplectic manifold with Riemannian metric, let us identify the physical Hilbert space as a subspace of quantization bundle sections that correspond to the lowest part of the spectrum of a Laplacian [61], since this reduces to the Kähler polarization in the special case of a Kähler manifold.

Definition 5.1.17 (see [45])**.** Let $(\mathcal{S}, \omega, g)$ be a symplectic manifold with Riemannian metric g, $\mathcal{L}_\hbar \to \mathcal{S}$ be a quantization bundle for some $\hbar \in I_*$. The **Bochner Laplacian** $\Delta_\hbar$ is an unbounded operator on sections $\Gamma(\mathcal{S}, \mathcal{L}_\hbar)$ determined by the

quantization bundle connection $\nabla_\hbar$ and metric g,

$$\Delta_\hbar = \nabla_\hbar^* \nabla_\hbar. \tag{5.31}$$

In the case of a Kähler manifold, let ∇_i denote the holomorphic and $\nabla_{\bar{\jmath}}$ the anti-holomorphic components of the connection $\nabla_\hbar$, with $i \in [1, N]$, $\bar{\jmath} \in [\bar{1}, \bar{N}]$. There is another, naturally defined Laplace operator, the Kodaira Laplacian

$$\Delta_\hbar^{\mathrm{K}} = -g^{i\bar{\jmath}} \nabla_i \nabla_{\bar{\jmath}}, \tag{5.32}$$

where I use the summation convention over the indices i and $\bar{\jmath}$. The Kodaira Laplacian is related to the Bochner Laplacian,

$$2\Delta_\hbar^{\mathrm{K}} = \Delta_\hbar - \frac{N}{\hbar}. \tag{5.33}$$

With the Kähler polarization, the physical Hilbert space is constructed from the space of holomorphically polarized sections with respect to the complex structure of the Kähler manifold. The kernel of the Kodaira Laplacian (5.32) is precisely this space of holomorphic sections. The Kodaira and the Bochner Laplacian are positive so the holomorphic section space is the eigenspace of the Bochner Laplacian corresponding to the lowest eigenvalue $\frac{N}{\hbar}$, by (5.33). Thus, the physical Hilbert space is determined by the spectral decomposition of the Bochner Laplacian.

In Guillemin and Uribe [45], it was shown how to use a renormalized Bochner Laplacian for a natural generalization to almost Kähler manifolds (with a non-integrable, almost complex structure). The renormalized Bochner Laplacian is a generalization of the expression on the right-hand side of (5.33) and coincides with $2\Delta_\hbar^{\mathrm{K}}$ in the Kähler case, see also Borthwick and Uribe [18]. A choice of a physical Hilbert space is again given by the eigenspace corresponding to the lowest part of the spectrum, even though the lowest part does not have to be a single eigenvalue anymore.

For the arguments in Chapter 6, I will need yet an even further generalization to a symplectic manifold with Riemannian metric but without any pre-defined (almost) complex structure, see Ma and Marinescu [61], and [62]. Let us consider a $2N$-dimensional, compact, real, symplectic manifold $(\mathcal{S}, \omega)$ with quantization bundle $\mathcal{L}_\hbar \to \mathcal{S}$ and Riemannian metric g. Let $\Theta : \mathrm{T}\mathcal{S} \to \mathrm{T}\mathcal{S}$ be the anti-self-adjoint linear map such that for all $v_1, v_2 \in \mathrm{T}\mathcal{S}$

$$\omega(v_1, v_2) = g(v_1, \Theta v_2). \tag{5.34}$$

There exists an almost complex structure $J : \mathrm{T}\mathcal{S} \to \mathrm{T}\mathcal{S}$ such that $g(Jv_1, Jv_2) = g(v_1, v_2)$ and $\omega(Jv_1, Jv_2) = \omega(v_1, v_2)$ for all $v_1, v_2 \in \mathrm{T}\mathcal{S}$ [61]. Let η be the compatible metric such that for all $v_1, v_2 \in \mathrm{T}\mathcal{S}$

$$\eta(v_1, v_2) = \omega(v_1, Jv_2). \tag{5.35}$$

The almost complex structure commutes with Θ, so it is given by

$$J = -\Theta|\Theta|^{-1}. \tag{5.36}$$

At every point $x \in \mathcal{S}$, the operator Θ_x is an endomorphism on $\mathrm{T}_x\mathcal{S}$. Let half the trace of $|\Theta_x|$ be denoted as

$$\lambda(x) := \frac{1}{2}\operatorname{tr}(J_x\Theta_x) = \frac{1}{2}\operatorname{tr}|\Theta_x|. \tag{5.37}$$

Note that in the special case of a Kähler manifold with a Kähler metric, we have $|\Theta_x| = \mathbb{1}$ and this trace function is N, half the real dimension of $\mathcal{S}$. It was shown that the function $\lambda(x)$ is positive for all $x \in \mathcal{S}$ [61].

A renormalized Bochner Laplacian $\Delta_{\hbar,\Phi}$ is then defined with λ and a smooth Hermitian section Φ on a tensor product of the quantization line bundle with a vector bundle, see Ma and Marinescu [60]. They have shown — using Spin$^{\mathbb{C}}$ Dirac operators — that there exist two positive constants κ and μ that are independent of $\hbar$, such that the spectrum of the renormalized Bochner Laplacian fulfills

$$\operatorname{spec}(\Delta_{\hbar,\Phi}) \subset [-\kappa,\kappa] \cup \left[\frac{2\mu}{\hbar} - \kappa, \infty\right). \tag{5.38}$$

Given the spectrum condition (5.38) of the renormalized Bochner Laplacian on a symplectic manifold with a Riemannian metric $(\mathcal{S},\omega,g)$ and a quantization bundle $\mathcal{L}_\hbar \to \mathcal{S}$, the physical Hilbert space $\mathcal{H}_\hbar \subset \mathrm{L}^2(\mathcal{S},\mathcal{L}_\hbar)$ is spanned by the sections corresponding to the lower part of the spectrum i.e., the part contained in $[-\kappa,\kappa]$.

For the (on-shell) solution space of the real scalar field on a causet, I derived the symplectic vector space with inner product $\big(\mathcal{S},\omega,\langle\cdot,\cdot\rangle\big)$ in Section 2.3. I will use the method of the Bochner Laplacian to derive the physical Hilbert space $\mathcal{H}_\hbar$ in Chapter 6. The inner product determines a metric g and I will use a basis of holomorphic and anti-holomorphic vectors. This choice of a complex basis will allow me to write elements of the Hilbert space as holomorphic sections with respect to the complex structure J given by (5.36). A similar procedure is possible for the solution space over a spacetime manifold [94, Sec. 5.3], where the given inner product is determined by the symmetric part H of the operator B, see (5.58).

5.1.4 (Berezin)-Toeplitz Quantization and Dequantization

For a given symplectic manifold $(\mathcal{S},\omega)$, suppose that a Hilbert space $\mathcal{H}_\hbar$ has been constructed as a subspace of square-integrable sections of the quantization bundles $\mathrm{L}^2(\mathcal{S},\mathcal{L}_\hbar)$ discussed before. Let

$$\Pi_\hbar : \mathrm{L}^2(\mathcal{S},\mathcal{L}_\hbar) \to \mathcal{H}_\hbar \tag{5.39}$$

be the projector to this Hilbert space. Using this projector, a quantization map is defined as follows [30].

Definition 5.1.18. The **(Berezin)-Toeplitz quantization** map $T_\hbar$ assigns a bounded operator on the Hilbert space $\mathcal{H}_\hbar$ to every classical observable in a dense *-subalgebra $\mathcal{A}_0 \subset \mathfrak{A}_0$,

$$T_\hbar : \mathcal{A}_0 \to \mathcal{B}(\mathcal{H}_\hbar), \tag{5.40}$$

defined via the projector $\mathit{\Pi}_\hbar$ such that

$$\forall F \in \mathcal{A}_0 : \forall \psi \in \mathcal{H}_\hbar : \qquad T_\hbar(F)\psi = \mathit{\Pi}_\hbar(F\psi). \tag{5.41}$$

For each $\hbar \in I$, let $\mathfrak{A}_\hbar \subseteq \mathcal{B}(\mathcal{H}_\hbar)$ be a C*-algebra such that it contains the image of $T_\hbar$. The Toeplitz quantization map $T_\hbar$ is linear and respects involution of the *-algebra $\mathcal{A}_0 \subset \mathfrak{A}_0$. Its domain actually extends to all bounded functions $\mathrm{C_b}(\mathcal{S}, \mathbb{C})$ so that $1 \in \mathrm{C_b}(\mathcal{S}, \mathbb{C})$ is mapped to $\mathbb{1} \in \mathcal{B}(\mathcal{H}_\hbar)$. However, it will be easier to use the C*-algebra of compact operators $\mathfrak{A}_\hbar = \mathcal{K}(\mathcal{H}_\hbar)$ in the construction of a continuous field of C*-algebras. Note that $\mathfrak{A}_\hbar$ coincides with $\mathcal{B}(\mathcal{H}_\hbar)$ if $\dim \mathcal{H}_\hbar < \infty$. The restriction to a dense subalgebra $\mathcal{A}_0 \subset \mathfrak{A}_0$ is necessary for the construction of star products.

If the Toeplitz operators of compactly supported functions $\mathrm{C_c}(\mathcal{S}, \mathbb{C})$ on the physical Hilbert space $\mathcal{H}_\hbar$ are of trace-class, let us define a measure $\mu_\hbar$ such that

$$\mathrm{Tr}\Big(T_\hbar(F)\Big) = \int_{\mathcal{S}} F \, \mathrm{d}\mu_\hbar \tag{5.42}$$

holds for all $F \in \mathrm{C_c}(\mathcal{S}, \mathbb{C})$. When such a measure exists, there is an adjoint operation to Toeplitz quantization.

Definition 5.1.19. Suppose the measure $\mu_\hbar$ determined by (5.42) exists. The **(Berezin)-Toeplitz dequantization** is a family of linear maps

$$\mathit{\Xi}_\hbar : \mathfrak{A}_\hbar \to \mathfrak{A}_0, \tag{5.43}$$

such that for all complex-valued, compactly supported functions $F \in \mathrm{C_c}(\mathcal{S}, \mathbb{C})$ and all operators $A_\hbar \in \mathfrak{A}_\hbar$

$$\mathrm{Tr}\Big(A_\hbar T_\hbar(F)\Big) = \int_{\mathcal{S}} \mathit{\Xi}_\hbar(A_\hbar) F \, \mathrm{d}\mu_\hbar. \tag{5.44}$$

I only consider the case of a symplectic manifold with a physical Hilbert space $\mathcal{H}_\hbar$ where Toeplitz dequantization exists. If the algebras $\mathfrak{A}_\hbar$ are unital, then Toeplitz dequantization preserves the unit, $\mathit{\Xi}_\hbar(\mathbb{1}) = 1$ since the measure is normalized,

$$\forall F \in \mathrm{C_c}(\mathcal{S}, \mathbb{C}) : \qquad \int_{\mathcal{S}} \mathit{\Xi}_\hbar(\mathbb{1}) F \, \mathrm{d}\mu_\hbar = \int_{\mathcal{S}} F \, \mathrm{d}\mu_\hbar. \tag{5.45}$$

Definition 5.1.20 (see [58])**.** Let $\mathcal{A}_0$ be the algebra of classical observables over a symplectic manifold that admits Toeplitz quantization T and dequantization Ξ. The **Berezin transform** of a classical observable $F \in \mathcal{A}_0$ is $(\Xi_\hbar \circ T_\hbar)(F)$.

An observable $F \in \mathcal{A}_0$ is also known as the *contravariant* or *lower* symbol of the Toeplitz operator $T_\hbar(F)$, while the Berezin transform $(\Xi_\hbar \circ T_\hbar)(F)$ is called the *covariant* or *upper* symbol of $T_\hbar(F)$, see Berezin [13], where in general $(\Xi_\hbar \circ T_\hbar)(F) \neq F$.

5.2 States and Representations

For this section, I assume a basic understanding of a Hilbert space $\mathcal{H}_\hbar$ and its space of bounded linear operators $\mathcal{B}(\mathcal{H}_\hbar)$. At first, I review the algebraic perspective on physical observations as *states* and define the terminology to discuss the Sorkin-Johnston state which is commonly considered for the scalar quantum field theory on a causet Sorkin [102], and [103].

In the algebraic framework, states are defined as follows [33].

Definition 5.2.1. Let $\mathcal{A}$ be a *-algebra, see Definition 2.1.4. A **state** is a linear functional $\sigma : \mathcal{A} \to \mathbb{C}$ that is positive,

$$\forall A \in \mathcal{A} : \qquad \sigma(A^*A) \geq 0, \tag{5.46}$$

and has unit norm.

Definition 5.2.2. A state $\sigma : \mathcal{A} \to \mathbb{C}$ is **mixed** if there exists a convex combination of two other, distinct states $\sigma_{1,2} : \mathcal{A} \to \mathbb{C}$,

$$\exists \lambda \in (0,1) \subset \mathbb{R} : \qquad \sigma = \lambda\sigma_1 + (1-\lambda)\sigma_2. \tag{5.47}$$

A state is **pure** if it is not mixed.

5.2.1 Representations

The algebraic notion of states is independent of a particular Hilbert space formulation and hence also useful for abstract *-algebras like those constructed with the methods of deformation quantization, see Subsection 5.1.1 and Subsection 5.1.2. However, in some cases it might be necessary or at least useful to have a representation of an abstract *-algebra as an algebra on a Hilbert space. So let us briefly review the representation of an abstract *-algebra following Khavkine and Moretti [52], and Dereziński and Gérard [31].

Definition 5.2.3. Let $\mathcal{A}_1$ and $\mathcal{A}_2$ be (unital) *-algebras. A ***-morphism** is a map $\alpha : \mathcal{A}_1 \to \mathcal{A}_2$ that preserves the algebraic structure and the involution, meaning that $\forall A, A' \in \mathcal{A}_1 : \forall c, c' \in \mathbb{C}$:

$$\alpha(AA') = \alpha(A)\alpha(A'), \tag{5.48a}$$
$$\alpha(cA + c'A') = c\alpha(A) + c'\alpha(A'), \tag{5.48b}$$
$$\alpha(A^*) = \alpha(A)^*, \tag{5.48c}$$

and if the algebras are unital, then

$$\alpha(\mathbb{1}) = \mathbb{1}. \tag{5.48d}$$

Notice that the algebra of bounded, linear operators on a dense subset of a Hilbert space is a *-algebra, which leads us to the following definition.

Definition 5.2.4. Let $\mathcal{H}$ be a Hilbert space and let $\mathcal{K} \subseteq \mathcal{H}$ be a dense subspace. A **representation** of a *-algebra $\mathcal{A}$ is a *-morphism $\rho : \mathcal{A} \to \mathcal{B}(\mathcal{K})$. The representation ρ is **faithful** if $\ker \rho = \{0\}$ and it is **irreducible** if every subspace of $\mathcal{H}$ invariant under the image of ρ is trivial.

There is a further property of representations (unitary equivalence) that will be necessary to follow the details of the Gelfand-Naimark-Segal (GNS) construction, which yields a Hilbert space representation of any abstract *-algebra and a state. However, for this brief review here, let me just summarize the main statement of the GNS theorem without a proof.

Theorem 5.2.5. *Let $\mathcal{A}$ be a unital *-algebra and $\sigma : \mathcal{A} \to \mathbb{C}$ a state. There exists a representation ρ_σ on a dense subset $\mathcal{K}_\sigma$ of some Hilbert space $\mathcal{H}_\sigma$ (with inner product $\langle \cdot, \cdot \rangle$) and a unit vector (the "vacuum") $\Omega_\sigma \in \mathcal{H}_\sigma$ such that*

$$\forall A \in \mathcal{A} : \qquad \sigma(A) = \langle \Omega_\sigma, \rho_\sigma(A)\Omega_\sigma \rangle , \tag{5.49a}$$
$$\mathcal{H}_\sigma = \rho_\sigma(\mathcal{A})\Omega_\sigma. \tag{5.49b}$$

Proof. For example, see [52, Thm. 5.1.13].

Note that the GNS construction is useful whenever we want to find a representation for a given *-algebra in terms of bounded operators on some Hilbert space. However, using the method of geometric quantization, we directly obtain a physical Hilbert space and the quantum algebra is (a subset of) the space of bounded operators on that Hilbert space. For the case of a finite causet, I will use such a geometric construction in Chapter 6.

5.2.2 Weyl Algebras and Quasi-Free States

Let us now return to the case of a scalar field theory on a spacetime or causet $\mathcal{X}$, following the arguments and definitions given in [94] and [29], respectively.

Recall from Chapter 2 the space of regular (off-shell) observables $\mathcal{F}_{\text{reg}}(\mathcal{X})$. The *Moyal-Weyl star product* $\star_0$ of two regular observables $F_1, F_2 \in \mathcal{F}_{\text{reg}}(\mathcal{X})$ at a point $\varphi \in \mathcal{E}(\mathcal{X})$ is given by

$$(F_1 \star_0 F_2)(\varphi) := \sum_{k=0}^{\infty} \frac{1}{k!} \left\langle F_1^{(k)}(\varphi), \left(\tfrac{\mathrm{i}}{2}\pi_{\text{off}}^{\sharp}\right)^{\otimes k} F_2^{(k)}(\varphi) \right\rangle \hbar^k. \tag{5.50}$$

I write the pointwise product of the algebra as $p : F_1 \otimes F_2 \mapsto F_1 F_2$. For any bilinear form B on $\mathcal{F}_{\text{reg}}(\mathcal{X})$, let D_B be a map such that

$$D_B(F_1 \otimes F_2)(\varphi_1 \otimes \varphi_2) := \left\langle F_1^{(1)}(\varphi_1), B^{\sharp} F_2^{(1)}(\varphi_2) \right\rangle, \tag{5.51}$$

which is the Poisson bracket in the case where $B = \pi_{\text{off}}$ and $\varphi_1 = \varphi_2$. With this notation, the Moyal-Weyl star product takes the exponential expression

$$F_1 \star_0 F_2 = p \circ \exp\left(\frac{\mathrm{i}}{2}\hbar D_{\pi_{\text{off}}}\right)(F_1 \otimes F_2). \tag{5.52}$$

For any $\phi \in \mathcal{E}(\mathcal{X})$, recall that there is a linear functional Φ_ϕ given by (2.9) for causets and given by (2.10) for spacetimes.

Definition 5.2.6. Let $\mathcal{E}$ be the space of fields over a spacetime or causet $\mathcal{X}$ and let $\mathcal{F}_{\text{lin}}(\mathcal{X})$ be the space of linear observables. Let $\{\cdot,\cdot\}$ be a Poisson bracket for (regular) observables. A **Weyl algebra** $(\mathfrak{W}_\hbar, \bullet_\hbar, {}^*)$ is a C*-algebra with a (non-commutative) product $\bullet_\hbar$ that is spanned by the image of a map $W : \mathcal{F}_{\text{lin}}(\mathcal{X}) \to \mathfrak{W}_\hbar$ and any two elements in the image fulfill the **Weyl relations**:

$$\forall \phi, \phi' \in \mathcal{E} : \quad W(\Phi_\phi) \bullet_\hbar W(\Phi_{\phi'}) = \exp\left(-\frac{\mathrm{i}\hbar}{2}\{\Phi_\phi, \Phi_{\phi'}\}\right) W(\Phi_\phi + \Phi_{\phi'}), \tag{5.53a}$$

$$\forall \phi \in \mathcal{E} : \quad W(\Phi_\phi)^* = W(-\Phi_\phi), \tag{5.53b}$$

$$W(0) = \mathbb{1}. \tag{5.53c}$$

Let us define the Weyl functional $W : \mathcal{F}_{\text{lin}}(\mathcal{X}) \to \mathcal{F}_{\text{reg}}(\mathcal{X})$ such that for all $\Phi_\phi \in \mathcal{F}_{\text{lin}}(\mathcal{X})$:

$$W(\Phi_\phi) := \exp\left(\mathrm{i}\Phi_\phi\right). \tag{5.54}$$

The image of the map W spans the algebra $\left(\mathcal{F}_{\text{reg}}(\mathcal{X})[[\hbar]], \star_0\right)$ that fulfills the Weyl relations (and can be completed to a C*-algebra) as shown in [29, Sec. IV.B] for causets and in [94, Sec. 5.1] for spacetimes.

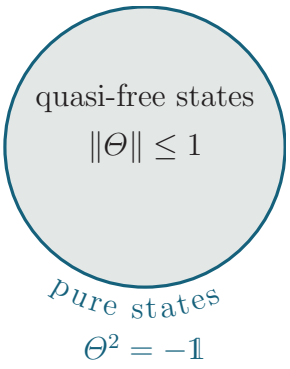

Figure 5.2: Illustration of the operator norm of Θ determined by the symplectic form and the inner product η_{qf} as given in (5.57). For pure states, the operator norm lies on the boundary (has unit norm) and Θ is a complex structure.

Definition 5.2.7 (see [31])**.** Let $\mathfrak{W}_\hbar$ be a Weyl algebra with the generator map $W_\hbar : \mathcal{F}_{\text{lin}}(\mathcal{X}) \to \mathfrak{W}_\hbar$ as in Definition 5.2.6. A **quasi-free (or Gaussian) state** is a state $\sigma_\hbar : \mathfrak{W}_\hbar \to \mathbb{C}$ that is determined by a symmetric, bilinear form γ, called **covariance**, so that for all $\Phi \in \mathcal{F}_{\text{lin}}$:

$$\sigma_\hbar\Big(W_\hbar(\Phi)\Big) = \exp\left(-\frac{\hbar}{4}\gamma(\Phi,\Phi)\right). \tag{5.55}$$

Given a Weyl algebra $\mathfrak{W}_\hbar$ for a symplectic space $(\mathcal{S},\omega)$ — like the symplectic space constructed in Subsection 2.4.2 — and a quasi-free state $\sigma_\hbar : \mathfrak{W}_\hbar \to \mathbb{C}$ with covariance γ, let us consider the bilinear form $\eta_{\text{qf}} := \gamma^{-1}$. The bilinear forms ω and η_{qf} satisfy the Cauchy-Schwarz inequality, $\forall \varphi, \psi \in \mathcal{S}$:

$$|\omega(\varphi,\psi)|^2 \leq \eta_{\text{qf}}(\varphi,\varphi)\eta_{\text{qf}}(\psi,\psi), \tag{5.56}$$

known as the domination condition for quasi-free states, see Fewster and Verch [39]. We may express the bilinear form η_{qf} in terms of the symplectic form and some operator $\Theta \in \text{End}(\mathcal{S})$ given such that for all $\varphi, \psi \in \mathcal{S}$:

$$\omega(\varphi,\Theta\psi) = \eta_{\text{qf}}(\varphi,\psi). \tag{5.57}$$

The domination condition is equivalent to the fact that this operator is bounded by one, $\|\Theta\| \leq 1$. Figure 5.2 illustrates this condition on the operator norm. A pure, quasi-free state saturates the Cauchy-Schwartz inequality with $\Theta^2 = -\mathbb{1}$ (circle boundary, blue), meaning that Θ is a complex structure and the pair $(\omega, \eta_{\text{qf}})$ is Kähler, see Definition 5.1.16.

5.2.3 Exponential Star Products and Hadamard States

Let us continue with a review of the relation between star products and quasi-free states, following analogous arguments for a spacetime or causet $\mathcal{X}$ [94, 29].

The Moyal-Weyl star product with the exponential form (5.52) is a special case of an exponential star product for regular observables $\mathcal{F}_{\text{reg}}(\mathcal{X})$. Any exponential star product is fully determined by the first order term in the power series (5.5). With some symmetric, bilinear form H, this first order term is given by

$$B = H + \frac{\mathrm{i}}{2}\pi_{\text{off}}. \tag{5.58}$$

For any regular observables $F_1, F_2 \in \mathcal{F}_{\text{reg}}(\mathcal{X})$ the exponential star product is

$$F_1 \star_H F_2 = p \circ \exp\Big(\hbar D_B\Big)(F_1 \otimes F_2). \tag{5.59}$$

For a finite causet C, for example, the 1-st order term $B_1 = B$ in an exponential star product $\star_H$ is composed of the Pauli-Jordan operator E and a symmetric term H,

$$B^{ij} = H^{ij} + \frac{\mathrm{i}}{2}E^{ij}. \tag{5.60}$$

The higher orders (5.5) are given as follows

$$(B_k)^{i_1 i_2 \dots i_k j_1 j_2 \dots j_k} = \prod_{n=1}^{k} B^{i_n j_n}. \tag{5.61}$$

As discussed in [29], the term B has the physical interpretation of a *two-point function* when the symmetric part H is chosen such that, for all $\Phi_f \in \mathcal{F}_{\text{lin}}(C)$ with $f \in \mathcal{D}(C)$, the first order form B (or its corresponding operator $B^\sharp : (\mathcal{E}^*)^{\mathbb{C}}(C) \to \mathcal{E}^{\mathbb{C}}(C)$) has the properties

$$\text{positivity:} \qquad \Big\langle B, \overline{f} \otimes f \Big\rangle \geq 0, \tag{5.62a}$$

$$\text{imaginary part:} \qquad 2\,\mathrm{Im}\, B^\sharp = \pi_{\text{off}}^\sharp, \tag{5.62b}$$

$$\text{e.o.m.-compatibility:} \qquad \ker(B^\sharp) \subseteq \ker(\pi_{\text{off}}^\sharp). \tag{5.62c}$$

Let $\star_H$ denote the star product for some map H that fulfills these conditions. So we obtain a quantum algebra $\mathfrak{A}_{\hbar,H}(C)$ of formal power series in $\hbar$ with the star product $\star_H$.

For a spacetime manifold M, the conditions (5.62) become the following properties of the *Wightman propagator* or *two-point function* B, where for all $f, f' \in \mathcal{D}(M)$:

$$\text{positivity:} \qquad \Big\langle B, \overline{f} \otimes f \Big\rangle \geq 0, \tag{5.63a}$$

$$\text{imaginary part:} \qquad 2\,\mathrm{Im}\, B^\sharp = \pi_{\text{off}}^\sharp, \tag{5.63b}$$

$$\text{e.o.m.-compatibility:} \qquad \langle B, Pf \otimes f' \rangle = \langle B, f \otimes Pf' \rangle = 0. \tag{5.63c}$$

For a spacetime manifold, B has to fulfill another property namely a condition on its *wavefront set*, see Radzikowski [90]. Here, I follow closely to the definitions given in Khavkine and Moretti [52].

Definition 5.2.8. Let (M, g) be a (4-dimensional) spacetime manifold, $t \in \mathrm{C}^\infty(M, \mathbb{R})$ a time function with timelike, future directed gradient everywhere, and let

$$h(x, y) := \frac{1}{2} g\Big(\exp_x^{-1}(y), \exp_x^{-1}(y)\Big), \tag{5.64a}$$

$$h_\varepsilon(x, y) := h(x, y) + 2\mathrm{i}\varepsilon\Big(t(x) - t(y)\Big) + \varepsilon^2. \tag{5.64b}$$

A bi-distribution B is **Hadamard** if for every point $x_0 \in M$ there exists a convex neighbourhood N_0 such that for all $n \in \mathbb{N}$ there exist functions $u, v_0, v_1, \ldots \in \mathrm{C}^\infty(M^2, \mathbb{R})$ that are uniquely determined by the local geometry, see Moretti [81, Appx. A], and a length scale $\lambda > 0$ as well as a function $w_n \in \mathrm{C}^{2n+1}(M^2, \mathbb{R})$, such that the bi-distribution as a local map $B : N_0 \times N_0 \to \mathbb{R}$ takes the form

$$B = \lim_{\varepsilon \to 0^+} \left(\frac{u}{h_\varepsilon} + \sum_{j=0}^{n} h^j v_j \log\left(\frac{h_\varepsilon}{\lambda^2}\right) + w_n \right). \tag{5.65}$$

A **Hadamard state** is a state with a two-point function that is Hadamard.

Hadamard states are the class of states for a given spacetime manifold that are generally consider as *physical* states, for example, see Fewster and Verch [40]. For a scalar field theory, a Wightman propagator B with the properties (5.63) (including the Hadamard condition) always exists, but it is not unique. The star product $\star_H$ extends from $\mathcal{F}_{\mathrm{reg}}(M)$ to $\mathcal{F}_{\mu\mathrm{c}}(M)$ as shown in Dütsch and Fredenhagen [36], and [37].

Two exponential star products $\star_H$ and $\star_{H'}$ can be equivalent in the following sense.

Definition 5.2.9. Let $\mathcal{X}$ be a spacetime/causet. A **gauge equivalence** is a linear map $\alpha : \mathcal{F}_{\mathrm{reg}}(\mathcal{X}) \to \mathcal{F}_{\mathrm{reg}}[[\hbar]](\mathcal{X})$ determined by differential operators $\alpha_n : \mathcal{F}_{\mathrm{reg}}(\mathcal{X}) \to \mathcal{F}_{\mathrm{reg}}(\mathcal{X})$ such that

$$\alpha = \mathbb{1} + \sum_{n=1}^{\infty} \hbar^n \alpha_n. \tag{5.66}$$

Any two star products $\star_H$ and $\star_{H'}$ are related by a gauge equivalence $\alpha_{H-H'}$ such that for all $F_1, F_2 \in \mathcal{F}_{\mathrm{reg}}(\mathcal{X})$:

$$\alpha_{H-H'}(F_1) \star_H \alpha_{H-H'}(F_2) = \alpha_{H-H'}\left(F_1 \star_{H'} F_2\right), \tag{5.67}$$

where $H - H'$ is a smooth functional [94]. This isomorphism splits into the gauge equivalence $\alpha_{H-H'} = \alpha_H \alpha_{H'}^{-1}$, where for all $F \in \mathcal{F}_{\mathrm{reg}}(\mathcal{X})$ and at all points $\varphi \in \mathcal{E}(\mathcal{X})$,

$$d_H(F)(\varphi) := \left\langle H, F^{(2)}(\varphi) \right\rangle, \tag{5.68a}$$

$$\alpha_H := \exp\left(\frac{\hbar}{2} d_H\right). \tag{5.68b}$$

Note that $\mathfrak{A}_{\hbar,H}(\mathcal{X})$ is off-shell and the on-shell algebras are determined via a quotient as discussed in Subsection 2.4.2.

The covariance of a quasi-free state is the symmetric part H in the term $B = H + \frac{\mathrm{i}}{2}\pi^\sharp$ that determines an exponential star product, for example, with $\pi = \omega^{-1}$ for the on-shell Poisson algebras (see Subsection 2.4.2). The inequality (5.56) is equivalent to the positivity condition of B as given in (5.62a) for causets and in (5.63a) for spacetimes, and the inequalities are equivalent to the existence of a quasi-free state with covariance $\gamma = H$. For the proofs of the equivalences of these statements, see for example [31].

5.2.4 The Sorkin-Johnston State

Writing the original definition of the state given by Sorkin [103] and Johnston [50] with the previously defined terms, we have the following.

Definition 5.2.10. Let $\mathcal{S}$ be a symplectic space with a symplectic form (2.68) in terms of the on-shell Pauli-Jordan operator E_{on}, and a symmetric, bilinear form η such that $\forall \varphi, \psi \in \mathcal{S}$:

$$\eta(\varphi, \psi) = \omega\left(\varphi, (-E_{\mathrm{on}}^{-1}|E_{\mathrm{on}}|)\psi\right). \tag{5.69}$$

Let $\mathfrak{W}_\hbar$ be the Weyl algebra for $\mathcal{S}$ with the map $W_\hbar : \mathcal{S}^* \to \mathfrak{W}_\hbar$ that yields the generators of the algebra. The **Sorkin-Johnston state** is the quasi-free state $\sigma_{\mathrm{SJ}} : \mathfrak{W}_\hbar \to \mathbb{C}$, so that for all $\phi \in \mathcal{S}^*$:

$$\sigma_{\mathrm{SJ}}\Big(W_\hbar(\phi)\Big) = \exp\left(-\frac{\hbar}{4}\eta^{-1}(\phi, \phi)\right), \tag{5.70}$$

meaning that η^{-1} is the covariance of the state.

The fact that (ω, η) is Kähler means that the Sorkin-Johnston state is pure. By the one-to-one correspondence between quasi-free states and two-point functions, the Sorkin-Johnston state corresponds to a two-point function B_{SJ} determined by the on-shell (restricted) Pauli-Jordan operator

$$A_{\mathrm{SJ}} = \frac{1}{2}\Big(|E| + \mathrm{i}E\Big). \tag{5.71}$$

Let us call A_{SJ} the *Sorkin-Johnston operator*.

Sorkin and Johnston formulated the properties of the state σ_{SJ} as a set of axioms on the Sorkin-Johnston operator [50, 102, 103]. So the expression (5.71)

is the unique solution to the axioms

$$\text{positivity:} \qquad A_{\mathrm{SJ}} \geq 0, \tag{5.72a}$$

$$\text{commutator:} \qquad A_{\mathrm{SJ}} - \overline{A}_{\mathrm{SJ}} = \mathrm{i}E, \tag{5.72b}$$

$$\text{purity:} \qquad A_{\mathrm{SJ}}\overline{A}_{\mathrm{SJ}} = 0. \tag{5.72c}$$

Notice that these axioms are very similar to the conditions that one would get on a two-point function B as shown in (5.62). However, these axioms depend on the choice of an inner product on $\mathcal{S}$, which is particularly important for the last axiom (5.72c) that involves an operator multiplication. This multiplication is only defined between operators on $\mathcal{S}$, but not for a two-point function B. Hence, the uniqueness of the Sorkin-Johnston operator as solution to the axioms is a mere consequence of the fixed inner product (implicit in the operator E).

In order to derive (5.71) from the axioms (5.72), let us introduce the operator

$$F := 2A_{\mathrm{SJ}} - \mathrm{i}E \tag{5.73}$$

and we recall that E is real by definition, $\overline{E} = E$. The positivity axiom implies that F is positive semi-definite such that for all $v \in \mathcal{S}^{\mathbb{C}}$

$$0 \leq \langle v, Fv\rangle + \mathrm{i}\,\langle v, Ev\rangle = \langle v, Fv\rangle\,, \tag{5.74a}$$

Second, the commutator axiom states that the operator F is real (has real components). So, the third axiom splits into a real and an imaginary condition,

$$F^2 + E^2 = 0, \tag{5.74b}$$

$$EF - FE = 0. \tag{5.74c}$$

Since we have $|E| = \sqrt{-E^2}$ in a polar decomposition of the non-degenerate operator E, these conditions imply that $F = \pm|E|$. With the positivity axiom, there is only one solution

$$F = |E|, \tag{5.75}$$

which yields (5.71).

A generalization of the Sorkin-Johnston state to (globally hyperbolic) spacetime manifolds was first suggested in Afshordi, Aslanbeigi, and Sorkin [2]. However, due to the implicit use of an inner product on the symplectic space $\mathcal{S}$, the Sorkin-Johnston state is only unique up to the choice of the inner product. The two-point function of a Sorkin-Johnston state is not Hadamard in general [39, 40]. For example, choosing the inner product corresponding to the metric induced volume form dvol on a ultrastatic slab spacetime $M = (-\tau, \tau) \times \Sigma$ (for some $\tau > 0$

around some Cauchy slice Σ in a larger spacetime manifold) leads to a Sorkin-Johnston state that is not Hadamard [29]. The Sorkin-Johnston state does become Hadamard if an inner product with an appropriately chosen, smooth function u (that tends to zero towards the boundaries of M) is used to define a modified volume measure $\frac{1}{u}$dvol, but the constructed state does now clearly depend on the choice of u. For more details on the construction, see Wingham [109].

Chapter 6

Geometric Construction of the Sorkin-Johnston State

Recall from Subsection 2.4.2 the image of the Pauli-Jordan operator for a finite causal set, which is a $2N$-dimensional, real, symplectic vector space with an inner product $\big(\mathcal{S}, \omega, \langle\cdot,\cdot\rangle\big)$, for some $N \in \mathbb{N}$. There exists a non-degenerate operator, the restricted Pauli-Jordan operator $E_{\text{on}} \in \text{End}(\mathcal{S})$ such that for all $\psi_1, \psi_2 \in \mathcal{S}$:

$$\omega(\psi_1, \psi_2) = \left\langle \psi_1,\, E_{\text{on}}^{-1}\psi_2 \right\rangle . \tag{2.68'}$$

For a shorter notation, however, I drop the subscript "on", knowing that E^{-1} is only defined on the vector space $\mathcal{S}$.

6.1 Geometric Quantization and the Bochner Laplacian

I reviewed the general idea of geometric quantization for a symplectic manifold with Riemannian metric in Subsection 5.1.3. For the vector space, I want to construct the physical Hilbert space $\mathcal{H}_\hbar$ as a subspace of square integrable sections $\mathrm{L}^2(\mathcal{S}, \mathcal{L}_\hbar)$ of the quantization bundle $\mathcal{L}_\hbar \to \mathcal{S}$. I will derive the spectrum of the Bochner Laplacian (5.31) and then define the Hilbert space $\mathcal{H}_\hbar$ from the sections corresponding to the lowest part of the spectrum — which will turn out to be a single eigenvalue as in the Kähler case.

For the derivation of the spectrum, I will apply the idea discussed in Subsection 5.1.3. I define the strictly positive operator (modulus of the restricted Pauli-Jordan operator)

$$|E| := \sqrt{-E^2}. \tag{6.1}$$

Similarly to the general case shown in (5.36), a complex structure J is given by

$$J = -E^{-1}|E|, \tag{6.2}$$

so the real vector space $\mathcal{S}$ turns into a complex vector space $\mathcal{S}_J$ by defining complex scalar multiplication as in [56, Ch. IX, Sec. 1],

$$\forall \varphi \in \mathcal{S} : \forall x, y \in \mathbb{R} : \qquad (x + \mathrm{i}y)\varphi := x\varphi + yJ\varphi. \tag{6.3}$$

However, the complex structure will serve merely as a tool in the derivation of the spectrum so that it becomes obvious that the Hilbert space (corresponding to the lowest spectral value of the Laplacian) is determined by the space of holomorphic sections. So, for a shorter notation, I will also denote the complex vector space as $\mathcal{S}$, meaning $\mathcal{S}_J$ whenever I use complex coordinates.

6.1.1 The Quantization Bundle

Given an exact symplectic form $\omega = -\mathrm{d}\,\theta$, let us consider a trivial line bundle $\mathcal{L}_\hbar = \mathcal{S} \times \mathbb{C}$ with the non-trivial connection

$$\nabla_\hbar = \mathrm{d} + \frac{\mathrm{i}}{\hbar}\theta \tag{6.4}$$

parametrized by $\hbar$. The operator $\nabla_\hbar$ increases the total degree $p+q$ of $\mathcal{L}_\hbar$-valued differential forms $\Omega^{p,q}$ by 1. With the complex structure (6.2), the connection decomposes into an operator $\mathcal{D}^+_\hbar : \Omega^{p,q} \to \Omega^{p+1,q}$ raising the holomorphic degree and an operator $\overline{\mathcal{D}}^+_\hbar : \Omega^{p,q} \to \Omega^{p,q+1}$ raising the anti-holomorphic degree,

$$\nabla_\hbar = \mathcal{D}^+_\hbar + \overline{\mathcal{D}}^+_\hbar. \tag{6.5}$$

Let $* : \Omega^{p,q} \to \Omega^{N-q,N-p}$ be the Hodge dual operator. The space of square-integrable sections is equipped with an inner product that reads for any $\psi, \phi \in \Omega^{p,q}$

$$\langle \psi, \phi \rangle_\Omega := \int_{\mathcal{S}} \overline{\psi} \wedge *\phi. \tag{6.6}$$

The Cauchy completion of the space of square-integrable sections (such that the inner product (6.6) is finite) is a Hilbert space. The adjoint operators of the split in (6.5) are

$$\mathcal{D}^-_\hbar := -*\overline{\mathcal{D}}^+_\hbar *, \tag{6.7a}$$

$$\overline{\mathcal{D}}^-_\hbar := -*\mathcal{D}^+_\hbar *. \tag{6.7b}$$

I illustrate the domains and codomains of the complex differential operators in Figure 6.1. My main focus lies on the forms with $p = q = 0$ i.e., the sections of the line bundle $\psi \in \Omega^{0,0}$ (marked in blue), so that the operators $\mathcal{D}^-_\hbar$ and $\overline{\mathcal{D}}^-_\hbar$ annihilate them, $\mathcal{D}^-_\hbar \psi = 0, \overline{\mathcal{D}}^-_\hbar \psi = 0$ (they are omitted in Figure 6.1).

For the following computation, I use complex coordinates $z^i = x^i + \mathrm{i}y^i$ with holomorphic indices $i \in [1, N]$ and anti-holomorphic indices $\bar{\imath} \in [\bar{1}, \bar{N}]$

$$\left(z^1, \ldots, z^i, \ldots, z^N, \bar{z}^{\bar{1}}, \ldots, \bar{z}^{\bar{\imath}}, \ldots, \bar{z}^{\bar{N}}\right) \tag{6.8}$$

in which $|E|^{-1}$ is diagonal with diagonal components ϑ_i. The indices are raised with the constant metric $g^{\bar{\imath}i}$ determined by the inner product on $\mathcal{S}$. Raising an

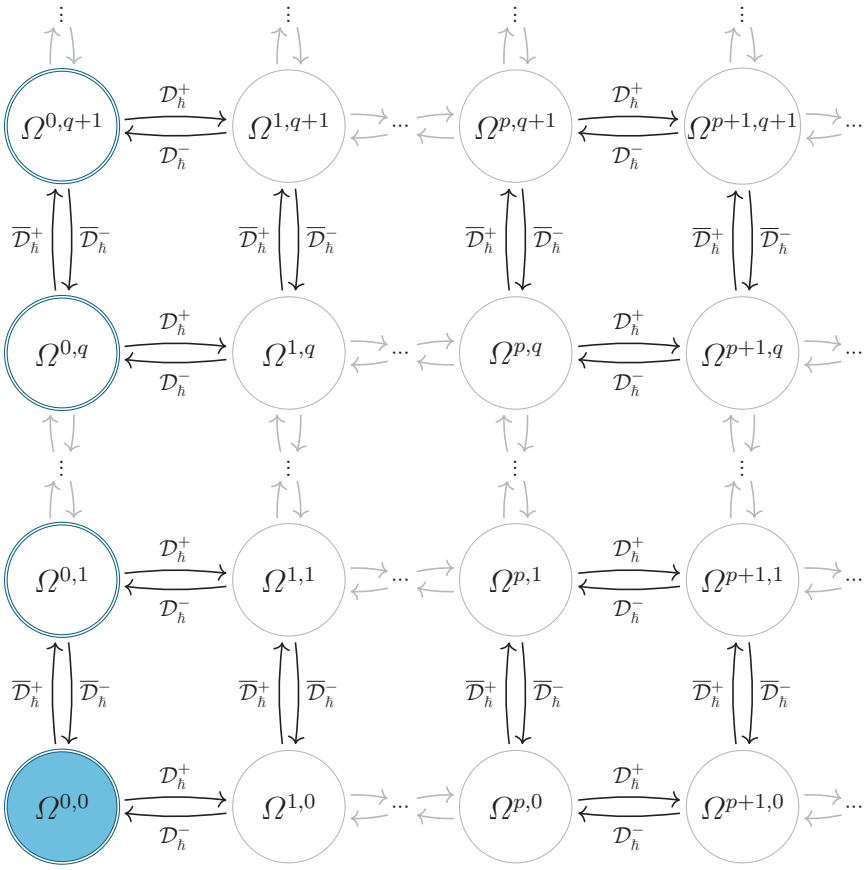

Figure 6.1: The spaces of $\mathcal{L}_\hbar$-valued differential forms and the holomorphic/ anti-holomorphic differential operators. For the derivation of the spectrum, my main attention lies on the $(0,0)$-forms (shaded, blue) and the anti-holomorphic forms (double circles, dark blue).

index also changes it from holomorphic to anti-holomorphic and vice versa. For a slightly compacter notation, I omit the $\hbar$ subscript whenever the connection $\nabla_\hbar$ is expressed in coordinates.

Let $\psi \in \Omega^{p,q}$ be a (p,q)-form with coefficients in the quantization bundle $\mathcal{L}_\hbar$, which I write in the complex coordinates (using the summation convention) as

$$\psi = \frac{1}{p!q!}\psi_{i_1\dots i_p\bar{\imath}_1\dots\bar{\imath}_q} \bigwedge_{a=1}^{p} \mathrm{d}z^{i_a} \wedge \bigwedge_{b=1}^{q} \mathrm{d}\overline{z}^{\bar{\imath}_b}. \tag{6.9}$$

The actions of the operators $\mathcal{D}_\hbar^\pm$, $\overline{\mathcal{D}}_\hbar^\pm$ turn a (p,q)-form into a $(p\pm1,q)$- or $(p,q\pm1)$-form, respectively, as shown in Figure 6.1,

$$\mathcal{D}_\hbar^+\psi = \frac{(-1)^p}{p!q!}\nabla_m\psi_{i_1i_2\dots i_p\bar{\imath}_1\bar{\imath}_2\dots\bar{\imath}_q} \bigwedge_{a=1}^{p} \mathrm{d}z^{i_a} \wedge \mathrm{d}z^m \wedge \bigwedge_{b=1}^{q} \mathrm{d}\overline{z}^{\bar{\imath}_b}, \tag{6.10a}$$

$$\overline{\mathcal{D}}_\hbar^+\psi = \frac{(-1)^{p+q}}{p!q!}\nabla_{\bar{m}}\psi_{i_1i_2\dots i_p\bar{\imath}_1\bar{\imath}_2\dots\bar{\imath}_q} \bigwedge_{a=1}^{p} \mathrm{d}z^{i_a} \wedge \bigwedge_{b=1}^{q} \mathrm{d}\overline{z}^{\bar{\imath}_b} \wedge \mathrm{d}\overline{z}^{\bar{m}}, \tag{6.10b}$$

$$\mathcal{D}_\hbar^-\psi = \frac{(-1)^p}{(p-1)!q!}g^{\bar{m}m}\nabla_{\bar{m}}\psi_{i_1\dots i_{p-1}m\bar{\imath}_1\dots\bar{\imath}_{q-1}} \bigwedge_{a=1}^{p-1} \mathrm{d}z^{i_a} \wedge \bigwedge_{b=1}^{q} \mathrm{d}\overline{z}^{\bar{\imath}_b}, \tag{6.10c}$$

$$\overline{\mathcal{D}}_\hbar^- \psi = \frac{(-1)^{p+q}}{p!(q-1)!} g^{m\bar{m}} \nabla_m \psi_{i_1 \dots i_p \bar{\imath}_1 \dots \bar{\imath}_{q-1} \bar{m}} \bigwedge_{a=1}^{p} \mathrm{d}z^{i_a} \wedge \bigwedge_{b=1}^{q-1} \mathrm{d}\overline{z}^{\bar{\imath}_b}. \tag{6.10d}$$

For the derivation of the spectrum of the Bochner Laplacian discussed below, I focus on the $(0,q)$-forms (double circled in Figure 6.1). I compute the following second order derivatives,

$$\mathcal{D}_\hbar^- \mathcal{D}_\hbar^+ \psi = -\frac{1}{q!} g^{\bar{m}n} \nabla_{\bar{m}} \nabla_n \psi_{\bar{\imath}_1 \dots \bar{\imath}_q} \bigwedge_{b=1}^{q} \mathrm{d}\overline{z}^{\bar{\imath}_b}, \tag{6.11a}$$

$$\overline{\mathcal{D}}_\hbar^- \overline{\mathcal{D}}_\hbar^+ \psi = -\frac{1}{q!} g^{m\bar{n}} \nabla_m \nabla_{\bar{n}} \psi_{\bar{\imath}_1 \dots \bar{\imath}_q} \bigwedge_{b=1}^{q} \mathrm{d}\overline{z}^{\bar{\imath}_b} + \frac{q}{q!} g^{m\bar{n}} \nabla_m \nabla_{\bar{\imath}_1} \psi_{\bar{n}\bar{\imath}_2 \dots \bar{\imath}_q} \bigwedge_{b=1}^{q} \mathrm{d}\overline{z}^{\bar{\imath}_b}, \tag{6.11b}$$

$$\overline{\mathcal{D}}_\hbar^+ \overline{\mathcal{D}}_\hbar^- \psi = -\frac{q}{q!} g^{m\bar{n}} \left(\nabla_m \nabla_{\bar{\imath}_1} - [\nabla_m, \nabla_{\bar{\imath}_1}]_- \right) \psi_{\bar{n}\bar{\imath}_2 \dots \bar{\imath}_q} \bigwedge_{b=1}^{q} \mathrm{d}\overline{z}^{\bar{\imath}_b}. \tag{6.11c}$$

Note that the difference of (6.11a) and (6.11b) and the sum of (6.11b) and (6.11c) are respectively given by

$$\begin{aligned} &\left(\mathcal{D}_\hbar^- \mathcal{D}_\hbar^+ - \overline{\mathcal{D}}_\hbar^- \overline{\mathcal{D}}_\hbar^+ \right) \psi \\ &\quad = \frac{1}{q!} g^{m\bar{n}} \left([\nabla_m, \nabla_{\bar{n}}]_- \psi_{\bar{\imath}_1 \dots \bar{\imath}_q} - \frac{q}{q!} \nabla_m \nabla_{\bar{\imath}_1} \psi_{\bar{n}\bar{\imath}_2 \dots \bar{\imath}_q} \right) \bigwedge_{b=1}^{q} \mathrm{d}\overline{z}^{\bar{\imath}_b}, \end{aligned} \tag{6.12a}$$

$$\begin{aligned} &\left(\overline{\mathcal{D}}_\hbar^- \overline{\mathcal{D}}_\hbar^+ + \overline{\mathcal{D}}_\hbar^+ \overline{\mathcal{D}}_\hbar^- \right) \psi \\ &\quad = \frac{1}{q!} \left(-g^{m\bar{n}} \nabla_m \nabla_{\bar{n}} \psi_{\bar{\imath}_1 \dots \bar{\imath}_q} + q g^{m\bar{n}} [\nabla_m, \nabla_{\bar{\imath}_1}]_- \psi_{\bar{n}\bar{\imath}_2 \dots \bar{\imath}_q} \right) \bigwedge_{b=1}^{q} \mathrm{d}\overline{z}^{\bar{\imath}_b}. \end{aligned} \tag{6.12b}$$

The commutator, which appears in both equations, is the quantization bundle curvature that is determined by the symplectic form, hence

$$[\nabla_i, \nabla_{\bar{\jmath}}]_- = -\frac{\mathrm{i}}{\hbar} \omega_{i\bar{\jmath}}. \tag{6.13}$$

The second term in both equations (6.12a) and (6.12b) vanishes for $(0,0)$-forms where $q = 0$. I use the results of this computation to simplify the Bochner Laplacian in the following.

6.1.2 The Bochner Laplacian

In terms of the connection (6.5) and its dual (6.7), the Bochner Laplacian (5.31) reads

$$\Delta_\hbar = \mathcal{D}_\hbar^- \mathcal{D}_\hbar^+ + \mathcal{D}_\hbar^- \overline{\mathcal{D}}_\hbar^+ + \overline{\mathcal{D}}_\hbar^- \mathcal{D}_\hbar^+ + \overline{\mathcal{D}}_\hbar^- \overline{\mathcal{D}}_\hbar^+. \tag{6.14}$$

As shown in Figure 6.1, for sections of the quantization bundle $\mathcal{L}_\hbar$, i.e. $(0,0)$-forms, only the left-most and right-most summand remain, because $\forall p \in [0,N] \subset \mathbb{N} : \mathcal{D}_\hbar^- \Omega^{p,0} = 0$ and $\forall q \in [0,N] \subset \mathbb{N} : \overline{\mathcal{D}}_\hbar^- \Omega^{0,q} = 0$. Following the result (6.12a) for

$(0,0)$-forms, the difference of the first and last operator pair is given by

$$\mathcal{D}_\hbar^- \mathcal{D}_\hbar^+ - \overline{\mathcal{D}}_\hbar^- \overline{\mathcal{D}}_\hbar^+ = g^{\bar{\imath}j} \left[\nabla_j, \nabla_{\bar{\imath}}\right]_- \tag{6.15a}$$

$$= -\frac{\mathrm{i}}{\hbar} g^{\bar{\imath}j} \omega_{j\bar{\imath}} =: \lambda_\hbar. \tag{6.15b}$$

I use this identity to replace the first operator pair of the Bochner Laplacian (5.31) by the anti-holomorphic operators $\overline{\mathcal{D}}_\hbar^\pm$ along with the positive constant $\lambda_\hbar$, such that for all $(0,0)$-forms

$$\Delta_\hbar = 2\overline{\mathcal{D}}_\hbar^- \overline{\mathcal{D}}_\hbar^+ + \lambda_\hbar \mathbb{1}. \tag{6.16}$$

The constant $\lambda_\hbar$ is (up to the quantization parameter $\hbar$) half the trace of $|E|^{-1}$,

$$\lambda_\hbar = \frac{1}{2\hbar} \operatorname{tr} |E|^{-1}. \tag{6.17}$$

In the chosen complex coordinates where $|E|^{-1}$ is diagonal, this constant is half the sum over all the diagonal components divided by $\hbar$.

Let us combine the operators $\overline{\mathcal{D}}_\hbar^\pm : \Omega^{0,q} \to \Omega^{0,q\pm1}$ that increase and decrease the anti-holomorphic degree to a self-adjoint operator,

$$\overline{\mathcal{D}}_\hbar := \overline{\mathcal{D}}_\hbar^+ + \overline{\mathcal{D}}_\hbar^-. \tag{6.18}$$

So the Bochner Laplacian acting on $(0,0)$-forms $\psi \in \Omega^{0,0}$ becomes

$$\Delta_\hbar \psi = 2\overline{\mathcal{D}}_\hbar^2 \psi + \lambda_\hbar \psi. \tag{6.19}$$

Since, by construction, the Bochner Laplacian and the operator $\overline{\mathcal{D}}_\hbar^2$ (Kodaira Laplacian) are self-adjoint and positive, $\lambda_\hbar$ is the lower bound on the spectrum of the Bochner Laplacian. I want to derive the spectrum of the Laplacian operators to find the space of eigensections corresponding to lowest part of the spectrum. I will consider this space as the physical Hilbert space for which I will construct an algebra of quantum observables.

Recall the definition of a spectrum for an operator on a Hilbert space (Banach space) given in Definition 2.4.3. Starting with the spectrum of $\overline{\mathcal{D}}_\hbar^2$, let $\Omega^{0,*}$ denote the space of sections of the powers of the anti-holomorphic cotangent bundle i.e., $(0,q)$-forms for any q. Let $\mathfrak{H}_\hbar^{0,\pm}$ be the Hilbert spaces of $(0,q)$-forms with even ($+$ superscript) or odd value ($-$ superscript) for the degree q. The operators $\overline{\mathcal{D}}_\hbar^\pm$ map between these Hilbert spaces as adjoint operators to each other, see also Figure 6.1.

6.1.3 Spectral Gap of the Laplacian

In order to derive the spectrum, I make use of the diagonal form of $|E|^{-1}$ in the chosen coordinates. The operator $\overline{\mathcal{D}}_\hbar^2 = \overline{\mathcal{D}}_\hbar^- \overline{\mathcal{D}}_\hbar^+$ acts on sections of the quantization line bundle $\mathcal{L}_\hbar$ and has the coordinate representation

$$\overline{\mathcal{D}}_\hbar^2 = -g^{i\bar{\jmath}} \nabla_i \nabla_{\bar{\jmath}}, \tag{6.20}$$

which is composed of holomorphic (∇_i) and anti-holomorphic ($\nabla_{\bar{\jmath}}$) derivative components of the covariant derivative, using the summation convention. The operator in (6.20) is the square of a self-adjoint operator and thus has a real, positive spectrum. The components of the symmetric bilinear form or metric g (corresponding to the inner product $\langle\cdot,\cdot\rangle$) are

$$\left(g_{i\bar{\jmath}}\right)_{i\in[1,N],\bar{\jmath}\in[\bar{1},\bar{N}]} = \operatorname{diag}\left(\frac{1}{\vartheta_1},\frac{1}{\vartheta_2},\dots,\frac{1}{\vartheta_N}\right), \tag{6.21a}$$

$$\left(g^{i\bar{\jmath}}\right)_{i\in[1,N],\bar{\jmath}\in[\bar{1},\bar{N}]} = \operatorname{diag}\left(\vartheta_1,\vartheta_2,\dots,\vartheta_N\right). \tag{6.21b}$$

I decompose the operator $\overline{\mathcal{D}}^2_\hbar$ into the operator sum

$$\overline{\mathcal{D}}^2_\hbar = (-\nabla_i)(g^{i\bar{\jmath}}\nabla_{\bar{\jmath}}) =: (\delta_{i\bar{\imath}}A^{\bar{\imath}})(B^i), \tag{6.22}$$

where $\delta^{i\bar{\jmath}}$ denotes the Kronecker delta. The components of the covariant derivative operator fulfill the commutation relations

$$[\nabla_i,\nabla_j]_- = 0, \tag{6.23a}$$

$$[\nabla_i,\nabla_{\bar{\jmath}}]_- = -\frac{\mathrm{i}}{\hbar}\omega_{i\bar{\jmath}} = \frac{1}{\hbar}\delta_{i\bar{\jmath}}, \tag{6.23b}$$

$$[\nabla_{\bar{\imath}},\nabla_{\bar{\jmath}}]_- = 0. \tag{6.23c}$$

Thus commuting the operators $A^{\bar{\imath}}$ and B^i gives

$$B^iA^{\bar{\imath}} = A^{\bar{\imath}}B^i + \frac{1}{\hbar}g^{i\bar{\imath}}. \tag{6.24}$$

Since both operator orders $B^iA^{\bar{\imath}}$ and $A^{\bar{\imath}}B^i$ are positive operators the spectrum of $B^iA^{\bar{\imath}}$ has the lower bound $g^{i\bar{\imath}}/\hbar$. With the help of the following lemma, the lower bound implies a spectral gap for $A^{\bar{\imath}}B^i$.

Lemma 6.1.1. *Let $A:\mathfrak{H}_1\to\mathfrak{H}_2$ and $B:\mathfrak{H}_2\to\mathfrak{H}_1$ be operators between Hilbert spaces $\mathfrak{H}_1$ and $\mathfrak{H}_2$; then*

$$\{0\}\cup\operatorname{spec}(AB) = \{0\}\cup\operatorname{spec}(BA). \tag{6.25}$$

Proof. To get the idea of the proof, first consider a pair of *bounded* operators $A\in\mathcal{B}(\mathfrak{H}_1,\mathfrak{H}_2)$ and $B\in\mathcal{B}(\mathfrak{H}_2,\mathfrak{H}_1)$ between two Hilbert spaces. For every $\lambda\in\operatorname{resol}(AB)\backslash\{0\}$ that is above the operator bound, $|\lambda|>\|AB\|$, there is a Neumann series

$$R = \frac{1}{\lambda}\left(\mathbb{1}+\sum_{n=1}^{\infty}\left(\frac{AB}{\lambda}\right)^n\right), \tag{6.26}$$

which converges in norm. This operator limit is the inverse of $(\lambda\mathbb{1}-AB)$ because

$$(\lambda\mathbb{1}-AB)R = \mathbb{1}+\sum_{n=1}^{\infty}\left(\frac{AB}{\lambda}\right)^n - \frac{AB}{\lambda} - \sum_{n=2}^{\infty}\left(\frac{AB}{\lambda}\right)^n = \mathbb{1}. \tag{6.27}$$

For the bounded operators, the series

$$\sum_{n=1}^{\infty}\left(\frac{BA}{\lambda}\right)^{n}=\frac{1}{\lambda}B\left(\sum_{n=1}^{\infty}\left(\frac{AB}{\lambda}\right)^{n-1}\right)A=\frac{1}{\lambda}BRA \tag{6.28}$$

is also well-defined. The right-hand side of equation (6.28) does not include a summation anymore, thus it can be calculated for any resolvent R with $\lambda \neq 0$. So let us conclude the lemma with the proof for any (unbounded) operator pair A and B as follows.

Let $\lambda \in \mathrm{resol}(AB) \setminus \{0\}$ be any element not in the spectrum and not zero. Let R be the resolvent for λ and define

$$\tilde{R} := \frac{1}{\lambda}\left(\mathbb{1} + BRA\right). \tag{6.29}$$

Because R exists, so does $\tilde{R}$. The multiplication with $(\lambda\mathbb{1} - BA)$ from the left yields

$$\begin{aligned}(\lambda\mathbb{1} - BA)\tilde{R} &= \mathbb{1} - \frac{1}{\lambda}BA + BRA - \frac{1}{\lambda}BABRA && \text{(6.30a)}\\ &= \mathbb{1} - \frac{1}{\lambda}BA + B\frac{1}{\lambda}(\lambda\mathbb{1} - AB)RA && \text{(6.30b)}\\ &= \mathbb{1} && \text{(6.30c)}\end{aligned}$$

and a multiplication from the right is shown similarly. This verifies that $\tilde{R}$ is a resolvent of BA, therefore $\lambda \in \mathrm{resol}(BA)$. Considering all $\lambda \in \mathrm{resol}(AB) \setminus \{0\}$, it follows that

$$\mathrm{resol}(AB) \setminus \{0\} \subset \mathrm{resol}(BA). \tag{6.31}$$

Repeating this procedure for the operator order BA, we have

$$\mathrm{resol}(BA) \setminus \{0\} \subset \mathrm{resol}(AB). \tag{6.32}$$

Finally, remove the zero element on the right-hand sides of both equations (6.31), (6.32) and combine them to

$$\mathrm{resol}(AB) \setminus \{0\} = \mathrm{resol}(BA) \setminus \{0\}. \tag{6.33}$$

Because the spectrum is the complement of the resolvent set, equation (6.33) implies that the union of the spectra with zero are identical too. □

Lemma 6.1.2. *The positive, self-adjoint operator pair $A^{\bar{\imath}}B^{i}$ (with $A^{\bar{\imath}} : \mathfrak{H}_{\hbar}^{0,\pm} \to \mathfrak{H}_{\hbar}^{0,\mp}$ and $B^{i} : \mathfrak{H}_{\hbar}^{0,\mp} \to \mathfrak{H}_{\hbar}^{0,\pm}$) that fulfills the commutation relation* (6.24)*:*

$$B^i A^{\bar{\imath}} = A^{\bar{\imath}} B^i + \frac{1}{\hbar} g^{i\bar{\imath}},$$

has a spectral gap between the spectral values 0 *and* $g^{i\bar{\imath}}/\hbar$.

Proof. The operator pairs $A^{\bar{\imath}}B^i$ and $B^i A^{\bar{\imath}}$ are positive and self-adjoint, so

$$\operatorname{spec}(A^{\bar{\imath}} B^i) \subset [0, \infty)\,, \tag{6.34a}$$
$$\operatorname{spec}(B^i A^{\bar{\imath}}) \subset [0, \infty)\,. \tag{6.34b}$$

Because $B^i = g^{i\bar{\jmath}}\nabla_{\bar{\jmath}}$, $0 \in \operatorname{spec}(B^i)$ and thus $0 \in \operatorname{spec}(A^{\bar{\imath}}B^i)$ with any holomorphic section as eigensection i.e., the sections ψ that fulfill

$$\nabla_{\bar{\imath}}\psi = \left(\frac{\partial}{\partial \overline{z}^{\bar{\imath}}} + \frac{\mathrm{i}}{\hbar}\theta_{\bar{\imath}}\right)\psi = 0. \tag{6.35}$$

The spectral values of the operator pair $B^i A^{\bar{\imath}}$ are identical to those of $A^{\bar{\imath}}B^i$ up to the constant term given in (6.24), so that

$$0 \in \operatorname{spec}(A^{\bar{\imath}} B^i) \Rightarrow \min\Big(\operatorname{spec}(B^i A^{\bar{\imath}})\Big) = \frac{1}{\hbar} g^{i\bar{\imath}}. \tag{6.36}$$

After applying Lemma 6.1.1, in summary, I have

$$\left\{0, \frac{1}{\hbar} g^{i\bar{\imath}}\right\} \subset \operatorname{spec}(A^{\bar{\imath}} B^i), \tag{6.37a}$$
$$\left(0, \frac{1}{\hbar} g^{i\bar{\imath}}\right) \not\subset \operatorname{spec}(A^{\bar{\imath}} B^i). \tag{6.37b}$$

So the only spectral value of $A^{\bar{\imath}}B^i$ smaller than $g^{i\bar{\imath}}/\hbar$ is 0. □

To obtain an explicit expression for the eigensections to the eigenvalue $0 \in \operatorname{spec}(A^{\bar{\imath}}B^i)$, I choose a gauge for the symplectic potential such that

$$\theta = \frac{\mathrm{i}}{2}\delta_{i\bar{\jmath}}\left(\overline{z}^{\bar{\jmath}}\mathrm{d}z^i - z^i \mathrm{d}\overline{z}^{\bar{\jmath}}\right), \tag{6.38}$$

and I write

$$|z|^2 = \delta_{i\bar{\imath}} z^i \overline{z}^{\bar{\imath}}. \tag{6.39}$$

In this gauge, any holomorphic section ψ — as a solution to (6.35) — is determined by an arbitrary, smooth, holomorphic function α, so that for all $z \in \mathcal{S}$:

$$\psi(z) = \frac{\alpha(z)}{\sqrt{2\pi\hbar}^N} \exp\left(-\frac{1}{2\hbar}|z|^2\right). \tag{6.40}$$

In the following, I repeat the application of the above lemma to determine the spectrum of the Bochner Laplacian.

6.1.4 Full Spectrum of the Laplacian

Any holomorphic section $\psi \in \Omega^{0,0}$, as given in (6.40), is also a solution of the differential equation

$$\overline{\mathcal{D}}_\hbar^- \overline{\mathcal{D}}_\hbar^+ \psi = -g^{i\bar{\jmath}} \nabla_i \nabla_{\bar{\jmath}} \psi = 0. \tag{6.41}$$

This follows from the fact that $\overline{\mathcal{D}}_\hbar^-$ is the adjoint to $\overline{\mathcal{D}}_\hbar^+$ and thus

$$\left\langle \psi, \overline{\mathcal{D}}_\hbar^- \overline{\mathcal{D}}_\hbar^+ \psi \right\rangle_\Omega = \left\langle \overline{\mathcal{D}}_\hbar^+ \psi, \overline{\mathcal{D}}_\hbar^+ \psi \right\rangle_\Omega \tag{6.42}$$

implies that $\overline{\mathcal{D}}_\hbar^+ \psi$ has to vanish whenever $\overline{\mathcal{D}}_\hbar^- \overline{\mathcal{D}}_\hbar^+ \psi$ does. Due to the diagonal form, all components $\nabla_{\bar{\jmath}} \psi$ have to vanish. Consequently, the eigenspace of $\Delta_\hbar$ for the eigenvalue (6.17),

$$\Delta_\hbar \psi = \lambda_\hbar \psi, \tag{6.43}$$

is spanned by the holomorphic sections (6.40). The following theorem then concludes my derivation of the spectrum.

Theorem 6.1.3. *Let $\Delta_\hbar$ be the Bochner Laplacian for sections of the quantization bundle $\mathcal{L}_\hbar \to \mathcal{S}$ over a $2N$-dimensional, real, symplectic vector space $\left(\mathcal{S}, \omega, \langle \cdot, \cdot \rangle\right)$ with a non-degnerate symplectic form ω and an inner product $\langle \cdot, \cdot \rangle$. Let ϑ_i be the diagonal components as given in* (6.21)*. The spectrum of the Laplacian is given by*

$$\operatorname{spec}(\Delta_\hbar) = \left\{ \frac{1}{\hbar} \sum_{i=1}^{N} (2n_i + 1)\vartheta_i \;\middle|\; n_i \in \mathbb{N} \right\}. \tag{6.44}$$

Proof. Recall the spectral relation (6.24):

$$\operatorname{spec}(B^i A^{\bar{\imath}}) = \operatorname{spec}(A^{\bar{\imath}} B^i) + \frac{1}{\hbar} g^{i\bar{\imath}}.$$

Applying Lemma 6.1.1 to the spectral gap shown in Lemma 6.1.1 yields a secondary spectral gap,

$$\left\{ \frac{1}{\hbar} g^{i\bar{\imath}}, \frac{2}{\hbar} g^{i\bar{\imath}} \right\} \subset \operatorname{spec}(B^i A^{\bar{\imath}}), \tag{6.45a}$$

$$\left(\frac{1}{\hbar} g^{i\bar{\imath}}, \frac{2}{\hbar} g^{i\bar{\imath}} \right) \not\subset \operatorname{spec}(B^i A^{\bar{\imath}}). \tag{6.45b}$$

An iteratively repeated application of Lemma 6.1.1 then yields the discrete spectra (where only the second one includes zero)

$$\operatorname{spec}(B^i A^{\bar{\imath}}) = \frac{1}{\hbar} g^{i\bar{\imath}} \mathbb{N}_*, \tag{6.46a}$$

$$\operatorname{spec}(A^{\bar{\imath}} B^i) = \frac{1}{\hbar} g^{i\bar{\imath}} \mathbb{N}. \tag{6.46b}$$

Recombining the operators for all the N components as defined in (6.21) and (6.22) gives

$$\operatorname{spec}\left(\overline{\mathcal{D}}_\hbar^- \overline{\mathcal{D}}_\hbar^+\right) = \left\{ \frac{1}{\hbar} \sum_{i=1}^{N} n_i \vartheta_i \;\middle|\; n_i \in \mathbb{N} \right\} \tag{6.47}$$

such that (6.44) follows by a scaling with 2 and shifting by $\lambda_\hbar$ according to (6.16) (and the general argument on spectra given in Subsection 2.4.3). □

Figure 6.2 shows an illustration of the spectrum, which gets denser towards infinity (page upwards). Note that one does not need any complex structure to determine the spectrum (6.44) and the spectrum is independent of J. I used J given by (6.2) merely as a tool in the derivation of the spectrum. The physical Hilbert space is determined by the eigenspace corresponding to the lowest part of the spectrum of the Laplacian. Since the lower part of the spectrum (6.44) is given by the single eigenvalue (6.17), note that the corresponding eigenspace is identical to the space of holomorphic sections (6.40) with respect to the complex structure J.

6.2 (Berezin)-Toeplitz Quantization and Dequantization

In the following, I use the space of eigensections at the lowest spectral value of the Bochner Laplacian as the physical Hilbert space $\mathcal{H}_\hbar$ to discuss Toeplitz quantization and its adjoint operation — Berezin-Toeplitz dequantization.

6.2.1 The Physical Hilbert Space and Toeplitz Quantization

Following the general construction from Subsection 5.1.3, I define the physical Hilbert space $\mathcal{H}_\hbar \subset \mathrm{L}^2(\mathcal{S}, \mathcal{L}_\hbar)$ as the part corresponding to the lowest part of the spectrum as given in Theorem 6.1.3. The lowest part of the spectrum is given by the single eigenvalue $\lambda_\hbar$ and the Hilbert space is the space spanned by *holomorphic* sections (6.40) of the quantization bundle $\mathcal{L}_\hbar$. The Hilbert space has the inner product

$$\langle \psi_1 | \psi_2 \rangle_\hbar = \int_{\mathcal{S}} \overline{\psi_1} \psi_2 \operatorname{dvol}, \tag{6.48a}$$

$$\operatorname{dvol} = (-1)^{\frac{1}{2}N(N-1)} \frac{1}{N!} \bigwedge_{i=1}^{N} \omega. \tag{6.48b}$$

Let $\mathfrak{A}_0$ be the C*-algebra of functions vanishing at infinity $\mathrm{C}_0(\mathcal{S}, \mathbb{C})$ with the dense subalgebra of Schwartz functions $\mathcal{A}_0 := \mathrm{C}^\infty_{\mathrm{S}}(\mathcal{S}, \mathbb{C})$, and let $\mathfrak{A}_\hbar$ be the C*-algebra of compact operators $\mathcal{K}(\mathcal{H}_\hbar)$. For Toeplitz quantization $T_\hbar : \mathcal{A}_0 \to \mathfrak{A}_\hbar$, I follow Definition 5.1.18 with the projector $\mathit{\Pi}_\hbar : \mathrm{L}^2(\mathcal{S}, \mathcal{L}_\hbar) \to \mathcal{H}_\hbar$, see (5.39). Note

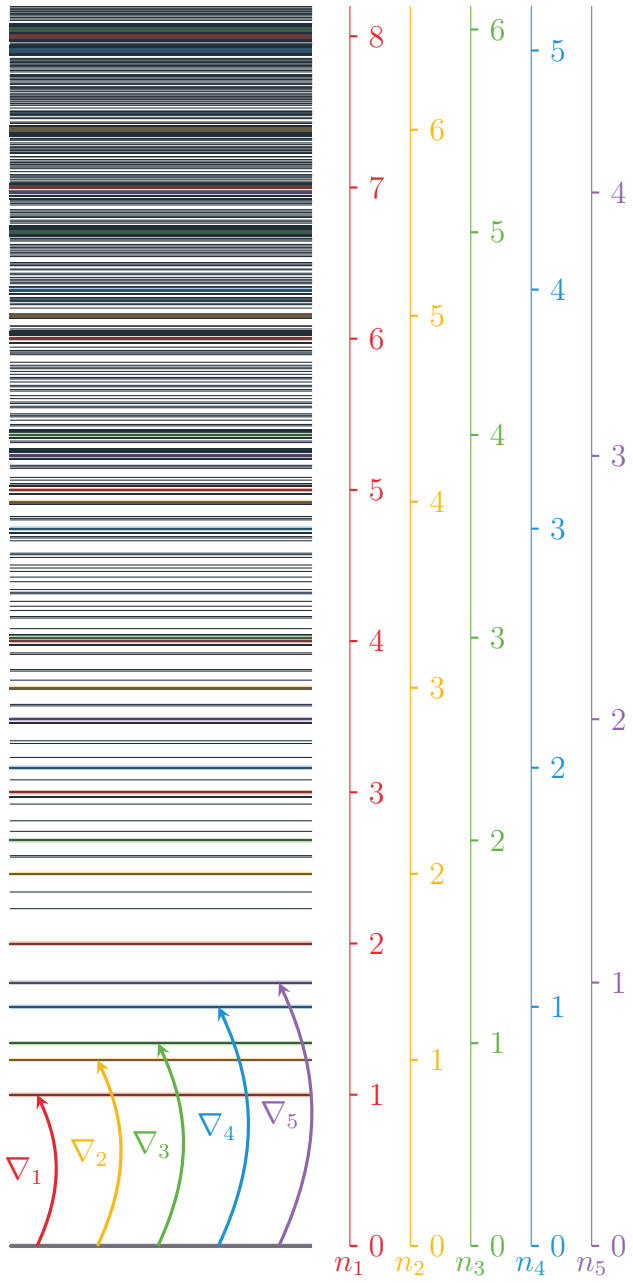

Figure 6.2: Illustration of the spectrum of the Bochner Laplacian $\Delta_\hbar = \nabla_\hbar^* \nabla_\hbar$ obtained with the holomorphic components of the covariant derivative ∇_i for $N = 5$ dimensions weighted by distinct components $\vartheta_i \in \mathbb{R}$. All dark lines represent a value in the spectrum of the Laplacian reached by linear combinations of the components ∇_1 to ∇_5 (different colours). The lowest eigenvalue (thick line, black) corresponds to the space of holomorphic sections (6.40).

that Toeplitz quantization actually extends to a map from bounded functions to bounded operators, $\mathrm{C_b}(\mathcal{S},\mathbb{C}) \to \mathcal{B}(\mathcal{H}_\hbar)$ — where the unit function $1 \in \mathrm{C_b}(\mathcal{S},\mathbb{C})$ is mapped to the identity operator — but I will restrict to Schwartz functions to obtain a well-defined continuous field of C*-algebras later on.

For any two holomorphic sections $\psi_{1,2}$ as in (6.40) with some smooth, holomorphic functions $\alpha_{1,2}$, the inner product reads

$$\langle\psi_1|\psi_2\rangle_\hbar = \frac{1}{(2\pi\hbar)^N}\int\limits_{\mathcal{S}} \overline{\alpha_1}\alpha_2 \exp\left(-\frac{1}{\hbar}|z|^2\right)\,\mathrm{dvol}. \tag{6.49}$$

I use the section basis given in ket-notation for any multi-index $\boldsymbol{n} = (n_1,\dots,n_N) \in \mathbb{N}^N$:

$$|\boldsymbol{n}\rangle_\hbar := \left|\frac{1}{\sqrt{2\pi\hbar}^N}\left(\prod_{i=1}^N \frac{1}{\sqrt{n_i!}}\left(\frac{z^i}{\sqrt{\hbar}}\right)^{n_i}\right)\exp\left(-\frac{1}{2\hbar}|z|^2\right)\right\rangle_\hbar . \tag{6.50}$$

For example if $N = 1$, consider two holomorphic sections $\psi^{(m,n)}$ with holomorphic functions $z^m = r^m\mathrm{e}^{\mathrm{i}m\varphi}$ and $z^n = r^n\mathrm{e}^{\mathrm{i}n\varphi}$, so the inner product simplifies to

$$\left\langle\psi^{(m)}\middle|\psi^{(n)}\right\rangle_\hbar = \frac{1}{2\pi\hbar}\int\limits_{r=0}^{\infty}\int\limits_{\varphi=0}^{2\pi} r^{m+n+1}\mathrm{e}^{\mathrm{i}(n-m)\varphi}\exp\left(-\frac{r^2}{\hbar}\right)\,\mathrm{d}\varphi\,\mathrm{d}r, \tag{6.51a}$$

$$= \delta_{mn}\frac{1}{\hbar}\int\limits_0^\infty r^{2m+1}\exp\left(-\frac{r^2}{\hbar}\right)\mathrm{d}r, \tag{6.51b}$$

$$= \delta_{mn} m!\hbar^m. \tag{6.51c}$$

This generalizes to an arbitrary dimension N implying that the basis (6.50) is orthonormal,

$$\langle\boldsymbol{m}|\boldsymbol{n}\rangle_\hbar = \prod_{i=1}^N \delta_{m_i n_i}. \tag{6.52}$$

I define unbounded ladder operators (in the summation convention)

$$a_{\bar\imath}^+ := \frac{1}{\sqrt{\hbar}}\delta_{\bar\imath i}z^i - \sqrt{\hbar}\nabla_{\bar\imath} \tag{6.53a}$$

$$a_i^- := \frac{1}{\sqrt{\hbar}}\delta_{i\bar\imath}\overline{z}^{\bar\imath} + \sqrt{\hbar}\nabla_i, \tag{6.53b}$$

which are adjoint to each other for each holomorphic–anti-holomorphic index pair $(i,\bar\imath)$. Using the commutators of the quantization bundle connection (6.23), the commutators for the ladder operators are those known from an N-dimensional quantum mechanical harmonic oscillator,

$$\left[a_i^\pm, a_{\bar\jmath}^\pm\right]_- = 0, \tag{6.54a}$$

$$\left[a_i^-, a_{\bar\jmath}^+\right]_- = \delta_{i\bar\jmath}\mathbb{1}. \tag{6.54b}$$

The action of the ladder operators on the Hilbert space basis yields

$$a_i^+ \,|n_1,\ldots,n_i,\ldots,n_N\rangle_\hbar = \sqrt{n_i+1}\,|n_1,\ldots,n_i+1,\ldots,n_N\rangle_\hbar\,, \tag{6.55a}$$

$$a_i^- \,|n_1,\ldots,n_i,\ldots,n_N\rangle_\hbar = \sqrt{n_i}\,|n_1,\ldots,n_i-1,\ldots,n_N\rangle_\hbar\,, \tag{6.55b}$$

hence they are known as the creation and annihilation operators, respectively. The heuristic relation between the Toeplitz operators of the (unbounded) coordinate functions z^i and $\overline{z}^{\bar{\imath}}$ with the ladder operators as well as examples for anti-normal ordering of Toeplitz quantization are given in Subsection 6.2.3.

6.2.2 Dequantization and the Berezin Transform

Let the dequantization map $\Xi_\hbar : \mathfrak{A}_\hbar \to \mathfrak{A}_0$ be given as the adjoint to Toeplitz quantization by the relation (5.44), which is

$$\mathrm{Tr}\Big(A_\hbar T_\hbar(F)\Big) = \frac{1}{(2\pi\hbar)^N}\int\limits_{\mathcal{S}} \Xi_\hbar(A_\hbar)F \;\mathrm{dvol} \tag{6.56}$$

for the $2N$-dimensional vector space $\mathcal{S}$, and any $F \in \mathcal{A}_0$, $A_\hbar \in \mathfrak{A}_\hbar$. Similarly to Toeplitz quantization, one may extend the domain of Berezin-Toeplitz dequantization to all bounded operators, however, the trace is only partially defined (denoted by Tr). For all trace-class operators $A_\hbar$ and all complex-valued Schwartz functions $F \in \mathcal{A}_0 = \mathrm{C}^\infty_{\mathrm{S}}(\mathcal{S},\mathbb{C})$, the trace on the left-hand side written in the section basis (6.50) is

$$\mathrm{Tr}\Big(A_\hbar T_\hbar(F)\Big) = \sum_{\boldsymbol{n}\in\mathbb{N}^N} \langle \boldsymbol{n}|_\hbar\, A_\hbar T_\hbar(F)\,|\boldsymbol{n}\rangle_\hbar\,. \tag{6.57}$$

Note that the dequantization of a projector $|\boldsymbol{j}\rangle_\hbar\,\langle\boldsymbol{j}|_\hbar$ for any $\boldsymbol{j}\in\mathbb{N}^N$ is the function

$$\Xi_\hbar\Big(|\boldsymbol{j}\rangle_\hbar\,\langle\boldsymbol{j}|_\hbar\Big)(z) = \exp\left(-\frac{1}{\hbar}|z|^2\right)\prod_{k=1}^N \frac{1}{j_k!}\left(\frac{|z^k|^2}{\hbar}\right)^{j_k}. \tag{6.58}$$

Let us take this as a consistency check and notice that the identity operator $\mathbb{1} \in \mathcal{B}(\mathcal{H}_\hbar)$ dequantizes to the constant function 1 when extending the domain of the dequantization map to bounded operators and the codomain to bounded functions.

The exponential factor in (6.58) contains the Berezin transform kernel $b_\hbar$, for any $z\in\mathcal{S}$, given by

$$b_\hbar(z) := \frac{1}{(2\pi\hbar)^N}\exp\left(-\frac{1}{\hbar}|z|^2\right). \tag{6.59}$$

Let $\circledast$ denote the convolution product between any pair of functionals $F_1, F_2 \in \mathrm{L}^1(\mathcal{S},\mathbb{C})$ such that

$$(F_1 \circledast F_2)(z) = \int\limits_{\mathcal{S}} F_1(z-z')F_2(z')\;\mathrm{dvol}(z'). \tag{6.60}$$

Expanding any Toeplitz operator in terms of the projectors $|\boldsymbol{j}\rangle_\hbar \langle \boldsymbol{j}|_\hbar$ and then using the dequantization (6.58), I derive the explicit expression for the Berezin transform of any Schwartz function $F \in \mathcal{A}_0$ (or even any bounded function) as a convolution with the Berezin kernel (6.59),

$$(\Xi_\hbar \circ T_\hbar)(F) = b_\hbar \circledast F, \tag{6.61}$$

which is also an element of $\mathcal{A}_0$. An example for a Berezin transform is given in Subsection 6.2.3. Note that in the classical limit $\hbar \to 0$, the Gaussian function (6.59) converges to a delta distribution — the identity with respect to convolution, or equivalently

$$\lim_{\hbar\to 0}(\Xi_\hbar \circ T_\hbar)(F) = F. \tag{6.62}$$

These observations are useful for the construction of a continuous field of C*-algebras (including the classical limit $\hbar = 0$) further below.

6.2.3 Normal and Anti-Normal Ordering

Toeplitz quantization and dequantization relate to anti-normal and normal ordering, respectively, as I will discuss here.

Beyond the extension to bounded functions, heuristically, one may even extend the Toeplitz quantization map (5.40) to a map from continuous, unbounded functions to unbounded operators. In particular for the coordinate functions (with any $i \in [1, N]$), this yields

$$T_\hbar\left(\delta_{i\bar{i}} z^i\right) = \sqrt{\hbar} a^+_{\bar{i}} \qquad\qquad T_\hbar\left(\delta_{i\bar{i}} \overline{z}^{\bar{i}}\right) = \sqrt{\hbar} a^-_i\,, \tag{6.63}$$

where the summation over the Kronecker delta turns the vectors $z, \overline{z} \in \mathcal{S}$ into the coordinate functions. In a similar way, the dequantization map Ξ extends heuristically to give

$$\Xi_\hbar\left(\sqrt{\hbar} a^+_{\bar{i}}\right) = \delta_{i\bar{i}} z^i \qquad\qquad \Xi_\hbar\left(\sqrt{\hbar} a^-_i\right) = \delta_{i\bar{i}} \overline{z}^{\bar{i}}. \tag{6.64}$$

Notice that the dequantization map is the inverse to the quantization map only on these coordinate functions. For a general monomial, for example, the quantization is

$$T_\hbar\left(\delta_{i\bar{i}} \left(z^i\right)^m \delta_{j\bar{j}} \left(\overline{z}^j\right)^n\right) = \hbar^{\frac{m+n}{2}} \left(a^-_j\right)^n \left(a^+_{\bar{i}}\right)^m \tag{6.65}$$

and the dequantization takes the reverse operator order back to the coordinate functions

$$\Xi_\hbar\left(\hbar^{\frac{m+n}{2}} \left(a^+_{\bar{i}}\right)^m \left(a^-_j\right)^n\right) = \delta_{i\bar{i}} \left(z^i\right)^m \delta_{j\bar{j}} \left(\overline{z}^{\bar{j}}\right)^n. \tag{6.66}$$

Thus, quantization corresponds to *anti-normal* ordering and the annihilation operators a_j^- appear to the left of creation operators a_i^+, while dequantization respects the opposite or *normal* ordering.

As a example that is in the domain $\mathcal{A}_0 = \mathrm{C}_{\mathrm{S}}^{\infty}(\mathcal{S}, \mathbb{C})$ of the Toeplitz map, consider a Schwartz function $F \in \mathcal{A}_0$ that is an N-fold product of Gaussian functions with variances $\beta_i > \hbar$ for all $i \in [1, N]$, given by

$$F(z) := \prod_{i=1}^{N} \frac{1}{2\pi\beta_i} \exp\left(-\frac{(x^i)^2 + (y^i)^2}{\beta_i}\right) \tag{6.67a}$$

$$= \prod_{i=1}^{N} \frac{1}{2\pi\beta_i} \exp\left(-\frac{|z^i|^2}{\beta_i}\right). \tag{6.67b}$$

It expands as a product of Taylor series

$$F(z) = \prod_{i=1}^{N} \frac{1}{2\pi\beta_i} \sum_{k=0}^{\infty} \frac{1}{k!} \left(-\frac{1}{\beta_i}\right)^k \left(z^i\right)^k \left(\overline{z}^i\right)^k \tag{6.68}$$

and its Toeplitz operator may be expanded similarly in terms of the unbounded ladder operators,

$$T_\hbar(F) = \prod_{i=1}^{N} \frac{1}{2\pi\beta_i} \sum_{k=0}^{\infty} \frac{1}{k!} \left(-\frac{\hbar}{\beta_i}\right)^k \left(a_i^-\right)^k \left(a_i^+\right)^k. \tag{6.69}$$

Note that the k-th power of the lowering operator appears to the left of the k-th power of the raising operator. Thus the function F is the anti-normal ordering corresponding to the Toeplitz operator $T_\hbar(F)$.

Now let us consider an observable A with a similar expansion as (6.69), but with the opposite ordering of the ladder operators,

$$A := \prod_{i=1}^{N} \frac{1}{2\pi\beta_i} \sum_{k=0}^{\infty} \frac{1}{k!} \left(-\frac{\hbar}{\beta_i}\right)^k \left(a_i^+\right)^k \left(a_i^-\right)^k. \tag{6.70}$$

In contrast to (6.69), here the k-th power of the creation operator $(a_i^+)^k$ appear to the left of the k-th power of the annihilation operator $(a_i^-)^k$. The Ξ-dequantization of the operator A is

$$\Xi_\hbar(A) = F. \tag{6.71}$$

Thus the operator A corresponds to the function F by normal-ordering. This example shows the correspondence of Toeplitz quantization to anti-normal, and Toeplitz dequantization to normal ordered expressions.

Taking the dequantization of the Toeplitz operator $T_\hbar(F)$, the Berezin transform, here written with the convolution $\circledast$ as defined in (6.60), is

$$(\Xi_\hbar \circ T_\hbar)(F)(z) = \frac{1}{(2\pi\hbar)^N} \exp\left(-\frac{1}{\hbar}|z|^2\right) \circledast F(z) \tag{6.72a}$$

$$= \frac{1}{(2\pi\hbar)^N} \int_{\mathcal{S}} \exp\left(-\frac{1}{\hbar}|\zeta|^2\right) \times \prod_{i=1}^{N} \frac{1}{2\pi\beta_i} \exp\left(-\frac{1}{\beta_i}\left|z^i - \zeta^i\right|^2\right) \mathrm{dvol}(\zeta). \tag{6.72b}$$

Because the Gaussian function F is a product of independent Gaussian functions, the $2N$-fold integration splits into N double-integrals which are solved by completing the square in the exponents,

$$(\Xi_\hbar \circ T_\hbar)(F)(z) = \prod_{i=1}^{N} \frac{1}{(2\pi\beta_i)(2\pi\hbar)} \times \iint \exp\left(-\frac{1}{\hbar}\left|\zeta^i\right|^2 - \frac{1}{\beta_i}\left|z^i - \zeta^i\right|^2\right) \mathrm{i}\, \mathrm{d}\zeta^i \mathrm{d}\overline{\zeta}^i \tag{6.73a}$$

$$= \prod_{i=1}^{N} \frac{1}{(2\pi\beta_i)(2\pi\hbar)} \exp\left(-\frac{|z^i|^2}{\beta_i + \hbar}\right) \times \underbrace{\iint \exp\left(-\frac{\beta_i + \hbar}{\beta_i \hbar}\left|\zeta^i - \frac{\hbar}{\beta_i + \hbar} z^i\right|^2\right) \mathrm{i}\, \mathrm{d}\zeta^i \mathrm{d}\overline{\zeta}^i}_{=2\pi\frac{\beta_i\hbar}{\beta_i+\hbar}} \tag{6.73b}$$

$$= \prod_{i=1}^{N} \frac{1}{2\pi(\beta_i + \hbar)} \exp\left(-\frac{|z^i|^2}{\beta_i + \hbar}\right). \tag{6.73c}$$

The Berezin transform of the Gaussian function F is again a Gaussian function with variance increased by $\hbar$.

6.3 Relation to Strict Deformation (De)Quantization

The geometric construction of the quantum algebra $\mathfrak{A}_\hbar$ for the physical Hilbert space $\mathcal{H}_\hbar$ in the previous section is a quantization parametrized by $\hbar$. In this section, I want to analyse the relationship to star products and the construction of a continuous field of C*-algebras over the quantization parameter range $I = [0, \infty)$.

6.3.1 The Weyl Generators and Algebra

I introduce the Weyl generators that span a Weyl algebra as defined in Definition 5.2.6 for the finite dimensional symplectic vector space $\mathcal{S}$. Weyl generators are useful to prove continuity of the field of C*-algebras below and to analyse the properties of the Sorkin-Johnston state determined by dequantization.

Lemma 6.3.1. *Let $\mathfrak{W}_\hbar$ be the Weyl C*-algebra over the vector space $\mathcal{S}$ with Weyl generators labelled by covectors $\phi \in \mathcal{S}^* = \mathrm{Hom}(\mathcal{S}, \mathbb{R})$ given by complex components $\phi_i \in \mathbb{C}$ such that (in the summation convention)*

$$\phi(z) = \phi_i z^i + \phi_{\bar{\imath}} \overline{z}^{\bar{\imath}}. \tag{6.74}$$

I define a corresponding linear combination with the creation a_j^+ and annihilation operators a_j^- by

$$\Phi_\hbar(\phi) := \sqrt{\hbar}\, \delta^{i\bar{\imath}} \left(\phi_i a_{\bar{\imath}}^+ + \phi_{\bar{\imath}} a_i^- \right). \tag{6.75}$$

Let $W_\hbar : \mathcal{S}^* \to \mathcal{B}(\mathcal{H}_\hbar)$ be the map from covectors to Weyl generators

$$W_\hbar(\phi) := \exp\Big(\mathrm{i} \Phi_\hbar(\phi) \Big). \tag{6.76}$$

These Weyl generators fulfill the Weyl relations given in Definition 5.2.6, Subsection 5.1.1.

Proof. The unit of the Weyl algebra (5.53c) is obviously given by $W_\hbar(0)$. For the involution (5.53b), note that $(a_j^\pm)^* = a_j^\mp$ and thus (6.75) is self-adjoint. Hence

$$W_\hbar(\phi)^* = W_\hbar(-\phi). \tag{6.77}$$

For the product of two generators (5.53a), compute the commutator

$$\begin{aligned}
[\Phi_\hbar(\phi), \Phi_\hbar(\phi')]_- &= \hbar \delta^{i\bar{\imath}} \delta^{j\bar{\jmath}} \left[\phi_i a_{\bar{\imath}}^+ + \phi_{\bar{\imath}} a_i^-, \phi'_j a_{\bar{\jmath}}^+ + \phi'_{\bar{\jmath}} a_j^- \right]_- && \text{(6.78a)} \\
&= -\hbar \delta^{i\bar{\imath}} \delta^{j\bar{\jmath}} \left(\phi_i \phi'_{\bar{\jmath}} - \phi_{\bar{\imath}} \phi'_j \right) \delta_{\bar{\imath} j} \mathbb{1} && \text{(6.78b)} \\
&= \mathrm{i}\hbar \{\phi, \phi'\} \mathbb{1}. && \text{(6.78c)}
\end{aligned}$$

It is seen that the commutator of this expression with $\Phi_\hbar(\phi)$ vanishes so that the Baker-Campbell-Hausdorff formula yields

$$\begin{aligned}
\exp\Big(\mathrm{i}\Phi_\hbar(\phi)\Big) \exp\Big(\mathrm{i}\Phi_\hbar(\phi')\Big) = \exp\left(-\frac{1}{2} [\Phi_\hbar(\phi), \Phi_\hbar(\phi')]_- \right) \\
\times \exp\Big(\mathrm{i}\Phi_\hbar(\phi + \phi')\Big).
\end{aligned} \tag{6.79}$$

Replacing the commutator in (6.79) with the expression (6.78c) shows that the generators (6.76) also fulfill the product relation (5.53a), and thus all Weyl relations (5.53). □

The Berezin-Toeplitz quantization respects anti-normal ordering and dequantization respects normal ordering (see Subsection 6.2.3). To reorder the terms in the series expansion of a Weyl generator (6.76), I use the commutation relations

(6.54) and derive commutators for powers of ladder operators in anti-normal or normal order. For an index pair $(i,\bar{\imath}) \in \{(1,\bar{1}),(2,\bar{2}),\dots,(N,\bar{N})\}$, the two orders of the commutators are, respectively,

$$\Big[(a_i^-)^m,(a_{\bar{\imath}}^+)^n\Big]_- = \sum_{l=1}^{\min(m,n)} (-1)^{l+1} l! \binom{m}{l}\binom{n}{l} (a_i^-)^{m-l}(a_{\bar{\imath}}^+)^{n-l}, \tag{6.80a}$$

$$\Big[(a_i^-)^m,(a_{\bar{\imath}}^+)^n\Big]_- = \sum_{l=1}^{\min(m,n)} l! \binom{m}{l}\binom{n}{l} (a_{\bar{\imath}}^+)^{n-l}(a_i^-)^{m-l}, \tag{6.80b}$$

while for all indices $(i,\bar{\imath}) \notin \{(1,\bar{1}),(2,\bar{2}),\dots,(N,\bar{N})\}$ these commutators vanish. For the second order term, for example, the operator reordering yields one extra term that is the same for quantization and dequantization but with opposite sign,

$$\Big(\mathrm{i}\Phi_\hbar(\phi)\Big)^2 = -\hbar\delta^{i\bar{\imath}}\delta^{j\bar{\jmath}}\Big(\underbrace{\phi_i\phi_j a_{\bar{\imath}}^+ a_{\bar{\jmath}}^+ + 2\phi_{\bar{\imath}}\phi_j a_i^- a_{\bar{\jmath}}^+ + \phi_{\bar{\imath}}\phi_{\bar{\jmath}} a_i^- a_j^-}_{\text{anti-normal ordered, by } T\text{-quantization}} - \phi_{\bar{\imath}}\phi_{\bar{\jmath}}\delta_{i\bar{\jmath}}\mathbb{1}\Big) \tag{6.81a}$$

$$= -\hbar\delta^{i\bar{\imath}}\delta^{j\bar{\jmath}}\Big(\underbrace{\phi_i\phi_j a_{\bar{\imath}}^+ a_{\bar{\jmath}}^+ + 2\phi_i\phi_{\bar{\jmath}} a_{\bar{\imath}}^+ a_j^- + \phi_{\bar{\imath}}\phi_{\bar{\jmath}} a_i^- a_j^-}_{\text{normal ordered, for } \Xi\text{-dequantization}} + \phi_i\phi_{\bar{\jmath}}\delta_{i\bar{\jmath}}\mathbb{1}\Big). \tag{6.81b}$$

The extra terms of all orders yield an exponential factor depending on $\hbar$ and $|\phi|^2 = \sum_{i=1}^N |\phi_i|^2$,

$$W_\hbar(\phi) = \exp\left(\frac{\hbar}{2}|\phi|^2\right) T_\hbar\left(\mathrm{e}^{\mathrm{i}\phi}\right). \tag{6.82}$$

Similarly, dequantization of the Weyl generators gives

$$\Xi_\hbar\Big(W_\hbar(\phi)\Big) = \exp\left(-\frac{\hbar}{2}|\phi|^2\right)\mathrm{e}^{\mathrm{i}\phi}. \tag{6.83}$$

Weyl quantization is a family of quantization maps $Q_{\mathrm{W},\hbar} : \mathcal{A}_0 \to \mathfrak{A}_\hbar$ such that on the extended domain of bounded functions, $Q_{\mathrm{W},\hbar} : \exp(\mathrm{i}\phi) \mapsto W_\hbar(\phi)$. Note that, in the limit $\hbar \to 0$, the quantization (6.82) and dequantization (6.83) coincide with $\exp(\mathrm{i}\phi)$, which is used in showing that Weyl quantization is a strict deformation quantization and also continuous in the classical limit; see Landsman [58] for a detailed discussion.

Any Toeplitz operator of a Schwartz function $F \in \mathrm{C}^\infty_{\mathrm{S}}(\mathcal{S},\mathbb{C})$ can also be written in terms of Weyl generators. For this, consider the Fourier transform,

$$\widehat{F}(\phi) = \frac{1}{(2\pi)^{2N}} \int_{\mathcal{S}} F(z)\mathrm{e}^{-\mathrm{i}\phi(z)}\,\mathrm{dvol}(z), \tag{6.84}$$

and its inverse transform (with the volume form dvol^* on $\mathcal{S}^*$),

$$F(z) = \int_{\mathcal{S}^*} \widehat{F}(\phi)\mathrm{e}^{\mathrm{i}\phi(z)}\,\mathrm{dvol}^*(\phi). \tag{6.85}$$

Recall that the result (6.83) is related to (6.82) by a Berezin transform. The Weyl quantization is related to "half" a Berezin transform, so I write

$$\sqrt{\widehat{b}_\hbar}(\phi) = \frac{1}{(2\pi)^N} \exp\left(-\frac{\hbar}{2}|\phi|^2\right). \tag{6.86}$$

Note that the exponential function here is exactly the same as in the dequantization (6.83). The Toeplitz operator of F is then

$$T_\hbar(F) = \int_{\mathcal{S}^*} \widehat{F}(\phi) T_\hbar\left(\mathrm{e}^{\mathrm{i}\phi}\right) \,\mathrm{dvol}^*(\phi) \tag{6.87a}$$

$$= (2\pi)^N \int_{\mathcal{S}^*} \widehat{F}(\phi)\sqrt{\widehat{b}_\hbar}(\phi) W_\hbar(\phi) \,\mathrm{dvol}^*(\phi). \tag{6.87b}$$

Note that in the classical limit $\hbar \to 0$, $F_\hbar \to F$, similarly to the limit of the Berezin transform, the left-hand side of (6.87) becomes F, and the right-hand side of (6.87) becomes the inverse Fourier transform (6.85). More details on the Weyl algebra and its relation to Toeplitz operators are given in Landsman [58, ch. II].

In the following, I use the results on the Weyl generators discussed above to formulate star products for (Berezin)-Toeplitz quantization and dequantization.

6.3.2 Infinite Order Strict Deformation (De)Quantization

Let $(\mathfrak{A}_\hbar)_{\hbar\in I}$ be the family of C*-algebras with $\mathfrak{A}_0 = \mathrm{C}_0(\mathcal{S}, \mathbb{C})$ — as the closure of $\mathcal{A}_0 = \mathrm{C}^\infty_{\mathrm{S}}(\mathcal{S}, \mathbb{C})$ — and compact operators $\mathfrak{A}_\hbar = \mathcal{K}(\mathcal{H}_\hbar)$ for $\hbar \in I_*$. There exists a continuous field of C*-algebras $\left(I, (\mathfrak{A}_\hbar)_{\hbar\in I}, \Gamma\right)$ equivalently determined by Weyl quantization and Toeplitz quantization [58, Ch. II, Sec. 2.6]. As an instance of my general discussion of star products and dequantization expandibility in Subsection 5.1.1 and Subsection 5.1.2, I discuss Ξ-dequantization expandibility and the star product for Toeplitz sections as well the star product corresponding to Berezin-Toeplitz dequantization.

As a special case of the quantization sections defined in (5.17), the Toeplitz section of any $F \in \mathcal{A}_0$ is given by the map

$$T(F) : \hbar \mapsto \begin{cases} F & \hbar = 0, \\ T_\hbar(F) & \hbar \in I_*. \end{cases} \tag{6.88}$$

Similarly, the family of Weyl generators of any $\phi \in \mathcal{S}^*$ forms a vector field in $\prod_{\hbar\in I} \mathcal{B}(\mathcal{H}_\hbar)$,

$$W(\phi) : \hbar \mapsto \begin{cases} \mathrm{e}^{\mathrm{i}\phi} & \hbar = 0, \\ W_\hbar(\phi) & \hbar \in I_*. \end{cases} \tag{6.89}$$

Notice that $\mathrm{e}^{\mathrm{i}\phi} \notin \mathcal{A}_0$ and the Weyl generators $W_\hbar(\phi)$ are bounded operators, while for the Weyl quantization map $Q_{\mathrm{W},\hbar} : \mathcal{A}_0 \to \mathfrak{A}_\hbar$ the domain is restricted to $\mathcal{A}_0$.

Nevertheless, it will be helpful to decompose operators in $\mathfrak{A}_\hbar$ in terms of Weyl generators, see Subsection 6.3.1.

In the proofs below, I have to bound k-th order remainders $\mathrm{er}_k \in \mathrm{C}^\infty(\mathbb{C},\mathbb{C})$ for any order $k \in \mathbb{N}$ of the Taylor expansion of the exponential function,

$$\mathrm{er}_k(\zeta) = \mathrm{e}^\zeta - \sum_{i=0}^{k} \frac{\zeta^j}{j!}. \tag{6.90}$$

Lemma 6.3.2. *For every $k \in \mathbb{N}$, there exists a real constant $C_k > 0$ such that for all $\zeta \in \mathbb{C}$*

$$\left|\mathrm{er}_k(\zeta)\right| \leq C_k \left(1 + \mathrm{e}^{\mathrm{Re}\,\zeta}\right) |\zeta|^{k+1}. \tag{6.91}$$

Proof. Taylor's theorem states that

$$\left|\mathrm{er}_k(\zeta)\right| = \mathcal{O}\left(|\zeta|^{k+1}\right) \tag{6.92}$$

as $|\zeta|$ becomes small. To find a bound for $|\zeta| \to \infty$, I use the triangle inequality,

$$\left|\mathrm{er}_k(\zeta)\right| \leq \mathrm{e}^{\mathrm{Re}\,\zeta} + \sum_{j=0}^{k} \frac{|\zeta|^k}{j!}. \tag{6.93}$$

Adding the two bounds (6.92) and (6.93) together yields (6.91). □

Proposition 6.3.3. *Given any Schwartz function $F \in \mathrm{C}^\infty_{\mathrm{S}}(\mathcal{S},\mathbb{C})$, the corresponding Toeplitz section $T(F)$ is Ξ-expandable.*

Proof. I use the Toeplitz section $A = T(F)$ from (6.88) — setting the dequantization $\Upsilon = \Xi$ — to obtain a condition for the Berezin transform of F,

$$\lim_{\hbar\to 0} \frac{1}{\hbar^k} \left\| (\Xi_\hbar \circ T_\hbar)(F) - \sum_{j=0}^{k} F_j \hbar^j \right\| = 0. \tag{6.94}$$

This condition is fulfilled by the functions

$$F_j(z) = \frac{1}{j!} \left(\delta^{i\bar{\imath}} \frac{\partial}{\partial z^i} \frac{\partial}{\partial \overline{z^i}} \right)^j F(z) \tag{6.95}$$

for all orders $j, k \in \mathbb{N}$. To show that the functions F_j indeed fulfill the condition, first consider a Schwartz function $F \in \mathrm{C}^\infty_{\mathrm{S}}(\mathcal{S},\mathbb{C})$, use the Fourier transforms $\widehat{F}$ and $\widehat{b}_\hbar$ with the convolution theorem. The derivatives in (6.95) become $\mathrm{i}\phi_i$ and

$\mathrm{i}\phi_{\bar{\imath}}$, respectively, so

$$\left\|(\Xi_\hbar \circ T_\hbar)(F) - \sum_{j=0}^{k} F_j \hbar^j \right\| = \left\| \int_{\mathcal{S}^*} \mathrm{er}_k\left(-\hbar|\phi|^2\right) \widehat{F}(\phi) \mathrm{e}^{\mathrm{i}\phi} \, \mathrm{dvol}^*(\phi) \right\| \tag{6.96a}$$

$$\leq \int_{\mathcal{S}^*} \left|\mathrm{er}_k\left(-\hbar|\phi|^2\right)\right| \left|\widehat{F}(\phi)\right| \, \mathrm{dvol}^*(\phi). \tag{6.96b}$$

Now apply Lemma 6.3.2 and note that here the argument ζ is non-positive, such that

$$\left\|(\Xi_\hbar \circ T_\hbar)(F) - \sum_{j=0}^{k} F_j \hbar^j \right\| \leq 2C_k \hbar^{k+1} \int_{\mathcal{S}^*} |\phi|^{2(k+1)} \left|\widehat{F}(\phi)\right| \, \mathrm{dvol}^*(\phi). \tag{6.97}$$

When F is Schwartz, then $\widehat{F}$ is Schwartz, the integral is finite, and we obtain an upper bound given by some finite constant times $\hbar^{k+1}$. So the limit expression (6.94) vanishes for all $k \in \mathbb{N}$. □

Recall that a quantization star product $\star_Q$ is determined by the conditions (5.19). Toeplitz quantization T is an instance of a quantization that admits a star product. It has an exponential expression with directed derivatives that act only on the function to the left $F_1 \in \mathcal{A}_0$ or on the right $F_2 \in \mathcal{A}_0$ as indicated with an arrow,

$$F_1 \star_T F_2 = F_1 \exp\left(-\hbar \frac{\overleftarrow{\partial}}{\partial z^i} \delta^{i\bar{\imath}} \frac{\overrightarrow{\partial}}{\partial \overline{z}^{\bar{\imath}}}\right) F_2. \tag{6.98}$$

Similarly, Berezin-Toeplitz dequantization determines a dequantization star product $\star_\Xi$ such that the conditions (5.24) are fulfilled for all $F_1, F_2 \in \mathcal{A}_0$ with the exponential expression

$$F_1 \star_\Xi F_2 = F_1 \exp\left(\hbar \frac{\overleftarrow{\partial}}{\partial \overline{z}^{\bar{\imath}}} \delta^{\bar{\imath}i} \frac{\overrightarrow{\partial}}{\partial z^i}\right) F_2. \tag{6.99}$$

Note that the holomorphic and anti-holomorphic derivatives of these two star products act in different directions and the exponentials have opposite sign.

Proposition 6.3.4. *Toeplitz quantization is an infinite order strict deformation quantization over the algebra of Schwartz functions* $\mathcal{A}_0 = \mathrm{C}^\infty_{\mathrm{S}}(\mathcal{S}, \mathbb{C})$ *with the star product* (6.98)*.*

Proof. In [58, Ch. II, Sec. 2.6], it was shown that there exists a continuous field of C*-algebras $\left(I, (\mathfrak{A}_\hbar)_{\hbar \in I}, \Gamma\right)$ including the Toeplitz sections $T(F)$ for $F \in \mathcal{A}_0$ as sections, $T(F) \in \Gamma$. It remains to show that the star product (6.98) fulfills the conditions (5.19) in all orders $k \in \mathbb{N}$.

Recall the Fourier decomposition (6.87) of the Toeplitz operators $T_\hbar(F)$ and $T_\hbar(F')$ for any functions $F, F' \in \mathrm{C}^\infty_\mathrm{S}(\mathcal{S}, \mathbb{C})$ into Toeplitz operators $T_\hbar(\mathrm{e}^{\mathrm{i}\phi})$ and $T_\hbar(\mathrm{e}^{\mathrm{i}\phi'})$ that are related to the respective Weyl generators via (6.82). The k-th remainder (5.18) is bounded from above by the double integral

$$R^k_T(F, F', \hbar) \leq \iint\limits_{\mathcal{S}^*} \left|\widehat{F}(\phi)\right| \left|\widehat{F}'(\phi')\right| R^k_T\left(\mathrm{e}^{\mathrm{i}\phi}, \mathrm{e}^{\mathrm{i}\phi'}, \hbar\right) \,\mathrm{dvol}^*(\phi)\,\mathrm{dvol}^*(\phi'). \tag{6.100}$$

The remainder inside the integral is given by

$$R^k_T\left(\mathrm{e}^{\mathrm{i}\phi}, \mathrm{e}^{\mathrm{i}\phi'}, \hbar\right) = \frac{1}{\hbar^k}\left\| T_\hbar\left(\mathrm{e}^{\mathrm{i}\phi}\right) T_\hbar\left(\mathrm{e}^{\mathrm{i}\phi'}\right) - \sum_{j=0}^{k} \frac{\hbar^j}{j!}\left(\delta^{i\bar{\imath}}\phi_i\phi'_{\bar{\imath}}\right)^j T_\hbar\left(\mathrm{e}^{\mathrm{i}(\phi+\phi')}\right)\right\|. \tag{6.101}$$

Notice that the Weyl relation (5.53a) implies

$$T_\hbar\left(\mathrm{e}^{\mathrm{i}\phi}\right) T_\hbar\left(\mathrm{e}^{\mathrm{i}\phi'}\right) = \exp\left(\hbar\delta^{i\bar{\imath}}\phi_i\phi'_{\bar{\imath}}\right) T_\hbar\left(\mathrm{e}^{\mathrm{i}(\phi+\phi')}\right) \tag{6.102}$$

so that the operator $T_\hbar\left(\mathrm{e}^{\mathrm{i}(\phi+\phi')}\right)$ pulls out of the two terms in (6.101). To apply Lemma 6.3.2, I choose $\zeta \in \mathbb{C}$ such that

$$\zeta = \hbar\delta^{i\bar{\imath}}\phi_i\phi'_{\bar{\imath}}, \tag{6.103a}$$

$$\mathrm{Re}\,\zeta = \frac{\hbar}{2}\delta^{i\bar{\imath}}\left(\phi_i\phi'_{\bar{\imath}} + \phi_{\bar{\imath}}\phi'_i\right). \tag{6.103b}$$

Thus, we have

$$R^k_T\left(\mathrm{e}^{\mathrm{i}\phi}, \mathrm{e}^{\mathrm{i}\phi'}, \hbar\right) = \frac{1}{\hbar^k}\left|\mathrm{er}_k(\zeta)\right| \left\|T_\hbar\left(\mathrm{e}^{\mathrm{i}(\phi+\phi')}\right)\right\| \tag{6.104a}$$

$$\leq C_k\hbar\left|\delta^{i\bar{\imath}}\phi_i\phi'_{\bar{\imath}}\right|^{k+1}\left(\left\|T_\hbar\left(\mathrm{e}^{\mathrm{i}(\phi+\phi')}\right)\right\| + \mathrm{e}^{\mathrm{Re}\,\zeta}\left\|T_\hbar\left(\mathrm{e}^{\mathrm{i}(\phi+\phi')}\right)\right\|\right). \tag{6.104b}$$

The two terms with the operator norm follow from (6.82) and $\|W_\hbar(\phi)\| = 1$ (for any $\phi \in \mathcal{S}^*$), implying that the Toeplitz map is norm contracting,

$$\left\|T_\hbar\left(\mathrm{e}^{\mathrm{i}(\phi+\phi')}\right)\right\| = \exp\left(-\frac{\hbar}{2}|\phi+\phi'|^2\right), \tag{6.105a}$$

$$\mathrm{e}^{\mathrm{Re}\,\zeta}\left\|T_\hbar\left(\mathrm{e}^{\mathrm{i}(\phi+\phi')}\right)\right\| = \exp\left(-\frac{\hbar}{2}|\phi|^2 - \frac{\hbar}{2}|\phi'|^2\right). \tag{6.105b}$$

Both of these exponentials are bounded by 1. So (6.104) is bounded by

$$R^k_T\left(\mathrm{e}^{\mathrm{i}\phi}, \mathrm{e}^{\mathrm{i}\phi'}, \hbar\right) \leq 2C_k\hbar\left|\delta^{i\bar{\imath}}\phi_i\phi'_{\bar{\imath}}\right|^{k+1}. \tag{6.106a}$$

The modulus in the $(k+1)$ order polynomial is bounded from above by the sum of $|\phi_i|$ and $|\phi'_i|$ all to the power of $k+1$. Inserted back into the integration (6.100) yields

$$R_T^k(F,F',\hbar) \leq 2C_k\hbar \iint\limits_{\mathcal{S}^*} \left(\sum_{i=1}^N |\phi_i|\,|\phi'_i|\right)^{k+1} \times \left|\widehat{F}(\phi)\right| \left|\widehat{F}'(\phi')\right| \,\mathrm{dvol}^*(\phi)\,\mathrm{dvol}^*(\phi'). \tag{6.107}$$

The factor with the sum is a polynomial in ϕ and ϕ' and the integration with the Schwartz functions $\widehat{F}$ and $\widehat{F}'$ is finite. Therefore, the remainder $R_T^k(F,F',\hbar)$ is bounded by a constant (independent of $\hbar$) times $\hbar$, which vanishes in the limit $\hbar \to 0$ for all $k \in \mathbb{N}$.

Poisson compatibility of this star product follows from the first order terms

$$F \star_T F' - F' \star_T F = -\hbar \sum_{i=1}^N \left(\frac{\partial F}{\partial z^i}\frac{\partial F'}{\partial \overline{z}^i} - \frac{\partial F'}{\partial z^i}\frac{\partial F}{\partial \overline{z}^i}\right) + \mathcal{O}\left(\hbar^2\right) \tag{6.108a}$$

$$= \mathrm{i}\hbar\,\{F,\,F'\} + \mathcal{O}\left(\hbar^2\right). \tag{6.108b}$$

Notice that the star product is also self-adjoint and differential, which follows immediately from the differential form (6.98). □

Proposition 6.3.5. *Berezin-Toeplitz dequantization is an infinite order strict deformation dequantization of the algebra of Schwartz functions $\mathcal{A}_0$ with the star product* (6.99).

Proof. According to [58, Ch. II, Thm. 2.6.5], the continuous fields of the Weyl quantization and Berezin-Toeplitz quantization coincide.

Even though the Weyl operators $W_\hbar(\phi)$ are not elements of $\mathfrak{A}_\hbar = \mathcal{K}(\mathcal{H}_\hbar)$, they are Ξ-expandable following a similar argument as in Proposition 6.3.3 with the coefficients

$$w_j^\phi = \frac{1}{j!}\left(-\frac{1}{2}|\phi|^2\right)^j \mathrm{e}^{\mathrm{i}\phi}. \tag{6.109}$$

So, we write a Ξ-expandable section $A_F \in \Gamma$ as

$$A_F(\hbar) = \int\limits_{\mathcal{S}^*} \widehat{F}(\phi,\hbar) W_\hbar(\phi)\,\mathrm{dvol}^*(\phi) \tag{6.110}$$

with a continuous function $\widehat{F} \in \mathrm{C}(\mathcal{S}^* \times I, \mathbb{C})$ such that $F(\cdot,\hbar) \in \mathcal{A}_0$ for all $\hbar \in I$. The conditions of the continuous field of C*-algebras $\left(I, (\mathfrak{A}_\hbar)_{\hbar\in I}, \Gamma\right)$ in Definition 5.1.7 imply that all sections of the form A_F are a total subset (span

a dense subspace) of Γ. This means that for any section $A \in \Gamma$ there exists a Ξ-expandable section (6.110) such that

$$\forall \delta > 0 : \exists N_0 \subset I : \forall \hbar' \in N_0 : \|A(\hbar') - A_F(\hbar')\| \leq \delta, \tag{6.111}$$

where N_0 is a neighborhood around $\hbar = 0$.

Taking the dequantization yields the smooth function

$$\Xi_\hbar\Big(A_F(\hbar)\Big) = \int\limits_{\mathcal{S}^*} \widehat{F}(\phi, \hbar) \exp\left(-\frac{\hbar}{2}|\phi|^2\right) \mathrm{e}^{\mathrm{i}\phi} \,\mathrm{dvol}(\phi), \tag{6.112}$$

which is the convolution of the pointwise Fourier transformed function $F(\cdot, \hbar)$ with "half" the Berezin kernel.

Now let us consider the dequantization of a product of two such sections, $A_F A_{F'}$, for $F, F' \in \mathcal{A}_0$. With the same identification of ζ as in (6.103), I rewrite the Weyl relation (5.53a) in terms of the complex conjugated value $\overline{\zeta} = \hbar\delta^{i\overline{\imath}}\phi_i\phi'_{\overline{\imath}}$,

$$W_\hbar(\phi)W_\hbar(\phi') = \mathrm{e}^{-\mathrm{i}\,\mathrm{Im}\,\overline{\zeta}} W_\hbar(\phi + \phi'). \tag{6.113}$$

Similar to the previous proof, notice that

$$\Xi_\hbar\Big(W_\hbar(\phi + \phi')\Big) = \exp\left(-\frac{\hbar}{2}|\phi + \phi'|^2\right) \mathrm{e}^{\mathrm{i}(\phi+\phi')}, \tag{6.114a}$$

$$\mathrm{e}^{\mathrm{Re}\,\overline{\zeta}}\Xi_\hbar\Big(W_\hbar(\phi + \phi')\Big) = \exp\left(-\frac{\hbar}{2}|\phi|^2 - \frac{\hbar}{2}|\phi'|^2\right) \mathrm{e}^{\mathrm{i}(\phi+\phi')} \tag{6.114b}$$

$$= \Xi_\hbar\Big(W_\hbar(\phi)\Big)\Xi_\hbar\Big(W_\hbar(\phi')\Big). \tag{6.114c}$$

I combine the exponentials as $\overline{\zeta} = \mathrm{Re}\,\overline{\zeta} + \mathrm{i}\,\mathrm{Im}\,\overline{\zeta}$, so that the dequantization of the product (6.113) reads

$$\Xi_\hbar\Big(W_\hbar(\phi)W_\hbar(\phi')\Big) = \mathrm{e}^{-\overline{\zeta}}\Xi_\hbar\Big(W_\hbar(\phi)\Big)\Xi_\hbar\Big(W_\hbar(\phi')\Big). \tag{6.115}$$

Thus the product of sections and its dequantization are, respectively,

$$(A_F A_{F'})(\hbar) = \iint\limits_{\mathcal{S}^*} \widehat{F}(\phi, \hbar)\widehat{F}'(\phi', \hbar) W_\hbar(\phi)W_\hbar(\phi') \,\mathrm{d}^2\mathrm{vol}^*, \tag{6.116a}$$

$$\Xi_\hbar\Big((A_F A_{F'})(\hbar)\Big) = \iint\limits_{\mathcal{S}^*} \widehat{F}(\phi, \hbar)\widehat{F}'(\phi', \hbar) \times \Xi_\hbar\Big(W_\hbar(\phi)\Big)\mathrm{e}^{-\overline{\zeta}}\Xi_\hbar\Big(W_\hbar(\phi')\Big) \,\mathrm{d}^2\mathrm{vol}^*. \tag{6.116b}$$

The exponential factor $\mathrm{e}^{-\overline{\zeta}}$ is the Fourier transform of the derivatives that act on the $\mathrm{e}^{\mathrm{i}\phi}$ and $\mathrm{e}^{\mathrm{i}\phi'}$ functions of the dequantizations of the Weyl generator (6.114),

$$\mathrm{e}^{\mathrm{i}\phi}\mathrm{e}^{-\overline{\zeta}}\mathrm{e}^{\mathrm{i}\phi'} = \mathrm{e}^{\mathrm{i}\phi}\left(\sum_{j=0}^{\infty}\frac{1}{j!}\left(\frac{\overleftarrow{\partial}}{\partial\overline{z}^{\overline{\imath}}}\delta^{\overline{\imath}i}\frac{\overrightarrow{\partial}}{\partial z^{i}}\right)^{j}\hbar^{j}\right)\mathrm{e}^{\mathrm{i}\phi'}. \tag{6.117}$$

Hence, the integration in (6.116b) separates into the integral expression (6.110) for the sections A_F and $A_{F'}$,

$$\Xi_\hbar\Big((A_F A_{F'})(\hbar)\Big) = A_F\left(\sum_{j=0}^{\infty}\frac{1}{j!}\left(\frac{\overleftarrow{\partial}}{\partial\overline{z}^{\overline{\imath}}}\delta^{\overline{\imath}i}\frac{\overrightarrow{\partial}}{\partial z^{i}}\right)^{j}\hbar^{j}\right)A_{F'}. \tag{6.118}$$

From the assumptions, I know that A_F and $A_{F'}$ are Ξ-expandable with the expansion truncated at any order $k \in \mathbb{N}$ given by

$$\Sigma^k_\Xi(A_F,\hbar) = \sum_{j=0}^{k} F_j\hbar^j \tag{6.119}$$

and similarly for $A_{F'}$. I express the result (6.118) for both A_F and $A_{F'}$ by the respective expansions (6.119) leading to

$$\Sigma^\infty_\Xi(A_F,\hbar)\exp\left(\hbar\frac{\overleftarrow{\partial}}{\partial\overline{z}^{\overline{\imath}}}\delta^{\overline{\imath}i}\frac{\overrightarrow{\partial}}{\partial z^{i}}\right)\Sigma^\infty_\Xi(A_{F'},\hbar) = \Sigma^\infty_\Xi(A_F,\hbar)\star_\Xi\Sigma^\infty_\Xi(A_{F'},\hbar). \tag{6.120}$$

The dequantization star product is again Poisson compatible, self-adjoint and differential, which is analogously shown as in the previous proposition for the quantization star product. □

Recall Definition 5.2.9 of the star product gauge equivalence and notice that the relation between the quantization star product $\star_T$ and the dequantization star product $\star_\Xi$, $\forall F, F' \in \mathcal{A}_0$,

$$(\Xi_\hbar\circ T_\hbar)\Big(F\star_T F'\Big) = \Big((\Xi_\hbar\circ T_\hbar)(F)\Big)\star_\Xi\Big((\Xi_\hbar\circ T_\hbar)(F')\Big), \tag{6.121}$$

is the series expansion with the coefficients (6.95), determined by the expansion terms of the Berezin transform.

In the final step of my construction, I use dequantization to define a state and compare its properties to the Sorkin-Johnston state using the Weyl algebra.

6.4 The Sorkin-Johnston State from Dequantization

Finally, I want to come to the main result of the construction of the family of quantum algebras $(\mathfrak{A}_\hbar)_{\hbar\in I_*}$. Recall that the construction started with the vector

space $\mathcal{S} = \mathrm{img}(E)$ as discussed in Subsection 2.4.2. This space has the symplectic form ω and an inner product so that the method of geometric quantization gave an algebra $\mathfrak{A}_\hbar$ for each $\hbar \in I_*$. Now I show that the Sorkin-Johnston state as discussed in Section 5.2 is the "ground state of the system" that is equivalently determined via the dequantization map.

Theorem 6.4.1. *The linear map $\sigma_\hbar : \mathfrak{A}_\hbar \to \mathbb{C}$ given by*

$$\sigma_\hbar(A) := \Xi_\hbar(A)(0) \tag{6.122}$$

is the Sorkin-Johnston state.

Proof. In order to show that this map is the Sorkin-Johnston state (5.70), I need to evaluate it on Weyl generators. Recall the result (6.83) when dequantizing the Weyl generator $W_\hbar(\phi)$ of any covector $\phi \in \mathcal{S}^*$. The evaluation at $0 \in \mathcal{S}$ yields

$$\sigma_\hbar\Big(W_\hbar(\phi)\Big) = \exp\left(-\frac{\hbar}{2}|\phi|^2\right). \tag{6.123}$$

I want to express this in terms of the Kähler metric η defined in (5.29), which is compatible with the complex structure (6.2) and the symplectic form ω. Notice that

$$\eta^{-1}(\phi,\phi) = \delta^{i\bar{\imath}}\phi_i\phi_{\bar{\imath}} + \delta^{\bar{\imath}i}\phi_{\bar{\imath}}\phi_i = 2|\phi|^2 \tag{6.124}$$

so that

$$|\phi|^2 = \frac{1}{2}\eta^{-1}(\phi,\phi). \tag{6.125}$$

This is the inverse of the bilinear form η on $\mathcal{S}$, which is identical to the covariance of the Sorkin-Johnston state given in Definition 5.2.10. The form η is compatible with the complex structure J yielding a Kähler vector space $(\mathcal{S}, \omega, \eta, J)$. □

Given any $F \in \mathcal{A}_0$, the Sorkin-Johnston state of the Toeplitz operator $T_\hbar(F) \in \mathfrak{A}_\hbar$ is the Berezin transform of F evaluated at 0,

$$\sigma_\hbar\Big(T_\hbar(F)\Big) = \int_{\mathcal{S}} b_\hbar(z)F(z)\ \mathrm{dvol}(z). \tag{6.126}$$

Note that the dequantization state is parametrized by $\hbar$, so $(\sigma_\hbar)_{\hbar\in I}$ is a family of states with the classical limit $\sigma_0(F) := F(0)$. For any section A of the continuous field of C*-algebras $\Big(I, (\mathfrak{A}_\hbar)_{\hbar\in I}, \Gamma\Big)$, the map $\sigma(A) : I \to \mathbb{C}$ given by

$$\sigma(A)(\hbar) := \sigma_\hbar\Big(A(\hbar)\Big) \tag{6.127}$$

is continuous, because $\Xi(A) : \mathcal{S} \times I \to \mathbb{C}$ defined as in (5.25) is continuous.

In the classical limit $\hbar \to 0$, the Sorkin-Johnston state is simply the evaluation of an observable at 0. For all other values $\hbar > 0$, a dequantization map lets us identify the quantum observables with classsical observables. Berezin-Toeplitz dequantization is the simplest choice of a dequantization map from the geometric construction and it leads to the Sorkin-Johnston state via evaluation at 0. The geometric construction of the Sorkin-Johnston state via the lowest part of the Bochner-Laplacian spectrum generalizes to symplectic manifolds with a Riemannian metric as mentioned in Subsection 5.1.3 based on the publications by Ma and Marinescu [60], [61], and [62]. The geometric construction allows for a non-perturbative generalization to interacting field theory and leads to a state via dequantization.

Chapter 7

Conclusion and Outlook

In this thesis, I have reviewed classical and quantum real scalar field theory on spacetime manifolds and causal sets. Most of the notations and formulations were discussed for spacetime manifolds and causal sets in parallel to highlight similarities and difference.

My investigations led to several results (of which some are already published and some other are close to publication) and point to further research questions. In the following, let me summarize the results and briefly discuss open problems.

7.1 Summary of the Research Results

In Chapter 1, I discussed Cauchy surfaces in globally hyperbolic spacetimes, reviewed two notions of Cauchy slices for causal sets (one determined by volume thickening and one based on layers) and defined a new one (based on steps). Cauchy slices are constructed from Cauchy antichains that are extended by one of three methods, a volume thickening (see Major, Rideout, and Surya [64]), a layer thickening, or a time step thickening, see Subsection 1.3.3. Since a Cauchy slice is a subset of a causet on which initial field data is specified, the appropriate choice of antichain thickening depends on the method that is used to discretize the Klein-Gordon field equations. For the discretization method based on the preferred past structure, as proposed in [29], initial field data has to be specified on a 2-layer or 2-step Cauchy slice, while for my generalization shown in Subsection 2.3.1, we also need the preferred past of the preferred past — hence a 4-step Cauchy slice — to have a well-defined initial value problem.

The preferred past structure is supplementary to a causet and there is an obvious choice of lattices described in Subsection 2.3.1. For causets that are sprinkled on Minkowski spacetime (of dimensions $1+1$, $1+2$ and $1+3$), I compared six criteria to obtain subsets of the rank 2 past for causet events in order to determine a preferred past structure by investigating the corresponding past diamonds. These results are published in [38] and my MATLAB source code is accessible via my GitHub repositories [76, 77]. My numerical results showed that criterion 6 (see Subsection 3.2.2) performs best in selecting a unique diamond with the highest probability among the investigated criteria. The distribution of the proper time separation for the past diamonds selected by criterion 6 has a relatively small

expectation value and small variance. The selected rank 2 past events are approximately uniformly distributed on the unit past hyperboloid, which indicates that criterion 6 tends towards Lorentz invariance in the Minkowski spacetime limit of an increasing sprinkling region.

My numerical results on diamonds between next-to-nearest neighbours along geodesic paths through the sprinkled causets shown in Section 3.4 are consistent with dimensional reduction for small causal intervals in causets as argued in Carlip [27]. One might hope that a discretization method for field equations on causal sets should be independent of the spacetime dimension, which is an emergent property rather than built in as a fundamental parameter. Further studies with an explicit comparison to the field equations on spacetime manifolds and investigations of sprinkles on curved spacetimes are open tasks.

In Chapter 4, I discussed the construction of the sprinkling probability space for arbitrary spacetime manifolds and its application to the computation of the expected cardinality of the past infinity in finite causets, sprinkled on causal intervals of Minkowski spacetime. For causal intervals of 2-dimensional Minkowski spacetime, there exists a combinatorial method to determine the probability for a causet to arise from a sprinkling process. I developed a LaTeX-package that utilizes this method to create Hasse diagrams, not only for causets that embed in 2-dimensional Minkowski spacetime, but for arbitrary causets as well [68].

In the second main part of this thesis, I reviewed quantization methods (see Chapter 5) in order to apply them to the on-shell phase space for some free field theory on a finite causet that has both a symplectic structure and inner product. I constructed a physical Hilbert space as subspace of square-integrable sections of the quantization bundle and the quantum algebra on a causet using geometric and Toeplitz quantization. Toeplitz quantization has an adjoint operation, called Berezin-Toeplitz dequantization, which I used to define a state and showed it is the Sorkin-Johnston state [50, 102]. I also discussed the relationship of (Berezin)-Toeplitz (de)quantization to star products and strict deformation quantization with a continuous field of C*-algebras where the quantization parameter $\hbar$ takes values including the classical limit $\hbar = 0$.

7.2 Open Questions

In the following, I would like to mention some further research questions based on the findings presented in this thesis and summarized above.

In the introductory chapter, I mentioned the causal hierarchy to draw our attention to further properties of causets inspired by globally hyperbolic spacetime manifolds. We noticed that causets are not necessarily distinguishing and I fur-

ther introduced the property of sliceability (see Subsection 1.3.3). Among generic causets, there is a large class of causets that are only composed of three time steps (that are equal to a 3-step Cauchy slice), which are known as Kleitman-Rothschild orders, see Kleitman and Rothschild [55], and Dowker [34]. How can the causet properties be used to define *physically relevant* causets? For a physically relevant causet, one may consider a sliceable causet such that any of its slicings has a number of Cauchy antichains that increases with the causet cardinality.

In the numerical investigations, I have focused on a method to determine a preferred past structure in finite, sprinkled causets on causal intervals of Minkowski spacetime. While this method should also work for compact spacetime regions in a curved spacetime that are approximately flat, it remains to test it for curved spacetime manifolds, for example, on de Sitter spacetime (with a global curvature parameter). Does the method still work on compact subsets of curved spacetime manifolds? Is there a physical interpretation of the events that have no unique preferred past (at least, according to criterion 6)? What are the properties of a preferred past chosen uniformly at random from the rank 2 pasts? On infinite causal sets, we cannot expect that any of the criteria presented in Subsection 3.2.2 would still select a singleton subset with high probability. How do we construct a preferred past structure for infinite causal sets? Since the preferred past structure is essentially a future-directed timelike vector field, it may be determined by a causet slicing. In general, is the discretized d'Alembertian with a preferred past structure a good approximation for the d'Alembertian on the represented spacetime manifold?

The new discretization method(s) via a preferred past structure may find further applications, for example, in the formulation of a discrete analogue to an action functional. What is the expression of the Benincasa-Dowker action [11] using a discretization with a preferred past structure? Furthermore, how is the method of relative Cauchy evolution (as shown in Subsection 2.3.4) related to an action principle? What does relative Cauchy evolution tell us about the energy momentum tensor in causal set theory?

We have reviewed the mathematical aspects of the sprinkling process to construct causets for a given spacetime manifold in Chapter 4. Ideally, one may want to start with a causet (or an ensemble of causets) and "reconstruct" the properties of a corresponding spacetime manifold. What is a good way to reconstruct a spacetime manifold or, at least, find a suitable class of spacetime manifolds that embed a given causet (see Reid [92])? For example, one may start with a Cauchy slice and determine a notion of spatial separation; see also Major, Rideout, and Surya [64].

The geometric construction of the quantum algebra and the Sorkin-Johnston

state from Chapter 6 may generalize to non-linear field theories. Some aspects of the perturbation theory have already been considered in the end of [29]. The continuous field of C*-algebras as discussed in Section 6.3 may also be generalized to non-linear theories non-perturbatively. It may also find an application in a mathematical formulation of a "continuum limit" or "continuum correspondence" between causal sets on the microscopic level and emergent spacetime manifolds on the macroscopic level [15, 100, 63, 92]. Assume that we have a sequence of (ensembles of) causets that embed in a given spacetime manifold and the causets get increasingly denser approaching a dense subset of the manifold. Can this problem be formulated such that there exists a continuous field of C*-algebras including the classical and quantum algebras of the causets and the spacetime manifold? What would such a continuous field tell us about the correspondence between causal sets and spacetime manifolds?

Glossary

Notation	Explanation	p.
General notations		
$\mathbb{N}$, $\mathbb{N}_* := \mathbb{N} \setminus \{0\}$	Natural numbers including/excluding 0	
$[a, b] \subset \mathbb{N}$	Interval of natural numbers from a to b	
$[a, b] \subset \mathbb{R}$	Closed interval of real numbers from a to b	
$\overline{c}$	Complex conjugation of a scalar $c \in \mathbb{C}$ (or component-wise for matrices)	
$A^m B_m := \sum_m A^m B_m$	Summation convention over the index m (once as superscript, once as subscript) for (co)vectors A, B, for a finite causet with N events, the sum runs from 1 to N	
$A^{[mn]} = \frac{1}{2}(A^{mn} - A^{nm})$	Anti-symmetric part of a 2-tensor A in index notation	
$A^{(mn)} = \frac{1}{2}(A^{mn} + A^{nm})$	Symmetric part of a 2-tensor A in index notation	
$\mathrm{C}_0(\Omega, \mathbb{K})$, $\mathrm{C}_\mathrm{b}(\Omega, \mathbb{K})$	Continuous functions that vanish at infinity, and continuous, bounded functions on Ω (valued in $\mathbb{K}$)	
$\mathrm{C}^\infty(\Omega, \mathbb{K})$, $\mathrm{C}^m(\Omega, \mathbb{K})$	Smooth functions, and m-fold differentiable functions on Ω (valued in $\mathbb{K}$)	
$\mathrm{C}^\infty_\mathrm{S}(\Omega, \mathbb{K})$	Schwartz functions on Ω (valued in $\mathbb{K}$)	
$\mathcal{B}(\mathcal{H})$	Bounded, linear operators on a Hilbert (Banach) space $\mathcal{H}$	
$\mathrm{resol}(D)$	Resolvent set of an operator D on a Hilbert (Banach) space	54
$\mathrm{spec}(D)$	Spectrum of an operator D on a Hilbert (Banach) space	54
Causality		
(M, g, u)	Globally hyperbolic spacetime manifold M with metric g and future-directed timelike, smooth vector field u (the time orientation)	18
$(+, -, -, \dots)$	Spacetime signature	12

continued on the next page

continued from the previous page

Notation	Meaning	p.
$\ll$	Chronological relation between events of spacetime manifold	15
$(C, \preceq)$	Causal set (causet) with causal relation $\preceq$	12
$(C, \preceq^{\mathrm{op}})$	Opposite causet/poset to the causet/poset $(C, \preceq)$	13
$\mathcal{X}$	(Placeholder for) a spacetime manifold/ causet object	31
$\prec$	Strict causal relation between events of a spacetime/causet; for a causet, it is used as the chronological relation	17
$\prec *$	Link relation between events in a causet; edges in a Hasse diagram	16
$\boldsymbol{C}$, $\boldsymbol{L}$	(Past) causal and link matrices for a finite causet	17
$[x, y]$, (x, y)	Closed/Open interval	14
$J^{\pm}(A)$ (or $J^{\pm}[\mathcal{X}](A)$)	Past/Future of a subset $A \subseteq \mathcal{X}$ (within a spacetime or causal set $\mathcal{X}$)	14
$J^{\pm}_{*}(A)$ (or $J^{\pm}_{*}[\mathcal{X}](A)$)	Strict past/future of a subset $A \subseteq \mathcal{X}$ (within a spacetime or causal set $\mathcal{X}$)	14
i^{-}, i^{+}	Penrose diagrams: timelike past/future infinity	14
i^{0}	Penrose diagrams: spacelike infinity	14
$\mathscr{I}^{\mp}$	Penrose diagrams: past/future null infinity	14
$\bar{\mathrm{X}}_x$, $\bar{\mathrm{X}}^{\pm}_x$	Closed future/past lightcone at event $x \in M$ (in a spacetime M), $\pm$ for only the future/ past lightcone	
Subsets of causal sets and local structure		
$\mathrm{paths}(x, y)$	Causal paths from event x to event y in a causet	16
$\mathrm{rk}(y, x)$	Rank of event y with respect to event x in a causet (minimal path length)	20
$\mathrm{step}(y, x)$	Step of event y with respect to event x in a causet (maximal path length)	21
$L^{\pm}_{k}(\cdot)$ (and $L^{\pm}_{[0,k]}(\cdot)$)	Layer k future/past of a causet event or subset (and the union of layer 0 to k)	20

continued on the next page

continued from the previous page

Notation	Meaning	p.
$R_k^{\pm}(\cdot)$ (and $R_{[0,k]}^{\pm}(\cdot)$)	Rank k future/past of a causet event or subset (and the union of rank 0 to k)	20
$S_k^{\pm}(\cdot)$ (and $S_{[0,k]}^{\pm}(\cdot)$)	Step k future/past of a causet event or subset (and the union of step 0 to k)	21
$\mathcal{I}^{\pm}$ (or $\mathcal{I}^{\pm}[C]$)	Subset of events without a strict future/past (in the causet C) i.e., future/past infinity	20
$\mathcal{I}^{\pm}_{k\text{-layer}}$, $\mathcal{I}^{\pm}_{k\text{-rank}}$, $\mathcal{I}^{\pm}_{k\text{-step}}$	k-layer/k-rank/k-step future/past infinity	20–21
$\Lambda^{\mp}$	Preferred past (or future) structure	41
$\mathrm{prm}(y, x)$	Number of perimetral events in a causet C diamond $[x, y] \subset C$	45
$\mathrm{itn}(y, x)$	Number of internal events in a causet C diamond $[x, y] \subset C$	45
$D^{-}_{\mathrm{crit}\,k}(x) \subseteq R_2^{-}(x)$	Subset of the rank 2 past of a causet event x determined by criterion k	63–65
Field kinematics		
$\mathcal{E}$ (or $\mathcal{E}(\mathcal{X})$)	Space of real scalar field configurations (on the spacetime/causet $\mathcal{X}$)	31
$\mathcal{E}_{\mathrm{s}}, \mathcal{E}_{\mathrm{p}}, \mathcal{E}_{\mathrm{f}}, \mathcal{E}_{\mathrm{t}} \subseteq \mathcal{E}$	Space of field configurations with spatial/past/future/timelike-compact or -finite support	32
$\mathcal{D} \subseteq \mathcal{E}$	Space of compactly or finitely supported fields	32
$\mathcal{E}_A(C) \subset \mathcal{E}(C)$	Field configurations that are supported on a timelike-finite subset $A \subset C$ of the causet C	47
$\mathcal{F}$ or $\mathcal{F}(\mathcal{X})$	Space of observables i.e. smooth functionals on $\mathcal{E}$ over the spacetime/causet $\mathcal{X}$	32
$\left\langle F^{(k)}(\varphi), \psi_1 \otimes \dots \psi_k \right\rangle$	k-th Gâteaux differential of a functional F at point $\varphi \in \mathcal{E}$ in directions $\psi_1, \dots, \psi_k \in \mathcal{E}$	33
$\Phi_f(\varphi)$	Linear observable evaluated at $\varphi \in \mathcal{E}$, the linear observable is determined by some pairing of the configuration φ with a compactly/finitely supported function $f \in \mathcal{D}^{\mathbb{C}}(\mathcal{X})$ on a spacetime/causet $\mathcal{X}$	34
$\mathcal{F}_{\mathrm{lin}} \subset \mathcal{F}$	Space of linear observables	32
$\mathcal{F}_{(\mathrm{m})\mathrm{loc}} \subset \mathcal{F}$	Space of (multi)local observables	35
$\mathcal{F}_{\mathrm{reg}} \subset \mathcal{F}$	Space of regular observables	35

continued on the next page

continued from the previous page

Notation	Meaning	p.
$F^* \in \mathcal{F}$	Involution of F as element of the *-algebra $\mathcal{F}$	34
Field dynamics		
$P = -(\Box + m^2 + \xi R)$	Klein-Gordon field operator for a boson with mass m, coupled to the scalar curvature R by the coupling constant ξ	36
E^+, E^-	Retarded and advanced Green's operator corresponding to P	37, 46
$E := E^+ - E^-$	Pauli-Jordan (causal) operator	37, 46
$\boldsymbol{E}$ (and $\boldsymbol{E}^\mathsf{T}$)	Pauli-Jordan matrix (and its transpose) for a finite causet	46
$\mathcal{S} = \mathrm{img}(E)$	Symplectic space to the classical field equation	52
$(g^{\leftarrow} f)(x) := f\Big(g(x)\Big)$	Pullback of the function f by the function g (evaluated at spacetime/causet event $x \in \mathcal{X}$); [This unconventional symbol is used to avoid confusion with other meanings of the commonly used symbol *.]	47
Poisson algebra		
$\{\cdot, \cdot\}$	Poisson bracket	50
$\mathcal{F}_{(\mathrm{s})\mu\mathrm{c}}(M)$	(Strongly) microcausal observables on a spacetime M	50
$\pi^\sharp_{\mathrm{off}} : (\mathcal{E}^*)^{\mathbb{C}}(\mathcal{X}) \to \mathcal{E}^{\mathbb{C}}(\mathcal{X})$	Poisson structure as linear map from the continuous dual of the (complexified) configuration space $\mathcal{E}^{\mathbb{C}}(\mathcal{X})$ to the configuration space on the spacetime/causet $\mathcal{X}$	50
Causet sprinkling		
$\rho, \ell = \rho^{-\frac{1}{d}}$	Sprinkling density and fundamental length scale (depending on the dimension d)	83
$\Big(Q_U, \mathrm{B}\sigma(Q_U), \mu_U\Big)$	Probability space for a compact spacetime subset U with sprinkling configuration space Q_U, Borel σ-algebra $\mathrm{B}\sigma(Q_U)$, and Poisson measure μ_U	85
$[C]_U \subset Q_U$	Causet isomorphism class of sprinkles on U that are isomorphic ($\sim$) to a given causet C	86

continued on the next page

continued from the previous page

Notation	Meaning	p.
$\mathsf{S} \in Q_U$, $\mathsf{x} \in S$	Random sprinkle on U, and a uniformly chosen random event in a sprinkle S	86
Quantization methods		
$[A_1, A_2]_-$ $:= A_1A_2 - A_2A_1$	Commutator for elements of a non-commutative algebra $\mathfrak{A} \ni A_1, A_2$	101
$f(\hbar) = \mathrm{o}\big(g(\hbar)\big)$	Little-o notation, meaning that $\lim_{\hbar\to 0} \frac{f(\hbar)}{g(\hbar)} = 0$	
$\mathcal{F}[[\hbar]]$, $\star$	Formal power series with coefficients in the (Poisson) algebra $\mathcal{F}$, and a star product	102
$\star_{(0)}$	Moyal-Weyl star product	102
$\star_{(H)}$	Exponential star product with symmetric part given by the bi-distribution H	102
$\hbar \in I \subset \mathbb{R}$, (I_*)	Quantization parameter $\hbar$ in a real interval I including (and without) the classical limit	103
$\mathcal{A}_0 \subset \mathfrak{A}_0$	Classical algebra, dense in the C*-algebra $\mathfrak{A}_0$	103
$\mathfrak{A}_\hbar$	Quantum algebra (C*-algebra) for $\hbar \in I$	103
$\big(I, (\mathfrak{A}_\hbar)_{\hbar\in I}, \Gamma\big)$	Continuous field of C*-algebras with the space of (continuous) sections Γ	104
Q, (Υ)	Family of (de)quantization maps	104
$\star_Q$, $(\star_\Upsilon)$	(De)quantization star product	106
$\Delta_\hbar$	Bochner-Laplacian on the quantization bundle $\mathcal{L}_\hbar \to \mathcal{S}$ (where $\mathcal{S}$ is an N-dimensional, symplectic vector space for a finite causet)	109
tr, (Tr)	Trace defined for all operators (or only partially-defined)	
$T_\hbar$, $\Xi_\hbar$	Toeplitz quantization map, Berezin-Toeplitz dequantization map	112
$\vert\boldsymbol{n}\rangle_\hbar$	Hilbert space basis vector with multi-index $\boldsymbol{n} \in \mathbb{N}^N$	134
$a^{\mp}_{i,\bar{\imath}}$	Annihilation/Creation operator for holomorphic ($i \in [1, N] \subset \mathbb{N}$) and anti-holomorphic components ($\bar{\imath} \in [\bar{1}, \bar{N}] \subset \mathbb{N}$)	134
$b_\hbar$	Kernel of the Berezin transform	135
$\circledast$	Convolution	135
$W_\hbar(\phi)$	Weyl generator for $\phi \in \mathcal{S}^*$	138

Bibliography

[1] J. Abajian and S. Carlip. “Dimensional reduction in manifoldlike causal sets”. In: *Physical Review D* 97.6 (2018), p. 066007.

[2] N. Afshordi, S. Aslanbeigi, and R. D. Sorkin. “A distinguished vacuum state for a quantum field in a curved spacetime: Formalism, features, and cosmology”. In: *Journal of High Energy Physics* 2012.8 (2012).

[3] S. Albeverio, Y. G. Kondratiev, and M. Röckner. “Diffeomorphism groups and current algebras: Configuration space analysis in quantum theory”. In: *Reviews in Mathematical Physics* 11.01 (1999), pp. 1–23.

[4] S. Albeverio, Y. G. Kondratiev, and M. Röckner. “Analysis and geometry on configuration spaces”. In: *Journal of Functional Analysis* 154 (1998), pp. 444–500.

[5] S. T. Ali and M. Engliš. “Quantization methods: A guide for physicists and analysts”. In: *Reviews in Mathematical Physics* 17.04 (2005), pp. 391–490.

[6] S. Aslanbeigi, M. Saravani, and R. D. Sorkin. “Generalized causal set d’ Alembertians”. In: *Journal of High Energy Physics* 2014.6 (2014), p. 24.

[7] E. Bachmat. “Discrete spacetime and its applications”. In: *Random Matrices, Integrable Systems and Applications: A Conference in Honor of Percy Deift’s 60th Birthday*. Ed. by J. Baik, L.-C. Li, T. Kriecherbauer, K. McLaughlin, and C. Tomei. Providence, RI: American Mathematical Society, 2008.

[8] C. Bär. “Green-hyperbolic operators on globally hyperbolic spacetimes”. In: *Communications in Mathematical Physics*. Vol. 333. 3. Springer, 2015, pp. 1585–1615.

[9] C. Bär, N. Ginoux, and F. Pfäffle. *Wave Equations on Lorentzian Manifolds and Quantization*. Vol. 3. European Mathematical Society, 2007.

[10] A. Bastiani. “Applications différentiables et variétés différentiables de dimension infinie”. In: *Journal d’Analyse Mathématique* 13.1 (1964), pp. 1–114.

[11] D. M. Benincasa and F. Dowker. “Scalar curvature of a causal set”. In: *Physical Review Letters* 104.18 (2010), p. 181301.

[12] M. Benini and C. Dappiaggi. "Models of free quantum field theories on curved backgrounds". In: *Advances in Algebraic Quantum Field Theory*. Ed. by R. Brunetti, C. Dappiaggi, K. Fredenhagen, and J. Yngvason. Springer, 2015.

[13] F. A. Berezin. "Covariant and contravariant symbols of operators". In: *Mathematics of the USSR-Izvestiya* 6.5 (1972). Translated by L. W. Longdon., p. 1117.

[14] A. N. Bernal and M. Sánchez. "Globally hyperbolic spacetimes can be defined as 'causal' instead of 'strongly causal'". In: *Classical and Quantum Gravity* 24.3 (2007), pp. 745–749.

[15] L. Bombelli. "Statistical Lorentzian geometry and the closeness of Lorentzian manifolds". In: *Journal of Mathematical Physics* 41.10 (2000), pp. 6944–6958.

[16] L. Bombelli, J. Lee, D. Meyer, and R. D. Sorkin. "Space-time as a causal set". In: *Physical Review Letters* 59.5 (1987), p. 521.

[17] M. Bordemann, E. Meinrenken, and M. Schlichenmaier. "Toeplitz quantization of Kähler manifolds and $gl(N)$, $N \to \infty$ limits". In: *Communications in Mathematical Physics* 165.2 (1994), pp. 281–296.

[18] D. Borthwick and A. Uribe. "Almost complex structures and geometric quantization". In: *Mathematical Research Letters* 3.6 (1996), pp. 845–861.

[19] G. Brightwell and R. Gregory. "Structure of random discrete spacetime". In: *Physical Review Letters* 66.3 (1991), p. 260.

[20] G. Brightwell, J. Henson, and S. Surya. "A 2D model of causal set quantum gravity: The emergence of the continuum". In: *Classical and Quantum Gravity* 25.10 (2008), p. 105025.

[21] G. Brinkmann and B. D. McKay. "Posets on up to 16 points". In: *Order* 19.2 (2002), pp. 147–179.

[22] C. Brouder, N. V. Dang, C. Laurent-Gengoux, and K. Rejzner. "Properties of field functionals and characterization of local functionals". In: *Journal of Mathematical Physics* 59.2 (2018), p. 023508.

[23] R. Brunetti, M. Dütsch, and K. Fredenhagen. "Perturbative algebraic quantum field theory and the renormalization groups". In: *Advances in Theoretical and Mathematical Physics* 13.5 (2009), pp. 1541–1599.

[24] R. Brunetti, K. Fredenhagen, and K. Rejzner. "Quantum gravity from the point of view of locally covariant quantum field theory". In: *Communications in Mathematical Physics* 345.3 (2016), pp. 741–779.

[25] R. Brunetti, K. Fredenhagen, and P. L. Ribeiro. "Algebraic structure of classical field theory I: Kinematics and linearized dynamics for real scalar fields". In: *Communications in Mathematical Physics* 368.2 (2019), pp. 519–584.

[26] R. Brunetti, K. Fredenhagen, and R. Verch. "The generally covariant locality principle – A new paradigm for local quantum field theory". In: *Communications in Mathematical Physics* 237.1 (2003), pp. 31–68.

[27] S. Carlip. "Dimensional reduction in causal set gravity". In: *Classical and Quantum Gravity* 32.23 (2015), p. 232001.

[28] A. C. Da Silva. *Lectures on symplectic geometry*. Number 1764 of the series Lecture Notes in Mathematics. Springer, 2008.

[29] E. Dable-Heath, C. J. Fewster, K. Rejzner, and N. Woods. "Algebraic classical and quantum field theory on causal sets". In: *Physical Review D* 101.6 (2020), p. 065013.

[30] L. B. De Monvel and V. Guillemin. *The Spectral Theory of Toeplitz Operators*. Vol. 99. Annals of Mathematics Studies. Princeton University Press, 1981.

[31] J. Dereziński and C. Gérard. *Mathematics of Quantization and Quantum Fields*. Cambridge University Press, 2013.

[32] J. Dixmier. *Les C*-algèbres et leurs représentations*. Cahiers scientifiques, fasc. 29. Paris: Gauthier-Villars, 1964.

[33] J. Dixmier. *C*-Algebras*. Vol. 15. Translation of Les C*-algèbres et leurs repésentations by Francis Jellett. North-Holland, 1977.

[34] F. Dowker. "Causal sets and the deep structure of spacetime". In: *100 Years of Relativity: Space-Time Structure: Einstein and Beyond*. World Scientific, 2005, pp. 445–464. ISBN: 978-981-256-394-1.

[35] F. Dowker and L. Glaser. "Causal set d'Alembertians for various dimensions". In: *Classical and Quantum Gravity* 30.19 (2013), p. 195016.

[36] M. Dütsch and K. Fredenhagen. "Algebraic quantum field theory, perturbation theory, and the loop expansion". In: *Communications in Mathematical Physics* 219.1 (2001), pp. 5–30.

[37] M. Dütsch and K. Fredenhagen. "Perturbative algebraic field theory, and deformation quantization". In: *Mathematical Physics in Mathematics and Physics. Quantum and Operator Algebraic Aspects. Proceedings of a Conference, Siena, Italy, June 20–24, 2000.* Providence, RI: AMS, American Mathematical Society, 2001, pp. 151–160.

[38] C. J. Fewster, E. Hawkins, C. Minz, and K. Rejzner. "Local structure of sprinkled causal sets". In: *Physical Review D* 103.8 (2021), p. 086020.

[39] C. J. Fewster and R. Verch. "On a recent construction of vacuum-like quantum field states in curved spacetime". In: *Classical and Quantum Gravity* 29.20 (2012).

[40] C. J. Fewster and R. Verch. "The necessity of the Hadamard condition". In: *Classical and Quantum Gravity* 30.23 (2013).

[41] K. Fredenhagen and K. Rejzner. "Batalin-Vilkovisky formalism in the functional approach to classical field theory". In: *Communications in Mathematical Physics* 314.1 (2012), pp. 93–127.

[42] K. Fredenhagen and K. Rejzner. "Perturbative construction of models of algebraic quantum field theory". In: *Advances in Algebraic Quantum Field Theory*. Ed. by R. Brunetti, C. Dappiaggi, K. Fredenhagen, and J. Yngvason. Springer, 2015.

[43] L. Glaser. "A closed form expression for the causal set d'Alembertian". In: *Classical and Quantum Gravity* 31.9 (2014), p. 095007.

[44] H. J. Groenewold. "On the principles of elementary quantum mechanics". In: *Physica XII*. Utrecht, 1946, pp. 405–460.

[45] V. Guillemin and A. Uribe. "The Laplace operator on the N-th tensor power of a line bundle: Eigenvalues which are uniformly bounded in N". In: *Asymptotic Analysis* 1.2 (1988), pp. 105–113.

[46] R. Haag and D. Kastler. "An algebraic approach to quantum field theory". In: *Journal of Mathematical Physics* 5.7 (1964), pp. 848–861.

[47] S. W. Hawking and G. F. R. Ellis. *The Large Scale Structure of Space-time*. Vol. 1. Cambridge University Press, 1973.

[48] E. Hawkins. "An obstruction to quantization of the sphere". In: *Communications in Mathematical Physics* 283.3 (2008), pp. 675–699.

[49] E. Hawkins and K. Rejzner. "The star product in interacting quantum field theory". In: *Letters in Mathematical Physics* (2020), pp. 1257–1313.

[50] S. Johnston. "Quantum Fields on Causal Sets". PhD thesis. Imperial College London, Sept. 2010.

[51] A. V. Karabegov and M. Schlichenmaier. "Identification of Berezin-Toeplitz deformation quantization". In: *Journal für die reine und angewandte Mathematik (Crelle's Journal)* 2001.540 (2001), pp. 49–76.

[52] I. Khavkine and V. Moretti. "Algebraic QFT in curved spacetime and quasifree Hadamard states: An introduction". In: *Advances in Algebraic Quantum Field Theory*. Ed. by R. Brunetti, C. Dappiaggi, K. Fredenhagen, and J. Yngvason. Springer, 2015.

[53] J. F. C. Kingman. *Poisson Processes*. Vol. 3. Oxford: Clarendon Press, 1993.

[54] E. Kirchberg and S. Wassermann. "Operations on continuous bundles of C*-algebras". In: *Mathematische Annalen* 303.1 (1995), pp. 677–697.

[55] D. J. Kleitman and B. L. Rothschild. "Asymptotic enumeration of partial orders on a finite set". In: *Transactions of the American Mathematical Society* 205 (1975), pp. 205–220.

[56] S. Kobayashi and K. Nomizu. *Foundations of differential geometry*. Vol. 2. John Wiley & Sons, 1969.

[57] M. Kontsevich. "Deformation quantization of Poisson manifolds". In: *Letters in Mathematical Physics* 66.3 (2003), pp. 157–216.

[58] N. P. Landsman. *Mathematical Topics between Classical and Quantum Mechanics*. Springer Science & Business Media, 1998.

[59] H. B. Lawson Jr. "Foliations". In: *Bulletin of the American Mathematical Society* 80.3 (1974), pp. 369–418.

[60] X. Ma and G. Marinescu. "The spin^c Dirac operator on high tensor powers of a line bundle". In: *Mathematische Zeitschrift* 240.3 (2002), pp. 651–664.

[61] X. Ma and G. Marinescu. "Generalized Bergman kernels on symplectic manifolds". In: *Advances in Mathematics* 217.4 (2008), pp. 1756–1815.

[62] X. Ma and G. Marinescu. "Toeplitz operators on symplectic manifolds". In: *Journal of Geometric Analysis* 18.2 (2008), pp. 565–611.

[63] S. Major, D. Rideout, and S. Surya. "On recovering continuum topology from a causal set". In: *Journal of Mathematical Physics* 48.3 (2007).

[64] S. A. Major, D. Rideout, and S. Surya. "Spatial hypersurfaces in causal set cosmology". In: *Classical and Quantum Gravity* 23.14 (2006), p. 4743.

[65] D. A. Meyer. "The Dimension of Causal Sets". PhD thesis. Massachusetts Institute of Technology, 1988.

[66] A. D. Michal. "Differentials of functions with arguments and values in topological abelian groups". In: *Proceedings of the National Academy of Sciences of the United States of America* 26.5 (1940), p. 356.

[67] E. Minguzzi and M. Sánchez. "The causal hierarchy of spacetimes". In: *Recent Developments in Pseudo-Riemannian Geometry (ESI Lectures in Mathematics and Physics)*. Ed. by D. V. Alekseevsky and H. Baum. Vol. 4. European Mathematical Society Publishing House, Zurich, Switzerland, 2008, 299ff.

[68] C. Minz. *LaTeX-package 'causets' for drawing causal set (Hasse) diagrams*. `https://ctan.org/pkg/causets`. 2020.

[69] C. Minz. *Causal 2-simplex in Minkowski spacetime | Causal set theory*. `https://youtu.be/2LnYMXsoCIc`. 2021.

[70] C. Minz. *Causal 2-simplex with one edge flipped in Minkowski spacetime | Causal set theory*. `https://youtu.be/BDxuvpTmMMo`. 2021.

[71] C. Minz. *Causal 2-simplex with two edges flipped in Minkowski spacetime | Causal set theory*. `https://youtu.be/m6kAMXJIp3E`. 2021.

[72] C. Minz. *Causal set of a 3D-lattice slab in Minkowski spacetime | Causal set theory*. `https://youtu.be/F8sbslcMKnI`. 2021.

[73] C. Minz. *Causal set of a perturbed 3D-lattice slab in Minkowski spacetime | Causal set theory*. `https://youtu.be/QJ9YICw3YHM`. 2021.

[74] C. Minz. *Causal set of the future infinity of a 3D-lattice slab in Minkowski spacetime | Causal set theory*. `https://youtu.be/pN1DJ8gUVGk`. 2021.

[75] C. Minz. *Causal set of the past infinity of a 3D-lattice slab in Minkowski spacetime | Causal set theory*. `https://youtu.be/pPm06w-ncOo`. 2021.

[76] C. Minz. *MATLAB source code for causal set sprinklings I: Simulations on Minkowski spacetimes*. `https://github.com/c-minz/diamondsprinkling`. 2021.

[77] C. Minz. *MATLAB source code for causal set sprinklings II: Simulation results*. `https://github.com/c-minz/diamondresults`. 2021.

[78] C. Minz. *Subset of a causal 2D-lattice in Minkowski spacetime | Causal set theory*. `https://youtu.be/U8AZqbhHEj8`. 2021.

[79] C. Minz. *Subset of a causal 3D-lattice in Minkowski spacetime | Causal set theory*. `https://youtu.be/VOXtmuGf-kc`. 2021.

[80] C. Minz. *Subset of a causal 4D-lattice in Minkowski spacetime | Causal set theory*. `https://youtu.be/B8DOx5e9U8U`. 2021.

[81] V. Moretti. "Comments on the stress-energy tensor operator in curved spacetime". In: *Communications in Mathematical Physics* 232.2 (2003), pp. 189–221.

[82] J. Myrheim. *Statistical Geometry*. Tech. rep. CERN, 1978.

[83] K.-H. Neeb. "Monastir summer school: Infinite dimensional Lie groups". In: *TU Darmstadt Preprint* 2433 (2006).

[84] A. Newlander and L. Nirenberg. "Complex analytic coordinates in almost complex manifolds". In: *Annals of Mathematics* (1957), pp. 391–404.

[85] OEIS Foundation Inc. *The On-Line Encyclopedia of Integer Sequences*. Number of partially ordered sets ("posets") with n unlabeled elements. `http://oeis.org/A000112`. A000112 (2020).

[86] K. R. Parthasarathy. *Probability Measures on Metric Spaces*. Vol. 352. American Mathematical Soc., 2005.

[87] R. E. Peierls. "The commutation laws of relativistic field theory". In: *Selected Scientific Papers of Sir Rudolf Peierls (with Commentary)*. World Scientific, 1997, pp. 367–382.

[88] R. Penrose. "Asymptotic properties of fields and space-times". In: *Phys. Rev. Lett.* 10.2 (1963), pp. 66–68.

[89] R. Penrose. *Techniques of Differential Topology in Relativity*. Vol. 7. Society for Industrial and Applied Mathematics, Philadelphia, Pa., 1972.

[90] M. J. Radzikowski. "Micro-local approach to the Hadamard condition in quantum field theory on curved space-time". In: *Communications in Mathematical Physics* 179.3 (1996), pp. 529–553.

[91] M. Reed and B. Simon. *Methods of Modern Mathematical Physics, I: Functional Analysis*. Vol. 1. Academic Press, 1980.

[92] D. D. Reid. "Embeddings of causal sets". In: *AIP Conference Proceedings*. Vol. 1140. 1. American Institute of Physics. 2009, pp. 60–68.

[93] D. D. Reid. "Manifold dimension of a causal set: Tests in conformally flat spacetimes". In: *Physical Review D* 67.2 (2003), pp. 1–8.

[94] K. Rejzner. *Perturbative Algebraic Quantum Field Theory - An Introduction for Mathematicians*. Mathematical Physics Studies. Springer, 2016.

[95] D. Rideout and S. Zohren. "Evidence for an entropy bound from fundamentally discrete gravity". In: *Classical and Quantum Gravity* 23.22 (2006), p. 6195.

[96] M. A. Rieffel. "Questions on quantization". In: *Contemporary Mathematics* 228 (1998), pp. 315–326.

[97] M. Roy, D. Sinha, and S. Surya. "The discrete geometry of a small causal diamond". In: *Physical Review D* 87.4 (2013), p. 044046.

[98] M. E. Rudin. *Lectures on Set Theoretic Topology*. Vol. 23. American Mathematical Soc., 1975.

[99] M. Schlichenmaier. "Berezin-Toeplitz quantization for compact Kähler manifolds. A review of results". In: *Advances in Mathematical Physics* 2010 (2010).

[100] R. D. Sorkin. "Causal Sets: Discrete Gravity". In: *Lectures on Quantum Gravity*. Springer, 2005, pp. 305–327.

[101] R. D. Sorkin. "Does locality fail at intermediate length-scales". In: *Approaches to Quantum Gravity: Towards a New Understanding of Space, Time and Matter* (2009). Ed. by D. Oriti, pp. 26–43.

[102] R. D. Sorkin. "Scalar field theory on a causal set in histories form". In: *Journal of Physics: Conference Series*. Vol. 306. 2011.

[103] R. D. Sorkin. "From Green function to quantum field". In: *International Journal of Geometric Methods in Modern Physics* 14.08 (2017), p. 1740007.

[104] S. Surya. "The causal set approach to quantum gravity". In: *Living Reviews in Relativity* 22.1 (2019), pp. 1–75.

[105] F. Treves. *Topological Vector Spaces, Distributions and Kernels: Pure and Applied Mathematics*. Vol. 25. Elsevier, 2016.

[106] L. C. P. Van Hove. "Sur certaines représentations unitaires d'un groupe infini de transformations". PhD thesis. Bruxelles U., 1951.

[107] R. M. Wald. *General Relativity*. University of Chicago Press, 1984.

[108] A. Weinstein. *Deformation Quantization*. 1994.

[109] F. L. Wingham. "Generalised Sorkin-Johnston and Brum-Fredenhagen States for Quantum Fields on Curved Spacetimes". PhD thesis. University of York, 2019.

[110] P. Winkler. "Random orders". In: *Order* 1.4 (1985), pp. 317–331.

[111] P. Winkler. "Random orders of dimension 2". In: *Order* 7.4 (1990), pp. 329–339.

[112] N. M. J. Woodhouse. *Geometric Quantization*. Vol. 1. Oxford University Press, 1997.

[113] N. X, F. Dowker, and S. Surya. "Scalar field Green functions on causal sets". In: *Classical and Quantum Gravity* 34.12 (2017), p. 124002.